Quadrature Amplitude Modulation:
From Basics to Adaptive Trellis-Coded,
Turbo-Equalised and Space-Time Coded OFDM,
CDMA and MC-CDMA Systems

by

L. Hanzo, S.X. Ng, T. Keller, W.T. Webb

Contents

Related Wiley and IEEE Press Books [1]

- R. Steele, L. Hanzo (Ed): *Mobile Radio Communications: Second and Third Generation Cellular and WATM Systems*, John Wiley and IEEE Press, 2nd edition, 1999, ISBN 07 273-1406-8, 1064 pages
- L. Hanzo, W. Webb, and T. Keller, *Single- and Multi-Carrier Quadrature Amplitude Modulation: Principles and Applications for Personal Communications, WLANs and Broadcasting*, John Wiley and IEEE Press, 2000, 739 pages
- L. Hanzo, F.C.A. Somerville, J.P. Woodard: *Voice Compression and Communications: Principles and Applications for Fixed and Wireless Channels*; IEEE Press and John Wiley, 2001, 642 pages
- L. Hanzo, P. Cherriman, J. Streit: *Wireless Video Communications: Second to Third Generation and Beyond*, IEEE Press and John Wiley, 2001, 1093 pages
- L. Hanzo, T.H. Liew, B.L. Yeap: *Turbo Coding, Turbo Equalisation and Space-Time Coding*, John Wiley and IEEE Press, 2002, 751 pages
- J.S. Blogh, L. Hanzo: *Third-Generation Systems and Intelligent Wireless Networking: Smart Antennas and Adaptive Modulation*, John Wiley and IEEE Press, 2002, 408 pages
- L. Hanzo, C.H. Wong, M.S. Yee: *Adaptive wireless transceivers: Turbo-Coded, Turbo-Equalised and Space-Time Coded TDMA, CDMA and OFDM systems*, John Wiley and IEEE Press, 2002, 737 pages
- L. Hanzo, M. Münster, B.J. Choi and T. Keller: *OFDM and MC-CDMA for Broadband Multi-user Communications, WLANs and Broadcasting*, John Wiley - IEEE Press, May 2003, 980 pages
- L. Hanzo, L-L. Yang, E-L. Kuan and K. Yen: *Single- and Multi-Carrier CDMA: Multi-User Detection, Space-Time Spreading, Synchronisation, Standards and Networking*, John Wiley and IEEE Press, June 2003, 1060 pages

[1] For detailed contents and sample chapters please refer to http://www-mobile.ecs.soton.ac.uk

Part I

QAM Basics

Chapter 1

Introduction and Background

This book is concerned with the issues of transmitting digital signals via multilevel modulation. We will be concerned with digital signals originating from a range of sources such as from speech or video encoding, or data from computers. A typical digital information transmission system is shown in Figure 1.1. The source encoder may be used to remove some of the redundancy which occurs in many sources such as speech, typically reducing the transmission rate of the source. The forward error correction (FEC) block then paradoxically inserts redundancy, but in a carefully controlled manner. This redundancy is in the form of parity check bits, and allows the FEC decoder to remove transmission errors caused by channel impairments, but at the cost of an increase in transmission rate. The interleaver systematically rearranges the bits to be transmitted, which has the effect of dispersing a short burst of errors at the receiver, allowing the FEC to work more effectively. Lastly, the modulator generates bandlimited waveforms which can be transmitted over the bandwidth-limited channel to the receiver, where the reverse functions are performed. Whilst we will discuss all aspects of Figure 1.1, it is the generation of waveforms in the modulator in a manner which reduces errors and increases the transmission rate within a given bandwidth, and the subsequent decoding in the demodulator, which will be our main concern in this book.

It is assumed that the majority of readers will be familiar with binary modulation schemes such as binary phase shift keying (BPSK), frequency shift keying (FSK), etc. Those readers who possess this knowledge might like to jump to Section 1.2. For those who are not familiar with modulation schemes we give a short non-mathematical explanation of modulation and constellation diagrams before detailing the history of QAM.

1.1 Modulation Methods

Suppose the data we wish to transmit is digitally encoded speech having a bit rate of 16 kbit/s, and after FEC coding the data rate becomes 32 kb/s. If the radio channel to be used is centred around 1 GHz, then in order to transmit the 32 kb/s we must arrange for some feature of a 1 GHz carrier to change at the data rate of 32 kb/s. If the phase of the carrier is switched at the rate of 32 kb/s, being at $0\,\mathrm{deg}$ and $180\,\mathrm{deg}$ for bits having logical 0 or logical 1, respectively,

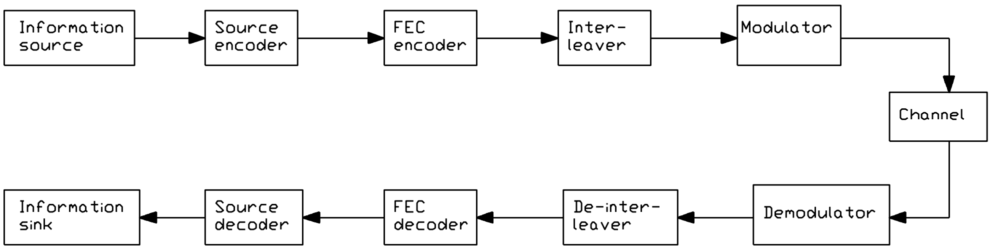

Figure 1.1: Typical digital information transmission system

then there are $1 \times 10^9/32 \times 10^3 \; = \; 31,250$ radio frequency (RF) oscillations per bit transmitted. Figure 1.2(a) and (b) show the waveforms at the output of the modulator when the data is a logical 0 and a logical 1, respectively. On the left is the phasor diagram for a logical

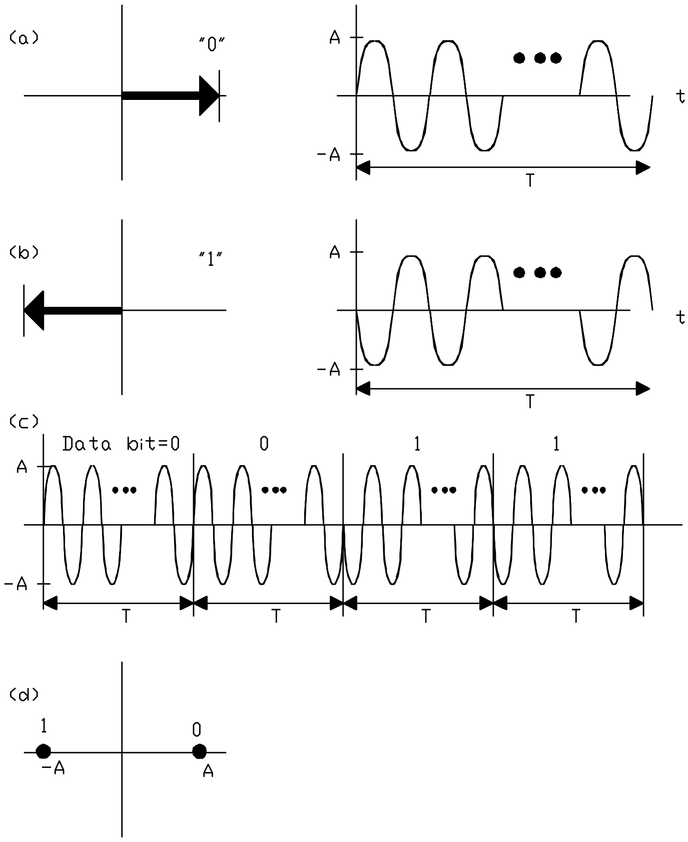

Figure 1.2: Carrier waveform for binary input data

0 and a logical 1 where the logical 0 is represented by a phasor along the positive x-axis, and

the logical 1 by a phasor along the negative x-axis. This negative phasor represents a phase shift of the carrier by $180\,\mathrm{deg}$. Figure 1.2(c) shows the modulator output for a sequence of data bits. Note that no filtering is used in this introductory example. Here the waveform can be seen to change abruptly at the boundary between some of the data symbols. We will see later that such abrupt changes can be problematic since they theoretically require an infinite bandwidth, and ways are sought to avoid them. Figure 1.2(d) is called a constellation diagram of phasor points, and as we are transmitting binary data there are only two points. As these two points are at equal distance from the origin we would expect them to represent equal magnitude carriers, and that the magnitude is indeed constant can be seen in Figure 1.2(c). The bandwidth of the modulated signal in this example will be in excess of the signalling

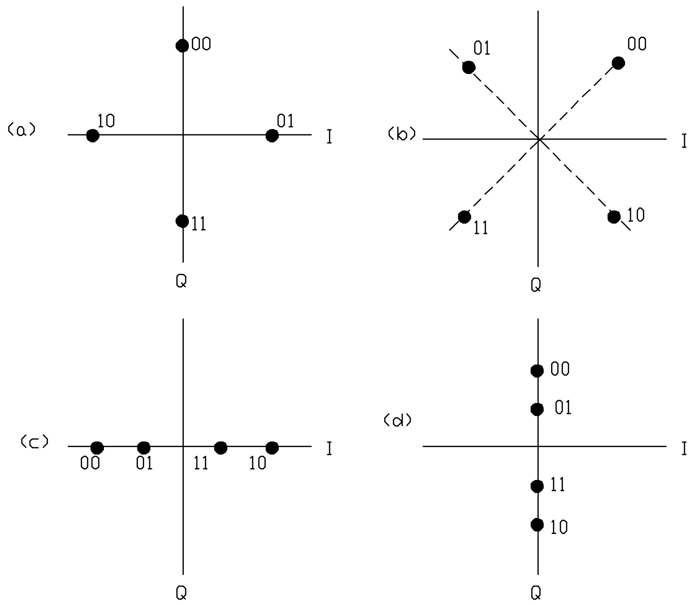

Figure 1.3: Examples of four-level constellations

rate of 32 kb/s due to the sudden transition between phase states. Later we will consider the bandwidth of modulated signals in-depth. Suffice to say here that if we decreased the signalling rate to 16 kb/s the bandwidth of the modulated signal will decrease. If the data rate is 32 kb/s, and the signalling rate becomes 16 kb/s, then every symbol transmitted must carry two bits of information. This means that we must have four points on the constellation, and clearly this can be done in many ways. Figure 1.3 shows some four-point constellations. The two bits of information associated with every constellation point are marked on the figure. In Figure 1.3(a) and (b) so-called quadrature modulation has been used as the points can only be uniquely described using two orthogonal coordinate axes, each passing through the origin. The orthogonal coordinate axes have a phase rotation of $90\,\mathrm{deg}$ with respect to each other, and hence they have a so-called quadrature relationship. The pair of coordinate axes can be associated with a pair of quadrature carriers, normally a sine and a cosine waveform, which can be independently modulated and then transmitted within the same frequency band. Due to their orthogonality they can be separated by the receiver. This implies that whatever symbol is chosen on one axis (say the x-axis in the case of Figure 1.3(a)) it will have no effect on the data demodulated on the y-axis. Data can therefore be independently transmitted via these two quadrature or orthogonal channels without any increase in error rate, although some increase may result in practice and this is considered in later chapters. We have used I and Q to signify the in-phase and quadrature components, respectively, where in-phase normally represents the x-axis and quadrature the y-axis. Figure 1.3(c) and (d) show constellations where the four points are only on one line. These are not quadrature constellations but actually represent multilevel amplitude and phase modulation where both the carrier amplitude and phase can take two discrete values.

For the constellations in Figure 1.3(a) and (b) we have a constant amplitude signal, but the carrier phase values at the beginning of each symbol period in Figure 1.3(b) would be either $45\deg, 135\deg, 225\deg or 315\deg$. There are two magnitude values and two phase values for the constellations in Figure 1.3(c) and (d).

In order to reduce the bandwidth of the modulated signal whilst maintaining the same information transmission rate we can further decrease the symbol rate by adding more points in the constellation. Such a reduction in the bandwidth requirement will allow us to transmit more information in the spectrum we have been allocated. Such capability is normally considered advantageous. If we combine the constellations of Figure 1.3(c) and (d) we obtain the square QAM constellation having four bits per constellation point as displayed in Figure 1.4. We will spend much time in dealing with this constellation in this book. In general, grouping n bits into one signalling symbol yields 2^n constellation points, which are often referred to as phasors, or complex vectors. The phasors associated with these points may have different amplitude and/or phase values, and this type of modulation is therefore referred to as multilevel modulation, where the number of levels is equal to the number of constellation points. After transmission through the channel the receiver must identify the phasor transmitted, and in doing so can determine the constellation point and hence the bits associated with this point. In this way the data is recovered. There are many problems with attempting to recover data transmitted over both fixed channels such as telephone lines and radio channels and many of these problems are given a whole chapter in this book. These problems are generally exacerbated by changing from binary to multilevel modulation, and this is why binary modulation is often preferred, despite its lower capacity. In order to introduce these problems, and to provide a historical perspective to quadrature amplitude modulation (QAM), a brief history of the development of QAM is presented.

1.2 History of Quadrature Amplitude Modulation

1.2.1 Determining the Optimum Constellation

Towards the end of the 1950s there was a considerable amount of interest in digital phase modulation transmission schemes [1] as an alternative to digital amplitude modulation. Digital phase modulation schemes are those whereby the amplitude of the transmitted carrier is held constant but the phase changed in response to the modulating signal. Such schemes have constellation diagrams of the form shown in Figure 1.3(a). It was a natural extension of this trend to consider the simultaneous use of both amplitude and phase modulation. The first paper to suggest this idea was by C.R. Cahn in 1960, who described a combined phase and

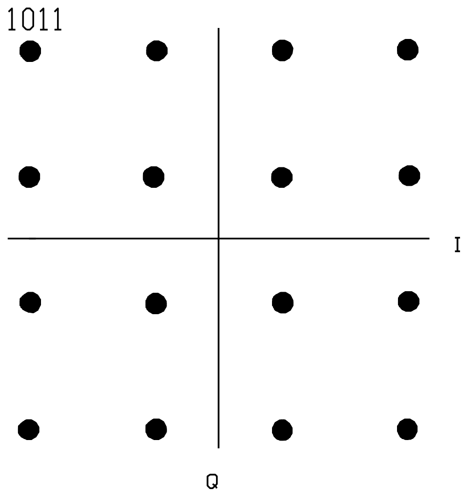

Figure 1.4: Square QAM constellation

amplitude modulation system [2]. He simply extended phase modulation to the multilevel case by allowing there to be more than one transmitted amplitude at any allowed phase. This had the effect of duplicating the original phase modulation or phase shift keying (PSK) constellation which essentially formed a circle. Such duplication led to a number of concentric circles depending on the number of amplitude levels selected. Each circle had the same number of phase points on each of its rings. Only Gaussian channels characteristic of telephone lines impaired by thermal noise were considered. Using a series of approximations and a wholly theoretical approach, he came to the conclusion that these amplitude and phase modulation (AM-PM) systems allowed an increased throughput compared to phase modulation systems when 16 or more states were used and suggested that such a system was practical to construct.

1.2.1.1 Coherent and Non-Coherent Reception

The fundamental problem with PSK is that of determining the phase of the transmitted signal and hence decoding the transmitted information. This problem is also known as carrier recovery as an attempt is made to recover the phase of the carrier. When a phase point at, say, $90\deg$ is selected to reflect the information being transmitted, the phase of the transmitted carrier is set to $90\deg$. However, the phase of the carrier is often changed by the transmission channel with the result that the receiver measures a different phase. This means that unless the receiver knew what the phase change imposed by the channel was it would be unable to determine the encoded information.

This problem can be overcome in one of two ways. The first is to measure the phase change imposed by the channel by a variety of means. The receiver can then determine the transmitted phase. This is known as coherent detection. The second is to transmit differences in phase, rather than absolute phase. The receiver then merely compares the previous phase with the current phase and the phase change of the channel is removed. This assumes that any phase change within the channel is relatively slow. This differential system is known as non-coherent transmission. In his paper, Cahn considered both coherent and non-coherent transmission, although for coherent transmission he assumed a hypothetical and unrealisable perfect carrier recovery device. The process of carrier recovery is considered in Chapter 6, and the details of differential transmission are explained in Chapter 4.

1.2.1.2 Clock Recovery

Alongside carrier recovery runs the problem of clock recovery. The recovered clock signal is used to ensure appropriate sampling of the received signal. In Figure 1.2(c) a carrier signal was shown which had vertical lines indicating each bit or symbol period. It was the phase at the start of this period which was indicative of the encoded information. Unfortunately, the receiver has no knowledge of when these periods occur although it might know their approximate duration. It is determining these *symbol periods* which is the task of clock recovery. So carrier recovery estimates the phase of the transmitted carrier and clock recovery estimates the instances at which the data changes from one symbol to another. Whilst the need for carrier recovery can be removed through differential or non-coherent detection, there is no way to remove the requirement for clock recovery.

Clock recovery schemes tend to seek certain periodicities in the received signal and use these to estimate the start of a symbol (actually they often attempt to select the centre of a symbol for reasons which will be explained in later chapters). Clock recovery is often a complex procedure, and poor clock recovery can substantially increase the bit error rate (BER). The issue of clock recovery is considered in Chapter 6. In his work, Cahn overcame the problem of clock recovery by assuming that he had some device capable of perfect clock recovery. Such devices do not exist, so Cahn acknowledged that the error rate experienced in practice would be worse than the value he had calculated, but as he was unable to compute the errors introduced by a practical clock recovery system, this was the only course open to him.

1.2.1.3 The Type I, II and III Constellations

A few months later a paper was published by Hancock and Lucky [3] in which they expanded upon the work of Cahn. In this paper they realised that the performance of the circular type constellation could be improved by having more points on the outer ring than on the inner ring. The rationale for this was that errors were caused when noise introduced into the signal moved the received phasor from the transmitted constellation point to a different one. The further apart constellation points could be placed, the less likely this was to happen. In Cahn's constellation, points on the inner ring were closest together in distance terms and so most vulnerable to errors. They conceded that a system with unequal numbers of points on each amplitude ring would be more complicated to implement, particularly in the case of non-coherent detection. They called the constellation proposed by Cahn a Type I system, and theirs a Type II system. Again using a mathematical approach they derived results similar to Cahn's for Type I systems and a 3 dB improvement for the Type II over the Type I system.

The next major publication was some 18 months later, in 1962, by Campopiano and Glazer [4]. They developed on the work of the previous papers but also introduced a new constellation - the square QAM system, which they termed a Type III system. They described

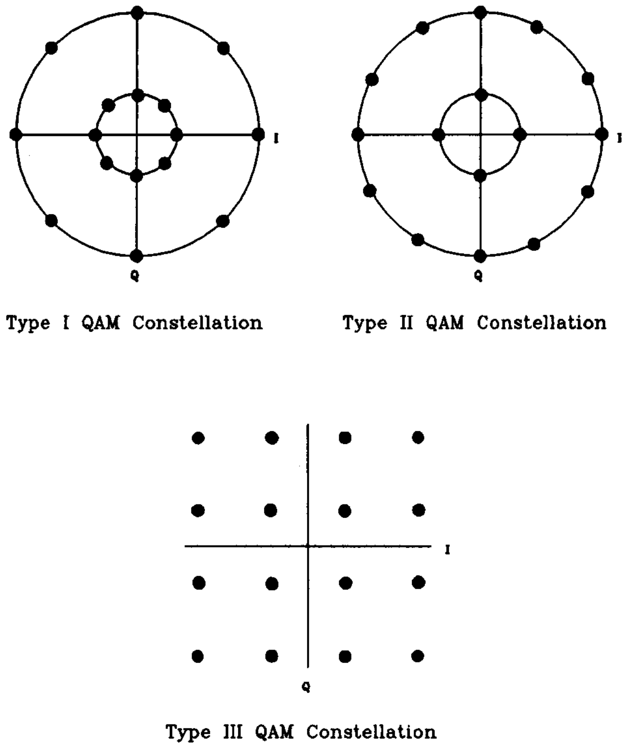

Figure 1.5: Examples of types I, II and III QAM constellations

this system as "essentially the amplitude modulation and demodulation of two carriers that have the same frequency but are in quadrature with each other" - the first time that combined amplitude and phase modulation had been thought of as amplitude modulation on quadrature carriers, although the acronym QAM was not suggested. They realised that the problem with their Type III system was that it had to be used in a phase coherent mode, that is non-coherent detection was not possible and so carrier recovery was necessary. Again, a theoretical analysis was performed for Gaussian noise channels and the authors came to the conclusion that the Type III system offered a very small improvement in performance over the Type II system, but thought that the implementation of the Type III system would be considerably simpler than that of Types I and II. Examples of the different types of constellation are shown in Figure 1.5.

Three months later another paper was published by Hancock and Lucky [5] in which they were probably unaware of the work done by Campopiano and Glazer. They attempted to improve on their previous work on the Type II system by carrying out a theoretical analysis, supposedly leading to the optimal constellation for Gaussian channels. In this paper they decided that the optimum 16-level constellation had two amplitude rings with eight equispaced points on each ring but with the rings shifted by $22.5\deg$ from each other. This constellation is shown in Figure 1.6.

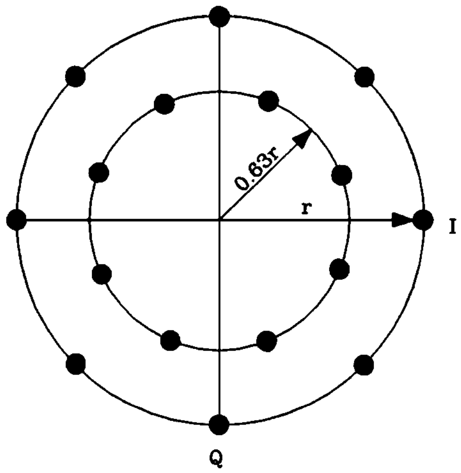

Figure 1.6: Optimum 16-level constellation according to Lucky [5] ©IRE, 1962

Again, they concluded that 16 was the minimum number of levels for AM-PM modulation and that a SNR of at least 11 dB was required for efficient operation with a low probability of bit error.

After this paper there was a gap of nine years before any further significant advances were published. This was probably due to the difficulties in implementing QAM systems with the technology available and also because the need for increased data throughput was not yet pressing. During this period the work discussed in the above papers was consolidated into a number of books, particularly that by Lucky, Salz and Weldon [6]. Here they clearly distinguished between quadrature amplitude modulation (QAM) schemes using square constellations and combined amplitude and phase modulation schemes using circular constellations. It was around this period that the acronym QAM started appearing in common usage along with AM-PM to describe the different constellations.

One of the earliest reports of the actual construction of a QAM system came from Salz, Sheenhan and Paris [7] of Bell Labs in 1971. They implemented circular constellations with 4 and 8 phase positions and 2 and 4 amplitude levels using coherent and non-coherent demodulation. Neither carrier nor clock recovery was attempted. Their results showed reasonable agreement with the theoretical results derived up to that time. This work was accompanied by that of Ho and Yeh [8] who improved the theory of circular AM-PM systems with algorithms that could be solved on digital computers which were by that time becoming increasingly available.

Interest in QAM remained relatively low, however, until 1974. In that year there was a number of significant papers published, considerably extending knowledge about quadrature amplitude modulation schemes. At this time, interest into optimum constellations was revived with two papers, one from Foschini, Gitlin and Weinstein [9] and the other from Thomas, Weidner and Durrani [10]. Foschini *et al.* attempted a theoretical derivation of the ideal constellation using a gradient calculation approach. They came to the conclusion that

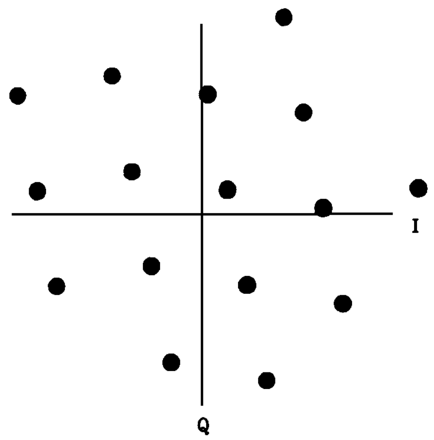

Figure 1.7: Optimum 16-level constellation according to Foschini [9] ©IEEE, 1974

the ideal constellation was based around an equilateral triangle construction leading to the unusual 16-level constellation shown in Figure 1.7. This constellation has not found favour in practical applications, since the complexities involved in its employment outweigh the associated gains that were claimed for it.

Their conclusions were that this constellation, when limited in terms of power and operated over Gaussian channels, offered a performance improvement of 0.5 dB over square QAM constellations. Meanwhile Thomas *et al.*, working at COMSAT, empirically generated 29 constellations and compared their error probabilities.

1.2.2 Satellite Links

In the paper by Thomas *et al.* [10] they also mentioned the first application of QAM, for use in satellite links. Satellite links have a particular problem in that satellites only have a limited power available to them. Efficient amplifiers are necessary to use this power carefully, and these had tended to employ a device known as a travelling wave tube (TWT). Such a device introduces significant distortion in the transmitted signal and Thomas *et al.* considered the effects of this distortion on the received waveform. They came to the interesting conclusion that the Type II constellation (in this case 3 points on the inner ring and 5 on the outer) was inferior to the Type I (4 points on inner and outer rings) due to the increased demand in peak-to-average power ratio of the Type II constellation. Their overall conclusion was that circular Type I constellations are superior in all cases. When they considered TWT distortion they discovered that AM-PM schemes were inferior to PSK schemes because of the need to significantly back off the amplifier to avoid severe amplitude distortion, and concluded that better linear amplifiers would be required before AM-PM techniques could be successfully used for satellite communications. They also considered the difficulties of implementing various carrier recovery techniques, advising that decision directed carrier recovery would be most appropriate, although few details were given as to how this was to be implemented. Decision directed carrier recovery is a process whereby the decoded signal is compared with the closest constellation point and the phase difference between them is used to estimate the error in the recovered carrier. This is discussed in more detail in Chapter 6.

Commensurate with the increasing interest as to possible applications for QAM were the two papers published in 1974 by Simon and Smith which concentrated on carrier recovery and detection techniques. In the first of these [11] they noted the interest in QAM that was then appearing for bandlimited systems, and addressed the problems of carrier recovery. They considered only the 16-level square constellation and noted that the generation of a highly accurate reconstructed carrier was essential for adequate performance. Their solution was to demodulate the signal, quantise it, and then establish the polarity of error from the nearest constellation point, and use it to update the voltage controlled oscillator (VCO) used in the carrier generation section. They provided a theoretical analysis and concluded that their carrier recovery technique worked well in the case of high signal-to-noise (SNR) ratio Gaussian noise, although they noted that gain control was required and would considerably complicate the implementation. They extended their work in Reference [12] where they considered offset QAM or O-QAM. In this modulation scheme the signal to one of the quadrature arms was delayed by half a symbol period in an attempt to prevent dramatic fluctuations of the signal envelope, which was particularly useful in satellite communications. They noted similar results for their decision directed carrier recovery scheme as when non-offset modulation was used.

1.2.2.1 Odd-Bit Constellations

Despite all the work on optimum constellations, by 1975 interest had centred on the square QAM constellation. The shape of this was evident for even numbers of bits per symbol, but if there was a requirement for an odd number of bits per symbol to be transmitted, the ideal shape of the constellation was not obvious, with rectangular constellations having been tentatively suggested. Early in 1975 J.G. Smith, also working on satellite applications, published a paper addressing this problem [13]. He noted that for even numbers of bits per symbol "the square constellation was the only viable choice." In this paper he showed that what he termed "symmetric" constellations offered about a 1 dB improvement over rectangular constellations and he considered both constellations to be of the same implementational complexity. Figure 1.8 shows an example of his symmetric constellation when there are 5 bits per symbol,

1.2.3 QAM Modem Implementations

About this time, the Japanese started to show interest in QAM schemes as they considered they might have application in both satellite and microwave radio links. In 1976 Miyauchi, Seki and Ishio published a paper devoted to implementation techniques [14]. They considered implementation by superimposing two 4-level PSK modulation techniques at different amplitudes to achieve a square QAM constellation and using a similar process in reverse at the demodulator, giving them the advantage of being able to use existing PSK modulator and demodulator circuits. This method of implementing QAM is discussed in Chapter 4. They implemented a prototype system without clock or carrier recovery and concluded that its performance was sufficiently good to merit further investigation. Further groundwork was covered in 1978 by W. Weber, again working on satellite applications, who considered differ-

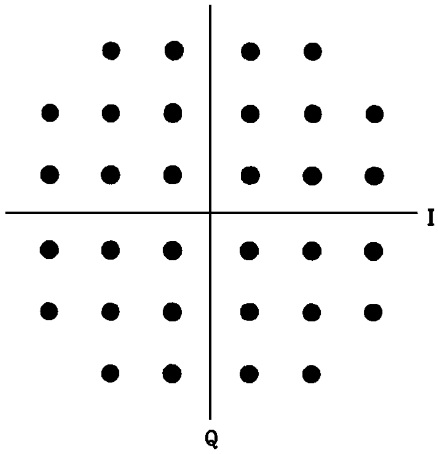

Figure 1.8: Optimum 32-level constellation according to Smith [13] ©IEEE, 1975

ential (i.e. non-coherent) encoding systems for the various constellations still in favour [15]. His paper essentially added a theoretical basis to the differential techniques that had been in use at that point, although suggesting that non-coherent demodulation techniques deserved more attention.

In late 1979 evidence of the construction of QAM prototype systems worldwide started to emerge. A paper from the CNET laboratories in France by Dupuis *et al.* [16] considered a 140 Mbit/s modem for use in point-to-point links in the 10-11 GHz band. This prototype employed the square 16-level constellation and included carrier recovery, although no details were given. Theoretical calculations of impairments were presented followed by measurements made over a 58 km hop near Paris. Their conclusions were that QAM had a number of restrictions in its use, relating to its sensitivity to non-linearities, and that in the form they had implemented it, PSK offered improved performance. However, they suggested that with further work these problems might be overcome.

The Japanese simultaneously announced results from a prototype 200 Mbit/s 16-QAM system in a paper by Horikawa, Murase and Saito [17]. They used differential coding coupled with a new form of carrier recovery based on a decision feedback method (detailed in Chapter 6). Their modem was primarily designed for satellite applications and their experiment included the use of TWT amplifiers, but was only carried out back-to-back in the laboratory. Their conclusions were that their prototype had satisfactory performance and was an efficient way to increase bandwidth efficiency.

One of the last of the purely theoretical, as opposed to practical papers on QAM appeared in April 1980, marking the progression of QAM from a technical curiosity into a practical system, some twenty years after its introduction. This came from V. Prabhu of Bell Labs [18], further developing the theory to allow calculation of error probabilities in the presence of co-channel interference. Prabhu concluded that 16-QAM had a co-channel interference immunity superior to 16-PSK but inferior to 8-PSK.

1.2.3.1 Non-Linear Amplification

In 1982 there came a turning point in the use of QAM for satellite applications when Feher turned his attention to this problem. His first major publication in this field [19] introduced a new method of generation of QAM signals using highly non-linear amplifiers which he termed non-linear amplified QAM (NLA-QAM). Two separate amplifiers for the 16-QAM case were used, one operating with half the output power of the other. The higher power amplifier coded the two most significant bits of the 4-bit symbol only, and the lower power amplifier coded only the two least significant bits. The amplified coded signals were then summed at full output power to produce the QAM signal. Because both amplifiers were therefore able to use constant envelope modulation they could be run at full power with resulting high efficiency, although with increased complexity due to the need for two amplifiers and a hybrid combiner, compared to previous systems which used only a single amplifier. However, in satellite applications, complexity was relatively unimportant compared to power efficiency, and this NLA technique offered a very substantial 5 dB power gain, considerably increasing the potential of QAM in severely power limited applications.

1.2.3.2 Frequency Selective Fading and Channel Equalisers

This work was soon followed by a performance study of a NLA 64-state system [20] which extended the NLA scheme to 64 levels by using three amplifiers all operating at different power levels. Performance estimates were achieved using computer simulation techniques which included the effects of frequency selective fading.

Frequency selective fading is essentially caused when there are a number of propagation paths between the transmitter and receiver, imposed for example by the reflection of the radio waves from nearby buldings or mountains. When the time delay of the longest path compared to that of the shortest path becomes comparable to a symbol period, intersymbol interference (ISI) arises. Since every time domain effect has an equivalent frequency domain effect, which are related to eachother through the Fourier transform, a dispersive channel impulse response results into an undulating frequency-domain channel transfer function, where the corresponding frequency-domain fluctuations are also referred to as 'frequency-selective' fading. This frequency-selective fading phenomenon may be mitigated with the aid of adaptive channel equaliser techniques, which attempt to remove the channel-induced ISI. They do so by calculating the ISI introduced and then subtracting it from the received signals. They are often extremely complex devices and are considered in detail in Chapter 7.

On a historical note, in the context of linear equalizers pioneering work was carried out amongst other researchers by Tufts [21], where the design of the transmitter and receiver was jointly optimised. The optimisation was based on the minimisation of the MSE between the transmitted signal and the equalized signal. This was achieved under the Zero Forcing (ZF) condition, where the ISI was completely mitigated at the sampling instances. Subsequently, Smith [22] introduced a similar optimisation criterion with and without applying the ZF condition. Similar works as a result of these pioneering contributions were achieved by amongst others Hänsler [23], Ericson [24] and Forney [25].

The development of the DFE was initiated by the idea of using previous detected symbols to compensate for the ISI in a dispersive channel, which was first proposed by Austin [26]. This idea was adopted by Monsen [27], who managed to optimise the DFE based on minimizing the MSE between the equalized symbol and the transmitted symbol. The optimisation of the DFE based on joint minimization of both the noise and ISI was undertaken by Salz [28], which was subsequently extended to QAM systems by Falconer and Foschini [29]. At about the same time, Price [30] optimised the DFE by utilizing the so-called ZF criterion, where all the ISI was compensated by the DFE. The pioneering work achieved so far assumed perfect decision feedback and that the number of taps of the DFE was infinite. A more comprehensive history of the linear equalizer and the DFE can be found in the classic papers by Lucky [31] or by Belfiore [32] and a more recent survey was produced by Qureshi [33].

In recent years, there has not been much development on the structure of the linear and decision feedback equalizers. However considerable effort has been given to the investigation of adaptive algorithms that are used to adapt the equalizers according to the prevalent CIR. These contributions will be elaborated in the next chapter. Nevertheless, some interesting work on merging the MLSE detectors with the DFE has been achieved by Cheung *et al.* [34,35], Wu *et al.* [36,37] and Gu *et al.* [38]. In these contributions, the structure of the MLSE and DFE was merged in order to yield an improved BER performance, when compared to the DFE, albeit at the cost of increased complexity. However, the complexity incurred was less, when compared to that of the MLSE.

In the context of error propagation in the DFE, which will be explained in Chapter 7, this phenomenon has been reported and researched in the past by Duttweiler *et al.* [39] and more recently by Smee *et al.* [40] and Altekar *et al.* [41]. In this respect some solutions have been proposed by amongst others, Tomlinson [42], Harashima [43], Russell *et al.* [44] and Chiani [45], in reducing the impact of error propagation.

1.2.3.3 History of Blind Equalisation

The philosophy of channel equalisation is that the transmitter sends known so-called channel-sounding symbols to the receiver. Upon receiving these known symbols the receiver typically evaluates the difference between the pre-agreed transmitted signal as well as the received signal and uses this error signal for adaptively adjusting the response of the equaliser, so that it eliminates the channel-induced ISI. When the wireless channel's impulse response changes rapidly, the channel's response has to be estimated at regular intervals, which requires the frequent transmission of redundant channel-sounding symbols.

By contrast, the principle of blind equalization is that no known channel-sounding symbols are transmitted over the channel for the sake of estimating its response, which allows the system to maximise its effective throughput. This blind equalisation concept was originally proposed by Sato [46]. Five years after Sato's publication, the blind equalization problem was further studied for example by Benveniste, Goursat and Ruget in [47], where several blind equalization issues were clarified and a new algorithm was proposed [48]. At the same time Godard [49] introduced a criterion, namely the so-called "constant modulus" (CM) criterion, leading to a new class of blind equalizers. Following Godard's contribution a range of studies were conducted employing the constant modulus criterion. Foschini [50] was the first researcher studying the convergence properties of Godard's equalizer upon assuming an infinite equalizer length. Later, Ding *et al.* continued this study [51] and provided an indepth analysis of the convergence issue in the context of a realistic equalizer. Although numerous researchers studied this issue, nevertheless, a general solution is yet to be found. A plethora of authors have studied Godard's equalizer, rendering it the most widely studied blind equalizer. A well–known algorithm of the so-called Bussgang type [52, 53] was also proposed by Picchi and Prati [54]. Their “Stop-and-Go” algorithm constitutes a combination of the Decision-Directed algorithm [55] with Sato’s algorithm [46]. After 1991, a range of different solutions to the blind equalization problem were proposed. Seshadri [56] suggested the employment of the so-called M-algorithm, as a “substitute” for the Viterbi algorithm [57] for the blind scenario, combined with the so-called “least mean squares (LMS)” based CIR estimation. This CIR estimation was replaced by “recursive least squares (RLS)” estimation by Raheli, Polydoros and Tzou [58], combining the associated convolutional decoding with the CIR estimation, leading to what was termed as “*Per-Survivor Processing*”. Since then a number of papers have focused on this technique [58–67]. At the same time as Seshadri, Tong *et al.* [68] proposed a different approach to blind equalization, which used oversampling in order to create a so-called “cyclostationary” received signal, and performed CIR estimation by measuring the autocorrelation function of this signal and by exploiting this signal’s cyclostationarity. This technique was also applied to the case of ‘sampling’ the received signals of different antennas (instead of oversampling the signal of a single antenna) and further extended by Moulines *et al.* using a different method of CIR estimation, namely the so–called subspace method in [69]. Furthermore, Tsatsanis and Giannakis suggested that the cyclostationarity can be induced by the transmitter upon transmitting the signal more than once [70]. A number of further contributions have also been published in the context of these techniques [71–86]. Finally, nearly coincidentally with Seshadri [56] and Tong *et al.* [68], Hatzinakos and Nikias [87] proposed a more sophisticated approach to blind equalization by exploiting the so-called “tricepstrum” of the received signal. Until today, the blind equalization problem is an open research topic, attracting significant amount of research. A general answer to the fundamental question “*Under what circumstances is it preferable to use a blind equalizer to a trained–equalizer ?*” is yet to be provided. Despite the scarcity of reviews on the topic, in the context of the Global System of Mobile Communications known as GSM an impressive effort was made by Boss, Kammeyer and Petermann [88], who also proposed two novel blind algorithms. We recommend furthermore the fractionally–spaced equalization review of Endres *et al.* [89] and the Constant Modulus overview of Johnson *et al.* [90] based on a specific type of equalizers, namely on the so-called “fractionally-spaced” equalizers. A review of subspace–ML multichannel blind equalizers was provided by Tong and Perreau [91]. Further important references are the monograph by Haykin [55], the relevant section by Proakis [92] and the blind deconvolution book due to Nandi [93]. Comparative performance studies between various blind equalizers have also been performed. We recommend the second–order statistics-based comparative performance studies of Becchetti *et al.* [94], Kristensson *et al.* [95] and Altuna *et al.* [96], which is based on the mobile environment as well as the second–order statistics and PSP-based comparative study of Skowratanont and Chambers [97]. Furthermore, we recommend the fractionally–spaced Bussgang algorithm based comparative performance study by Shynk *et al.* [98], the CMA comparative performance study of Schirtzinger *et al.* [99] and the comparative convergence study by Endres *et al.* [100].

1.2.3.4 Filtering

In a book published around this time [101], Feher also suggested the use of non-linear filtering (NLF) for QAM satellite communications. Since the I and Q components of the time domain QAM signal change their amplitude abruptly at the signalling intervals their transmission would require an infinite bandwidth. These abrupt changes are typically smoothed by a bandlimiting filter. The design an implementation of such filters is critical, particularly when the NLA-QAM signal is filtered at high power level. In order to alleviate these problems Feher developed the NLF technique along with Huang in 1979 which simplified filter design by simply fitting a quarter raised cosine segment between two initially abruptly changing symbols for both of the quadrature carriers. We have already hinted that filtering is required to prevent abrupt changes in the transmitted signal. This issue is considered in more rigour in Chapter 4. This allowed the generation of jitter-free bandlimited signals, which had previously been a problem, improving clock recovery techniques. Feher's work continued to increase the number of levels used, with a paper on 256-QAM in May 1985 [102] noting the problems that linear group delay distortion caused, and a paper in April 1986 on 512-QAM [103] which came to similar conclusions.

1.2.4 Advanced Prototypes

Work was still continuing in France, Japan and also in New Zealand. CNET were continuing their attempt to overcome the problems they had found in their initial trials reported in 1979. A paper published in 1985 by M. Borgne [104] compared the performance of 16, 32, 64 and 128 level QAM schemes using computer simulation with particular interest in the impairments likely to occur over point-to-point radio links. Borgne concluded that non-linearity cancellers and adaptive equalisers would be necessary for this application. Soon after this, the first major paper on adaptive equalisers for QAM was published by Shafi and Moore [105]. Much of this paper was concerned with clock and carrier recovery without going into detail as to how these operations were performed. Details were provided of a fractional decision feedback equaliser (DFE) which they considered suitable for point-to-point radio links. They concluded that carrier recovery and clock timing was critical and likely to cause major problems, which were somewhat ameliorated by their fractionally spaced system.

Although lagging somewhat behind Feher, the Japanese made up for this delay by publishing a very detailed paper describing the development of a 256-level QAM modem in August 1986. In this paper from Saito and Nakamura [106], the authors developed on the work announced in 1979 by Saito *et al.* [14] which was discussed earlier. In this new paper they detailed automatic gain control (which he termed automatic threshold control) and carrier recovery methods. The carrier recovery was a slight enhancement to the system announced in 1979 and the AGC system was based on decision directed methods. Details were given as to how false lock problems were avoided (see Chapter 6) and the back-to-back prototype experiments gave results which the authors considered showed the feasibility of the 256-QAM modem. Evidence of the ever increasing interest in QAM was that in the IEEE special issue on advances in digital communications by radio there was a substantial section devoted to high-level modulation techniques. In a paper by Rustako *et al.* [107] which considered point-to-point applications, the standard times-two carrier recovery method for binary modulation was expanded for QAM. The authors claimed the advantage of not requiring accurate data decisions or interacting with any equaliser. They acknowledged that their system had the disadvantage of slow reacquisition after fades and suggested that it would only be superior in certain situations. This form of carrier recovery is considered in some detail in Chapter 6.

Clearly, until the late 1980s developments were mainly targeted at telephone line and point-to-point radio applications, which led to the definition of the CCITT telephone circuit modem standards V.29 to V.33 based on various QAM constellations ranging from uncoded 16-QAM to trellis coded (TC) 128-QAM. The basic concept of coded modulation is introduced in Chapter 8 along with the members of CCITT standard V-series modem scheme family, including the V.29 - V.33 modems designed for telephone lines.

1.2.5 QAM for Wireless Communications

Another major development occurred in 1987 when Sundberg, Wong and Steele published a pair of papers [108, 109] considering QAM for voice transmission over Rayleigh fading channels, the first major paper considering QAM for mobile radio applications. In these papers, it was recognized that when a Gray code mapping scheme was used, some of the bits constituting a symbol had different error rates from other bits. Gray coding is a method of assigning bits to be transmitted to constellation points in an optimum manner and is discussed in Chapter 5. For the 16-level constellation two classes of bits occurred, for the 64-level three classes and so on. Efficient mapping schemes for pulse code modulated (PCM) speech coding were discussed where the most significant bits (MSBs) were mapped onto the class with the highest integrity. A number of other schemes including variable threshold systems and weighted systems were also discussed. Simulation and theoretical results were compared and found to be in reasonable agreement. They used no carrier recovery, clock recovery or AGC, assuming these to be ideal, and came to the conclusion that channel coding and post-enhancement techniques would be required to achieve acceptable performance.

This work was continued, resulting in a publication in 1990 by Hanzo, Steele and Fortune [110], again considering QAM for mobile radio transmission, where again a theoretical argument was used to show that with a Gray encoded square constellation, the bits encoded onto a single symbol could be split into a number of subclasses, each subclass having a different average BER. The authors then showed that the difference in BER of these different subclasses could be reduced by constellation distortion at the cost of slightly increased total BER, but was best dealt with by using different error correction powers on the different 16-QAM subclasses. A 16 kbit/s sub-band speech coder was subjected to bit sensitivity analysis and the most sensitive bits identified were mapped onto the higher integrity 16-QAM subclasses, relegating the less sensitive speech bits to the lower integrity classes. Furthermore, different error correction coding powers were considered for each class of bits to optimise performance. Again ideal clock and carrier recovery were used, although this time the problem of automatic gain control (AGC) was addressed. It was suggested that as bandwidth became increasingly congested in mobile radio, microcells would be introduced supplying the required high SNRs with the lack of bandwidth being an incentive to use QAM.

In the meantime, CNET were still continuing their study of QAM for point-to-point applications, and Sari and Moridi published a paper [111] detailing an improved carrier recovery system using a novel combination of phase and frequency detectors which seemed promising. However, interest was now increasing in QAM for mobile radio usage and a paper was published in 1989 by J. Chuang of Bell Labs [112] considering NLF-QAM for mobile radio and concluding that NLF offered slight improvements over raised cosine filtering when there was mild intersymbol interference (ISI).

A technique, known as the transparent tone in band method (TTIB) was proposed by McGeehan and Bateman [113] from Bristol University, UK, which facilitated coherent detection of the square QAM scheme over fading channels and was shown to give good performance but at the cost of an increase in spectral occupancy. This important technique is discussed in depth in Chapter 10. At an IEE colloquium on multilevel modulation techniques in March 1990 a number of papers were presented considering QAM for mobile radio and point-to-point applications. Matthews [114] proposed the use of a pilot tone located in the centre of the frequency band for QAM transmissions over mobile channels.

Huish discussed the use of QAM over fixed links, which was becoming increasingly widespread [115]. Webb *et al.* presented two papers describing the problems of square QAM constellations when used for mobile radio transmissions and introduced the star QAM constellation with its inherent robustness in fading channels [116, 117].

During the 1990s a number of publications emerged, describing various techniques designed for enhancing the achievable performance of QAM transmissions schemes, when communicating over mobile radio channels. All of these techniques are described in detail in Part II of the book, namely in Chapters 9 - 13. In December 1991 a paper appeared in the *IEE Proceedings* [118] which considered the effects of channel coding, trellis coding and block coding when applied to the star QAM constellation. This was followed by another paper in the *IEE Proceedings* [119] considering equaliser techniques for QAM transmissions over dispersive mobile radio channels. A review paper appearing in July 1992 [120] considered areas where QAM could be put to most beneficial use within the mobile radio environment, and concluded that its advantages would be greatest in microcells. Further work on spectral efficiency, particularly of multilevel modulation schemes [121] concluded that variable level QAM modulation was substantially more efficient than all the other modulation schemes simulated. Variable level QAM was first discussed in a paper by Steele and Webb in 1991 [122].

Further QAM schemes for hostile fading channels characteristic of mobile telephony can be found in the following recent references [123–134, 134–157]. If Feher's previously mentioned NLA concept cannot be applied, then power-inefficient class A or AB linear amplification has to be used, which might become an impediment in lightweight, low-consumption handsets. However, the power consumption of the low-efficiency class A amplifier [132, 133] is less critical than that of the digital speech and channel codecs. In many applications 16-QAM, transmitting 4 bits per symbol reduces the signalling rate by a factor of 4 and hence mitigates channel dispersion, thereby removing the need for an equaliser, while the higher SNR demand can be compensated by diversity reception.

Significant contributions were made by Cavers, Stapleton *et al.* at Simon Fraser University, Burnaby, Canada in the field of pre- and post-distorter design. Out-of-band emissions due to class AB amplifier non-linearities and hence adjacent channel interferences can be reduced by some 15-20 dB using Stapleton's adaptive predistorter [134, 134, 135] and a class AB amplifier with 6 dB back-off, by adjusting the predistorter's adaptive coefficients using the complex convolution of the predistorter's input signal and the amplifier's output signal. Further aspects of linearised power amplifier design are considered in references [136] and [137].

A further important research trend is hallmarked by Cavers' work targeted at pilot symbol assisted modulation (PSAM) [138], where known pilot symbols are inserted in the information stream in order to allow the derivation of channel measurement information. The recovered received symbols are then used to linearly predict the channel's attenuation and phase. This arrangement will be considered in Chapter 10. A range of advanced QAM modems have also been proposed by Japanese researchers doing cutting-edge research in the field, including Sampei *et al.* [127, 128, 139, 140], Adachi [141] *et al.* and Sasaoka *et al.* [131].

Since QAM research has reached a mature stage, a number of mobile speech, audio and video transmission schemes have been proposed [156–168]. These system design examples demonstrated that substantial system performance benefits accrue, when the entire system is jointly optimised, rather than just a conglomerate of independent system components. A range of digital video broadcasting (DVB) schemes will be the topic of Chapter 30.

1.3 History of Near-Instantaneously Adaptive QAM

A comprehensive overview of adaptive transceivers was provided in [169] and this section is also based on [169]. As we noted in the previous chapters, mobile communications channels typically exhibit a near-instantaneously fluctuating time-variant channel quality [169–172] and hence conventional fixed-mode modems suffer from bursts of transmission errors, even if the system was designed for providing a high link margin. *An efficient approach to mitigating these detrimental effects is to adaptively adjust the modulation and/or the channel coding format as well as a range of other system parameters based on the near-instantaneous channel quality information perceived by the receiver, which is fed back to the transmitter with the aid of a feedback channel [173].* This plausible principle was recognised by Hayes [173] as early as 1968.

It was also shown in the previous sections that these near-instantaneously adaptive schemes require a reliable feedback link from the receiver to the transmitter. However, the channel quality variations have to be sufficiently slow for the transmitter to be able to adapt its modulation and/or channel coding format appropriately. The performance of these schemes can potentially be enhanced with the aid of *channel quality prediction techniques [174]*. As an efficient fading counter-measure, Hayes [173] proposed the employment of transmission power adaptation, while *Cavers [175] suggested invoking a variable symbol duration scheme* in response to the perceived channel quality at the expense of a variable bandwidth requirement. A disadvantage of the variable-power scheme is that it increases both the average transmitted power requirements and the level of co-channel interference imposed on other users, while requiring a high-linearity class-A or AB power amplifier, which exhibit a low power-efficiency. As a more attractive alternative, *the employment of AQAM was proposed by Steele and Webb*, which circumvented some of the above-mentioned disadvantages by employing various star-QAM constellations [122, 176].

With the advent of *Pilot Symbol Assisted Modulation (PSAM)* [138, 139, 177], Otsuki *et al.* [178] employed square-shaped AQAM constellations instead of star constellations [179], as a practical fading counter measure. With the aid of analysing the channel capacity of Rayleigh fading channels [180], *Goldsmith* et al. *[181] and Alouini* et al. *[182] showed that combined variable-power, variable-rate adaptive schemes are attractive* in terms of approaching the capacity of the channel and characterised the achievable throughput performance of variable-power AQAM [181]. However, they also found that *the extra throughput achieved by the additional variable-power assisted adaptation over the constant-power, variable-rate scheme is marginal* for most types of fading channels [181, 183].

In 1996 Torrance and Hanzo [184] proposed a set of *mode switching levels* s designed for achieving a high average BPS throughput, while maintaining the target average BER. Their method was based on defining a specific combined BPS/BER cost-function for transmission over narrowband Rayleigh channels, which incorporated both the BPS throughput as well as the target average BER of the system. *Powell's optimisation was invoked for finding a set of mode switching thresholds, which were constant,* regardless of the actual channel Signal to Noise Ratio (SNR) encountered, i.e. irrespective of the prevalent instantaneous channel conditions. However, in 2001 Choi and Hanzo [185] noted that a *higher BPS throughput can be achieved, if under high channel SNR conditions the activation of high-throughput AQAM modes is further encouraged by lowering the AQAM mode switching thresholds. More explicitly, a set of SNR-dependent AQAM mode switching levels was proposed [185]*, which keeps the average BER constant, while maximising the achievable throughput. We note furthermore that the set of switching levels derived in [184, 186] is based on Powell's multidimensional optimisation technique [187] and hence the optimisation process may become trapped in a local minimum. This problem was overcome by Choi and Hanzo upon deriving an *optimum set of switching levels [185], when employing the Lagrangian multiplier technique*. It was shown that this set of switching levels results in the global optimum in a sense that the corresponding AQAM scheme obtains the maximum possible average BPS throughput, while maintaining the target average BER. An important further development was Tang's contribution [188] in the area of contriving an *intelligent learning scheme for the appropriate adjustment of the AQAM switching thresholds.*

These contributions demonstrated that *AQAM exhibited promising advantages*, when compared to fixed modulation schemes in terms of spectral efficiency, BER performance and robustness against channel delay spread, etc. Various systems employing AQAM were also characterised in [179]. The *numerical upper bound performance of narrow-band BbB-AQAM* over slow Rayleigh flat-fading channels was evaluated by Torrance and Hanzo [189], while over *wide-band channels* by Wong and Hanzo [190, 191]. Following these developments, adaptive modulation was also studied *in conjunction with channel coding and power control techniques by Matsuoka et al. [192] as well as Goldsmith and Chua [193, 194].*

In the early phase of research more emphasis was dedicated to the system aspects of adaptive modulation in a narrow-band environment. A reliable method of transmitting the modulation control parameters was proposed by Otsuki *et al.* [178], where the parameters were embedded in the transmission frame's mid-amble using Walsh codes. Subsequently, at the receiver the Walsh sequences were decoded using maximum likelihood detection. Another technique of *signalling the required modulation mode used was proposed by Torrance and Hanzo [195], where the modulation control symbols were represented by unequal error protection 5-PSK symbols.* Symbol-by-Symbol (SbS) adaptive*, rather than BbB-adaptive systems were proposed by Lau and Maric in [196], where the transmitter is capable of transmitting each symbol in a different modem mode, depending on the channel conditions. Naturally, the receiver has to synchronise with the transmitter in terms of the SbS-adapted mode sequence, in order to correctly demodulate the received symbols and hence the employment of BbB-adaptivity is less challenging, while attaining a similar performance to that of BbB-adaptive arrangements under typical channel conditions.*

The adaptive modulation philosophy was then extended to wideband multi-path environments *amongst others for example by Kamio et al. [197] by utilizing a bi-directional Decision Feedback Equaliser (DFE)* in a micro- and macro-cellular environment. This equalization technique employed both forward and backward oriented channel estimation based on the pre-amble and post-amble symbols in the transmitted frame. Equalizer tap gain interpolation across the transmitted frame was also utilized for reducing the complexity in conjunction with space diversity [197]. The authors concluded that the cell radius could be enlarged in a macro-cellular system and a higher area-spectral efficiency could be attained for micro-cellular environments by utilizing adaptive modulation. The data transmission latency effect, which occurred when the input data rate was higher than the instantaneous transmission throughput was studied and solutions were formulated using *frequency hopping [198] and statistical multiplexing, where the number of Time Division Multiple Access (TDMA) timeslots allocated to a user was adaptively controlled [199].*

In reference [200] *symbol rate adaptive modulation* was applied, where the symbol rate or the number of modulation levels was adapted by using $\frac{1}{8}$-rate 16QAM, $\frac{1}{4}$-rate 16QAM, $\frac{1}{2}$-rate 16QAM as well as full-rate 16QAM and the criterion used for adapting the modem modes was based on the instantaneous received signal to noise ratio and channel delay spread. The slowly varying channel quality of the uplink (UL) and downlink (DL) was rendered similar by utilizing short frame duration Time Division Duplex (TDD) and the maximum normalised delay spread simulated was 0.1. A *variable channel coding rate* was then introduced by Matsuoka *et al.* in conjunction with adaptive modulation in reference [192], where the transmitted burst incorporated an outer Reed Solomon code and an inner convolutional code in order to achieve high-quality data transmission. The coding rate was varied according to the prevalent channel quality using the same method, as in adaptive modulation in order to achieve a certain target BER performance. A so-called *channel margin* was introduced in this contribution, which effectively increased the switching thresholds for the sake of preempting *the effects of channel quality estimation errors*, although this inevitably reduced the achievable BPS throughput.

In an effort to improve the achievable performance versus complexity trade-off in the context of AQAM, Yee and Hanzo [201] studied the design of various *Radial Basis Function (RBF) assisted neural network based schemes, while communicating over dispersive channels.* The advantage of these RBF-aided DFEs is that they are capable of delivering error-free decisions even in scenarios, when the received phasors cannot be error-freely detected by the conventional DFE, since they cannot be separated into decision classes with the aid of a linear decision boundary. In these so-called linearly non-separable decision scenarios the RBF-assisted DFE still may remain capable of classifying the received phasors into decision classes without decision errors. A further improved turbo BCH-coded version of this RBF-aided system was characterised by Yee *et al.* in [202], while a turbo-equalised RBF arrangement was the subject of the investigation conducted by Yee, Liew and Hanzo in [203, 204]. The RBF-aided AQAM research has also been extended to the turbo equalisation of a convolutional as well as space-time trellis coded arrangement proposed by Yee, Yeap and Hanzo [169,205,206]. The same authors then endeavoured to reduce the associated implementation complexity of an RBF-aided QAM modem with the advent of employing a separate in-phase / quadrature-phase turbo equalisation scheme in the quadrature arms of the modem.

As already mentioned above, the performance of *channel coding in conjunction with adaptive modulation in a narrow-band environment* was also characterised by Chua and Goldsmith [193]. In their contribution trellis and lattice codes were used without channel interleaving, invoking a feedback path between the transmitter and receiver for modem mode control purposes. Specifically, the simulation and theoretical results by Goldsmith and Chua showed that a 3dB coding gain was achievable at a BER of 10^{-6} for a 4-sate trellis code and 4dB by an 8-state trellis code in the context of the adaptive scheme over Rayleigh-fading channels, while a 128-state code performed within 5dB of the Shannonian capacity limit.

The *effects of the delay in the AQAM mode signalling feedback path* on the adaptive modem's performance were studied and this scheme exhibited a higher spectral efficiency, when compared to the non-adaptive trellis coded performance. Goeckel [207] also contributed in the area of adaptive coding and employed realistic outdated, rather than perfect fading estimates. Further research on adaptive multidimensional coded modulation was also conducted by Hole *et al.* [208] for transmissions over flat fading channels. *Pearce, Burr and Tozer [209] as well as Lau and Mcleod [210] have also analysed the performance trade-offs associated with employing channel coding and adaptive modulation or adaptive trellis coding*, respectively, as efficient fading counter measures. In an effort to provide a fair comparison of the various coded modulation schemes known at the time of writing, Ng, Wong and Hanzo have also studied Trellis Coded Modulation (TCM), Turbo TCM (TTCM), Bit-Interleaved Coded Modulation (BICM) and Iterative-Decoding assisted BICM (BICM-ID), where TTCM was found to be the best scheme at a given decoding complexity [211].

Subsequent contributions by Suzuki *et al.* [212] incorporated *space-diversity and power-adaptation* in conjunction with adaptive modulation, for example in order to combat the effects of the multi-path channel environment at a 10Mbits/s transmission rate. *The maximum tolerable delay-spread was deemed to be one symbol duration for a target mean BER performance of* 0.1%. This was achieved in a TDMA scenario, where the channel estimates were predicted based on the extrapolation of previous channel quality estimates. As mentioned above, variable transmitted power was applied in combination with adaptive modulation in reference [194], where the transmission rate and power adaptation was optimised for the sake of achieving an increased spectral efficiency. In their treatise a slowly varying channel was assumed and the instantaneous received power required for achieving a certain upper bound performance was assumed to be known prior to transmission. *Power control in conjunction with a pre-distortion type non-linear power amplifier compensator* was studied in the context of adaptive modulation in reference [213]. This method was used to mitigate the non-linearity effects associated with the power amplifier, when QAM modulators were used.

Results were also recorded concerning the performance of adaptive modulation in conjunction with *different multiple access schemes in a narrow-band channel environment*. In a TDMA system, *dynamic channel assignment* was employed by Ikeda *et al.*, where in addition to assigning a different modulation mode to a different channel quality, priority was always given to those users in their request for reserving time-slots, which benefitted from the best channel quality [214]. The performance was compared to fixed channel assignment systems, where substantial gains were achieved in terms of system capacity. Furthermore, a *lower call termination probability was recorded*. However, the probability of intra-cell hand-off increased as a result of the associated dynamic channel assignment (DCA) scheme, which constantly searched for a high-quality, high-throughput time-slot for supporting the actively communicating users. The application of adaptive modulation in packet transmission was introduced by Ue, Sampei and Morinaga [215], where the results showed an improved BPS throughput. The performance of adaptive modulation was also characterised in conjunction with an *automatic repeat request* (ARQ) system in reference [216], where the transmitted bits were encoded using a cyclic redundant code (CRC) and a convolutional punctured code in order to increase the data throughput.

A further treatise was published by Sampei, Morinaga and Hamaguchi [217] on *laboratory test results* concerning the utilization of adaptive modulation in a TDD scenario, where the modem mode switching criterion was based on the signal to noise ratio and on the normalised delay-spread. *In these experimental results, the channel quality estimation errors degraded the performance* and consequently - as laready alluded to earlier - a channel estimation error margin was introduced for mitigating this degradation. Explicitly, the channel estimation error margin was defined as the measure of how much extra protection margin must be added to the switching threshold levels for the sake of minimising the effects of the channel estimation errors. The delay-spread also degraded the achievable performance due to the associated irreducible BER, which was not compensated by the receiver. However, the performance of the adaptive scheme in a delay-spread impaired channel environment was better, than that of a fixed modulation scheme. *These experiments also concluded that the AQAM scheme can be operated for a Doppler frequency of* $f_d = 10$*Hz at a normalised delay spread of* 0.1 *or for* $f_d = 14$*Hz at a normalised delay spread of* 0.02*, which produced a mean BER of* 0.1*% at a transmission rate of* 1 *Mbits/s.*

Lastly, the *data buffering-induced latency and co-channel interference aspects* of AQAM modems were investigated in [218, 219]. Specifically, the latency associated with storing the information to be transmitted during severely degraded channel conditions was mitigated by frequency hopping or statistical multiplexing. As expected, the latency is increased, when either the mobile speed or the channel SNR are reduced, since both of these result in prolonged low instantaneous SNR intervals. It was demonstrated that as a result of the proposed measures, typically more than 4dB SNR reduction was achieved by the proposed adaptive modems in comparison to the conventional fixed-mode benchmark modems employed. However, the achievable gains depend strongly on the prevalant co-channel interference levels and hence interference cancellation was invoked in [219] on the basis of adjusting the demodulation decision boundaries after estimating the interfering channel's magnitude and phase.

The associated AQAM principles may also be invoked in the context of *multicarrier Orthogonal Frequency Division Multiplex (OFDM) modems [179]*. This principle was first proposed by Kalet [154] for employment in OFDM systems and was then further developed for example by Czylwik *et al.* [220] as well as by Chow, Cioffi and Bingham [221]. The associated concepts were detailed for example in [179] and they will also be augmented in Part III of this monograph. Let us now briefly review the recent history of OFDM-based QAM systems in the next section.

1.4 History of OFDM-based QAM

1.4.1 History of OFDM

The first QAM-related so-called orthogonal frequency division multiplexing (OFDM) scheme was proposed by Chang in 1966 [142] for dispersive fading channels, which has also undergone a dramatic evolution due to the efforts of Weinstein, Peled, Ruiz, Hirosaki, Kolb, Cimini, Schüssler, Preuss, Rückriem, Kalet *et al.* [142–155]. OFDM was standardised as the European digital audio broadcast (DAB) as well as digital video broadcast (DVB) scheme. It constituted also a credible proposal for the recent third-generation mobile radio standard competition in Europe. It was recently selected as the high performance local area network (HIPERLAN) transmission technique.

The system's operational principle is that the original bandwidth is divided in a high number of narrow sub-bands, in which the mobile channel can be considered non-dispersive. Hence no channel equaliser is required and instead of implementing a bank of sub-channel modems they can be conveniently implemented by the help of a single fast fourier Transformer (FFT). This scheme will be the topic of Chapters 15 - 20.

These OFDM systems - often also termed as frequency division multiplexing (FDM) or multi-tone systems - have been employed in military applications since the 1960s, for example by Bello [222], Zimmerman [143], Powers and Zimmerman [223], Chang and Gibby [224] and others. Saltzberg [225] studied a multi-carrier system employing orthogonal time–staggered quadrature amplitude modulation (O-QAM) of the carriers.

The employment of the discrete Fourier transform (DFT) to replace the banks of sinusoidal generators and the demodulators was suggested by Weinstein and Ebert [144] in 1971, which significantly reduces the implementation complexity of OFDM modems. In 1980, Hirosaki [155] suggested an equalisation algorithm in order to suppress both intersymbol and intersubcarrier interference caused by the channel impulse response or timing and frequency errors. Simplified OFDM modem implementations were studied by Peled [148] in 1980, while Hirosaki [149] introduced the DFT based implementation of Saltzberg's O-QAM OFDM system. From Erlangen University, Kolb [150], Schüßler [151], Preuss [152] and Rückriem [153] conducted further research into the application of OFDM. Cimini [145] and Kalet [154] published analytical and early seminal experimental results on the performance of OFDM modems in mobile communications channels.

More recent advances in OFDM transmission were presented in the impressive state-of-the-art collection of works edited by Fazel and Fettweis [226], including the research by Fettweis *et al.* at Dresden University, Rohling *et al.* at Braunschweig University, Vandendorp at Loeven University, Huber *et al.* at Erlangen University, Lindner *et al.* at Ulm University, Kammeyer *et al.* at Brehmen University and Meyr *et al.* [227, 228] at Aachen University, but the individual contributions are too numerous to mention.

While OFDM transmission over mobile communications channels can alleviate the problem of multipath propagation, recent research efforts have focused on solving a set of inherent difficulties regarding OFDM, namely the peak–to–mean power ratio, time and frequency synchronisation, and on mitigating the effects of the frequency selective fading channel. These issues are addressed below in slightly more depth, while a treatment is given in Chapters 15 - 20.

1.4.2 Peak-to-Mean Power Ratio

The peak-to-mean power ratio problem of OFDM systems has been detailed along with a range of mitigating techniques in [172]. It is plausible that the OFDM signal - which is the superposition of a high number of modulated sub-channel signals - may exhibit a high instantaneous signal peak with respect to the average signal level. Furthermore, large signal amplitude swings are encountered, when the time domain signal traverses from a low instantaneous power waveform to a high power waveform, which may results in a high out-of-band (OOB) harmonic distortion power, unless the transmitter's power amplifier exhibits an extremely high linearity across the entire signal level range (Section 4.5.1). This then potentially contaminates the adjacent channels with adjacent channel interference. Practical amplifiers exhibit a finite amplitude range, in which they can be considered almost linear. In order to prevent severe clipping of the high OFDM signal peaks - which is the main source of OOB emissions - the power amplifier must not be driven into saturation and hence they are typically operated with a certain so-called back-off, creating a certain "head room" for the signal peaks, which reduces the risk of amplifier saturation and OOB emmission. Two different families of solutions have been suggested in the literature, in order to mitigate these problems, either reducing the peak-to-mean power ratio, or improving the amplification stage of the transmitter.

More explicitly, Shepherd [229], Jones [230], and Wulich [231] suggested different coding techniques which aim to minimise the peak power of the OFDM signal by employing different data encoding schemes before modulation, with the philosophy of choosing block codes whose legitimate code words exhibit low so-called Crest factors or peak-to-mean power envelope fluctuation. Müller [232], Pauli [233], May [234] and Wulich [235] suggested different algorithms for post-processing the time domain OFDM signal prior to amplification, while Schmidt and Kammeyer [236] employed adaptive subcarrier allocation in order to reduce the crest factor. Dinis and Gusmão [237–239] researched the use of two-branch amplifiers, while the clustered OFDM technique introduced by Daneshrad, Cimini and Carloni [240] operates with a set of parallel partial FFT processors with associated transmitting chains. OFDM systems with increased robustness to non-linear distortion have been proposed by Okada, Nishijima and Komaki [241] as well as by Dinis and Gusmão [242].

1.4.3 Synchronisation

Time and frequency synchronisation between the transmitter and receiver are of crucial importance as regards to the performance of an OFDM link [243, 244]. A wide variety of techniques have been proposed for estimating and correcting both timing and carrier frequency offsets at the OFDM receiver. Rough timing and frequency acquisition algorithms relying on known pilot symbols or pilot tones embedded into the OFDM symbols have been suggested by Claßen [227], Warner [245], Sari [246], Moose [247], as well as Brüninghaus and Rohling [248]. Fine frequency and timing tracking algorithms exploiting the OFDM signal's cyclic extension were published by Moose [247], Daffara [249] and Sandell [250].

1.4.4 OFDM/CDMA

Combining OFDM transmissions with code division multiple access (CDMA) [171] allows us to exploit the wideband channel's inherent frequency diversity by spreading each symbol across multiple subcarriers. This technique has been pioneered by Yee, Linnartz and Fettweis [251], by Chouly, Brajal and Jourdan [252], as well as by Fettweis, Bahai and Anvari [253]. Fazel and Papke [254] investigated convolutional coding in conjunction with OFDM/CDMA. Prasad and Hara [255] compared various methods of combining the two techniques, identifying three different structures, namely multi-carrier CDMA (MC-CDMA), multi-carrier direct sequence CDMA (MC-DS-CDMA) and multi-tone CDMA (MT-CDMA). Like non-spread OFDM transmission, OFDM/CDMA methods suffer from high peak-to-mean power ratios, which are dependent on the frequency domain spreading scheme, as investigated by Choi, Kuan and Hanzo [256].

1.4.5 Adaptive Antennas in OFDM Systems

The employment of adaptive antenna techniques in conjunction with OFDM transmissions was shown to be advantageous in suppressing co-channel interference in cellular communications systems. Li, Cimini and Sollenberger [257–259], Kim, Choi and Cho [260], Lin, Cimini and Chuang [261] as well as Münster *et al.* [262] have investigated algorithms for multi-user channel estimation and interference suppression. To elaborate a little further, multiple antenna assisted wireless communications systems are discussed in [172] in detail, when incorporated in OFDM systems for the sake of increasing the number of users supported. Furthermore, multiple antenna aided space-time coding arrangements constitute the topic of [170], where the main objective is the mitigation of the channel-induced fading, since space-time codecs are capable of achieving substantial transmit diversity gains. A range of space-time spreading aided CDMA schemes, which were designed with a similar objective to space-time codecs, were characterised in [171]. Finally, multiple antenna based beamformers are discussed in [263], where the basic design objective is to achieve angular selectivity and hence mitigate the effects of co-channel interference.

1.4.6 Decision-Directed Channel Estimation for OFDM

1.4.6.1 Decision-Directed Channel Estimation for Single-User OFDM

In recent years numerous research contributions have appeared on the topic of channel transfer function estimation techniques designed for employment in single-user, single transmit antenna-assisted OFDM scenarios, since the availability of an accurate channel transfer function estimate is one of the prerequisites for coherent symbol detection with an OFDM receiver. The techniques proposed in the literature can be classified as *pilot-assisted, decision-directed* (DD) and *blind* channel estimation (CE) methods.

In the context of pilot-assisted channel transfer function estimation a subset of the available subcarriers is dedicated to the transmission of specific pilot symbols known to the receiver, which are used for ”sampling” the desired channel transfer function. Based on these samples of the frequency domain transfer function, the well-known process of interpolation is used for generating a transfer function estimate for each subcarrier residing between the pilots. This is achieved at the cost of a reduction in the number of useful subcarriers available for data transmission. The family of *pilot-assisted* channel estimation techniques was investigated for example by Chang and Su [288], Höher [264, 272, 273], Itami *et al.* [277], Li [280], Tufvesson and Maseng [271], Wang and Liu [283], as well as Yang *et al.* [279, 284, 290].

By contrast, in the context of Decision-Directed Channel Estimation (DDCE) all the sliced and remodulated subcarrier data symbols are considered as pilots. In the absence of symbol errors and also depending on the rate of channel fluctuation, it was found that accurate channel transfer function estimates can be obtained, which often are of better quality, in terms of the channel transfer function estimator’s mean-square error (MSE), than the estimates offered by pilot-assisted schemes. This is because the latter arrangements usually invoke relatively sparse pilot patterns.

The family of *decision-directed* channel estimation techniques was investigated for example by van de Beek *et al.* [267], Edfors *et al.* [268, 275], Li *et al.* [274], Li [286], Mignone and Morello [270], Al-Susa and Ormondroyd [278], Frenger and Svensson [269], as well as Wilson *et al.* [266]. Furthermore, the family of *blind* channnel estimation techniques was studied by Lu and Wang [285], Necker and Stüber [289], as well as by Zhou and Giannakis [282]. The various contributions have been summarized in Tables 1.1 and 1.2.

In order to render the various DDCE techniques more amenable to use in scenarios as-

Year	Author	Contribution
’91	Höher [264]	Cascaded 1D-FIR channel transfer factor interpolation was carried out in the frequency- and time-direction for frequency-domain PSAM.
’93	Chow, Cioffi and Bingham [265]	Subcarrier-by-subcarrier-based LMS-related channel transfer factor equalisation techniques were employed.
’94	Wilson, Khayata and Cioffi [266]	Linear channel transfer factor filtering was invoked in the time-direction for DDCE.
’95	van de Beek, Edfors, Sandell, Wilson and Börjesson [267]	DFT-aided CIR-related domain Wiener filter-based noise reduction was advocated for DDCE. The effects of leakage in the context of non-sample-spaced CIRs were analysed.
’96	Edfors, Sandell, van de Beek, Wilson and Börjesson [268]	SVD-aided CIR-related domain Wiener filter-based noise reduction was introduced for DDCE.
	Frenger and Svensson [269]	MMSE-based frequency-domain channel transfer factor prediction was proposed for DDCE.
	Mignone and Morello [270]	FEC was invoked for improving the DDCE’s remodulated reference.
’97	Tufvesson and Maseng [271]	An analysis of various pilot patterns employed in frequency-domain PSAM was provided in terms of the system’s BER for different Doppler frequencies. Kalman filter-aided channel transfer factor estimation was used.
	Höher, Kaiser and Robertson [272, 273]	Cascaded 1D-FIR Wiener filter channel interpolation was utilised in the context of 2D-pilot pattern-aided PSAM
’98	Li, Cimini and Sollenberger [274]	An SVD-aided CIR-related domain Wiener filter-based noise reduction was achieved by employing CIR-related tap estimation filtering in the time-direction.
	Edfors, Sandell, van de Beek, Wilson and Börjesson [275]	A detailed analysis of SVD-aided CIR-related domain Wiener filter-based noise reduction was provided for DDCE, which expanded the results of [268].
	Tufvesson, Faulkner and Maseng [276]	Wiener filter-aided frequency domain channel transfer factor prediction-assisted pre-equalisation was studied.
	Itami, Kuwabara, Yamashita, Ohta and Itoh [277]	Parametric finite-tap CIR model-based channel estimation was employed for frequency domain PSAM.

Table 1.1: Contributions to channel transfer factor estimation for single-transmit antenna-assisted OFDM; ©John Wiley and IEEE Press, 2003 [172].

Year	Author	Contribution
’99	Al-Susa and Ormondroyd [278]	DFT-aided Burg algorithm-assisted adaptive CIR-related tap prediction filtering was employed for DDCE.
	Yang, Letaief, Cheng and Cao [279]	Parametric, ESPRIT-assisted channel estimation was employed for frequency domain PSAM.
’00	Li [280]	Robust 2D frequency domain Wiener filtering was suggested for employment in frequency domain PSAM using 2D pilot patterns.
’01	Yang, Letaief, Cheng and Cao [281]	Detailed discussions of parametric, ESPRIT-assisted channel estimation were provided in the context of frequency domain PSAM [279].
	Zhou and Giannakis [282]	Finite alphabet-based channel transfer factor estimation was proposed.
	Wang and Liu [283]	Polynomial frequency domain channel transfer factor interpolation was contrived.
	Yang, Cao and Letaief [284]	DFT-aided CIR-related domain one-tap Wiener filter-based noise reduction was investigated, which is supported by variable frequency domain Hanning windowing.
	Lu and Wang [285]	A Bayesian blind turbo receiver was contrived for coded OFDM systems.
	Li and Sollenberger [286]	Various transforms were suggested for CIR-related tap estimation filtering-assisted DDCE.
	Morelli and Mengali [287]	LS- and MMSE-based channel transfer factor estimators were compared in the context of frequency domain PSAM.
’02	Chang and Su [288]	Parametric quadrature surface-based frequency domain channel transfer factor interpolation was studied for PSAM.
	Necker and Stüber [289]	Totally blind channel transfer factor estimation based on the finite alphabet property of PSK signals was investigated.

Table 1.2: Contributions to channel transfer factor estimation for single-transmit antenna-assisted OFDM; ©John Wiley and IEEE Press, 2003 [172].

sociated with a relatively high rate of channel variation expressed in terms of the OFDM symbol normalized Doppler frequency, linear prediction techniques well known from the speech coding literature [168, 291] can be invoked. To elaborate a little further, we will substitute the CIR-related tap estimation filter - which is part of the two-dimensional channel transfer function estimator proposed in [274] - by a CIR-related tap prediction filter. The employment of this CIR-related tap prediction filter enables a more accurate estimation of the channel transfer function encountered during the forthcoming transmission time slot and thus potentially enhances the performance of the channel estimator. We will be following the general concepts described by Duel-Hallen *et al.* [292] and the ideas presented by Frenger and Svensson [269], where frequency domain prediction filter-assisted DDCE was proposed. Furthermore, we should mention the contributions of Tufvesson *et al.* [276, 293], where a prediction filter-assisted frequency domain pre-equalisation scheme was discussed in the context of OFDM. In a further contribution by Al-Susa and Ormondroyd [278], adaptive prediction filter-assisted DDCE designed for OFDM has been proposed upon invoking techniques known from speech coding, such as the Levinson-Durbin algorithm or the Burg algorithm [291, 294, 295] in order to determine the predictor coefficients.

1.4.6.2 Decision-Directed Channel Estimation for Multi-User OFDM

In contrast to the above-mentioned single-user OFDM scenarios, in a multi-user OFDM scenario the signal received by each antenna is constituted by the superposition of the signal contributions associated with the different users or transmit antennas. Note that in terms of the multiple-input multiple-output (MIMO) structure of the channel the multi-user single-transmit antenna scenario is equivalent, for example, to a single-user space-time coded (STC) scenario using multiple transmit antennas. For the latter a Least-Squares (LS) error channel estimator was proposed by Li *et al.* [296], which aims at recovering the different transmit antennas' channel transfer functions on the basis of the output signal of a specific reception antenna element and by also capitalising on the remodulated received symbols associated with the different users. The performance of this estimator was found to be limited in terms of the mean-square estimation error in scenarios, where the product of the number of transmit antennas and the number of CIR taps to be estimated per transmit antenna approaches the total number of subcarriers hosted by an OFDM symbol. As a design alternative, in [297] a DDCE was proposed by Jeon *et al.* for a space-time coded OFDM scenario of two transmit antennas and two receive antennas.

Specifically, the channel transfer function[1] associated with each transmit-receive antenna pair was estimated on the basis of the output signal of the specific receive antenna upon *subtracting* the interfering signal contributions associated with the remaining transmit antennas. These interference contributions were estimated by capitalising on the knowledge of the channel transfer functions of all interfering transmit antennas predicted during the $(n-1)$-th OFDM symbol period for the n-th OFDM symbol, also invoking the corresponding remodulated symbols associated with the n-th OFDM symbol. To elaborate further, the difference between the subtraction-based channel transfer function estimator of [297] and the LS estimator proposed by Li *et al.* in [296] is that in the former the channel transfer functions predicted during the previous, i.e. the $(n-1)$-th OFDM symbol period for the current, i.e.

[1]In the context of the OFDM system the set of K different subcarriers' channel transfer factors is referred to as the channel transfer function, or simply as the channel.

Year	Author	Contribution
'99	Li, Seshadri and Ariyavisitakul [296]	The LS-assisted DDCE proposed exploits the cross-correlation properties of the transmitted subcarrier symbol sequences.
'00	Jeon, Paik and Cho [297]	Frequency-domain PIC-assisted DDCE is studied, which exploits the channel's slow variation versus time.
	Li [298]	Time-domain PIC-assisted DDCE is investigated as a simplification of the LS-assisted DDCE of [296]. Optimum training sequences are proposed for the LS-assisted DDCE of [296].
'01	Mody and Stüber [299]	Channel transfer factor estimation designed for frequency-domain PSAM based on CIR-related domain filtering is studied.
	Gong and Letaief [300]	MMSE-assisted DDCE is advocated which represents an extension of the LS-assisted DDCE of [300]. The MMSE-assisted DDCE is shown to be practical in the context of transmitting consecutive training blocks. Additionally, a low-rank approximation of the MMSE-assisted DDCE is considered.
	Jeon, Paik and Cho [301]	2D MMSE-based channel estimation is proposed for frequency-domain PSAM.
	Vook and Thomas [302]	2D MMSE based channel estimation is invoked for frequency domain PSAM. A complexity reduction is achieved by CIR-related domain-based processing.
	Xie and Georghiades [303]	Expectation maximization (EM) based channel transfer factor estimation approach for DDCE.
'02	Li [304]	A more detailed discussion on time-domain PIC-assisted DDCE is provided and optimum training sequences are proposed [298].
	Bölcskei, Heath and Paulraj [305]	Blind channel identification and equalisation using second-order cyclostationary statistics as well as antenna precoding were studied.
	Minn, Kim and Bhargava [306]	A reduced complexity version of the LS-assisted DDCE of [296] is introduced, based on exploiting the channel's correlation in the frequency-direction, as opposed to invoking the simplified scheme of [304], which exploits the channel's correlation in the time-direction. A similar approach was suggested by Slimane [307] for the specific case of two transmit antennas.
	Komninakis, Fragouli, Sayed and Wesel [308]	Fading channel tracking and equalisation were proposed for employment in MIMO systems assisted by Kalman estimation and channel prediction.

Table 1.3: Contributions on channel transfer factor estimation for multiple-transmit antenna assisted OFDM; ©John Wiley and IEEE Press, 2003 [172].

the n-th OFDM symbol are employed for both symbol detection *as well as* for obtaining an updated channel estimate for employment during the $(n+1)$-th OFDM symbol period. In the approach advocated in [297] the subtraction of the different transmit antennas' interfering signals is performed in the frequency domain.

By contrast, in [298] a similar technique was proposed by Li with the aim of simplifying the DDCE approach of [296], which operates in the time domain. A prerequisite for the operation of this parallel interference cancellation (PIC)-assisted DDCE is the availability of a reliable estimate of the various channel transfer functions for the current OFDM symbol, which are employed in the cancellation process in order to obtain updated channel transfer function estimates for the demodulation of the next OFDM symbol. In order to compensate for the channel's variation as a function of the OFDM symbol index, linear prediction techniques can be employed, as it was also proposed for example in [298]. However, due to the estimator's recursive structure, determining the optimum predictor coefficients is not as straightforward as for the transversal FIR filter-assisted predictor.

An overview of further publications on channel transfer factor estimation for OFDM systems supported by multiple antennas is provided in Table 1.3, although these topics are beyond the scope of this book. Various multiple antenna aided wireless communications systems are discussed in [172] in detail, when incorporated in OFDM systems. Furthermore, multiple antenna aided space-time coding arrangements constitute the topic of [170], while space-time spreading is addressed in [171]. Finally, multiple antenna based beamformers are discussed in [263].

1.4.7 Uplink Detection Techniques for Multi-User SDMA-OFDM

The related family of Space-Division-Multiple-Access (SDMA) communication systems has recently drawn wide reseach interests. In these systems the L different users' transmitted signals are separated at the base-station (BS) with the aid of their unique, user-specific spatial signature, which is constituted by the P-element vector of channel transfer factors between the users' single transmit antenna and the P different receiver antenna elements at the BS, upon assuming flat-fading channel conditions such as those often experienced in the context of each of the OFDM subcarriers.

A whole host of multi-user detection (MUD) techniques known from Code-Division-Multiple-Access (CDMA) communications lend themselves also to an application in the context of SDMA-OFDM on a per-subcarrier basis. Some of these techniques are the Least-Squares (LS) [318, 324, 332, 334], Minimum Mean-Square Error (MMSE) [310–313, 315, 318, 322, 326, 334–336], Successive Interference Cancellation (SIC) [309, 314, 318, 322, 324, 329, 331, 333, 334, 336], Parallel Interference Cancellation (PIC) [330, 334] and Maximum Likelihood (ML) detection [317, 319–323, 325, 328, 334, 336]. A comprehensive overview of recent publications on MUD techniques for MIMO systems is given in Tables 1.4 and 1.5.

1.4.8 OFDM Applications

Due to their implementational complexity, OFDM applications have been scarce until quite recently. Recently, however, OFDM has been adopted as the new European digital audio broadcasting (DAB) standard [146, 147, 337–339] as well as for the terrestrial digital video broadcasting (DVB) system [246, 340]. During this process the design of OFDM systems

Year	Author	Contribution
’96	Foschini [309]	The concept of the BLAST architecture was introduced.
’98	Vook and Baum [310]	SMI-assisted MMSE combining was invoked on an OFDM subcarrier basis.
	Wang and Poor [311]	Robust sub-space-based weight vector calculation and tracking were employed for co-channel interference suppression, as an improvement of the SMI-algorithm.
	Wong, Cheng, Letaief and Murch [312]	Optimization of an OFDM system was reported in the context of multiple transmit and receive antennas upon invoking the maximum SINR criterion. The computational was reduced by exploiting the channel’s correlation in the frequency direction.
	Li and Sollenberger [313]	Tracking of the channel correlation matrix’ entries was suggested in the context of SMI-assisted MMSE combining for multiple receiver antenna assisted OFDM, by capitalizing on the principles of [274].
’99	Golden, Foschini, Valenzuela and Wolniansky [314]	The SIC detection-assisted V-BLAST algorithm was introduced.
	Li and Sollenberger [315]	The system introduced in [313] was further detailed.
	Vandenameele, Van der Perre, Engels and de Man [316]	A comparative study of different SDMA detection techniques, namely that of MMSE, SIC and ML detection was provided. Further improvements of SIC detection were suggested by adaptively tracking multiple symbol decisions at each detection node.
	Speth and Senst [317]	Soft-bit generation techniques were proposed for MLSE in the context of a coded SDMA-OFDM system.
’00	Sweatman, Thompson, Mulgrew and Grant [318]	Comparisons of various detection algorithms including LS, MMSE, D-BLAST and V-BLAST (SIC detection) were carried out.
	van Nee, van Zelst and Awater [319–321]	The evaluation of ML detection in the context of a Space-Division Multiplexing (SDM) system was provided, considering various simplified ML detection techniques.
	Vandenameele, Van der Perre, Engels, Gyselinckx and de Man [322]	More detailed discussions were provided on the topics of [316].

Table 1.4: Contributions on multi-user detection techniques designed for multiple transmit antenna assisted OFDM systems; ©John Wiley and IEEE Press, 2003 [172].

Year	Author	Contribution
'00	Li, Huang, Lozano and Foschini [323]	Reduced complexity ML detection was proposed for multiple transmit antenna systems employing adaptive antenna grouping and multi-step reduced-complexity detection.
'01	Degen, Walke, Lecomte and Rembold [324]	An overview of various adaptive MIMO techniques was provided. Specifically, pre-distortion was employed at the transmitter, as well as LS- or BLAST detection were used at the receiver or balanced equalisation was invoked at both the transmitter and receiver.
	Zhu and Murch [325]	A tight upper bound on the SER performance of ML detection was derived.
	Li, Letaief, Cheng and Cao [326]	Joint adaptive power control and detection were investigated in the context of an OFDM/SDMA system, based on the approach of Farrokhi *et al.* [327].
	van Zelst, van Nee and Awater [328]	Iterative decoding was proposed for the BLAST system following the turbo principle.
	Benjebbour, Murata and Yoshida [329]	The performance of V-BLAST or SIC detection was studied in the context of backward iterative cancellation scheme employed after the conventional forward cancellation stage.
	Sellathurai and Haykin [330]	A simplified D-BLAST was proposed, which used iterative PIC capitalizing on the extrinsic soft-bit information provided by the FEC scheme used.
	Bhargave, Figueiredo and Eltoft [331]	A detection algorithm was suggested, which followed the concepts of V-BLAST or SIC. However, multiple symbols states are tracked from each detection stage, where - in contrast to [322] - an intermediate decision is made at intermediate detection stages.
	Thoen, Deneire, Van der Perre and Engels [332]	A constrained LS detector was proposed for OFDM/SDMA, which was based on exploiting the constant modulus property of PSK signals.
'02	Li and Luo [333]	The block error probability of optimally ordered V-BLAST was studied. Furthermore, the block error probability is also investigated for the case of tracking multiple parallel symbol decisions from the first detection stage, following an approach similar to that of [322].

Table 1.5: Contributions on detection techniques for MIMO systems and for multiple transmit antenna assisted OFDM systems;©John Wiley and IEEE Press, 2003 [172].

has matured and their wide-range employment has become a cost-efficient commercial reality. In recent years OFDM schemes have found their way into wireless local area networks (WLANs) as well, such as the 802.11 family.

For fixed-wire applications, OFDM is employed in the asynchronous digital subscriber line (ADSL) and high-bit-rate digital subscriber line (HDSL) systems [341–344] and it has also been suggested for power line communications systems [345, 346] due to its resilience to time dispersive channels and narrow band interferers.

OFDM applications were studied also within the various European Research projects [347]. The MEDIAN project investigated a 155 Mbps wireless asynchronous transfer mode (WATM) network [348–351], while the Magic WAND group [352,353] developed an OFDM-based WLAN. Hallmann and Rohling [354] presented a range of different OFDM systems that were applicable to the European Telecommunications Standardisation Institute's (ETSI) recent personal communications oriented air interface concept [355].

1.5 History of QAM-Based Coded Modulation

The history of channel coding or Forward Error Correction (FEC) coding dates back to Shannon's pioneering work [356] in 1948, in which he showed that it is possible to design a communication system with any desired small probability of error, whenever the rate of transmission is smaller than the capacity of the channel. While Shannon outlined the theory that explained the fundamental limits imposed on the efficiency of communications systems, he provided no insights into how to actually approach these limits. This motivated the search for codes that would produce arbitrarily small probability of error. Specifically, Hamming [357] and Golay [358] were the first to develop practical error control schemes. Convolutional codes [359] were later introduced by Elias in 1955, while Viterbi [360] invented a maximum likelihood sequence estimation algorithm in 1967 for efficiently decoding convolutional codes. In 1974, Bahl proposed the more complex Maximum A-Posteriori (MAP) algorithm, which is capable of achieving the minimum achievable BER.

The first successful application of channel coding was the employment of convolutional codes [359] in deep-space probes in the 1970s. However, for years to come, error control coding was considered to have limited applicability, apart from deep-space communications. Specifically, this is a power-limited scenario, which has no strict bandwidth limitation. By contrast mobile communications systems constitute a power- and bandwidth-limited scenario. In 1987, a bandwidth efficient Trellis Coded Modulation (TCM) [361] scheme employing symbol-based channel interleaving in conjunction with Set-Partitioning (SP) [362] assisted signal labelling was proposed by Ungerböck. Specifically, the TCM scheme, which is based on combining convolutional codes with multidimensional signal sets, constitutes a bandwidth efficient scheme that has been widely recognised as an efficient error control technique suitable for applications in mobile communications [363]. Another powerful coded modulation scheme utilising bit-based channel interleaving in conjunction with Gray signal labelling, which is referred to as Bit-Interleaved Coded Modulation (BICM), was proposed by Zehavi [364] as well as by Caire, Taricco and Biglieri [365]. Another breakthrough in the history of error control coding is the invention of turbo codes by Berrou, Glavieux and Thitimajshima [366] in 1993. Convolutional codes were used as the component codes and decoders based on the MAP algorithm were employed. The results proved that a performance close to the Shannon limit can be achieved in practice with the aid of binary codes. The attractive properties of turbo codes have attracted intensive research in this area [367–369]. As a result, turbo coding has reached a state of maturity within just a few years and was standardised in the recently ratified third-generation (3G) mobile radio systems [370].

However, turbo codes often have a low coding rate and hence require considerable bandwidth expansion. Therefore, one of the objectives of turbo coding research is the design of bandwidth-efficient turbo codes. In order to equip the family of binary turbo codes with a higher spectral efficiency, BICM-based Turbo Coded Modulation (TuCM) [371] was proposed in 1994. Specifically, TuCM uses a binary turbo encoder, which is linked to a signal mapper, after its output bits were suitably punctured and multiplexed for the sake of transmitting the desired number of information bits per transmitted symbol. In the TuCM scheme of [371] Gray-coding based signal labelling was utilised. For example, two 1/2-rate Recursive Systematic Convolutional (RSC) codes are used for generating a total of four turbo coded bits and this bit stream may be punctured for generating three bits, which are mapped to an 8PSK modulation scheme. By contrast, in separate coding and modulation scheme, any modulation schemes for example BPSK, may be used for transmitting the channel coded bits. Finally, without puncturing, 16QAM transmission would have to be used for maintaining the original transmission bandwidth. Turbo Trellis Coded Modulation (TTCM) [372] is a more recently proposed channel coding scheme that has a structure similar to that of the family of turbo codes, but employs TCM schemes as its component codes. The TTCM symbols are transmitted alternatively from the first and the second constituent TCM encoders and symbol-based interleavers are utilised for turbo interleaving and channel interleaving. It was shown in [372] that TTCM performs better than the TCM and TuCM schemes at a comparable complexity. In 1998, iterative joint decoding and demodulation assisted BICM referred to as BICM-ID was proposed in [373, 374], which uses SP based signal labelling. The aim of BICM-ID is to increase the Euclidean distance of BICM and hence to exploit the full advantage of bit interleaving with the aid of soft-decision feedback based iterative decoding [374]. Many other bandwidth efficient schemes using turbo codes have been proposed in the literature [368], but we will focus our study on TCM, BICM, TTCM and BICM-ID schemes in the context of wireless channels in this part of the book.

1.6 QAM in Multiple Antenna Based Systems

In recent years various smart antenna designs have emerged, which have found application in diverse scenarios, as seen in Table 1.6. The main objective of employing smart antennas is that of combating the effects of multipath fading on the desired signal and suppressing interfering signals, thereby increasing both the performance and capacity of wireless systems [375]. Specifically, in smart antenna assisted systems multiple antennas may be invoked at the transmitter and/or the receiver, where the antennas may be arranged for achieving spatial diversity, directional beamforming or for attaining both diversity and beamforming. In smart antenna systems the achievable performance improvements are usually a function of the antenna spacing and that of the algorithms invoked for processing the signals received by the antenna elements.

In beamforming arrangements [263] typically $\lambda/2$-spaced antenna elements are used for the sake of creating a spatially selective transmitter/receiver beam. Smart antennas using

Beamforming [263]	Typically $\lambda/2$-spaced antenna elements are used for the sake of creating a spatially selective transmitter/receiver beam. Smart antennas using beamforming have been employed for mitigating the effects of cochannel interfering signals and for providing beamforming gain.
Spatial Diversity [170] and Space-Time Spreading	In contrast to the $\lambda/2$-spaced phased array elements, in spatial diversity schemes, such as space-time block or trellis codes [170] the multiple antennas are positioned as far apart as possible, so that the transmitted signals of the different antennas experience independent fading, resulting in the maximum achievable diversity gain.
Space Division Multiple Access	SDMA exploits the unique, user-specific "spatial signature" of the individual users for differentiating amongst them. This allows the system to support multiple users within the same frequency band and/or time slot.
Multiple Input Multiple Output Systems [309]	MIMO systems also employ multiple antennas, but in contrast to SDMA arrangements, not for the sake of supporting multiple users. Instead, they aim for increasing the throughput of a wireless system in terms of the number of bits per symbol that can be transmitted by a given user in a given bandwidth at a given integrity.

Table 1.6: Applications of multiple antennas in wireless communications

beamforming have widely been employed for mitigating the effects of various interfering signals and for providing beamforming gain. Furthermore, the beamforming arrangement is capable of suppressing co-channel interference, which allows the system to support multiple users within the same bandwidth and/or same time-slot by separating them spatially. This spatial separation becomes however only feasible, if the corresponding users are separable in terms of the angle of arrival of their beams. These beamforming schemes, which employ appropriately phased antenna array elements that are spaced at distances of $\lambda/2$ typically result in an improved SINR distribution and enhanced network capacity [263].

In contrast to the $\lambda/2$-spaced phased array elements, **in spatial diversity schemes**, such as space-time coding [170] aided transmit diversity arrangements, the multiple antennas are positioned as far apart as possible. A typical antenna element spacing of 10λ [375] may be used, so that the transmitted signals of the different antennas experience independent fading, when they reach the receiver. This is because the maximum diversity gain can be achieved, when the received signal replicas experience independent fading. Although spatial diversity can be achieved by employing multiple antennas at either the base station, mobile station, or both, it is more cost effective and practical to employ multiple transmit antennas at the base station. A system having multiple receiver antennas has the potential of achieving receiver diversity, while that employing multiple transmit antennas exhibits transmit diversity. Recently, the family of transmit diversity schemes based on space-time coding, either space-time block codes or space-time trellis codes, has received wide attention and has been invoked in the 3rd-generation systems [263,376]. The aim of using spatial diversity is to provide both transmit as well as receive diversity and hence enhance the system's integrity/robustness. This typically results in a better physical-layer performance and hence a better network-layer performance, hence space-time codes indirectly increase not only the transmission integrity, but also the achievable spectral efficiency.

A third application of smart antennas is often referred to as **Space Division Multiple Access** (SDMA), which exploits the unique, user-specific "spatial signature" of the individual users for differentiating amongst them. In simple conceptual terms one could argue that both a conventional CDMA spreading code and the Channel Impulse Response (CIR) affect the transmitted signal similarly - they are namely convolved with it. Hence, provided that the CIR is accurately estimated, it becomes known and certainly unique, although - as opposed to orthogonal Walsh-Hadamad spreading codes, for example - not orthogonal to the other CIRs. Nonetheless, it may be used for uniquely identifying users after channel estimation and hence for supporting several users within the same bandwidth. Provided that a powerful multiuser detector is available, one can support even more users than the number of antennas. Hence this method enhances the achievable spectral efficiency directly.

Finally, Multiple Input Multiple Output (MIMO) systems [309, 377–380] also employ multiple antennas, but in contrast to SDMA arrangements, not for the sake of supporting multiple users. Instead, they aim for increasing the throughput of a wireless system in terms of the number of bits per symbol that can be transmitted by a single user in a given bandwidth at a given integrity.

1.7 Outline of the Book

1.7.1 Part I: QAM Basics

- In **Chapter 2** we consider the communications channels over which we wish to send our data. These channels are divided into Gaussian and mobile radio channels, and the characteristics of each are explained.

- **Chapter 3** provides an introduction to modems, considering the manner in which speech or other source waveforms are converted into a form suitable for transmission over a channel, and introducing some of the fundamentals of modems.

- **Chapter 4** provides a more detailed description of modems, specifically that of the modulator, considering QAM constellations, pulse shaping techniques, methods of generating and detecting QAM, as well as amplifier techniques to reduce the problems associated with non-linearities.

- **Chapter 5** elaborates on the details of decision theory and highlights the theoretical aspects of QAM transmission, showing how the BER can be mathematically computed for transmission over Gaussian channels.

- **Chapter 6** considers a range of classic clock and carrier recovery schemes, which are applicable mainly to systems operating over benign Gaussian channels, such as the times-two and the early-late recovery schemes as well as their derivatives.

- **Chapter 7** continues our discourse by considering channel equalisers. First the family of classic zero-forcing and least mean square equalisers, as well as Kalman filtering based schemes are discussed. Then a large part of this chapter is dedicated to the portrayal of blind channel equalisers.

- **Chapter 8** introduces the concept of classic trellis coded modulation schemes and deals with the historically important family of modems designed for Gaussian channels such as telephone lines.

1.7.2 Part II: Adaptive QAM Techniques for Fading Channels

- **Chapter 9** constitutes the first chapter of Part II of the book, focusing on QAM-based wireless communication by providing a theoretical analysis of QAM transmission over Rayleigh fading mobile radio channels using the so-called maximum minimum distance square-shaped constellation.

- **Chapter 10** introduces the concept of differentially encoded QAM, which was designed for maintaining a low detection complexity, when communicating over hostile wireless channels. These schemes are capable of operating without the employment coherent carrier recovery arrangements, which are prone to false locking in the presence of channel fading. This chapter also considers some of the practicalities of QAM transmissions over these wireless links, including the effects of intentional constellation distortions on the probabilities of the four individual bits of a 4-bit symbol and of hardware imperfections.

- **Chapter 11** details a range of various clock and carrier recovery schemes designed for mobile radio communications using QAM.

- **Chapter 22** provides a detailed mathematical characterisation of adaptive QAM systems, which are capable of appropriately adjusting the number of bits per QAM symbol on the basis of the instantaneous channel conditions. When the instantaneous channel quality is high, a high number of bits is transmitted. By contrast, under hostile channel conditions a low number of bits is transmitted for the sake of maintaining the target integrity. These concepts are also extended to sophisticated space-time coded multicarrier OFDM and MC-CDMA systems employing multiple transmitters and receivers.

- **Chapter 12** proposes a range of various channel equalisers designed for wideband QAM-aided transmissions.

- In **Chapter 13** we consider various orthogonal transmission and pulse shaping techniques in the context of quadrature-quadrature amplitude modulation also referred to as Q^2AQM.

- **Chapter 14** considers the spectral efficiency gains that can be achieved, when using QAM instead of conventional binary modulation techniques, when communicating in interference-limited cellular environments.

1.7.3 Part III: Advanced QAM Adaptive OFDM Systems

- **In Chapter 15** we focus our attention on the employment of the Fourier transform in order to show mathematically, how orthogonal frequency division multiplexing (OFDM) schemes may be implemented at the cost of a low complexity.

- In **Chapter 16** the BER performance of OFDM modems in AWGN channels is studied for a set of different modulation schemes in the subcarriers. The effects of amplitude limiting of the transmitter's output signal, caused by a simple clipping amplifier model, and of finite resolution D/A and A/D conversion on the system performance are investigated. Oscillator phase noise is considered as a source of intersubcarrier interference and its effects on the system performance are demonstrated.

- In **Chapter 17** the effects of time-dispersive frequency-selective Rayleigh fading channels on OFDM transmissions are demonstrated. Channel estimation techniques are presented which support the employment of coherent detection in frequency selective channels. Additionally, differential detection is investigated, and the resulting system performance over the different channels is compared.

- **Chapter 18** focuses our attention on the time and frequency synchronisation requirements of OFDM transmissions and the effects of synchronisation errors are demonstrated. Two novel synchronisation algorithms designed for both transmission frame and OFDM symbol synchronisation are suggested and compared. The resultant system performance recorded, when communicating over fading wideband channels is examined.

- In **Chapter 19**, based on the results of Chapter 22 and Chapter 17, the employment of adaptive modulation schemes is suggested for duplex point-to-point links over frequency-selective time-varying channels. Different bit allocation schemes are investigated and a simplified sub-band adaptivity OFDM scheme is suggested for alleviating the associated signalling constraints. A range of blind modulation scheme detection algorithms are also investigated and compared. The employment of long-block-length convolutional turbo codes is suggested for improving the system's throughput and the turbo coded adaptive OFDM modem's performance is compared using different sets of parameters. Then the effects of using pre-equalisation at the transmitter are examined, and a set of different pre-equalisation algorithms is introduced. A joint pre-equalisation and adaptive modulation algorithm is proposed and its BER and throughput performance is studied.

- In **Chapter 20** the adaptive OFDM transmission ideas of Chapter 22 and Chapter 19 are extended further, in order to include adaptive error correction coding, based on redundant residual number system (RRNS) and turbo BCH codes. A joint modulation and code rate adaptation scheme is presented.

- **Chapter 21** is dedicated to an OFDM-based system design study, which identifies the benefits and disadvantages of both space-time trellis as well as space-time block codes versus adaptive modulation under various propagation conditions.

1.7.4 Part IV: Advanced QAM Turbo-Equalised Adaptive TCM, TTCM, BICM, BICM-ID and Space-Time Coding Assisted OFDM, CDMA and MC-CDMA Systems

- In **Chapter 24** four different coded modulation schemes, namely TCM, TTCM, BICM and BICM-ID are introduced. The conceptual differences amongst these four coded modulation schemes are studied in terms of their coding structure, signal labelling philosophy, interleaver type and decoding philosophy. The symbol-based MAP algorithm operating in the logarithmic domain is also highlighted.

- **Chapter 25** studies the achievable performance of the above-mentioned coded modulation schemes, when communicating over AWGN and narrowband fading channels. Multi-carrier Orthogonal Frequency Division Multiplexing (OFDM) is also combined with the coded modulation schemes designed for communicating over wideband fading channels. With the aid of multi-carrier OFDM the wideband channel is divided into numerous narrowband sub-channels, each associated with an individual OFDM subcarrier. The performance trends of the coded modulation schemes are studied in the context of these OFDM sub-channels and compared in terms of the associated decoding complexity, coding delay and effective throughput under the assumption of encountering non-dispersive channel conditions in each sub-channel.

- In **Chapter 26** the channel equalisation concepts of Chapter 7 are developed further in the context of AQAM and both a conventional Decision Feedback Equaliser (DFE) and a Radial Basis Function (RBF) based DFE are introduced. These schemes are then combined with various coded modulation schemes communicating over wideband fading channels. The concepts of conventional DFE based adaptive modulation as well as RBF-based turbo equalisation and a reduced complexity RBF-based Inphase(I)/Quadrature-phase(Q) turbo equalisation scheme are also presented. We will incorporate the various coded modulation schemes considered into these systems and evaluate their performance in terms of the achievable BER, FER and effective throughput, when assuming a similar bandwidth, coding rate and decoding complexity for the various arrangements.

- In **Chapter 27** the performance of the various coded modulation schemes is also evaluated in conjunction with a Direct Sequence (DS) Code-Division Multiple Access (CDMA) system. Specifically, a DFE based Multi-User Detection (MUD) scheme is introduced for assisting the fixed-mode coded modulation schemes as well as the adaptive coded modulation schemes operating in conjunction with DS-CDMA, when communicating over wideband fading channels. The concept of Genetic Algorithm (GA) based MUD is also highlighted, which is invoked in conjunction with the coded modulation schemes for employment in the CDMA system. The performance of this MUD is compared to that of the optimum MUD.

- In **Chapter 28** IQ-interleaved Coded Modulation (IQ-CM) schemes are introduced for achieving IQ diversity. Space Time Block Coding (STBC) is also introduced for attaining additional space/transmit and time diversity. The concept of Double-Spreading aided Rake Receivers (DoS-RR) is proposed for achieving multipath diversity in a CDMA downlink, when transmitting over wideband fading channels. Finally, a STBC based IQ-CM assisted DoS-RR scheme is proposed for attaining transmit-, time-, IQ- and multipath-diversity, in a CDMA downlink, when communicating over wideband fading channels.

- **Chapter 29** provides a comparative study of the various coded modulation schemes studied in Part IV of the book, including suggestions for future research on coded modulation aided transceivers.

  Finally, in **Chapter 30** a variety of advanced QAM and OFDM assisted turbo-coded DVB schemes are proposed and analysed. Specifically, it compares the performance of schemes that use blind-equalised QAM modems. It is demonstrated that in comparison to the standard-based DVB systems the employment of turbo coding can provide an extra 5-6 dB channel SNR gain and this can be exploited for example to double the number of transmitted bits in a given bandwidth. This then ultimately allows us to improve for example the associated video quality that can be guaranteed in a given bandwidth at the cost of the associated additional implementational complexity.

1.8 Summary

Here we conclude our introduction to QAM and the review of publications concerning QAM as well as its various applications, spanning a period of four decades between the first theoretical study conducted in the context of Gaussian channels, leading to a whole host of applications in various sophisticated wireless systems operating in diverse propagation environments. We now embark on a detailed investigation of the topics introduced in this introductory chapter.

Part II

Adaptive QAM Techniques for Fading Channels

Part III

Advanced QAM:
Adaptive versus Space-Time
Block- and Trellis-Coded OFDM

Chapter 22

Adaptive QAM Optimisation for OFDM and MC-CDMA

B.J. Choi, L. Hanzo

22.1 Motivation

In Chapter 21 we have considered the design trade-offs of adaptive versus space-time coded transmissions. Although both methods aim for mitigating the effects of fading-induced channel quality fluctuations, their approach is fundamentally different. Adaptive QAM aims for adjusting the modulation modes for the sake of maintaining the target integrity, despite the channel quality fluctuations. By contrast, space-time coding [170] employs multiple transmitters and receivers for the sake of directly mitigating the channel quality undulations. It transpired that both techniques were capable of attaining a similar performance, although AQAM imposed a lower complexity owing to employing a single transmitter and receiver.

In this chapter our discourse evolves further by providing a comparative study of the various approaches developed for optimising the AQAM switching thresholds and then employing the thresholds in the context of both AQAM and space-time coded OFDM [172] as well aS frequency-domain spread MC-CDMA [172].

Let commence our detailed discourse with a glimpse of history. In recent years the concept of intelligent multi-mode, multimedia transceivers (IMMT) has emerged in the context of wireless systems [167–172, 179, 641, 647, 648]. The range of various existing solutions that have found favour in already operational standard systems was summarised in the excellent overview by Nanda *et al.* [648]. *The aim of these adaptive transceivers is to provide mobile users with the best possible compromise amongst a number of contradicting design factors, such as the power consumption of the hand-held portable station (PS), robustness against transmission errors, spectral efficiency, teletraffic capacity, audio/video quality and so forth [647].*

The fundamental limitation of wireless systems is constituted by their time- and frequency-domain channel fading, as illustrated in Figure 22.1 [170] in terms of the Signal-to-Noise Ratio (SNR) fluctuations experienced by a modem over a dispersive channel. The violent SNR fluctuations observed both versus time and versus frequency suggest that over these channels no fixed-mode transceiver can be expected to provide an attractive performance, complexity and delay trade-off. Motivated by the above mentioned performance limitations of fixed-mode transceivers, IMMTs have attracted considerable research interest in the past decade [167, 168, 179, 641, 647, 648]. Some of these research results are collated in this monograph.

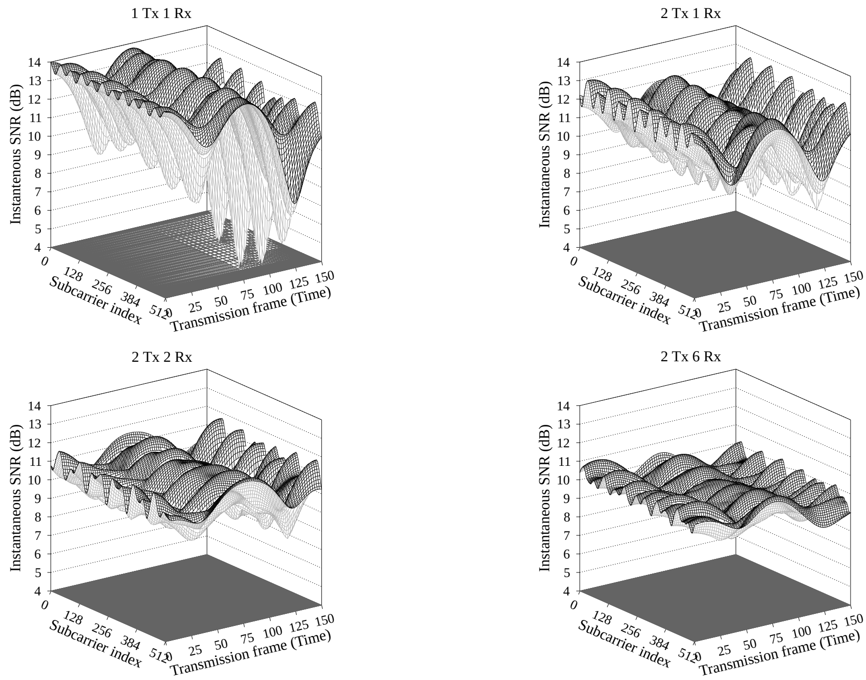

Figure 22.1: Instantaneous channel SNR versus time and frequency for a 512-subcarrier OFDM modem in the context of a single-transmitter single-receiver as well as for the space-time block code $\mathbf{G}_2$ [617] using one, two and six receivers when communicating over an indoor wireless channel. The average channel SNR is 10 dB. ©IEEE, Liew and Hanzo [170, 649], 2001

In Figure 22.1 we show the instantaneous channel SNR experienced by the 512-subcarrier OFDM symbols for a single-transmitter, single-receiver scheme and for the space-time block code $\mathbf{G}_2$ [617] using one, two and six receivers over the shortened WATM channel. The average channel SNR is 10 dB. We can see in Figure 22.1 that the variation of the instantaneous channel SNR for a single transmitter and single receiver is severe. The instantaneous channel SNR may become as low as 4 dB due to deep fades of the channel. On the other hand, we can see that for the space-time block code $\mathbf{G}_2$ using one receiver the variation in the instantaneous channel SNR is slower and less severe. Explicitly, by employing multiple transmit antennas as shown in Figure 22.1, we have reduced the effect of the channels' deep fades significantly. This is advantageous in the context of adaptive modulation schemes, since higher-order modulation modes can be employed, in order to increase the throughput of the system. However, as we increase the number of receivers, i.e. the diversity order, we observe that the variation of the channel becomes slower. Effectively, by employing higher-order diversity, the fading channels have been converted to AWGN-like channels, as evidenced by the scenario employing the space-time block code $\mathbf{G}_2$ using six receivers. Since adaptive modulation only offers advantages over fading channels, we argue that using adaptive modulation might become unnecessary, as the diversity order is increased. Hence, adaptive modulation can be viewed as a lower-complexity alternative to space-time coding, since only a single transmitter and receiver is required.

The above mentioned calamities inflicted by the wireless channel can be mitigated by contriving a suite of near-instantaneously adaptive or Burst-by-Burst Adaptive (BbBA) wideband single-carrier [179], multi-carrier or Orthogonal Frequency Division Multiplex [172] (OFDM) as well as Code Division Multiple Access (CDMA) [171] transceivers. The aim of these IMMTs is to communicate over hostile mobile channels at a higher integrity or higher throughput, than conventional fixed-mode transceivers. A number of existing wireless systems already support some grade of adaptivity and future research is likely to promote these principles further by embedding them into the already existing standards. For example, due to their high control channel rate and with the advent of the well-known Orthogonal Variable Spreading Factor (OVSF) codes the third-generation UTRA/IMT2000 systems are amenable to not only long-term spreading factor reconfiguration, but also to near-instantaneous reconfiguration on a 10ms transmission burst-duration basis. The High-Speed Data Packet Access (HSDPA) mode of the third-generation wireless systems has also opted for using adaptive modulation [169] and adaptive chennel coding [170].

With the advent of BbBA QAM, OFDM or CDMA transmissions it becomes possible for mobile stations (MS) to invoke for example in indoor scenarios or in the central propagation cell region - where typically benign channel conditions prevail - a high-throughput modulation mode, such as 4 bit/symbol Quadrature Amplitude Modulation (16QAM). By contrast, a robust, but low-throughput modulation mode, such as 1 bit/symbol Binary Phase Shift Keying (BPSK) can be employed near the edge of the propagation cell, where hostile propagation conditions prevail. The BbBA QAM, OFDM or CDMA mode switching regime is also capable of reconfiguring the transceiver at the rate of the channel's slow- or even fast-fading. This may prevent premature hand-overs and - more importantly - unnecessary powering up, which would inflict an increased interference upon co-channel users, resulting in further potential power increments. This detrimental process could result in all mobiles operating at unnecessarily high power levels.

A specific property of these transceivers is that their bit rate fluctuates, as a function of time. This is not an impediment in the context of data transmission. However, in interactive speech [168] or video [167] communications appropriate source codecs have to be designed, which are capable of promptly reconfiguring themselves according to the near-instantaneous bitrate budget provided by the transceiver.

The expected performance of our BbBA transceivers can be characterised with the aid of a whole plethora of performance indicators. In simple terms, adaptive modems outperform their individual fixed-mode counterparts, since given an average number of transmitted bits per symbol (BPS), their average BER will be lower than that of the fixed-mode modems. From a different perspective, at a given BER their BPS throughput will be always higher. In general, the higher the tolerable BER, the closer the performance to that of the Gaussian channel capacity. Again, this fact underlines the importance of designing programmable-rate, error-resilient source codecs - such as the Advanced Multi-Rate (AMR) speech codec to be employed in UMTS - which do not expect a low BER.

Similarly, when employing the above BbBA or AQAM principles in the frequency domain in the context of OFDM [179] or in conjunction with OVSF spreading codes in CDMA systems, attractive system design trade-offs and a high over-all performance can be attained [167]. However, despite the extensive research in the field by the international community, there is a whole host of problems that remain to be solved and this monograph intends to contribute towards these efforts.

22.2 Adaptation Principles

AQAM is suitable for duplex communication between the MS and BS, since the AQAM modes have to be adapted and signalled between them, in order to allow channel quality estimates and signalling to take place. The AQAM mode adaptation is the action of the transmitter in response to time–varying channel conditions. In order to efficiently react to the changes in channel quality, the following steps have to be taken:

- *Channel quality estimation:* In order to appropriately select the transmission parameters to be employed for the next transmission, a reliable estimation of the channel transfer function during the next active transmit timeslot is necessary.

- *Choice of the appropriate parameters for the next transmission:* Based on the prediction of the channel conditions for the next timeslot, the transmitter has to select the appropriate modulation and channel coding modes for the subcarriers.

- *Signalling or blind detection of the employed parameters:* The receiver has to be informed, as to which demodulator parameters to employ for the received packet. This information can either be conveyed within the OFDM symbol itself, at the cost of loss of effective data throughput, or the receiver can attempt to estimate the parameters employed by the remote transmitter by means of blind detection mechanisms [179].

22.3 Channel Quality Metrics

The most reliable channel quality estimate is the bit error rate (BER), since it reflects the channel quality, irrespective of the source or the nature of the quality degradation. The BER can be estimated invoking a number of approaches.

Firstly, the BER can be estimated with a certain granularity or accuracy, provided that the system entails a channel decoder or - synonymously - Forward Error Correction (FEC) decoder employing algebraic decoding [170].

Secondly, if the system contains a soft-in-soft-out (SISO) channel decoder, the BER can be estimated with the aid of the Logarithmic Likelihood Ratio (LLR), evaluated either at the input or the output of the channel decoder. A particularly attractive way of invoking LLRs is employing powerful turbo codecs, which provide a reliable indication of the confidence associated with a particular bit decision in the context of LLRs.

Thirdly, in the event that no channel encoder / decoder (codec) is used in the system, the channel quality expressed in terms of the BER can be estimated with the aid of the mean-squared error (MSE) at the output of the channel equaliser or the closely related metric of Pseudo-Signal-to-Noise-Ratio (Pseudo-SNR) [167]. The MSE or pseudo-SNR at the output of the channel equaliser have the important advantage that they are capable of quantifying the severity of the inter-symbol-interference (ISI) and/or Co-channel Interference (CCI) experienced, in other words quantifying the Signal to Interference plus Noise Ratio (SINR).

As an example, let us consider OFDM. In OFDM modems [179] the bit error probability in each subcarrier can be determined by the fluctuations of the channel's instantaneous frequency domain channel transfer function H_n, if no co-channel interference is present. The estimate $\hat{H}_n$ of the channel transfer function can be acquired by means of pilot–tone based channel estimation [179]. For CDMA transceivers similar techniques are applicable, which constitute the topic of this monograph.

The delay between the channel quality estimation and the actual transmission of a burst in relation to the maximal Doppler frequency of the channel is crucial as regards to the adaptive system's performance. If the channel estimate is obsolete at the time of transmission, then poor system performance will result [167].

22.4 Transceiver Parameter Adaptation

Different transmission parameters - such as the modulation and coding modes - of the AQAM single- and multi-carrier as well as CDMA transceivers can be adapted to the anticipated channel conditions. For example, adapting the number of modulation levels in response to the anticipated SNR encountered in each OFDM subcarrier can be employed, in order to achieve a wide range of different trade–offs between the received data integrity and throughput. Corrupted subcarriers can be excluded from data transmission and left blank or used for example for Crest–factor reduction. A range of different algorithms for selecting the appropriate modulation modes have to be investigated by future research. **The adaptive channel coding parameters entail code rate, adaptive interleaving and puncturing for convolutional and turbo codes, or varying block lengths for block codes [179].**

Based on the estimated frequency–domain channel transfer function, **spectral pre–distortion at the transmitter of one or both communicating stations can be invoked, in order to partially of fully counteract the frequency–selective fading of the time–dispersive channel**. Unlike frequency–domain equalisation at the receiver — which corrects for the amplitude– and phase–errors inflicted upon the subcarriers by the channel, but which cannot improve the SNR in poor quality OFDM subchannels — spectral pre–distortion at the OFDM transmitter can deliver near–constant signal–to–noise levels for all subcarriers and can be viewed as power control on a subcarrier–by–subcarrier basis.

In addition to improving the system's BER performance in time–dispersive channels, spectral pre–distortion can be employed in order to perform all channel estimation and equalisation functions at only one of the two communicating duplex stations. Low–cost, low power consumption mobile stations can communicate with a base station that performs the channel

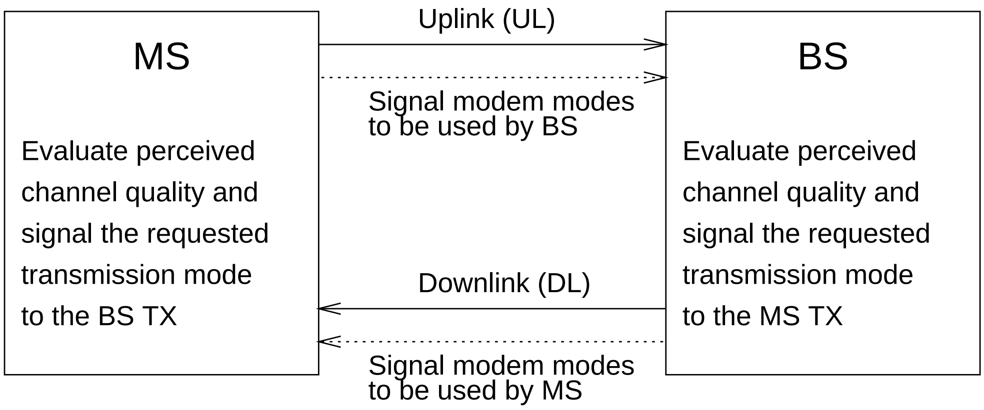

Figure 22.2: Parameter signalling in BbBA OFDM, CDMA and AQAM modems, IEEE Press-John Wiley, 2000, Hanzo, Webb, Keller [179].

estimation and frequency–domain equalisation of the uplink, and uses the estimated channel transfer function for pre–distorting the down–link OFDM symbol. This setup would lead to different overall channel quality on the up– and downlink, and the superior pre-equalised downlink channel quality could be exploited by using a computationally less complex channel decoder, having weaker error correction capabilities in the mobile station than in the base station.

If the channel's frequency–domain transfer function is to be fully counteracted by the spectral pre-distortion upon adapting the subcarrier power to the inverse of the channel transfer function, then the output power of the transmitter can become excessive, if heavily faded subcarriers are present in the system's frequency range. In order to limit the transmitter's maximal output power, hybrid channel pre–distortion and adaptive modulation schemes can be devised, which would de–activate transmission in deeply faded subchannels, while retaining the benefits of pre–distortion in the remaining subcarriers.

BbBA mode signalling plays an important role in adaptive systems and the range of signalling options is summarised in Figure 22.2 for **closed–loop signalling**. If the channel quality estimation and parameter adaptation have been performed at the transmitter of a particular link, based on open–loop adaptation, then the resulting set of parameters has to be communicated to the receiver in order to successfully demodulate and decode the OFDM symbol. Once the receiver determined the requested parameter set to be used by the remote transmitter, then this information has to be signalled to the remote transmitter in the reverse link. If this signalling information is corrupted, then the receiver is generally unable to correctly decode the OFDM symbol corresponding to the incorrect signalling information, yielding an OFDM symbol error.

Unlike adaptive serial systems, which employ the same set of parameters for all data symbols in a transmission packet [179], adaptive OFDM systems [179] have to react to the frequency selective nature of the channel, by adapting the modem parameters across the subcarriers. The resulting signalling overhead may become significantly higher than that for serial modems, and can be prohibitive for example for subcarrier–by–subcarrier based modulation mode adaptation. In order to overcome these limitations, efficient and reliable signalling techniques have to be employed for practical implementation of adaptive OFDM modems.

If some flexibility in choosing the transmission parameters is sacrificed in an adaptation scheme, like in sub–band adaptive OFDM schemes [179], then the amount of signalling can be reduced. Alternatively, blind parameter detection schemes can be devised, which require little or no OFDM mode signalling information, respectively [179].

In conclusion, fixed mode transceivers are incapable of achieving a good trade-off in terms of performance and complexity. The proposed BbB adaptive system design paradigm is more promising in this respect. A range of problems and solutions were highlighted in conceptual terms with reference to an OFDM-based example, indicating the areas, where substantial future research is required. A specific research topic, which raised substantial research interest recently is invoking efficient channel quality prediction techniques [174]. Before we commence our indepth discourse in the forthcoming chapters, in the next section we provide a brief historical perspective on adaptive modulation.

22.5 Milestones in Adaptive Modulation History

22.5.1 Adaptive Single- and Multi-carrier Modulation

A comprehensive overview of adaptive transceivers was provided in [169] and this section is also based on [169]. As we noted in the previous chapters, mobile communications channels typically exhibit a near-instantaneously fluctuating time-variant channel quality [169–172] and hence conventional fixed-mode modems suffer from bursts of transmission errors, even if the system was designed for providing a high link margin. *An efficient approach to mitigating these detrimental effects is to adaptively adjust the modulation and/or the channel coding format as well as a range of other system parameters based on the near-instantaneous channel quality information perceived by the receiver, which is fed back to the transmitter with the aid of a feedback channel [173].* This plausible principle was recognised by Hayes [173] as early as 1968.

It was also shown in the previous sections that these near-instantaneously adaptive schemes require a reliable feedback link from the receiver to the transmitter. However, the channel quality variations have to be sufficiently slow for the transmitter to be able to adapt its modulation and/or channel coding format appropriately. The performance of these schemes can potentially be enhanced with the aid of *channel quality prediction techniques [174]*. As an efficient fading counter-measure, Hayes [173] proposed the employment of transmission power adaptation, while *Cavers [175] suggested invoking a variable symbol duration scheme* in response to the perceived channel quality at the expense of a variable bandwidth requirement. A disadvantage of the variable-power scheme is that it increases both the average transmitted power requirements and the level of co-channel interference imposed on other users, while requiring a high-linearity class-A or AB power amplifier, which exhibit a low power-efficiency. As a more attractive alternative, *the employment of AQAM was proposed by Steele and Webb*, which circumvented some of the above-mentioned disadvantages by employing various star-QAM constellations [122, 176].

With the advent of *Pilot Symbol Assisted Modulation (PSAM)* [138, 139, 177], Otsuki *et al.* [178] employed square-shaped AQAM constellations instead of star constellations [179], as a practical fading counter measure. With the aid of analysing the channel capacity of Rayleigh fading channels [180], *Goldsmith* et al. *[181] and Alouini* et al. *[182] showed* *that combined variable-power, variable-rate adaptive schemes are attractive* in terms of approaching the capacity of the channel and characterised the achievable throughput performance of variable-power AQAM [181]. However, they also found that *the extra throughput achieved by the additional variable-power assisted adaptation over the constant-power, variable-rate scheme is marginal* for most types of fading channels [181, 183].

In 1996 Torrance and Hanzo [184] proposed a set of *mode switching levels* $\mathbf{s}$ designed for achieving a high average BPS throughput, while maintaining the target average BER. Their method was based on defining a specific combined BPS/BER cost-function for transmission over narrowband Rayleigh channels, which incorporated both the BPS throughput as well as the target average BER of the system. *Powell's optimisation was invoked for finding a set of mode switching thresholds, which were constant*, regardless of the actual channel Signal to Noise Ratio (SNR) encountered, i.e. irrespective of the prevalent instantaneous channel conditions. However, in 2001 Choi and Hanzo [185] noted that a *higher BPS throughput can be achieved, if under high channel SNR conditions the activation of high-throughput AQAM modes is further encouraged by lowering the AQAM mode switching thresholds. More explicitly, a set of SNR-dependent AQAM mode switching levels was proposed [185]*, which keeps the average BER constant, while maximising the achievable throughput. We note furthermore that the set of switching levels derived in [184, 186] is based on Powell's multidimensional optimisation technique [187] and hence the optimisation process may become trapped in a local minimum. This problem was overcome by Choi and Hanzo upon deriving an *optimum set of switching levels [185], when employing the Lagrangian multiplier technique*. It was shown that this set of switching levels results in the global optimum in a sense that the corresponding AQAM scheme obtains the maximum possible average BPS throughput, while maintaining the target average BER. An important further development was Tang's contribution [188] in the area of contriving an *intelligent learning scheme for the appropriate adjustment of the AQAM switching thresholds.*

These contributions demonstrated that *AQAM exhibited promising advantages*, when compared to fixed modulation schemes in terms of spectral efficiency, BER performance and robustness against channel delay spread, etc. Various systems employing AQAM were also characterised in [179]. The *numerical upper bound performance of narrow-band BbB-AQAM* over slow Rayleigh flat-fading channels was evaluated by Torrance and Hanzo [189], while over *wide-band channels* by Wong and Hanzo [190, 191]. Following these developments, adaptive modulation was also studied *in conjunction with channel coding and power control techniques by Matsuoka et al. [192] as well as Goldsmith and Chua [193, 194].*

In the early phase of research more emphasis was dedicated to the system aspects of adaptive modulation in a narrow-band environment. A reliable method of transmitting the modulation control parameters was proposed by Otsuki *et al.* [178], where the parameters were embedded in the transmission frame's mid-amble using Walsh codes. Subsequently, at the receiver the Walsh sequences were decoded using maximum likelihood detection. Another technique of *signalling the required modulation mode used was proposed by Torrance and Hanzo [195], where the modulation control symbols were represented by unequal error protection 5-PSK symbols.* Symbol-by-Symbol (SbS) adaptive, *rather than BbB-adaptive systems were proposed by Lau and Maric in [196], where the transmitter is capable of transmitting each symbol in a different modem mode, depending on the channel conditions. Naturally, the receiver has to synchronise with the transmitter in terms of the SbS-adapted mode sequence, in order to correctly demodulate the received symbols and hence the employment* *of BbB-adaptivity is less challenging, while attaining a similar performance to that of BbB-adaptive arrangements under typical channel conditions.*

The adaptive modulation philosophy was then extended to wideband multi-path environments *amongst others for example by Kamio et al. [197] by utilizing a bi-directional Decision Feedback Equaliser (DFE)* in a micro- and macro-cellular environment. This equalization technique employed both forward and backward oriented channel estimation based on the pre-amble and post-amble symbols in the transmitted frame. Equalizer tap gain interpolation across the transmitted frame was also utilized for reducing the complexity in conjunction with space diversity [197]. The authors concluded that the cell radius could be enlarged in a macro-cellular system and a higher area-spectral efficiency could be attained for micro-cellular environments by utilizing adaptive modulation. The data transmission latency effect, which occurred when the input data rate was higher than the instantaneous transmission throughput was studied and solutions were formulated using *frequency hopping [198] and statistical multiplexing, where the number of Time Division Multiple Access (TDMA) timeslots allocated to a user was adaptively controlled [199].*

In reference [200] *symbol rate adaptive modulation* was applied, where the symbol rate or the number of modulation levels was adapted by using $\frac{1}{8}$-rate 16QAM, $\frac{1}{4}$-rate 16QAM, $\frac{1}{2}$-rate 16QAM as well as full-rate 16QAM and the criterion used for adapting the modem modes was based on the instantaneous received signal to noise ratio and channel delay spread. The slowly varying channel quality of the uplink (UL) and downlink (DL) was rendered similar by utilizing short frame duration Time Division Duplex (TDD) and the maximum normalised delay spread simulated was 0.1. A *variable channel coding rate* was then introduced by Matsuoka *et al.* in conjunction with adaptive modulation in reference [192], where the transmitted burst incorporated an outer Reed Solomon code and an inner convolutional code in order to achieve high-quality data transmission. The coding rate was varied according to the prevalent channel quality using the same method, as in adaptive modulation in order to achieve a certain target BER performance. A so-called *channel margin* was introduced in this contribution, which effectively increased the switching thresholds for the sake of preempting *the effects of channel quality estimation errors,* although this inevitably reduced the achievable BPS throughput.

In an effort to improve the achievable performance versus complexity trade-off in the context of AQAM, Yee and Hanzo [201] studied the design of various *Radial Basis Function (RBF) assisted neural network based schemes, while communicating over dispersive channels.* The advantage of these RBF-aided DFEs is that they are capable of delivering error-free decisions even in scenarios, when the received phasors cannot be error-freely detected by the conventional DFE, since they cannot be separated into decision classes with the aid of a linear decision boundary. In these so-called linearly non-separable decision scenarios the RBF-assisted DFE still may remain capable of classifying the received phasors into decision classes without decision errors. A further improved turbo BCH-coded version of this RBF-aided system was characterised by Yee *et al.* in [202], while a turbo-equalised RBF arrangement was the subject of the investigation conducted by Yee, Liew and Hanzo in [203, 204]. The RBF-aided AQAM research has also been extended to the turbo equalisation of a convolutional as well as space-time trellis coded arrangement proposed by Yee, Yeap and Hanzo [169,205,206]. The same authors then endeavoured to reduce the associated implementation complexity of an RBF-aided QAM modem with the advent of employing a separate in-phase / quadrature-phase turbo equalisation scheme in the quadrature arms of the modem.

As already mentioned above, the performance of *channel coding in conjunction with adaptive modulation in a narrow-band environment* was also characterised by Chua and Goldsmith [193]. In their contribution trellis and lattice codes were used without channel interleaving, invoking a feedback path between the transmitter and receiver for modem mode control purposes. Specifically, the simulation and theoretical results by Goldsmith and Chua showed that a 3dB coding gain was achievable at a BER of 10^{-6} for a 4-sate trellis code and 4dB by an 8-state trellis code in the context of the adaptive scheme over Rayleigh-fading channels, while a 128-state code performed within 5dB of the Shannonian capacity limit. The *effects of the delay in the AQAM mode signalling feedback path* on the adaptive modem's performance were studied and this scheme exhibited a higher spectral efficiency, when compared to the non-adaptive trellis coded performance. Goeckel [207] also contributed in the area of adaptive coding and employed realistic outdated, rather than perfect fading estimates. Further research on adaptive multidimensional coded modulation was also conducted by Hole *et al.* [208] for transmissions over flat fading channels. *Pearce, Burr and Tozer [209] as well as Lau and Mcleod [210] have also analysed the performance trade-offs associated with employing channel coding and adaptive modulation or adaptive trellis coding,* respectively, as efficient fading counter measures. In an effort to provide a fair comparison of the various coded modulation schemes known at the time of writing, Ng, Wong and Hanzo have also studied Trellis Coded Modulation (TCM), Turbo TCM (TTCM), Bit-Interleaved Coded Modulation (BICM) and Iterative-Decoding assisted BICM (BICM-ID), where TTCM was found to be the best scheme at a given decoding complexity [211].

Subsequent contributions by Suzuki *et al.* [212] incorporated *space-diversity and power-adaptation* in conjunction with adaptive modulation, for example in order to combat the effects of the multi-path channel environment at a 10Mbits/s transmission rate. *The maximum tolerable delay-spread was deemed to be one symbol duration for a target mean BER performance of* 0.1%. This was achieved in a TDMA scenario, where the channel estimates were predicted based on the extrapolation of previous channel quality estimates. As mentioned above, variable transmitted power was applied in combination with adaptive modulation in reference [194], where the transmission rate and power adaptation was optimised for the sake of achieving an increased spectral efficiency. In their treatise a slowly varying channel was assumed and the instantaneous received power required for achieving a certain upper bound performance was assumed to be known prior to transmission. *Power control in conjunction with a pre-distortion type non-linear power amplifier compensator* was studied in the context of adaptive modulation in reference [213]. This method was used to mitigate the non-linearity effects associated with the power amplifier, when QAM modulators were used.

Results were also recorded concerning the performance of adaptive modulation in conjunction with *different multiple access schemes in a narrow-band channel environment*. In a TDMA system, *dynamic channel assignment* was employed by Ikeda *et al.*, where in addition to assigning a different modulation mode to a different channel quality, priority was always given to those users in their request for reserving time-slots, which benefitted from the best channel quality [214]. The performance was compared to fixed channel assignment systems, where substantial gains were achieved in terms of system capacity. Furthermore, a *lower call termination probability was recorded*. However, the probability of intra-cell hand-off increased as a result of the associated dynamic channel assignment (DCA) scheme, which constantly searched for a high-quality, high-throughput time-slot for supporting the actively communicating users. The application of adaptive modulation in packet transmission was introduced by Ue, Sampei and Morinaga [215], where the results showed an improved BPS throughput. The performance of adaptive modulation was also characterised in conjunction with an *automatic repeat request* (ARQ) system in reference [216], where the transmitted bits were encoded using a cyclic redundant code (CRC) and a convolutional punctured code in order to increase the data throughput.

A further treatise was published by Sampei, Morinaga and Hamaguchi [217] on *laboratory test results* concerning the utilization of adaptive modulation in a TDD scenario, where the modem mode switching criterion was based on the signal to noise ratio and on the normalised delay-spread. *In these experimental results, the channel quality estimation errors degraded the performance* and consequently - as laready alluded to earlier - a channel estimation error margin was introduced for mitigating this degradation. Explicitly, the channel estimation error margin was defined as the measure of how much extra protection margin must be added to the switching threshold levels for the sake of minimising the effects of the channel estimation errors. The delay-spread also degraded the achievable performance due to the associated irreducible BER, which was not compensated by the receiver. However, the performance of the adaptive scheme in a delay-spread impaired channel environment was better, than that of a fixed modulation scheme. *These experiments also concluded that the AQAM scheme can be operated for a Doppler frequency of $f_d = 10$Hz at a normalised delay spread of 0.1 or for $f_d = 14$Hz at a normalised delay spread of 0.02, which produced a mean BER of 0.1% at a transmission rate of 1 Mbits/s.*

Lastly, the *data buffering-induced latency and co-channel interference aspects* of AQAM modems were investigated in [218, 219]. Specifically, the latency associated with storing the information to be transmitted during severely degraded channel conditions was mitigated by frequency hopping or statistical multiplexing. As expected, the latency is increased, when either the mobile speed or the channel SNR are reduced, since both of these result in prolonged low instantaneous SNR intervals. It was demonstrated that as a result of the proposed measures, typically more than 4dB SNR reduction was achieved by the proposed adaptive modems in comparison to the conventional fixed-mode benchmark modems employed. However, the achievable gains depend strongly on the prevalant co-channel interference levels and hence interference cancellation was invoked in [219] on the basis of adjusting the demodulation decision boundaries after estimating the interfering channel's magnitude and phase.

The associated principles can also be invoked in the context of *multicarrier Orthogonal Frequency Division Multiplex (OFDM) modems [179].* This principle was first proposed by Kalet [154] and was then further developed for example by Czylwik *et al.* [220] as well as by Chow, Cioffi and Bingham [221]. The associated concepts were detailed for example in [179] and will be also augmented in this monograph. Let us now briefly review the recent history of the BbB adaptive concept in the context of CDMA in the next section.

22.5.2 Adaptive Code Division Multiple Access

The techniques described in the context of single- and multi-carrier modulation are conceptually similar to multi-rate transmission [650] in CDMA systems. However, in BbB adaptive CDMA the transmission rate is modified according to the near-instantaneous channel quality, instead of the service required by the mobile user. BbB-adaptive CDMA systems are also useful for employment in arbitrary propagation environments or in hand-over scenarios, such as those encountered, when a mobile user moves from an indoor to an outdoor environment or in a so-called 'birth-death' scenario, where the number of transmitting CDMA users changes frequently [651], thereby changing the interference dramatically. Various methods of multi-rate transmission have been proposed in the research literature. Below we will briefly discuss some of the recent research issues in multi-rate and adaptive CDMA schemes.

Ottosson and Svensson compared various multi-rate systems [650], including multiple spreading factor (SF) based, multi-code and multi-level modulation schemes. According to the multi-code philosophy, the SF is kept constant for all users, but multiple spreading codes transmitted simultaneously are assigned to users requiring higher bit rates. In this case - unless the spreading codes's perfect orthogonality is retained after transmission over the channel - the multiple codes of a particular user interfere with each other. This inevitebly reduces the system's performance.

Multiple data rates can also be supported by a variable SF scheme, where the chip rate is kept constant, but the data rates are varied, thereby effectively changing the SF of the spreading codes assigned to the users; at a fixed chip rate the lower the SF, the higher the supported data rate. Performance comparisons for both of these schemes have been carried out by Ottosson and Svensson [650], as well as by Ramakrishna and Holtzman [652], demonstrating that both schemes achieved a similar performance. Adachi, Ohno, Higashi, Dohi and Okumura proposed the employment of multi-code CDMA in conjunction with pilot symbol-assisted channel estimation, RAKE reception and antenna diversity for providing multi-rate capabilities [653, 654]. The employment of multi-level modulation schemes was also investigated by Ottosson and Svensson [650], where higher-rate users were assigned higher-order modulation modes, transmitting several bits per symbol. However, it was concluded that the performance experienced by users requiring higher rates was significantly worse, than that experienced by the lower-rate users. The use of M-ary orthogonal modulation in providing variable rate transmission was investigated by Schotten, Elders-Boll and Busboom [655]. According to this method, each user was assigned an orthogonal sequence set, where the number of sequences, M, in the set was dependent on the data rate required – the higher the rate required, the larger the sequence set. Each sequence in the set was mapped to a particular combination of $b = (\log_2 M)$ bits to be transmitted. The M-ary sequence was then spread with the aid of a spreading code of a constant SF before transmission. It was found [655] that the performance of the system depended not only on the MAI, but also on the Hamming distance between the sequences in the M-ary sequence set.

Saquib and Yates [656] investigated the employment of the decorrelating detector in conjunction with the multiple-SF scheme and proposed a modified decorrelating detector, which utilized soft decisions and maximal ratio combining, in order to detect the bits of the different-rate users. Multi-rate transmission schemes involving interference cancellation receivers have previously been investigated amongst others by Johansson and Svensson [657,658], as well as by Juntti [659]. Typically, multiple users transmitting at different bit rates are supported in the same CDMA system invoking multiple codes or different spreading factors. SIC schemes and multi-stage cancellation schemes were used at the receiver for mitigating the MAI [657–659], where the bit rate of the users was dictated by the user requirements. The performance comparison of various multiuser detectors in the context of a multiple-SF transmission scheme was presented for example by Juntti [659], where the detectors compared were the decorrelator, the PIC receiver and the so-called group serial interference cancellation (GSIC) receiver. It was concluded that the GSIC and the decorrelator performed better than the PIC receiver, but all the interference cancellation schemes including the GSIC, exhibited an error floor at high SNRs due to error propagation.

The bit rate of each user can also be adapted according to the near-instantaneous channel quality, in order to mitigate the effects of channel quality fluctuations. Kim [660] analysed the performance of two different methods of combating the near-instantaneous quality variations of the mobile channel. Specifically, Kim studied the adaptation of the transmitter power or the switching of the information rate, in order to suit the near-instantaneous channel conditions. It was demonstrated using a RAKE receiver that rate adaptation provided a higher average information rate, than power adaptation for a given average transmit power and a given BER [660]. Abeta, Sampei and Morinaga [661] conducted investigations into an adaptive packet transmission based CDMA scheme, where the transmission rate was modified by varying the channel code rate and the processing gain of the CDMA user, employing the carrier to interference plus noise ratio (CINR) as the switching metric. When the channel quality was favourable, the instantaneous bit rate was increased and conversely, the instantaneous bit rate was reduced when the channel quality dropped. In order to maintain a constant overall bit rate, when a high instantaneous bit rate was employed, the duration of the transmission burst was reduced. Conversely, when the instantaneous bit rate was low, the duration of the burst was extended. This resulted in a decrease in interference power, which translated to an increase in system capacity. Hashimoto, Sampei and Morinaga [662] extended this work also to demonstrate that the proposed system was capable of achieving a higher user capacity with a reduced hand-off margin and lower average transmitter power. In these schemes the conventional RAKE receiver was used for the detection of the data symbols. A variable-rate CDMA scheme – where the transmission rate was modified by varying the channel code rate and, correspondingly, the M-ary modulation constellations – was investigated by Lau and Maric [196]. As the channel code rate was increased, the bit-rate was increased by increasing M correspondingly in the M-ary modulation scheme. Another adaptive system was proposed by Tateesh, Atungsiri and Kondoz [663], where the rates of the speech and channel codecs were varied adaptively [663]. In their adaptive system, the gross transmitted bit rate was kept constant, but the speech codec and channel codec rates were varied according to the channel quality. When the channel quality was low, a lower rate speech codec was used, resulting in increased redundancy and thus a more powerful channel code could be employed. This resulted in an overall coding gain, although the speech quality dropped with decreasing speech rate. A variable rate data transmission scheme was proposed by Okumura and Adachi [664], where the fluctuating transmission rate was mapped to discontinuous transmission, in order to reduce the interference inflicted upon the other users, when there was no transmission. The transmission rate was detected blindly at the receiver with the help of cyclic redundancy check decoding and RAKE receivers were employed for coherent reception, where pilot-symbol-assisted channel estimation was performed.

The information rate can also be varied according to the channel quality, as it will be demonstrated shortly. However, in comparison to conventional power control techniques - which again, may disadvantage other users in an effort to maintain the quality of the links considered - the proposed technique does not disadvantage other users and increases the network capacity [169, 665]. The instantaneous channel quality can be estimated at the receiver and the chosen information rate can then be communicated to the transmitter via explicit signalling in a so-called closed-loop controlled scheme. Conversely, in an open-loop scheme - provided that the downlink and uplink channels exhibit a similar quality - the information rate

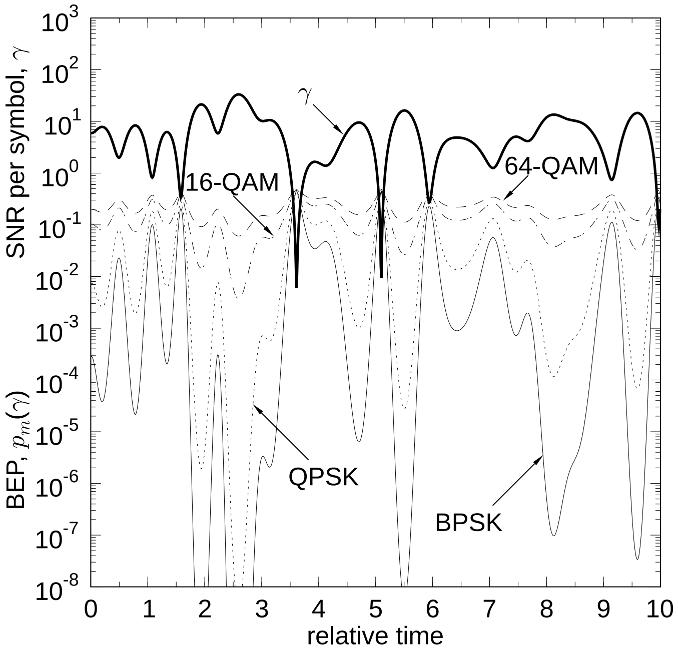

Figure 22.3: Instantaneous SNR per transmitted symbol, γ, in a flat Rayleigh fading scenario and the associated instantaneous bit error probability, $p_m(\gamma)$, of a fixed-mode QAM. The average SNR is $\bar{\gamma} = 10$dB. The fading magnitude plot is based on a normalized Doppler frequency of $f_N = 10^{-4}$ and for the duration of $100ms$, corresponding to a mobile terminal travelling at the speed of $54km/h$ and operating at $f_c = 2GHz$ frequency band at the sampling rate of $1MHz$.

for the downlink transmission can be chosen according to the channel quality estimate related to the uplink and vice versa. The validity of the uplink/downlink similarity in TDD-CDMA systems has been studied by Miya *et al.* [580], Kato *et al.* [581] and Jeong *et al.* [666].

22.6 Increasing the Average Transmit Power as a Fading Counter-Measure

The radio frequency (RF) signal radiated from the transmitter's antenna takes different routes, experiencing defraction, scattering and reflections, before it arrives at the receiver. Each multi-path component arriving at the receiver simultaneously adds constructively or destructively, resulting in fading of the combined signal. When there is no line-of-sight component amongst these signals, the combined signal is characterized by Rayleigh fading. The instantaneous SNR (iSNR), γ, per transmitted symbol[1] is depicted in Figure 22.3 for a typical Rayleigh fading using the thick line. The Probability Density Function (PDF) of γ is given

[1]When no diversity is employed at the receiver, the SNR per symbol, γ, is the same as the channel SNR, γ_c. In this case, we will use the term "SNR" without any adjective.

as [388]:

$$f_{\bar{\gamma}}(\gamma) = \frac{1}{\bar{\gamma}}\, e^{\gamma/\bar{\gamma}} \,, \tag{22.1}$$

where $\bar{\gamma}$ is the average SNR and $\bar{\gamma} = 10$dB was used in Figure 22.3.

The instantaneous Bit Error Probability (iBEP), $p_m(\gamma)$, of BPSK, QPSK, 16-QAM and 64-QAM is also shown in Figure 22.3 with the aid of four different thin lines. These probabilities are obtained from the corresponding bit error probability over AWGN channel conditioned on the iSNR, γ, which are given as [179]:

$$p_m(\gamma) = \sum_i A_i Q(\sqrt{a_i \gamma}) \,, \tag{22.2}$$

where $Q(x)$ is the Gaussian Q-function defined as $Q(x) \triangleq \frac{1}{\sqrt{2\pi}} \int_x^\infty e^{-t^2/2} dt$ and $\{A_i, a_i\}$ is a set of modulation mode dependent constants. For the Gray-mapped square QAM modulation modes associated with $m = 2, 4, 16, 64$ and 256, the sets $\{A_i, a_i\}$ are given as [179,667]:

$$\begin{array}{lcl}
m = 2, & \text{BPSK} & \{(1,2)\} \\
m = 4, & \text{QPSK} & \{(1,1)\} \\
m = 16, & \text{16-QAM} & \left\{ \left(\frac{3}{4}, \frac{1^2}{5}\right), \left(\frac{2}{4}, \frac{3^2}{5}\right), \left(-\frac{1}{4}, \frac{5^2}{5}\right) \right\} \\
m = 64, & \text{64-QAM} & \left\{ \left(\frac{7}{12}, \frac{1^2}{21}\right), \left(\frac{6}{12}, \frac{3^2}{21}\right), \left(-\frac{1}{12}, \frac{5^2}{21}\right), \left(\frac{1}{12}, \frac{9^2}{21}\right), \left(-\frac{1}{12}, \frac{13^2}{21}\right) \right\} \\
m = 256, & \text{256-QAM} & \left\{ \left(\frac{15}{32}, \frac{1^2}{85}\right), \left(\frac{14}{32}, \frac{3^2}{85}\right), \left(\frac{5}{32}, \frac{5^2}{85}\right), \left(-\frac{6}{32}, \frac{7^2}{85}\right), \left(-\frac{7}{32}, \frac{9^2}{85}\right), \right. \\
 & & \left(\frac{6}{32}, \frac{11^2}{85}\right), \left(\frac{9}{32}, \frac{13^2}{85}\right), \left(\frac{8}{32}, \frac{15^2}{85}\right), \left(-\frac{7}{32}, \frac{17^2}{85}\right), \left(-\frac{6}{32}, \frac{19^2}{85}\right), \\
 & & \left. \left(-\frac{1}{32}, \frac{21^2}{85}\right), \left(\frac{2}{32}, \frac{23^2}{85}\right), \left(\frac{3}{32}, \frac{25^2}{85}\right), \left(-\frac{2}{32}, \frac{27^2}{85}\right), \left(-\frac{1}{32}, \frac{29^2}{85}\right) \right\} .
\end{array} \tag{22.3}$$

As we can observe in Figure 22.3, $p_m(\gamma)$ exhibits high values during the deep channel envelope fades, where even the most robust modulation mode, namely BPSK, exhibits a bit error probability $p_2(\gamma) > 10^{-1}$. By contrast even the error probability of the high-throughput 16-QAM mode, namely $p_{16}(\gamma)$, is below 10^{-2}, when the iSNR γ exhibits a high peak. This wide variation of the communication link's quality is a fundamental problem in wireless radio communication systems. Hence, numerous techniques have been developed for combating this problem, such as increasing the average transmit power, invoking diversity, channel inversion, channel coding and/or adaptive modulation techniques. In this section we will investigate the efficiency of employing an increased average transmit power.

As we observed in Figure 22.3, the instantaneous Bit Error Probability (BEP) becomes excessive for sustaining an adequate service quality during instances, when the signal experiences a deep channel envelope fade. Let us define the cut-off BEP p_c, below which the Quality Of Service (QOS) becomes unacceptable. Then the outage probability P_{out} can be defined as:

$$P_{out}(\bar{\gamma}, p_c) \triangleq \Pr[\, p_m(\gamma) \, > \, p_c \,] \,, \tag{22.4}$$

where $\bar{\gamma}$ is the average channel SNR dependent on the transmit power, p_c is the cut-off BEP and $p_m(\gamma)$ is the instantaneous BEP, conditioned on γ, for an m-ary modulation mode, given for example by (22.2). We can reduce the outage probability of (22.4) by increasing the

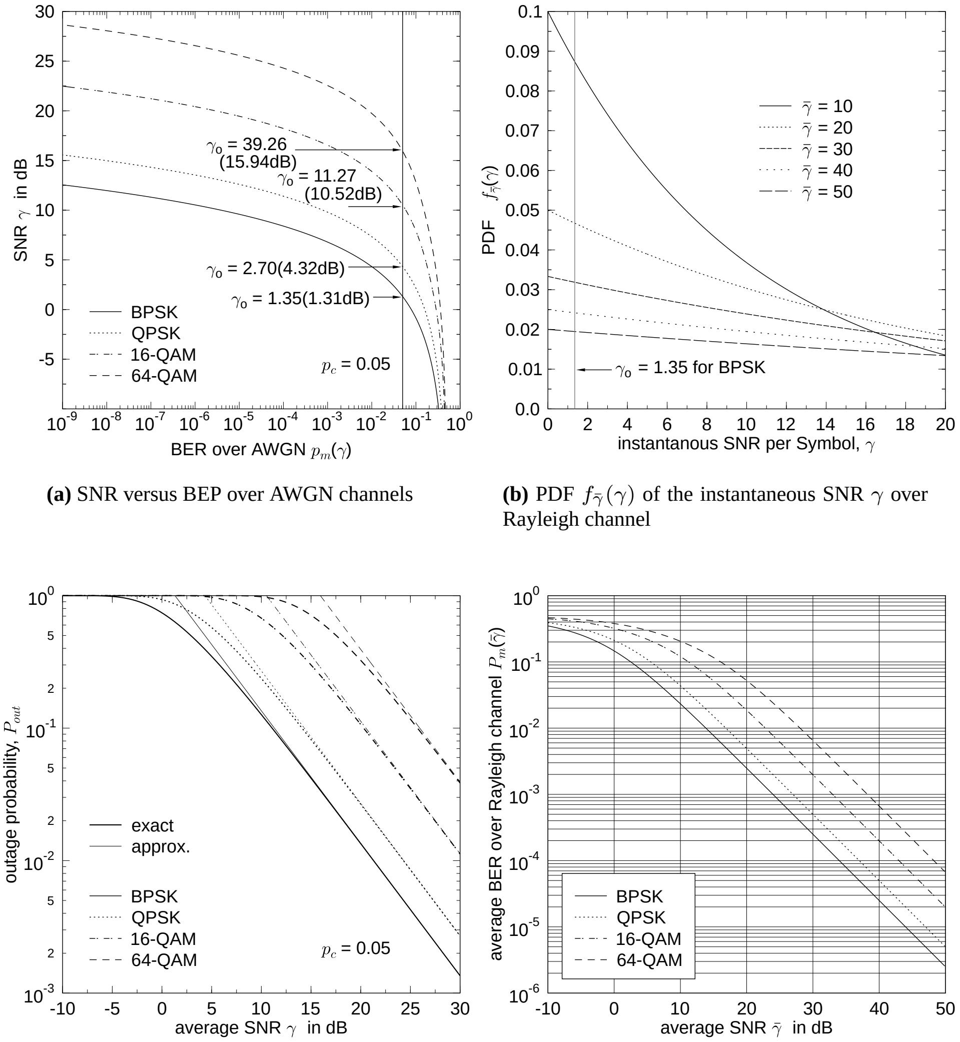

(a) SNR versus BEP over AWGN channels

(b) PDF $f_{\bar{\gamma}}(\gamma)$ of the instantaneous SNR γ over Rayleigh channel

(c) Outage Probability over Rayleigh channel

(d) BER over Rayleigh channel

Figure 22.4: The effects of an increased average transmit power. (a) The cut-off SNR γ_o versus the cut-off BEP p_c for BPSK, QPSK, 16-QAM and 64-QAM. (b) PDF of the iSNR γ over Rayleigh channel, where the outage probability is given by the area under the PDF curve surrounded by the two lines given by $\gamma = 0$ and $\gamma = \gamma_o$. An increased transmit power increases the average SNR $\bar{\gamma}$ and hence reduces the area under the PDF proportionately to $\bar{\gamma}$. (c) The exact outage probability versus the average SNR $\bar{\gamma}$ for BPSK, QPSK, 16-QAM and 64-QAM evaluated from (22.7) confirms this observation. (d) The average BEP is also inversely proportional to the transmit power for BPSK, QPSK, 16-QAM and 64-QAM.

transmit power, and hence increasing the average channel SNR $\bar{\gamma}$. Let us briefly investigate the efficiency of this scheme.

Figure 22.4(a) depicts the instantaneous BEP as a function of the instantaneous channel SNR. Once the cut-off BEP p_c is determined as a QOS-related design parameter, the corresponding cut-off SNR γ_o can be determined, as shown for example in Figure 22.4(a) for $p_c = 0.05$. Then, the outage probability of (22.4) can be calculated as:

$$P_{out} = \Pr[\,\gamma \,<\, \gamma_o\,]\,, \tag{22.5}$$

and in physically tangible terms its value is equal to the area under the PDF curve of Figure 22.4(b) surrounded by the left y-axis and $\gamma = \gamma_o$ vertical line. Upon taking into account that for high SNRs the PDFs of Figure 22.4(b) are near-linear, this area can be approximated by $\gamma_o/\bar{\gamma}$, considering that $f_{\bar{\gamma}}(0) = 1/\bar{\gamma}$. Hence, the outage probability is inversely proportional to the transmit power, requiring an approximately 10-fold increased transmit power for reducing the outage probability by an order of magnitude, as seen in Figure 22.4(c). The exact value of the outage probability is given by:

$$P_{out} = \int_0^{\gamma_o} f_{\bar{\gamma}}(\gamma)\,d\gamma \tag{22.6}$$

$$= 1 - e^{-\gamma_o/\bar{\gamma}}\,, \tag{22.7}$$

where we used the PDF $f_{\bar{\gamma}}(\gamma)$ given in (22.1). Again, Figure 22.4(c) shows the exact outage probabilities together with their linearly approximated values for several QAM modems recorded for the cut-off BEP of $p_c = 0.05$, where we can confirm the validity of the linearly approximated outage probability[2], when we have $P_{out} < 0.1$.

The average BEP $P_m(\bar{\gamma})$ of an m-ary Gray-mapped QAM modem is given by [179, 388, 668]:

$$P_m(\bar{\gamma}) = \int_0^{\infty} p_m(\gamma)\,f_{\bar{\gamma}}(\gamma)\,d\gamma \tag{22.8}$$

$$= \frac{1}{2}\sum_i A_i\{1 - \mu(\bar{\gamma}, a_i)\}\,, \tag{22.9}$$

where a set of constants $\{A_i, a_i\}$ is given in (22.3) and $\mu(\bar{\gamma}, a_i)$ is defined as:

$$\mu(\bar{\gamma}, a_i) \triangleq \sqrt{\frac{a_i\bar{\gamma}}{1 + a_i\bar{\gamma}}}\,. \tag{22.10}$$

In physical terms (22.8) implies weighting the BEP $p_m(\gamma)$ experienced at an iSNR γ by the probability of occurrence of this particular value of γ - which is quantified by its PDF $f_{\bar{\gamma}}(\gamma)$ - and then averaging, *i.e.* integrating, this weighted BEP over the entire range of γ. Figure 22.4(d) displays the average BER evaluated from (22.9) for the average SNR rage of -10dB $\geq\, \bar{\gamma}\, \geq$ 50dB. We can observe that the average BEP is also inversely proportional to the transmit power.

[2]The same approximate outage probability can be derived by taking the first term of the Taylor series of e^x of (22.7).

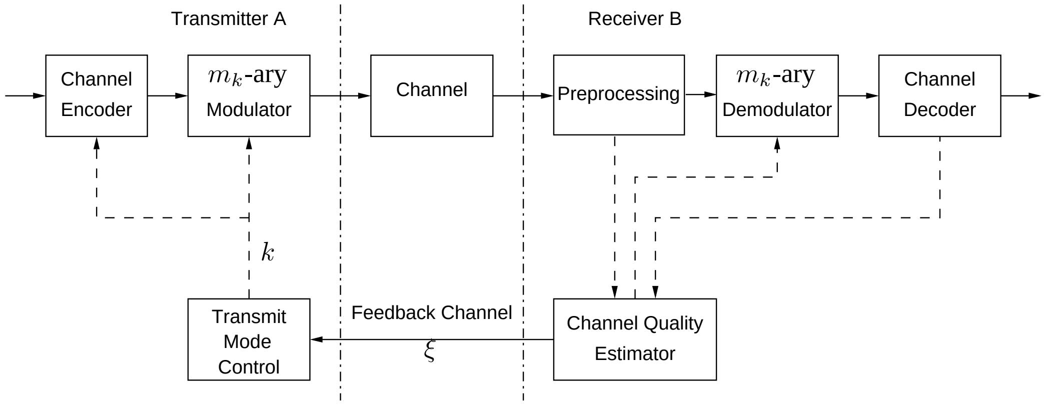

Figure 22.5: Stylised model of near-instantaneous adaptive modulation scheme.

In conclusion, we studied the efficiency of increasing the average transmit power as a fading counter-measure and found that the outage probability as well as the average bit error probability are inversely proportional to the average transmit power. Since the maximum radiated powers of modems are regulated in order to reduce the co-channel interference and transmit power, the acceptable transmit power increase may be limited and hence employing this technique may not be sufficiently effective for achieving the desired link performance. We will show that the AQAM philosophy of the next section is a more attractive solution to the problem of channel quality fluctuation experienced in wireless systems.

22.7 System Description

A stylised model of our adaptive modulation scheme is illustrated in Figure 22.5, which can be invoked in conjunction with any power control scheme. In our adaptive modulation scheme, the modulation mode used is adapted on a near-instantaneous basis for the sake of counteracting the effects of fading. Let us describe the detailed operation of the adaptive modem scheme of Figure 22.5. Firstly, the channel quality ξ is estimated by the remote receiver B. This channel quality measure ξ can be the instantaneous channel SNR, the Radio Signal Strength Indicator (RSSI) output of the receiver [176], the decoded BER [176], the Signal to Interference-and-Noise Ratio (SINR) estimated at the output of the channel equalizer [191], or the SINR at the output of a CDMA joint detector [669]. The estimated channel quality perceived by receiver B is fed back to transmitter A with the aid of a feedback channel, as seen in Figure 22.5. Then, the transmit mode control block of transmitter A selects the highest-throughput modulation mode k capable of maintaining the target BEP based on the channel quality measure ξ and the specific set of adaptive mode switching levels $\mathbf{s}$. Once k is selected, m_k-ary modulation is performed at transmitter A in order to generate the transmitted signal $s(t)$, and the signal $s(t)$ is transmitted through the channel.

The general model and the set of important parameters specifying our constant-power adaptive modulation scheme are described in the next subsection in order to develop the underlying general theory. Then, in Subsection 22.7.2 several application examples are introduced.

22.7.1 General Model

A K-mode adaptive modulation scheme adjusts its transmit mode k, where $k \in \{0, 1 \cdots K-1\}$, by employing m_k-ary modulation according to the near-instantaneous channel quality ξ perceived by receiver B of Figure 22.5. The mode selection rule is given by:

$$\text{Choose mode } k \text{ when } \quad s_k \le \xi < s_{k+1} \,, \tag{22.11}$$

where a switching level s_k belongs to the set $\mathbf{s} = \{s_k \mid k = 0, 1, \cdots, K\}$. The Bits Per Symbol (BPS) throughput b_k of a specific modulation mode k is given by $b_k = \log_2(m_k)$ if $m_k \neq 0$, otherwise $b_k = 0$. It is convenient to define the incremental BPS c_k as $c_k = b_k - b_{k-1}$, when $k > 0$ and $c_0 = b_0$, which quantifies the achievable BPS increase, when switching from the lower-throughput mode k–1 to mode k.

22.7.2 Examples

22.7.2.1 Five-Mode AQAM

A five-mode AQAM system has been studied extensively by many researchers, which was motivated by the high performance of the Gray-mapped constituent modulation modes used. The parameters of this five-mode AQAM system are summarised in Table 22.1. In our inves-

k	0	1	2	3	4
m_k	0	2	4	16	64
b_k	0	1	2	4	6
c_k	0	1	1	2	2
modem	No Tx	BPSK	QPSK	16-QAM	64-QAM

Table 22.1: The parameters of five-mode AQAM system.

tigation, the near-instantaneous channel quality ξ is defined as instantaneous channel SNR γ. The boundary switching levels are given as $s_0 = 0$ and $s_5 = \infty$. Figure 22.6 illustrates operation of the five-mode AQAM scheme over a typical narrow-band Rayleigh fading channel scenario. Transmitter A of Figure 22.5 keeps track of the channel SNR γ perceived by receiver B with the aid of a low-BER, low-delay feedback channel - which can be created for example by superimposing the values of ξ on the reverse direction transmitted messages of transmitter B - and determines the highest-BPS modulation mode maintaining the target BEP depending on which region γ falls into. The channel-quality related SNR regions are divided by the modulation mode switching levels s_k. More explicitly, the set of AQAM switching levels $\{s_k\}$ is determined such that the average BPS throughput is maximised, while satisfying the average target BEP requirement, P_{target}. We assumed a target BEP of $P_{target} = 10^{-2}$ in Figure 22.6. The associated instantaneous BPS throughput b is also depicted using the

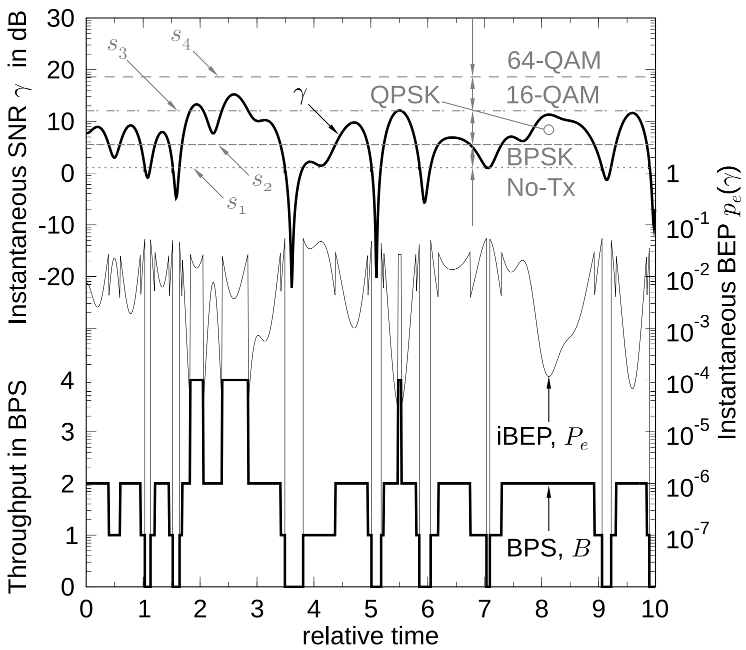

Figure 22.6: The operation of the five-mode AQAM scheme over a Rayleigh fading channel. The instantaneous channel SNR γ is represented as a thick line at the top part of the graph, the associated instantaneous BEP $P_e(\gamma)$ as a thin line at the middle, and the instantaneous BPS throughput $b(\gamma)$ as a thick line at the bottom. The average SNR is $\bar{\gamma} = 10\text{dB}$, while the target BEP is $P_{target} = 10^{-2}$.

thick stepped line at the bottom of Figure 22.6. We can observe that the throughput varied from 0 BPS, when the no transmission (No-Tx) QAM mode was chosen, to 4 BPS, when the 16-QAM mode was activated. During the depicted observation window the 64-QAM mode was not activated. The instantaneous BEP, depicted as a thin line using the middle trace of Figure 22.6, is concentrated around the target BER of $P_{target} = 10^{-2}$.

22.7.2.2 Seven-Mode Adaptive Star-QAM

Webb and Steele revived the research community's interest on adaptive modulation, although a similar concept was initially suggested by Hayes [173] in the 1960s. Webb and Steele reported the performance of adaptive star-QAM systems [176]. The parameters of their system are summarised in Table 22.2.

22.7.2.3 Five-Mode APSK

Our five-mode Adaptive Phase-Shift-Keying (APSK) system employs m-ary PSK constituent modulation modes. The magnitude of all the constituent constellations remained constant, where adaptive modem parameters are summarised in Table 22.3.

k	0	1	2	3	4	5	6
m_k	0	2	4	8	16	32	64
b_k	0	1	2	3	4	5	6
c_k	0	1	1	1	1	1	1
modem	No Tx	BPSK	QPSK	8-QAM	16-QAM	32-QAM	64-QAM

Table 22.2: The parameters of a seven-mode adaptive star-QAM system [176], where 8-QAM and 16-QAM employed four and eight constellation points allocated to two concentric rings, respectively, while 32-QAM and 64-QAM employed eight and 16 constellation points over four concentric rings, respectively.

k	0	1	2	3	4
m_k	0	2	4	8	16
b_k	0	1	2	3	4
c_k	0	1	1	1	1
modem	No Tx	BPSK	QPSK	8-PSK	16-PSK

Table 22.3: The parameters of the five-mode APSK system.

22.7.2.4 Ten-Mode AQAM

Hole, Holm and Øien [208] studied a trellis coded adaptive modulation scheme based on eight-mode square- and cross-QAM schemes. Upon adding the No-Tx and BPSK modes, we arrive at a ten-mode AQAM scheme. The associated parameters are summarised in Table 22.4.

k	0	1	2	3	4	5	6	7	8	9
m_k	0	2	4	8	16	32	64	128	256	512
b_k	0	1	2	3	4	5	6	7	8	9
c_k	0	1	1	1	1	1	1	1	1	1
modem	No Tx	BPSK	QPSK	8-Q	16-Q	32-C	64-Q	128-C	256-Q	512-C

Table 22.4: The parameters of the ten-mode adaptive QAM scheme based on [208], where m-Q stands for m-ary square QAM and m-C for m-ary cross QAM.

22.7.3 Characteristic Parameters

In this section, we introduce several parameters in order to characterize our adaptive modulation scheme. The constituent mode selection probability (MSP) $\mathcal{M}_k$ is defined as the probability of selecting the k-th mode from the set of K possible modulation modes, which can be calculated as a function of the channel quality metric ξ, regardless of the specific metric used, as:

$$\mathcal{M}_k = \Pr[\, s_k \le \xi < s_{k+1} \,] \tag{22.12}$$

$$= \int_{s_k}^{s_{k+1}} f(\xi)\, d\xi \;, \tag{22.13}$$

where s_k denotes the mode switching levels and $f(\xi)$ is the probability density function (PDF) of ξ. Then, the average throughput B expressed in terms of BPS can be described as:

$$B = \sum_{k=0}^{K-1} b_k \int_{s_k}^{s_{k+1}} f(\xi)\, d\xi \tag{22.14}$$

$$= \sum_{k=0}^{K-1} b_k\, \mathcal{M}_k \;, \tag{22.15}$$

which in simple verbal terms can be formulated as the weighted sum of the throughput b_k of the individual constituent modes, where the weighting takes into account the probability $\mathcal{M}_k$ of activating the various constituent modes. When $s_K = \infty$, the average throughput B can also be formulated as:

$$B = \sum_{k=0}^{K-1} b_k \int_{s_k}^{s_{k+1}} f(\xi)\, d\xi \tag{22.16}$$

$$= \sum_{k=0}^{K-1} c_k \int_{s_k}^{\infty} f(\xi)\, d\xi \tag{22.17}$$

$$= \sum_{k=0}^{K-1} c_k\, F_c(s_k), \tag{22.18}$$

where $F_c(\xi)$ is the complementary Cumulative Distribution Function (CDF) defined as:

$$F_c(\xi) \triangleq \int_{\xi}^{\infty} f(x)\, dx \;. \tag{22.19}$$

Let us now assume that we use the instantaneous SNR γ as the channel quality measure ξ, which implies that no co-channel interference is present. By contrast, when operating in a co-channel interference limited environment, we can use the instantaneous SINR as the channel quality measure ξ, provided that the co-channel interference has a near-Gaussian distribution. In such scenario, the mode-specific average BEP P_k can be written as:

$$P_k = \int_{s_k}^{s_{k+1}} p_{m_k}(\gamma)\, f(\gamma)\, d\gamma \;, \tag{22.20}$$

where $p_{m_k}(\gamma)$ is the BEP of the m_k-ary constituent modulation mode over the AWGN channel and we used γ instead of ξ in order to explicitly indicate the employment of γ as the channel quality measure. Then, the average BEP P_{avg} of our adaptive modulation scheme can be represented as the sum of the BEPs of the specific constituent modes divided by the average adaptive modem throughput B, formulated as [189]:

$$P_{avg} = \frac{1}{B} \sum_{k=0}^{K-1} b_k \, P_k \; , \tag{22.21}$$

where b_k is the BPS throughput of the k-th modulation mode, P_k is the mode-specific average BEP given in (22.20) and B is the average adaptive modem throughput given in (22.15) or in (22.18).

The aim of our adaptive system is to transmit as high a number of bits per symbol as possible, while providing the required Quality of Service (QOS). More specifically, we are aiming for maximizing the average BPS throughput B of (22.14), while satisfying the average BEP requirement of $P_{avg} \leq P_{target}$. Hence, we have to satisfy the constraint of meeting P_{target}, while optimizing the design parameter of $\mathbf{s}$, which is the set of modulation-mode switching levels. The determination of optimum switching levels will be investigated in Section 22.8. Since the calculation of the optimum switching levels typically requires the numerical computation of the parameters introduced in this section, it is advantageous to express the parameters in a closed form, which is the objective of the next section.

22.7.3.1 Closed Form Expressions for Transmission over Nakagami Fading Channels

Fading channels often are modelled as Nakagami fading channels [670]. The PDF of the instantaneous channel SNR γ over a Nakagami fading channel is given as [670]:

$$f(\gamma) = \left(\frac{m}{\bar{\gamma}}\right)^m \frac{\gamma^{m-1}}{\Gamma(m)} \, e^{-m\gamma/\bar{\gamma}} \; , \;\; \gamma \geq 0 \; , \tag{22.22}$$

where the parameter m governs the severity of fading and $\Gamma(m)$ is the Gamma function [671]. When $m = 1$, the PDF of (22.22) is reduced to the PDF of γ over Rayleigh fading channel, which is given in (22.1). As m increases, the fading behaves like Rician fading, and it becomes the AWGN channel, when m tends to ∞. Here we restrict the value of m to be a positive integer. In this case, the Nakagami fading model of (22.22), having a mean of $\bar{\gamma}_s = m\,\bar{\gamma}$, will be used to describe the PDF of the SNR per symbol γ_s in an m-antenna based diversity assisted system employing Maximal Ratio Combining (MRC).

When the instantaneous channel SNR γ is used as the channel quality measure ξ in our adaptive modulation scheme transmitting over a Nakagami channel, the parameters defined in Section 22.7.3 can be expressed in a closed form. Specifically, the mode selection probability $\mathcal{M}_k$ can be expressed as:

$$\mathcal{M}_k = \int_{s_k}^{s_{k+1}} f(\gamma)\, d\gamma \tag{22.23}$$

$$= F_c(s_k) - F_c(s_{k+1}) \; , \tag{22.24}$$

where the complementary CDF $F_c(\gamma)$ is given by:

$$F_c(\gamma) = \int_{\gamma}^{\infty} f(x)\, dx \tag{22.25}$$

$$= \int_{\gamma}^{\infty} \left(\frac{m}{\bar{\gamma}}\right)^m \frac{x^{m-1}}{\Gamma(m)}\, e^{-mx/\bar{\gamma}}\, dx \tag{22.26}$$

$$= e^{-m\gamma/\bar{\gamma}} \sum_{i=0}^{m-1} \frac{(m\gamma/\bar{\gamma})^i}{\Gamma(i+1)} \,. \tag{22.27}$$

In deriving (22.27) we used the result of the indefinite integral of [672]:

$$\int x^n e^{-ax}\, dx = -(e^{-ax}/a) \sum_{i=0}^{n} x^{n-i}/a^i\, n!/(n-i)!) \,. \tag{22.28}$$

In a Rayleigh fading scenario, *i.e.* when $m = 1$, the mode selection probability $\mathcal{M}_k$ of (22.24) can be expressed as:

$$\mathcal{M}_k = e^{-s_k/\bar{\gamma}} - e^{-s_{k+1}/\bar{\gamma}} \,. \tag{22.29}$$

The average throughput B of our adaptive modulation scheme transmitting over a Nakagami channel is given by substituting (22.27) into (22.18), yielding:

$$B = \sum_{k=0}^{K-1} c_k\, e^{-ms_k/\bar{\gamma}} \left\{ \sum_{i=0}^{m-1} \frac{(ms_k/\bar{\gamma})^i}{\Gamma(i+1)} \right\} \,. \tag{22.30}$$

Let us now derive the closed form expressions for the mode specific average BEP P_k defined in (22.20) for the various modulation modes when communicating over a Nakagami channel. The BER of a Gray-coded square QAM constellation for transmission over AWGN channels was given in (22.2) and it is repeated here for convenience:

$$p_{m_k,QAM}(\gamma) = \sum_i A_i\, Q(\sqrt{a_i \gamma}) \,, \tag{22.31}$$

where the values of the constants A_i and a_i were given in (22.3). Then, the mode specific average BEP $P_{k,QAM}$ of m_k-ary QAM over a Nakagami channel can be expressed as seen in

Appendix 31.3 as follows:

$$P_{k,QAM} = \int_{s_k}^{s_{k+1}} p_{m_k,QAM}(\gamma)\, f(\gamma)\, d\gamma \tag{22.32}$$

$$= \sum_i A_i \int_{s_k}^{s_{k+1}} Q(\sqrt{a_i\gamma}) \left(\frac{m}{\bar{\gamma}}\right)^m \frac{\gamma^{m-1}}{\Gamma(m)}\, e^{-m\gamma/\bar{\gamma}}\, d\gamma \tag{22.33}$$

$$= \sum_i A_i \left\{ -e^{-m\,\gamma/\bar{\gamma}}\, Q(\sqrt{a_i\gamma}\,) \sum_{j=0}^{m-1} \frac{(m\,\gamma/\bar{\gamma})^j}{\Gamma(j+1)} \right]_{s_k}^{s_{k+1}} + \sum_{j=0}^{m-1} X_j(\gamma, a_i) \Bigg]_{s_k}^{s_{k+1}} \Bigg\}\,, \tag{22.34}$$

where $g(\gamma)]_{s_k}^{s_{k+1}} \triangleq g(s_{k+1}) - g(s_k)$ and $X_j(\gamma, a_i)$ is given by:

$$X_j(\gamma, a_i) = \frac{\mu^2}{\sqrt{2a_i\pi}} \left(\frac{m}{\bar{\gamma}}\right)^j \frac{\Gamma(j+\frac{1}{2})}{\Gamma(j+1)} \sum_{k=1}^{j} \left(\frac{2\mu^2}{a_i}\right)^{j-k} \frac{\gamma^{k-\frac{1}{2}}}{\Gamma(k+\frac{1}{2})}\, e^{-a_i\gamma/(2\mu^2)}$$
$$+ \left(\frac{2\mu^2\, m}{a_i\bar{\gamma}}\right)^j \frac{1}{\sqrt{\pi}} \frac{\Gamma(j+\frac{1}{2})}{\Gamma(j+1)}\, \mu\, Q\left(\sqrt{a_i\gamma}/\mu\right)\,, \tag{22.35}$$

where, again, $\mu \triangleq \sqrt{\frac{a_i\bar{\gamma}}{2+a_i\bar{\gamma}}}$ and $\Gamma(x)$ is the Gamma function.

On the other hand, the high-accuracy approximated BEP formula of a Gray-coded m_k-ary PSK scheme ($k \geq 3$) transmitting over an AWGN channel is given as [673]:

$$p_{m_k,PSK} \simeq \frac{2}{k} \left\{ Q\left(\sqrt{2\gamma}\,\sin(\pi/2^k)\right) + Q\left(\sqrt{2\gamma}\,\sin(3\pi/2^k)\right) \right\} \tag{22.36}$$

$$= \sum_i A_i\, Q(\sqrt{a_i\gamma})\,, \tag{22.37}$$

where the set of constants $\{(A_i, a_i)\}$ is given by $\{(2/k,\ 2\sin^2(\pi/m_k)), (2/k,\ 2\sin^2(3\pi/m_k))\}$. Hence, the mode-specific average BEP $P_{k,PSK}$ can be represented using the same equation, namely (22.34), as for $P_{k,QAM}$.

22.8 Optimum Switching Levels

In this section we restrict our interest to adaptive modulation schemes employing the SNR per symbol γ as the channel quality measure ξ. We then derive the optimum switching levels as a function of the target BEP and illustrate the operation of the adaptive modulation scheme. The corresponding performance results of the adaptive modulation schemes communicating over a flat-fading Rayleigh channel are presented in order to demonstrate the effectiveness of the schemes.

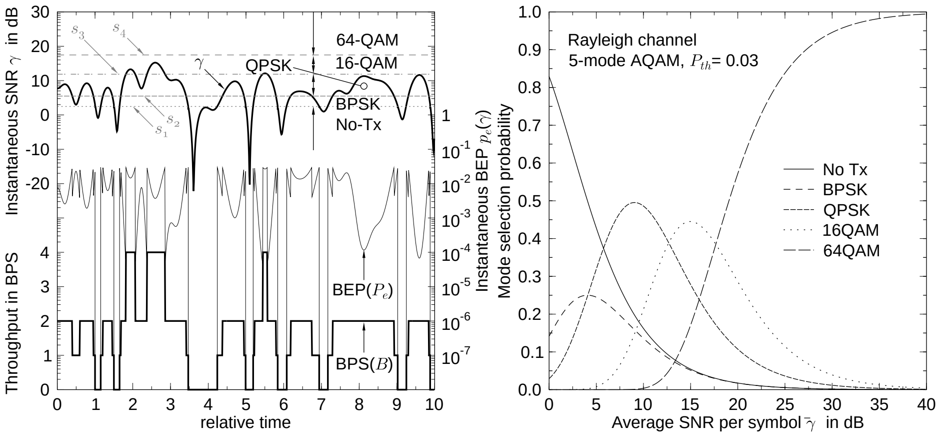

(a) operation of AQAM

(b) mode selection probability

Figure 22.7: Various characteristics of the five-mode AQAM scheme communicating over a Rayleigh fading channel employing the specific set of switching levels designed for limiting the peak instantaneous BEP to $P_{th} = 3 \times 10^{-2}$. (a) The evolution of the instantaneous channel SNR γ is represented by the thick line at the top of the graph, the associated instantaneous BEP $p_e(\gamma)$ by the thin line in the middle and the instantaneous BPS throughput $b(\gamma)$ by the thick line at the bottom. The average SNR is $\bar{\gamma} = 10$dB. (b) As the average SNR increases, the higher-order AQAM modes are selected more often.

22.8.1 Limiting the Peak Instantaneous BEP

The first attempt of finding the optimum switching levels that are capable of satisfying various transmission integrity requirements was made by Webb and Steele [176]. They used the BEP curves of each constituent modulation mode, obtained from simulations over an AWGN channel, in order to find the Signal-to-Noise Ratio (SNR) values, where each modulation mode satisfies the target BEP requirement [179]. This intuitive concept of determining the switching levels has been widely used by researchers [178, 183] since then. The regime proposed by Webb and Steele can be used for ensuring that the instantaneous BEP always remains below a certain threshold BEP P_{th}. In order to satisfy this constraint, the first modulation mode should be “no transmission”. In this case, the set of switching levels $\mathbf{s}$ is given by:

$$\mathbf{s} = \{\ s_0 = 0,\ s_k \mid p_{m_k}(s_k) = P_{th}\ \ k \geq 1\}\ . \tag{22.38}$$

Figure 22.7 illustrates how this scheme operates over a Rayleigh channel, using the example of the five-mode AQAM scheme described in Section 22.7.2.1. The average SNR was $\bar{\gamma} = 10$dB and the instantaneous target BEP was $P_{th} = 3 \times 10^{-2}$. Using the expression given in (22.2) for p_{m_k}, the set of switching levels can be calculated for the instantaneous target BEP, which is given by $s_1 = 1.769$, $s_2 = 3.537$, $s_3 = 15.325$ and $s_4 = 55.874$. We can observe that the instantaneous BEP represented as a thin line by the middle of trace of Figure 22.7(a)

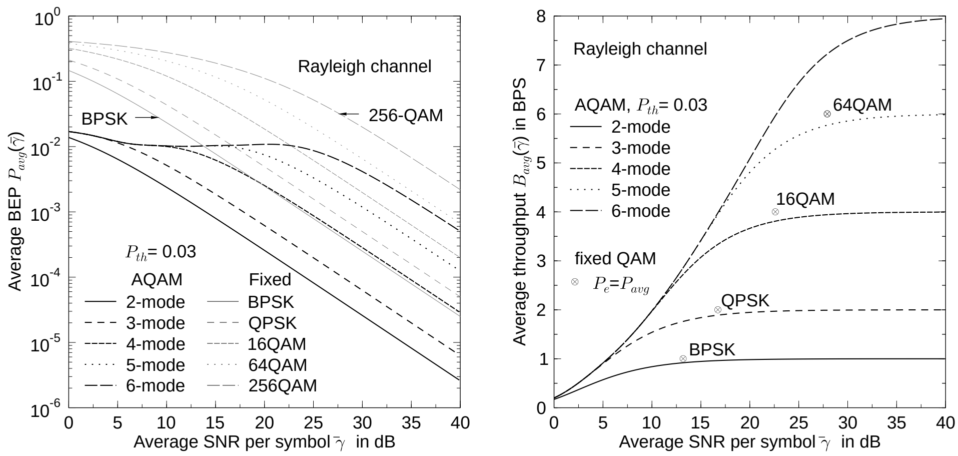

(a) average BER

(b) average throughput

Figure 22.8: The performance of AQAM employing the specific switching levels defined for limiting the peak instantaneous BEP to $P_{th} = 0.03$. (a) As the number of constituent modulation modes increases, the SNR region where the average BEP remains around $P_{avg} = 10^{-2}$ widens. (b) The SNR gains of AQAM over the fixed-mode QAM scheme required for achieving the same BPS throughput at the same average BEP of P_{avg} are in the range of 5dB to 8dB.

was limited to values below $P_{th} = 3 \times 10^{-2}$.

At this particular average SNR predominantly the QPSK modulation mode was invoked. However, when the instantaneous channel quality is high, 16-QAM was invoked in order to increase the BPS throughput. The mode selection probability $\mathcal{M}_k$ of (22.24) is shown in Figure 22.7(b). Again, when the average SNR is $\bar{\gamma} = 10$dB, the QPSK mode is selected most often, namely with the probability of about 0.5. The 16-QAM, No-Tx and BPSK modes have had the mode selection probabilities of 0.15 to 0.2, while 64-QAM is not likely to be selected in this situation. When the average SNR increases, the next higher order modulation mode becomes the dominant modulation scheme one by one and eventually the highest order of 64-QAM mode of the five-mode AQAM scheme prevails.

The effects of the number of modulation modes used in our AQAM scheme on the performance are depicted in Figure 22.8. The average BEP performance portrayed in Figure 22.8(a) shows that the AQAM schemes maintain an average BEP lower than the peak instantaneous BEP of $P_{th} = 3 \times 10^{-2}$ even in the low SNR region, at the cost of a reduced average throughput, which can be observed in Figure 22.8(b). As the number of the constituent modulation modes employed of the AQAM increases, the SNR regions, where the average BEP is near constant around $P_{avg} = 10^{-2}$ expands to higher average SNR values. We can observe that the AQAM scheme maintains a constant SNR gain over the highest-order constituent fixed QAM mode, as the average SNR increases, at the cost of a negligible BPS throughput degradation. This is because the AQAM activates the low-order modulation modes or disables transmissions completely, when the channel envelope is in a deep fade, in order to avoid

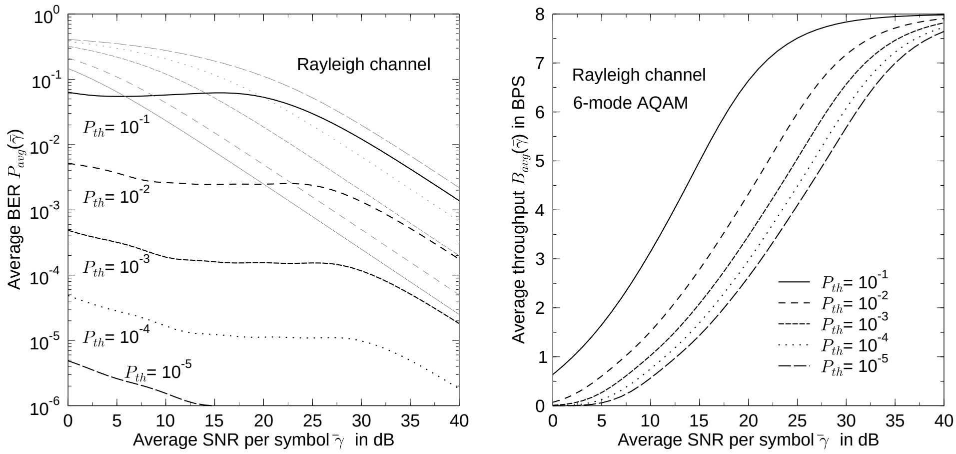

(a) average BER **(b)** average throughput

Figure 22.9: The performance of the six-mode AQAM employing the switching levels of (22.38) designed for limiting the peak instantaneous BEP.

inflicting bursts of bit errors.

Figure 22.8(b) compares the average BPS throughput of the AQAM scheme employing various numbers of AQAM modes and those of the fixed QAM constituent modes achieving the same average BER. When we want to achieve the target throughput of $B_{avg} = 1$ BPS using the AQAM scheme, Figure 22.8(b) suggest that 3-mode AQAM employing No-Tx, BPSK and QPSK is as good as four-mode AQAM, or in fact any other AQAM schemes employing more than four modes. In this case, the SNR gain achievable by AQAM is 7.7dB at the average BEP of $P_{avg} = 1.154 \times 10^{-2}$. For the average throughputs of $B_{avg} = 2$, 4 and 6, the SNR gains of the 6-mode AQAM schemes over the fixed QAM schemes are 6.65dB, 5.82dB and 5.12dB, respectively.

Figure 22.9 shows the performance of the six-mode AQAM scheme, which is an extended version of the five-mode AQAM of Section 22.7.2.1, for the peak instantaneous BEP values of $P_{th} = 10^{-1}$, 10^{-2}, 10^{-3}, 10^{-4} and 10^{-5}. We can observe in Figure 22.9(a) that the corresponding average BER P_{avg} decreases as P_{th} decreases. The average throughput curves seen in Figure 22.9(b) indicate that as anticipated the increased average SNR facilitates attaining an increased throughput by the AQAM scheme and there is a clear design trade-off between the achievable average throughput and the peak instantaneous BEP. This is because predominantly lower-throughput, but more error-resilient AQAM modes have to be activated, when the target BER is low. By contrast, higher-throughput but more error-sensitive AQAM modes are favoured, when the tolerable BEP is increased.

In conclusion, we introduced an adaptive modulation scheme, where the objective is to limit the peak instantaneous BEP. A set of switching levels designed for meeting this objective was given in (22.38), which is independent of the underlying fading channel and the average SNR. The corresponding average BEP and throughput formulae were derived in Section 22.7.3.1 and some performance characteristics of a range of AQAM schemes for transmitting over a flat Rayleigh channel were presented in order to demonstrate the effectiveness of the adaptive modulation scheme using the analysis technique developed in Section 22.7.3.1. The main advantage of this adaptive modulation scheme is in its simplicity regarding the design of the AQAM switching levels, while its drawback is that there is no direct relationship between the peak instantaneous BEP and the average BEP, which was used as our performance measure. In the next section a different switching-level optimization philosophy is introduced and contrasted with the approach of designing the switching levels for maintaining a given peak instantaneous BEP.

22.8.2 Torrance's Switching Levels

Torrance and Hanzo [184] proposed the employment of the following cost function and applied Powell's optimization method [187] for generating the optimum switching levels:

$$\Omega_T(\mathbf{s}) = \sum_{\bar{\gamma}=0\text{dB}}^{40\text{dB}} \left[10\log_{10}(\max\{P_{avg}(\bar{\gamma};\mathbf{s})/P_{th}, 1\}) + B_{max} - B_{avg}(\bar{\gamma};\mathbf{s})\right] , \qquad (22.39)$$

where the average BEP P_{avg} is given in (22.21), $\bar{\gamma}$ is the average SNR per symbol, $\mathbf{s}$ is the set of switching levels, P_{th} is the target average BER, B_{max} is the BPS throughput of the highest order constituent modulation mode and the average throughput B_{avg} is given in (22.14). The idea behind employing the cost function Ω_T is that of maximizing the average throughput B_{avg}, while endeavouring to maintain the target average BEP P_{th}. Following the philosophy of Section 22.8.1, the minimization of the cost function of (22.39) produces a set of constant switching levels across the entire SNR range. However, since the calculation of P_{avg} and B_{avg} requires the knowledge of the PDF of the instantaneous SNR γ per symbol, in reality the set of switching levels $\mathbf{s}$ required for maintaining a constant P_{avg} is dependent on the channel encountered and the receiver structure used.

Figure 22.10 illustrates the operation of a five-mode AQAM scheme employing *Torrance*'s SNR-independent switching levels designed for maintaining the target average BEP of $P_{th} = 10^{-2}$ over a flat Rayleigh channel. The average SNR was $\bar{\gamma} = 10$dB and the target average BEP was $P_{th} = 10^{-2}$. *Powell*'s minimization [187] involved in the context of (22.39) provides the set of optimised switching levels, given by $s_1 = 2.367$, $s_2 = 4.055$, $s_3 = 15.050$ and $s_4 = 56.522$. Upon comparing Figure 22.10(a) to Figure 22.7(a) we find that the two schemes are nearly identical in terms of activating the various AQAM modes according to the channel envelope trace, while the peak instantaneous BEP associated with Torrance's switching scheme is not constant. This is in contrast to the constant peak instantaneous BEP values seen in Figure 22.7(a). The mode selection probabilities depicted in Figure 22.10(b) are similar to those seen in Figure 22.7(b).

The average BEP curves, depicted in Figure 22.11(a) show that *Torrance*'s switching levels support the AQAM scheme in successfully maintaining the target average BEP of $P_{th} = 10^{-2}$ over the average SNR range of 0dB to 20dB, when five or six modem modes are employed by the AQAM scheme. Most of the AQAM studies found in the literature have applied *Torrance*'s switching levels owing to the above mentioned good agreement between the design target P_{th} and the actual BEP performance P_{avg} [674].

Figure 22.11(b) compares the average throughputs of a range of AQAM schemes employ-

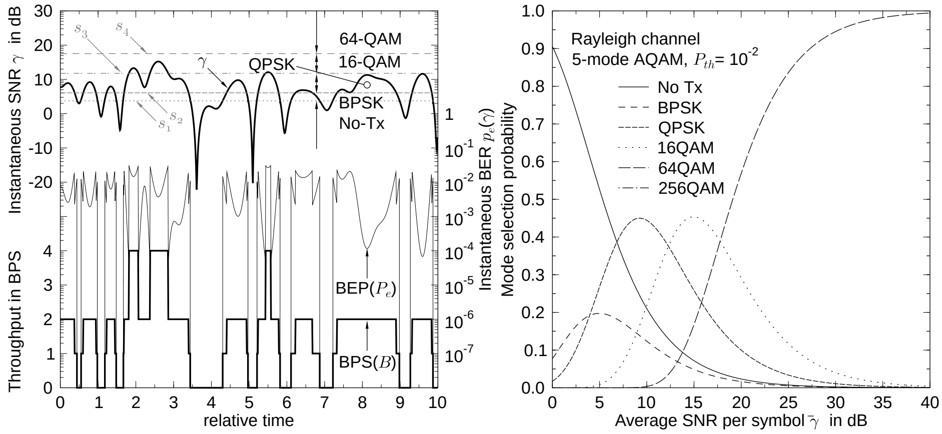

(a) operation of AQAM

(b) mode selection probability

Figure 22.10: Performance of the five-mode AQAM scheme over a flat Rayleigh fading channel employing the set of switching levels derived by Torrance and Hanzo [184] for achieving the target average BEP of $P_{th} = 10^{-2}$. (a) The instantaneous channel SNR γ is represented as a thick line at the top part of the graph, the associated instantaneous BEP $p_e(\gamma)$ as a thin line at the middle, and the instantaneous BPS throughput $b(\gamma)$ as a thick line at the bottom. The average SNR is $\bar{\gamma} = 10$dB. (b) As the SNR increases, the higher-order AQAM modes are selected more often.

ing various numbers of AQAM modes to the average BPS throughput of fixed-mode QAM arrangements achieving the same average BEP, *i.e.* $P_e = P_{avg}$, which is not necessarily identical to the target BEP of $P_e = P_{th}$. Specifically, the SNR values required by the fixed mode scheme in order to achieve $P_e = P_{avg}$ are represented by the markers '$\otimes$', while the SNRs, where the target average BEP of $P_e = P_{th}$ is achieved, is denoted by the markers '$\odot$'. Compared to the fixed QAM schemes achieving $P_e = P_{avg}$, the SNR gains of the AQAM scheme were 9.06dB, 7.02dB, 5.81dB and 8.74dB for the BPS throughput values of 1, 2, 4 and 6, respectively. By contrast, the corresponding SNR gains compared to the fixed QAM schemes achieving $P_e = P_{th}$ were 7.55dB, 6.26dB, 5.83dB and 1.45dB. We can observe that the SNR gain of the AQAM arrangement over the 64-QAM scheme achieving a BEP of $P_e = P_{th}$ is small compared to the SNR gains attained in comparison to the lower-throughput fixed-mode modems. This is due to the fact that the AQAM scheme employing *Torrance*'s switching levels allows the target BEP to drop at a high average SNR due to its sub-optimum thresholds, which prevents the scheme from increasing the average throughput steadily to the maximum achievable BPS throughput. This phenomenon is more visible for low target average BERs, as it can be observed in Figure 22.12.

In conclusion, we reviewed an adaptive modulation scheme employing Torrance's switching levels [184], where the objective was to maximize the average BPS throughput, while maintaining the target average BEP. Torrance's switching levels are constant across the entire SNR range and the average BEP P_{avg} of the AQAM scheme employing these switching lev-

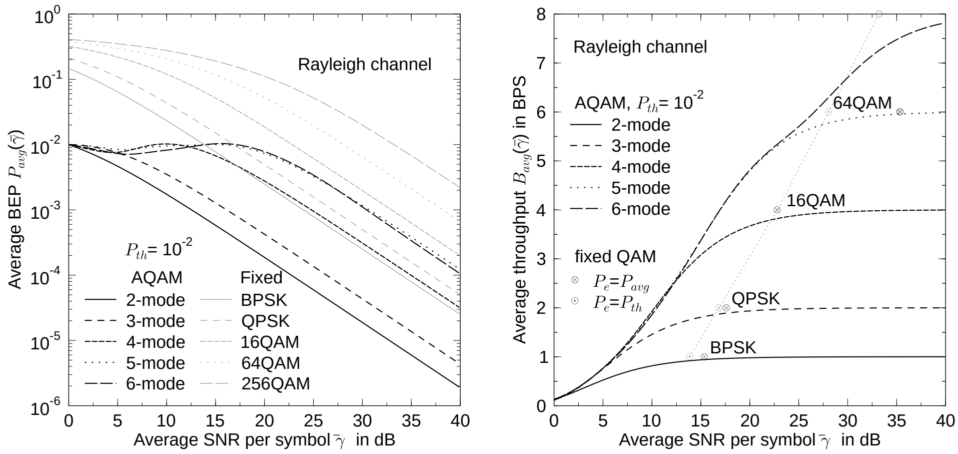

(a) average BER **(b)** average throughput

Figure 22.11: The performance of various AQAM systems employing *Torrance*'s switching levels [184] designed for the target average BEP of $P_{th} = 10^{-2}$. (a) The actual average BEP P_{avg} is close to the target BEP of $P_{th} = 10^{-2}$ over an average SNR range which becomes wider, as the number of modulation modes increases. However, the five-mode and six-mode AQAM schemes have a similar performance across much of the SNR range. (b) The SNR gains of the AQAM scheme over the fixed-mode QAM arrangements, while achieving the same throughput at the same average BEP, *i.e.* $P_e = P_{avg}$, range from 6dB to 9dB, which corresponds to a 1dB improvement compared to the SNR gains observed in Figure 22.8(b). However, the SNR gains over the fixed mode QAM arrangement achieving the target BEP of $P_e = P_{avg}$ are reduced, especially at high average SNR values, namely for $\bar{\gamma} > 25$dB.

els shows good agreement with the target average BEP P_{th}. However, the range of average SNR values, where $P_{avg} \simeq P_{th}$ was limited up to 25dB.

22.8.3 Cost Function Optimization as a Function of the Average SNR

In the previous section, we investigated *Torrance*'s switching levels [184] designed for achieving a certain target average BEP. However, the actual average BEP of the AQAM system was not constant across the SNR range, implying that the average throughput could potentially be further increased. Hence here we propose a modified cost function $\Omega(\mathbf{s};\bar{\gamma})$, putting more emphasis on achieving a higher throughput and optimise the switching levels for a given SNR, rather than for the whole SNR range [186]:

$$\Omega(\mathbf{s};\bar{\gamma}) = 10\log_{10}(\max\{P_{avg}(\bar{\gamma};\mathbf{s})/P_{th}, 1\}) + \rho\log_{10}(B_{max}/B_{avg}(\bar{\gamma};\mathbf{s})) \;, \quad (22.40)$$

where $\mathbf{s}$ is a set of switching levels, $\bar{\gamma}$ is the average SNR per symbol, P_{avg} is the average BEP of the adaptive modulation scheme given in (22.21), P_{th} is the target average BEP of the adaptive modulation scheme, B_{max} is the BPS throughput of the highest order constituent

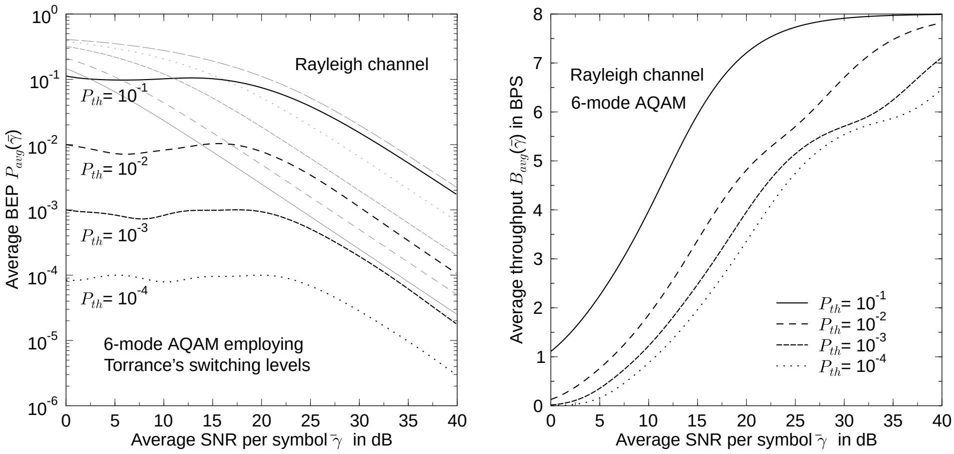

(a) average BER **(b)** average throughput

Figure 22.12: The performance of the six-mode AQAM scheme employing Torrance's switching levels [184] for various target average BERs. When the average SNR is over 25dB and the target average BEP is low, the average BEP of the AQAM scheme begins to decrease, preventing the scheme from increasing the average BPS throughput steadily.

modulation mode. Furthermore, the average throughput B_{avg} is given in (22.14) and ρ is a weighting factor, facilitating the above-mentioned BPS throughput enhancement. The first term at the right hand side of (22.40) corresponds to a cost function, which accounts for the difference, in the logarithmic domain, between the average BEP P_{avg} of the AQAM scheme and the target BEP P_{th}. This term becomes zero, when $P_{avg} \leq P_{th}$, contributing no cost to the overall cost function Ω. On the other hand, the second term of (22.40) accounts for the logarithmic distance between the maximum achievable BPS throughput B_{max} and the average BPS throughput B_{avg} of the AQAM scheme, which decreases, as B_{avg} approaches B_{max}. Applying Powell's minimization [187] to this cost function under the constraint of $s_{k-1} \leq s_k$, the optimum set of switching levels $\mathrm{s}_{opt}(\bar{\gamma})$ can be obtained, resulting in the highest average BPS throughput, while maintaining the target average BEP.

Figure 22.13 depicts the switching levels versus the average SNR per symbol optimised in this manner for a five-mode AQAM scheme achieving the target average BEP of $P_{th} = 10^{-2}$ and 10^{-3}. Since the switching levels are optimised for each specific average SNR value, they are not constant across the entire SNR range. As the average SNR $\bar{\gamma}$ increases, the switching levels decrease in order to activate the higher-order mode modulation modes more often in an effort to increase the BPS throughput. The low-order modulation modes are abandoned one by one, as $\bar{\gamma}$ increases, activating always the highest-order modulation mode, namely 64-QAM, when the average BEP of the fixed-mode 64-QAM scheme becomes lower, than the target average BEP P_{th}. Let us define the *avalanche SNR* $\bar{\gamma}_\alpha$ of a K-mode adaptive modulation scheme as the lowest SNR, where the target BEP is achieved, which can be

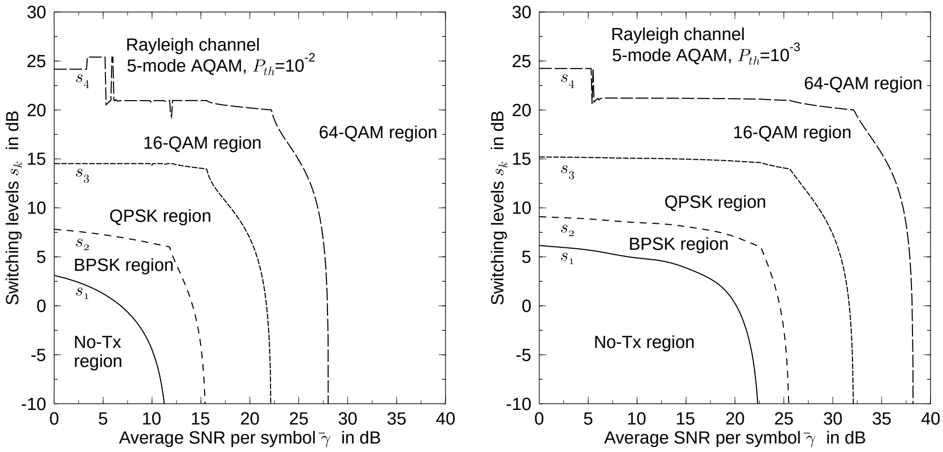

(a) $P_{th} = 10^{-2}$

(b) $P_{th} = 10^{-3}$

Figure 22.13: The switching levels optimised at each average SNR value in order to achieve the target average BEP of (a) $P_{th} = 10^{-2}$ and (b) $P_{th} = 10^{-3}$. As the average SNR $\bar{\gamma}$ increases, the switching levels decrease in order to activate the higher-order mode modulation modes more often in an effort to increase the BPS throughput. The low-order modulation modes are abandoned one by one as $\bar{\gamma}$ increases, activating the highest-order modulation mode, namely 64-QAM, all the time when the average BEP of the fixed-mode 64-QAM scheme becomes lower than the target average BEP P_{th}.

formulated as:

$$P_{e,m_K}(\bar{\gamma}_\alpha) = P_{th} \,, \tag{22.41}$$

where m_K is the highest order modulation mode, P_{e,m_K} is the average BEP of the fixed-mode m_K-ary modem activated at the average SNR of $\bar{\gamma}$ and P_{th} is the target average BEP of the adaptive modulation scheme. We can observe in Figure 22.13 that when the average channel SNR is higher than the avalanche SNR, *i.e.* $\bar{\gamma} \geq \bar{\gamma}_\alpha$, the switching levels are reduced to zero. Some of the optimised switching level versus SNR curves exhibit glitches, indicating that the multi-dimensional optimization might result in local optima in some cases.

The corresponding average BEP P_{avg} and the average throughput B_{avg} of the two to six-mode AQAM schemes designed for the target average BEP of $P_{th} = 10^{-2}$ are depicted in Figure 22.14. We can observe in Figure 22.14(a) that now the actual average BEP P_{avg} of the AQAM scheme is exactly the same as the target BEP of $P_{th} = 10^{-2}$, when the average SNR $\bar{\gamma}$ is less than or equal to the avalanche SNR $\bar{\gamma}_\alpha$. As the number of AQAM modulation modes K increases, the range of average SNRs where the design target of $P_{avg} = P_{th}$ is met extends to a higher SNR, namely to the avalanche SNR. In Figure 22.14(b), the average BPS throughputs of the AQAM modems employing the 'per-SNR optimised' switching levels introduced in this section are represented in thick lines, while the BPS throughput of the six-mode AQAM arrangement employing Torrance's switching levels [184] is represented using a solid thin

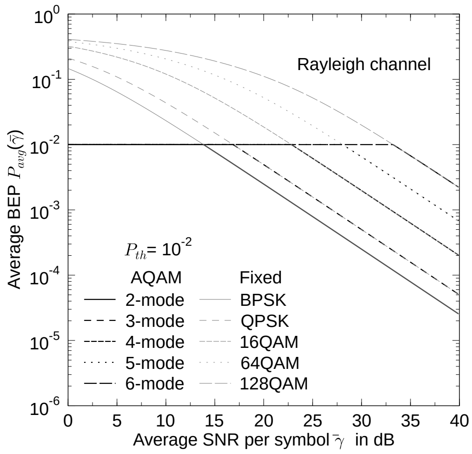

(a) average BEP

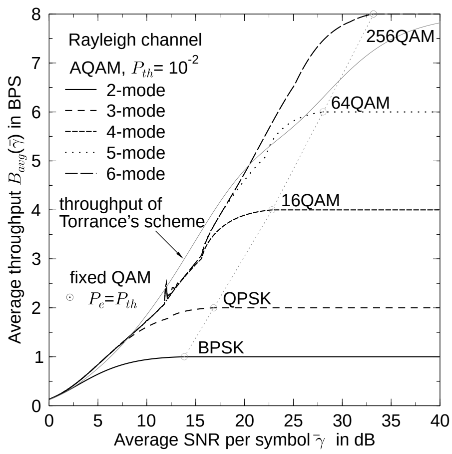

(b) average throughput

Figure 22.14: The performance of K-mode AQAM schemes for $K = 2, 3, 4, 5$ and 6, employing the switching levels optimised for each SNR value designed for the target average BEP of $P_{th} = 10^{-2}$. (a) The actual average BEP P_{avg} is exactly the same as the target BER of $P_{th} = 10^{-2}$, when the average SNR $\bar{\gamma}$ is less than or equal to the so-called avalanche SNR $\bar{\gamma}_\alpha$, where the average BEP of the highest-order fixed-modulation mode is equal to the target average BEP. (b) The average throughputs of the AQAM modems employing the 'per-SNR optimised' switching levels are represented in the thick lines, while that of the six-mode AQAM scheme employing Torrance's switching levels [184] is represented by a solid thin line.

line. The average SNR values required by the fixed-mode QAM scheme for achieving the target average BEP of $P_{e,m_K} = P_{th}$ are represented by the markers '$\odot$'. As we can observe in Figure 22.14(b) the new per-SNR optimised scheme produces a higher BPS throughput, than the scheme using Torrance's switching regime, when the average SNR $\bar{\gamma} > 20$dB. However, for the range of 8dB $< \bar{\gamma} <$ 20dB, the BPS throughput of the new scheme is lower than that of *Torrance*'s scheme, indicating that the multi-dimensional optimization technique might reach local minima for some SNR values.

Figure 22.15(a) shows that the six-mode AQAM scheme employing 'per-SNR optimised' switching levels satisfies the target average BEP values of $P_{th} = 10^{-1}$ to 10^{-4}. However, the corresponding average throughput performance shown in Figure 22.15(b) also indicates that the thresholds generated by the multi-dimensional optimization were not satisfactory. The BPS throughput achieved was heavily dependent on the value of the weighting factor ρ in (22.40). The glitches seen in the BPS throughput curves in Figure 22.15(b) also suggest that the optimization process might result in some local minima.

We conclude that due to these problems it is hard to achieve a satisfactory BPS throughput for adaptive modulation schemes employing the switching levels optimised for each SNR value based on the heuristic cost function of (22.40), while the corresponding average BEP exhibits a perfect agreement with the target average BEP.

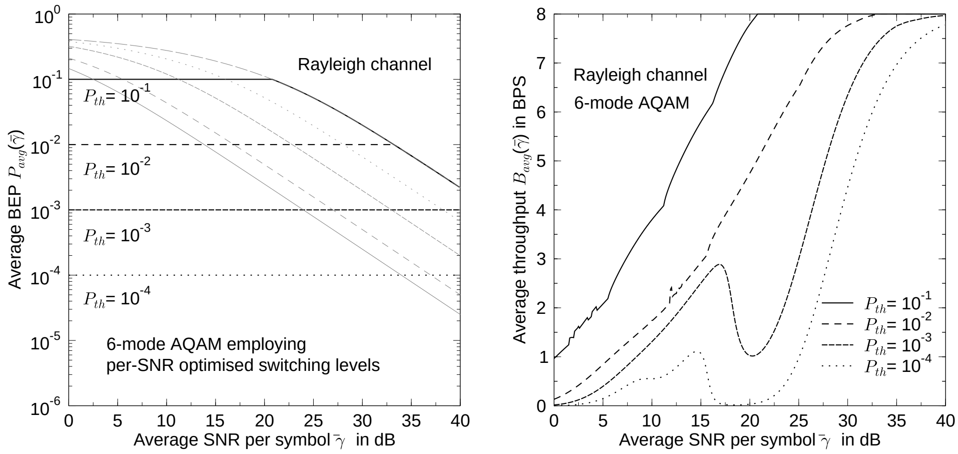

(a) average BER **(b)** average throughput

Figure 22.15: The performance of six-mode AQAM employing 'per-SNR optimised' switching levels for various values of the target average BEP. (a) The average BEP P_{avg} remains constant until the average SNR $\bar{\gamma}$ reaches the avalanche SNR, then follows the average BEP curve of the highest-order fixed-mode QAM scheme, *i.e.* that of 256-QAM. (b) For some SNR values the BPS throughput performance of the six-mode AQAM scheme is not satisfactory due to the fact that the multi-dimensional optimization algorithm becomes trapped in local minima and hence fails to reach the global minimum.

22.8.4 Lagrangian Method

As argued in the previous section, Powell's minimization [187] of the cost function often leads to a local minimum, rather than to the global minimum. Hence, here we adopt an analytical approach to finding the globally optimised switching levels. Our aim is to optimise the set of switching levels, $\mathbf{s}$, so that the average BPS throughput $B(\bar{\gamma};\mathbf{s})$ can be maximized under the constraint of $P_{avg}(\bar{\gamma};\mathbf{s}) = P_{th}$. Let us define P_R for a K-mode adaptive modulation scheme as the sum of the mode-specific average BEP weighted by the BPS throughput of the individual constituent mode:

$$P_R(\bar{\gamma};\mathbf{s}) \triangleq \sum_{k=0}^{K-1} b_k\, P_k\;, \tag{22.42}$$

where $\bar{\gamma}$ is the average SNR per symbol, $\mathbf{s}$ is the set of switching levels, K is the number of constituent modulation modes, b_k is the BPS throughput of the k-th constituent mode and the mode-specific average BEP P_k is given in (22.20) as:

$$P_k = \int_{s_k}^{s_{k+1}} p_{m_k}(\gamma)\, f(\gamma)\, d\gamma\;, \tag{22.43}$$

where again, $p_{m_k}(\gamma)$ is the BEP of the m_k-ary modulation scheme over the AWGN channel and $f(\gamma)$ is the PDF of the SNR per symbol γ. Explicitly, (22.43) implies weighting the BEP $p_{m_k}(\gamma)$ by its probability of occurrence quantified in terms of its PDF and then averaging, *i.e.* integrating it over the range spanning from s_k to s_{k+1}. Then, with the aid of (22.21), the average BEP constraint can also be written as:

$$P_{avg}(\bar{\gamma};\mathbf{s}) = P_{th} \iff P_R(\bar{\gamma};\mathbf{s}) = P_{th}\, B(\bar{\gamma};\mathbf{s}) \; . \tag{22.44}$$

Another rational constraint regarding the switching levels can be expressed as:

$$s_k \;\leq\; s_{k+1} \; . \tag{22.45}$$

As we discussed before, our optimization goal is to maximize the objective function $B(\bar{\gamma};\mathbf{s})$ under the constraint of (22.44). The set of switching levels $\mathbf{s}$ has $K+1$ levels in it. However, considering that we have $s_0 = 0$ and $s_K = \infty$ in many adaptive modulation schemes, we have $K-1$ independent variables in $\mathbf{s}$. Hence, the optimization task is a $K-1$ dimensional optimization under a constraint [675]. It is a standard practice to introduce a modified object function using a Lagrangian multiplier and convert the problem into a set of one-dimensional optimization problems. The modified object function Λ can be formulated employing a Lagrangian multiplier λ [675] as:

$$\Lambda(\mathbf{s};\bar{\gamma}) = B(\bar{\gamma};\mathbf{s}) + \lambda\left\{P_R(\bar{\gamma};\mathbf{s}) - P_{th}\, B(\bar{\gamma};\mathbf{s})\right\} \tag{22.46}$$

$$= (1-\lambda P_{th})\, B(\bar{\gamma};\mathbf{s}) + \lambda P_R(\bar{\gamma};\mathbf{s}) \; . \tag{22.47}$$

The optimum set of switching levels should satisfy:

$$\frac{\partial \Lambda}{\partial \mathbf{s}} = \frac{\partial}{\partial \mathbf{s}}\left(B(\bar{\gamma};\mathbf{s}) + \lambda\left\{P_R(\bar{\gamma};\mathbf{s}) - P_{th}\, B(\bar{\gamma};\mathbf{s})\right\}\right) = 0 \quad \text{and} \tag{22.48}$$

$$P_R(\bar{\gamma};\mathbf{s}) - P_t\, B(\bar{\gamma};\mathbf{s}) = 0 \; . \tag{22.49}$$

The following results are helpful in evaluating the partial differentiations in (22.48) :

$$\frac{\partial}{\partial s_k} P_{k-1} = \frac{\partial}{\partial s_k}\int_{s_{k-1}}^{s_k} p_{m_{k-1}}(\gamma)\, f(\gamma)\, d\gamma = p_{m_{k-1}}(s_k)\, f(s_k) \tag{22.50}$$

$$\frac{\partial}{\partial s_k} P_k = \frac{\partial}{\partial s_k}\int_{s_k}^{s_{k+1}} p_{m_k}(\gamma)\, f(\gamma)\, d\gamma = -p_{m_k}(s_k)\, f(s_k) \tag{22.51}$$

$$\frac{\partial}{\partial s_k} F_c(s_k) = \frac{\partial}{\partial s_k}\int_{s_k}^{\infty} f(\gamma)\, d\gamma = -f(s_k) \; . \tag{22.52}$$

Using (22.50) and (22.51), the partial differentiation of P_R defined in (22.42) with respect to s_k can be written as:

$$\frac{\partial P_R}{\partial s_k} = b_{k-1}\, p_{m_{k-1}}(s_k)\, f(s_k) - b_k\, p_{m_k}(s_k)\, f(s_k) \; , \tag{22.53}$$

where b_k is the BPS throughput of an m_k-ary modem. Since the average throughput is given by $B = \sum_{k=0}^{K-1} c_k\, F_c(s_k)$ in (22.18), the partial differentiation of B with respect to s_k can be written as, using (22.52) :

$$\frac{\partial B}{\partial s_k} = -c_k\, f(s_k)\ , \tag{22.54}$$

where c_k was defined as $c_k \triangleq b_k - b_{k-1}$ in Section 22.7.1. Hence (22.48) can be evaluated as:

$$\left[-c_k(1-\lambda\, P_{th}) + \lambda\left\{b_{k-1}\, p_{m_{k-1}}(s_k) - b_k p_{m_k}(s_k)\right\}\right]\ f(s_k) = 0 \ \text{ for } k = 1, 2, \cdots, K-1\ . \tag{22.55}$$

A trivial solution of (22.55) is $f(s_k) = 0$. Certainly, $\{s_k = \infty,\ k = 1, 2, \cdots, K-1\}$ satisfies this condition. Again, the lowest throughput modulation mode is 'No-Tx' in our model, which corresponds to no transmission. When the PDF of γ satisfies $f(0) = 0$, $\{s_k = 0,\ k = 1, 2, \cdots, K-1\}$ can also be a solution, which corresponds to the fixed-mode m_{K-1}-ary modem. The corresponding avalanche SNR $\bar{\gamma}_\alpha$ can obtained by substituting $\{s_k = 0,\ k = 1, 2, \cdots, K-1\}$ into (22.49), which satisfies:

$$p_{m_{K-1}}(\bar{\gamma}_\alpha) - P_{th} = 0\ . \tag{22.56}$$

When $f(s_k) \neq 0$, Equation (22.55) can be simplified upon dividing both sides by $f(s_k)$, yielding:

$$-c_k(1-\lambda\, P_{th}) + \lambda\left\{b_{k-1}\, p_{m_{k-1}}(s_k) - b_k p_{m_k}(s_k)\right\} = 0 \ \text{ for } k = 1, 2, \cdots, K-1\ . \tag{22.57}$$

Rearranging (22.57) for $k = 1$ and assuming $c_1 \neq 0$, we have:

$$1 - \lambda\, P_{th} = \frac{\lambda}{c_1}\left\{b_0\, p_{m_0}(s_1) - b_1 p_{m_1}(s_1)\right\}. \tag{22.58}$$

Substituting (22.58) into (22.57) and assuming $c_k \neq 0$ for $k \neq 0$, we have:

$$\frac{\lambda}{c_k}\left\{b_{k-1}\, p_{m_{k-1}}(s_k) - b_k p_{m_k}(s_k)\right\} = \frac{\lambda}{c_1}\left\{b_0\, p_{m_0}(s_1) - b_1 p_{m_1}(s_1)\right\}. \tag{22.59}$$

In this context we note that the Lagrangian multiplier λ is not zero because substitution of $\lambda = 0$ in (22.57) leads to $-c_k = 0$, which is not true. Hence, we can eliminate the Lagrangian multiplier dividing both sides of (22.59) by λ. Then we have:

$$y_k(s_k) = y_1(s_1) \ \text{ for } k = 2, 3, \cdots K-1\ , \tag{22.60}$$

where the function $y_k(s_k)$ is defined as:

$$y_k(s_k) \triangleq \frac{1}{c_k}\left\{b_k p_{m_k}(s_k) - b_{k-1}\, p_{m_{k-1}}(s_k)\right\}\ ,\ k = 2, 3, \cdots K-1\ , \tag{22.61}$$

which does not contain the Lagrangian multiplier λ and hence it will be referred to as the 'Lagrangian-free function'. This function can be physically interpreted as the normalized

BEP difference between the adjacent AQAM modes. For example, $y_1(s_1) = p_2(s_1)$ quantifies the BEP increase, when switching from the No-Tx mode to the BPSK mode, while $y_2(s_2) = 2\,p_4(s_2) - p_2(s_2)$ indicates the BEP difference between the QPSK and BPSK modes. These curve will be more explicitly discussed in the context of Figure 22.16. The significance of (22.60) is that the relationship between the optimum switching levels s_k, where $k = 2, 3, \cdots K-1$, and the lowest optimum switching level s_1 is independent of the underlying propagation scenario. Only the constituent modulation mode related parameters, such as b_k, c_k and $p_{m_k}(\gamma)$, govern this relationship.

Let us now investigate some properties of the Lagrangian-free function $y_k(s_k)$ given in (22.61). Considering that $b_k > b_{k-1}$ and $p_{m_k}(s_k) > p_{m_{k-1}}(s_k)$, it is readily seen that the value of $y_k(s_k)$ is always positive. When $s_k = 0$, $y_k(s_k)$ becomes:

$$y_k(0) \triangleq \frac{1}{c_k}\left\{b_k p_{m_k}(0) - b_{k-1}\,p_{m_{k-1}}(0)\right\} = \frac{1}{c_k}\left\{\frac{b_k}{2} - \frac{b_{k-1}}{2}\right\} = \frac{1}{2}\,. \tag{22.62}$$

The solution of $y_k(s_k) = 1/2$ can be either $s_k = 0$ or $b_k p_{m_k}(s_k) = b_{k-1}p_{m_{k-1}}(s_k)$. When $s_k = 0$, $y_k(s_k)$ becomes $y_k(\infty) = 0$. We also conjecture that

$$\frac{d\,s_k}{d\,s_1} = \frac{y_1^{'}(s_1)}{y_k^{'}(s_k)} \;>\; 0 \;\text{ when } y_k(s_k) = y_1(s_1), \tag{22.63}$$

which states that the k-th optimum switching level s_k always increases, whenever the lowest optimum switching level s_1 increases. Our numerical evaluations suggest that this conjecture appears to be true.

As an example, let us consider the five-mode AQAM scheme introduced in Section 22.7.2.1. The parameters of the five-mode AQAM scheme are summarised in Table 22.1. Substituting these parameters into (22.60) and (22.61), we have the following set of equations.

$$y_1(s_1) = p_2(s_1) \tag{22.64}$$
$$y_2(s_2) = 2\,p_4(s_2) - p_2(s_2) \tag{22.65}$$
$$y_3(s_3) = 2\,p_{16}(s_3) - p_4(s_3) \tag{22.66}$$
$$y_4(s_4) = 3\,p_{64}(s_4) - 2\,p_{16}(s_4) \tag{22.67}$$

The Lagrangian-free functions of (22.64) through (22.67) are depicted in Figure 22.16 for Gray-mapped square-shaped QAM. As these functions are basically linear combinations of BEP curves associated with AWGN channels, they exhibit waterfall-like shapes and asymptotically approach 0.5, as the switching levels s_k approach zero (or $-\infty$ expressed in dB). While $y_1(s_1)$ and $y_2(s_2)$ are monotonic functions, $y_3(s_3)$ and $y_4(s_4)$ cross the $y = 0.5$ line at $s_3 = -7.34$ dB and $s_4 = 1.82$ dB respectively, as it can be observed in Figure 22.16(b). One should also notice that the trivial solutions of (22.60) are $y_k = 0.5$ at $s_k = 0$, $k = 1,\,2,\,3,\,4$, as we have discussed before.

For a given value of s_1, the other switching levels can be determined as $s_2 = y_2^{-1}(y_1(s_1))$, $s_3 = y_3^{-1}(y_1(s_1))$ and $s_4 = y_4^{-1}(y_1(s_1))$. Since deriving the analytical inverse function of y_k is an arduous task, we can rely on a graphical or a numerical method. Figure 22.16(b) illustrates an example of the graphical method. Specifically, when $s_1 = \alpha_1$, we first find the point on the curve y_1 directly above the abscissa value of α_1 and then draw a horizontal

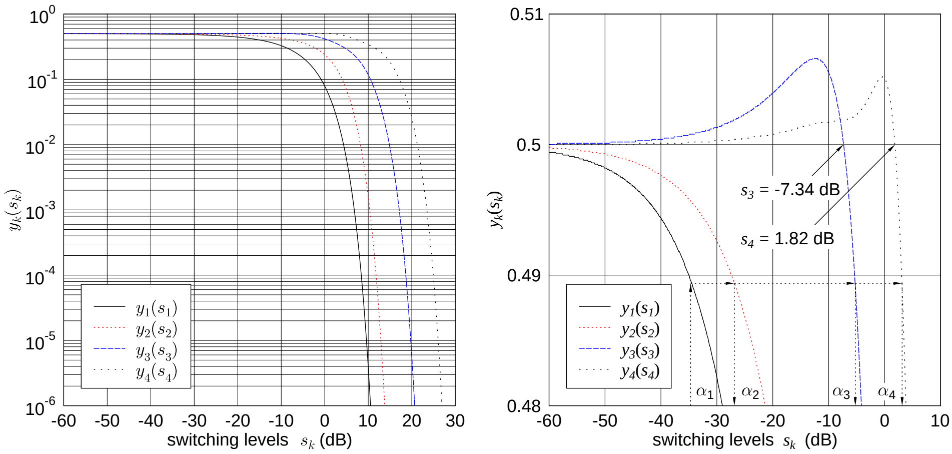

(a) global behaviour

(b) behaviour near 0.5

Figure 22.16: The Lagrangian-free functions $y_k(s_k)$ of (22.64) through (22.67) for Gray-mapped square-shaped QAM constellations. As s_k becomes lower $y_k(s_k)$ asymptotically approaches 0.5. Observe that while $y_1(s_1)$ and $y_2(s_2)$ are monotonic functions, $y_3(s_3)$ and $y_4(s_4)$ cross the $y = 0.5$ line.

line across the corresponding point. From the crossover points found on the curves of y_2, y_3 and y_4 with the aid of the horizontal line, we can find the corresponding values of the other switching levels, namely those of α_2, α_3 and α_4. In a numerical sense, this solution corresponds to a one-dimensional (1-D) root finding problem [187] (Chapter 9). Furthermore, the $y_k(s_k)$ values are monotonic, provided that we have $y_k(s_k) < 0.5$ and this implies that the roots found are unique. The numerical results shown in Figure 22.17 represent the direct relationship between the optimum switching level s_1 and the other optimum switching levels, namely s_2, s_3 and s_4. While the optimum value of s_2 shows a near-linear relationship with respect to s_1, those of s_3 and s_4 asymptotically approach two different constants, as s_1 becomes smaller. This corroborates the trends observed in Figure 22.16(b), where $y_3(s_3)$ and $y_4(s_4)$ cross the $y = 0.5$ line at $s_3 = -7.34$ dB and $s_4 = 1.82$ dB, respectively. Since the low-order modulation modes are abandoned at high average channel SNRs in order to increase the average throughput, the high values of s_1 on the horizontal axis of Figure 22.17 indicate encountering a low channel SNR, while low values of s_1 suggest that high channel SNRs are experienced, as it transpires for example from Figure 22.13.

Since we can relate the other switching levels to s_1, we have to determine the optimum value of s_1 for the given target BEP, P_{th}, and the PDF of the instantaneous channel SNR, $f(\gamma)$, by solving the constraint equation given in (22.49). This problem also constitutes a 1-D root finding problem, rather than a multi-dimensional optimization problem, which was the case in Sections 22.8.2 and 22.8.3. Let us define the constraint function $Y(\bar{\gamma}; \mathbf{s}(s_1))$ using

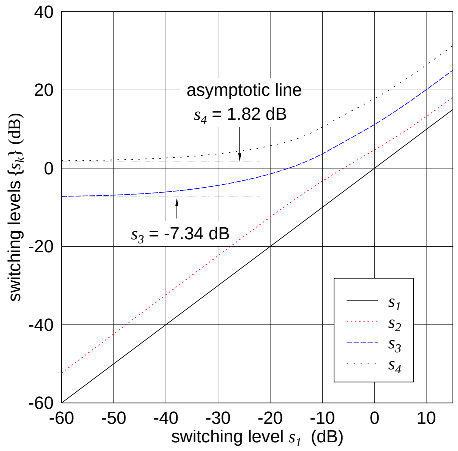

Figure 22.17: Optimum switching levels as functions of s_1, where the linear relationship of s_1 versus s_1 was also plotted for completeness. Observe that while the optimum value of s_2 shows a linear relationship with respect to s_1, those of s_3 and s_4 asymptotically approach constant values as s_1 is reduced.

(22.49) as:

$$Y(\bar{\gamma}; \mathbf{s}(s_1)) \triangleq P_R(\bar{\gamma}; \mathbf{s}(s_1)) - P_{th}\, B(\bar{\gamma}; \mathbf{s}(s_1)), \tag{22.68}$$

where we represented the set of switching levels as a vector, which is the function of s_1, in order to emphasise that s_k satisfies the relationships given by (22.60) and (22.61).

More explicitly, $Y(\bar{\gamma}; \mathbf{s}(s_1))$ of (22.68) can be physically interpreted as the difference between $P_R(\bar{\gamma}; \mathbf{s}(s_1))$, namely the sum of the mode-specific average BEPs weighted by the BPS throughput of the individual AQAM modes, as defined in (22.42) and the average BPS throughput $B(\bar{\gamma}; \mathbf{s}(s_1))$ weighted by the target BEP P_{th}. Considering the equivalence relationship given in (22.44), (22.68) reflects just another way of expressing the difference between the average BEP P_{avg} of the adaptive scheme and the target BEP P_{th}.

Even though the relationships implied in $\mathbf{s}(s_1)$ are independent of the propagation conditions and the signalling power, the constraint function $Y(\bar{\gamma}; \mathbf{s}(s_1))$ of (22.68) and hence the actual values of the optimum switching levels are dependent on propagation conditions through the PDF $f(\gamma)$ of the SNR per symbol and on the average SNR per symbol $\bar{\gamma}$.

Let us find the initial value of $Y(\bar{\gamma}; \mathbf{s}(s_1))$ defined in (22.68), when $s_1 = 0$. An obvious solution for s_k when $s_1 = 0$ is $s_k = 0$ for $k = 1, 2, \cdots, K-1$. In this case, $Y(\bar{\gamma}; \mathbf{s}(s_1))$ becomes:

$$Y(\bar{\gamma}; 0) = b_{K-1}\,(P_{m_{K-1}}(\bar{\gamma}) - P_{th}), \tag{22.69}$$

where b_{K-1} is the BPS throughput of the highest-order constituent modulation mode, while $P_{m_{K-1}}(\bar{\gamma})$ is the average BEP of the highest-order constituent modulation mode for transmission over the underlying channel scenario and P_{th} is the target average BEP. The value of $Y(\bar{\gamma}; 0)$ could be positive or negative, depending on the average SNR $\bar{\gamma}$ and on the target average BEP P_{th}. Another solution exists for s_k when $s_1 = 0$, if $b_k\, p_{m_k}(s_k) = b_{k-1}\, p_{m_{k-1}}(s_k)$.

The value of $Y(\bar{\gamma};0^+)$ using this alternative solution turns out to be close to $Y(\bar{\gamma};0)$. However, in the actual numerical evaluation of the initial value of Y, we should use $Y(\bar{\gamma};0^+)$ for ensuring the continuity of the function Y at $s_1 = 0$.

In order to find the minima and the maxima of Y, we have to evaluate the derivative of $Y(\bar{\gamma};\mathbf{s}(s_1))$ with respect to s_1. With the aid of (22.50) to (22.54), we have:

$$\begin{aligned}
\frac{dY}{ds_1} &= \sum_{k=1}^{K-1} \frac{\partial Y}{\partial s_k}\,\frac{ds_k}{ds_1} \\
&= \sum_{k=1}^{K-1} \frac{\partial}{\partial s_k}\,\{P_R - P_{th}\,B\}\,\frac{ds_k}{ds_1} \\
&= \sum_{k=1}^{K-1} \left\{b_{k-1}\,p_{m_{k-1}}(s_k) - b_k\,p_{m_k}(s_k) + P_{th}\,c_k\right\}\,f(s_k)\,\frac{ds_k}{ds_1} \\
&= \sum_{k=1}^{K-1} \left[\frac{c_k}{c_1}\,\{b_0\,p_{m_0}(s_1) - b_1\,p_{m_1}(s_1)\} + P_{th}\,c_k\right]\,f(s_k)\,\frac{ds_k}{ds_1} \\
&= \frac{1}{c_1}\,\{b_0\,p_{m_0}(s_1) - b_1\,p_{m_1}(s_1) + P_{th}\}\sum_{k=1}^{K-1} c_k\,f(s_k)\,\frac{ds_k}{ds_1}\;. \qquad (22.70)
\end{aligned}$$

Considering $f(s_k) \geq 0$ and using our conjecture that $\frac{ds_k}{ds_1} > 0$ given in (22.63), we can conclude from (22.70) that $\frac{dY}{ds_1} = 0$ has roots, when $f(s_k) = 0$ for all k or when $b_1\,p_{m_1}(s_1) - b_0\,p_{m_0}(s_1) = P_{th}$. The former condition corresponds to either $s_i = 0$ for some PDF $f(\gamma)$ or to $s_k = \infty$ for all PDFs. By contrast, when the condition of $b_1\,p_{m_1}(s_1) - b_0\,p_{m_0}(s_1) = P_{th}$ is met, $dY/ds_1 = 0$ has a unique solution. Investigating the sign of the first derivative between these zeros, we can conclude that $Y(\bar{\gamma};s_1)$ has a global minimum of Y_{min} at $s_1 = \zeta$ such that $b_1\,p_{m_1}(\zeta) - b_0\,p_{m_0}(\zeta) = P_{th}$ and a maximum of Y_{max} at $s_1 = 0$ and another maximum value at $s_1 = \infty$.

Since $Y(\bar{\gamma};s_1)$ has a maximum value at $s_1 = \infty$, let us find the corresponding maximum value. Let us first consider $\lim_{s_1\to\infty} P_{avg}(\bar{\gamma};\mathbf{s}(s_1))$, where upon exploiting (22.21) and (22.42) we have:

$$\lim_{s_1\to\infty} P_{avg}(\bar{\gamma};s_k) = \frac{\lim_{s_1\to\infty} P_R}{\lim_{s_1\to\infty} B} \qquad (22.71)$$

$$= \frac{0}{0}\;. \qquad (22.72)$$

When applying l'Hopital's rule and using Equations (22.50) through (22.54), we have:

$$\frac{\lim_{s_1\to\infty} P_R}{\lim_{s_1\to\infty} B} = \frac{\lim_{s_1\to\infty} \frac{d}{ds_1} P_R}{\lim_{s_1\to\infty} \frac{d}{ds_1} B} \qquad (22.73)$$

$$= \lim_{s_1\to\infty} \frac{1}{c_1}\,b_1\,p_{m_1}(s_1) - b_0\,p_{m_0}(s_1) \qquad (22.74)$$

$$= 0^+\;, \qquad (22.75)$$

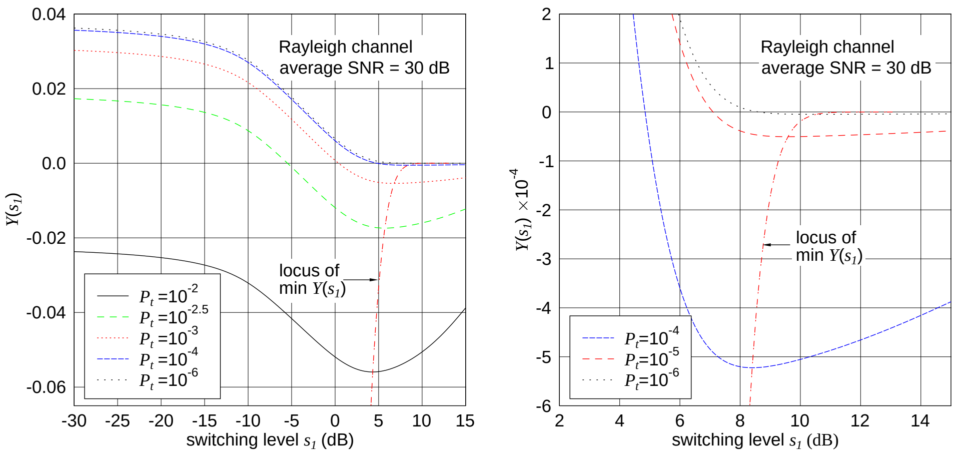

(a) global behaviour **(b)** behaviour near $Y(s_1) = 0$

Figure 22.18: The constraint function $Y(\bar{\gamma}; \mathbf{s}(s_1))$ defined in (22.68) for our five-mode AQAM scheme employing Gray-mapped square-constellation QAM operating over a flat Rayleigh fading channel. The average SNR was $\bar{\gamma} = 30$ dB and it is seen that Y has a single minimum value, while approaching 0^-, as s_1 increases. The solution of $Y(\bar{\gamma}; \mathbf{s}(s_1)) = 0$ exists, when $Y(\bar{\gamma}; 0) = 6\{p_{64}(\bar{\gamma}) - P_{th}\} > 0$ and is unique.

implying that $P_{avg}(\bar{\gamma}; s_k)$ approaches zero from positive values, when s_1 tends to ∞. Since according to (22.21), (22.42) and (22.68) the function $Y(\bar{\gamma}; \mathbf{s}(s_1))$ can be written as $B(P_{avg} - P_{th})$, we have:

$$\lim_{s_1 \to \infty} Y(\bar{\gamma}; s_1) = \lim_{s_1 \to \infty} B(P_{avg} - P_{th}) \tag{22.76}$$

$$= \lim_{s_1 \to \infty} B(0^+ - P_{th}) \tag{22.77}$$

$$= 0^- , \tag{22.78}$$

Hence $Y(\bar{\gamma}; \mathbf{s}(s_1))$ asymptotically approaches zero from negative values, as s_1 tends to ∞. From the analysis of the minimum and the maxima, we can conclude that the constraint function $Y(\bar{\gamma}; \mathbf{s}(s_1))$ defined in (22.68) has a unique zero only if $Y(\bar{\gamma}; 0^+) > 0$ at a switching value of $0 < s_1 < \zeta$, where ζ satisfies $b_1\, p_{m_1}(\zeta) - b_0\, p_{m_0}(\zeta) = P_{th}$. By contrast, when $Y(\bar{\gamma}; 0^+) < 0$, the optimum switching levels are all zero and the adaptive modulation scheme always employs the highest-order constituent modulation mode.

As an example, let us evaluate the constraint function $Y(\bar{\gamma}; s_1)$ for our five-mode AQAM scheme operating over a flat Rayleigh fading channel. Figure 22.18 depicts the values of $Y(s_1)$ for several values of the target average BEP P_{th}, when the average channel SNR is 30dB. We can observe that $Y(s_1) = 0$ may have a root, depending on the target BEP P_{th}.

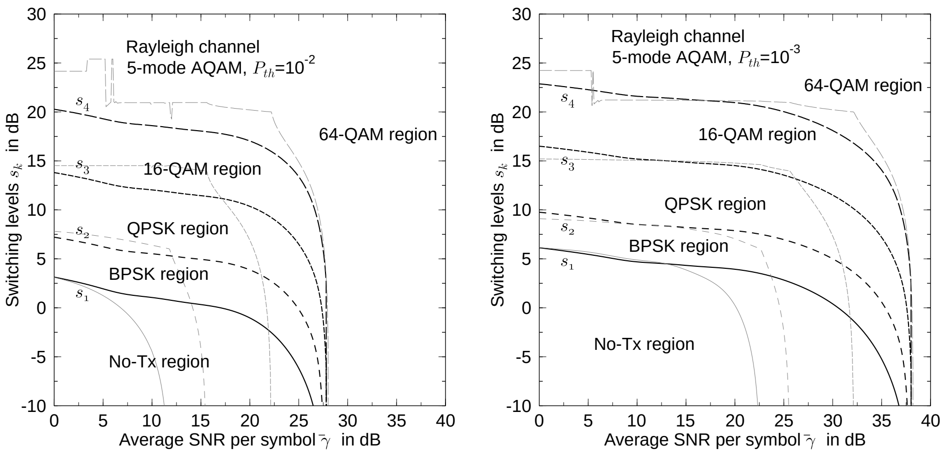

(a) $P_{th} = 10^{-2}$ **(b)** $P_{th} = 10^{-3}$

Figure 22.19: The switching levels for our five-mode AQAM scheme optimised at each average SNR value in order to achieve the target average BEP of (a) $P_{th} = 10^{-2}$ and (b) $P_{th} = 10^{-3}$ using the Lagrangian multiplier based method of Section 22.8.4. The switching levels based on Powell's optimization are represented in thin grey lines for comparison.

When $s_k = 0$ for $k < 5$, according to (22.21), (22.42) and (22.68) $Y(s_1)$ is reduced to

$$Y(\bar{\gamma}; 0) = 6(P_{64}(\bar{\gamma}) - P_{th}) \,, \tag{22.79}$$

where $P_{64}(\bar{\gamma})$ is the average BEP of 64-QAM over a flat Rayleigh channel. The value of $Y(\bar{\gamma}; 0)$ in (22.79) can be negative or positive, depending on the target BEP P_{th}.

We can observe in Figure 22.18 that the solution of $Y(\bar{\gamma}; \mathbf{s}(s_1)) = 0$ is unique, when it exists. The locus of the minimum $Y(s_1)$, *i.e.* the trace curve of points $(Y_{min}(s_{1,min}), s_{1,min})$, where Y has the minimum value, is also depicted in Figure 22.18. The locus is always below the horizontal line of $Y(s_1) = 0$ and asymptotically approaches this line, as the target BEP P_{th} becomes smaller.

Figure 22.19 depicts the switching levels optimised in this manner for our five-mode AQAM scheme maintaining the target average BEPs of $P_{th} = 10^{-2}$ and 10^{-3}. The switching levels obtained using Powell's optimization method in Section 22.8.3 are represented as the thin grey lines in Figure 22.19 for comparison. In this case all the modulation modes may be activated with a certain probability, until the average SNR reaches the avalanche SNR value, while the scheme derived using Powell's optimization technique abandons the lower throughput modulation modes one by one, as the average SNR increases.

Figure 22.20 depicts the average throughput B expressed in BPS of the AQAM scheme employing the switching levels optimised using the Lagrangian method. In Figure 22.20(a), the average throughput of our six-mode AQAM arrangement using Torrance's scheme discussed in Section 22.8.2 is represented as a thin grey line. The Lagrangian multiplier based scheme showed SNR gains of 0.6dB, 0.5dB, 0.2dB and 3.9dB for a BPS throughput of 1, 2, 4

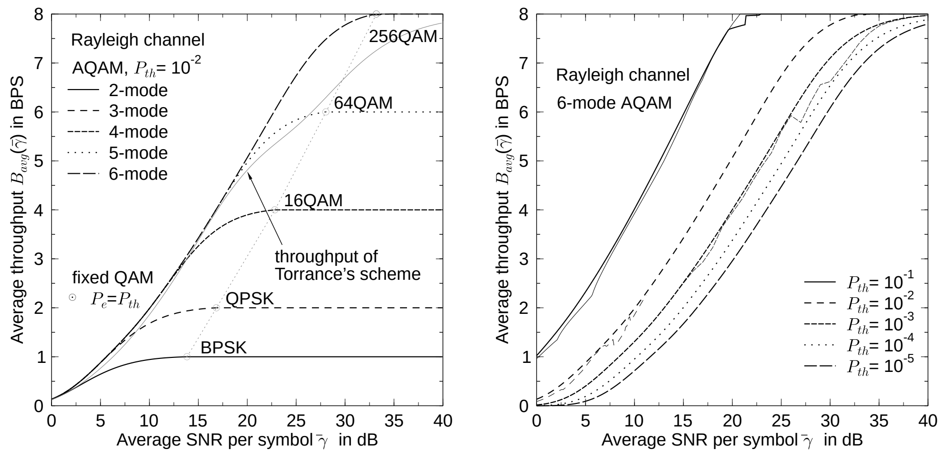

(a) $P_{th} = 10^{-2}$ **(b)** 6-mode AQAM

Figure 22.20: The average BPS throughput of various AQAM schemes employing the switching levels optimised using the Lagrangian multiplier method (a) for $P_{th} = 10^{-2}$ employing two to six-modes and (b) for $P_{th} = 10^{-2}$ to $P_{th} = 10^{-5}$ using six-modes. The average throughput of the six-mode AQAM scheme using Torrance's switching levels [184] is represented for comparison as the thin grey line in figure (a). The average throughput of the six-mode AQAM scheme employing per-SNR optimised thresholds using Powell's optimization method are represented by the thin lines in figure (b) for the target average BEP of $P_{th} = 10^{-1}$, 10^{-2} and 10^{-3}.

and 6, respectively, compared to Torrance's scheme. The average throughput of our six-mode AQAM scheme is depicted in Figure 22.20(b) for the several values of P_{th}, where the corresponding BPS throughput of the AQAM scheme employing per-SNR optimised thresholds determined using Powell's method are also represented as thin lines for $P_{th} = 10^{-1}$, 10^{-2} and 10^{-3}. Comparing the BPS throughput curves, we can conclude that the per-SNR optimised Powell method of Section 22.8.3 resulted in imperfect optimization for some values of the average SNR.

In conclusion, we derived an optimum mode-switching regime for a general AQAM scheme using the Lagrangian multiplier method and presented our numerical results for various AQAM arrangements. Since the results showed that the Lagrangian optimization based scheme is superior in comparison to the other methods investigated, we will employ these switching levels in order to further investigate the performance of various adaptive modulation schemes.

22.9 Results and Discussions

The average throughput performance of adaptive modulation schemes employing the globally optimised mode-switching levels of Section 22.8.4 is presented in this section. The mobile channel is modelled as a Nakagami-m fading channel. The performance results and discussions include the effects of the fading parameter m, that of the number of modulation modes, the influence of the various diversity schemes used and the range of Square QAM, Star QAM and MPSK signalling constellations.

22.9.1 Narrow-Band Nakagami-m Fading Channel

The PDF of the instantaneous channel SNR γ of a system transmitting over the Nakagami fading channel is given in (22.22). The parameters characterising the operation of the adaptive modulation scheme were summarised in Section 22.7.3.1.

22.9.1.1 Adaptive PSK Modulation Schemes

Phase Shift Keying (PSK) has the advantage of exhibiting a constant envelope power, since all the constellation points are located on a circle. Let us first consider the BEP of fixed-mode PSK schemes as a reference, so that we can compare the performance of adaptive PSK and fixed-mode PSK schemes. The BEP of Gray-coded coherent M-ary PSK (MPSK), where $M = 2^k$, for transmission over the AWGN channel can be closely approximated by [673]:

$$p_{MPSK}(\gamma) \simeq \sum_{i=1}^{2} A_i \, Q(\sqrt{a_i \gamma}\,) \,, \tag{22.80}$$

where $M \geq 8$ and the associated constants are given by [673]:

$$A_1 = A_2 = 2/k \tag{22.81}$$

$$a_1 = 2\sin^2(\pi/M) \tag{22.82}$$

$$a_2 = 2\sin^2(3\pi/M) \,. \tag{22.83}$$

Figure 22.21(a) shows the BEP of BPSK, QPSK, 8PSK, 16PSK, 32PSK and 64PSK for transmission over the AWGN channel. The differences of the required SNR per symbol, in order to achieve the BER of $p_{MPSK}(\gamma) = 10^{-6}$ for the modulation modes having a throughput difference of 1 BPS are around 6dB, except between BPSK and QPSK, where a 3dB difference is observed.

The average BEP of MPSK schemes over a flat Nakagami-m fading channel is given as:

$$P_{MPSK}(\bar{\gamma}) = \int_0^{\infty} p_{MPSK}(\gamma)\, f(\gamma)\, d\gamma \,, \tag{22.84}$$

where the BEP $p_{MPSK}(\gamma)$ for a transmission over the AWGN channel is given by (22.80) and the PDF $f(\gamma)$ is given by (22.22). A closed form solution of (22.84) can be readily obtained for an integer m using the results given in Section (14-4-15) of [388], which can be expressed as:

$$P_{MPSK}(\bar{\gamma}) = \sum_{i=1}^{2} A_i \left[\tfrac{1}{2}(1-\mu_i)\right]^m \sum_{j=0}^{m-1} \binom{m-1+j}{j} \left[\tfrac{1}{2}(1+\mu_i)\right]^j \,, \tag{22.85}$$

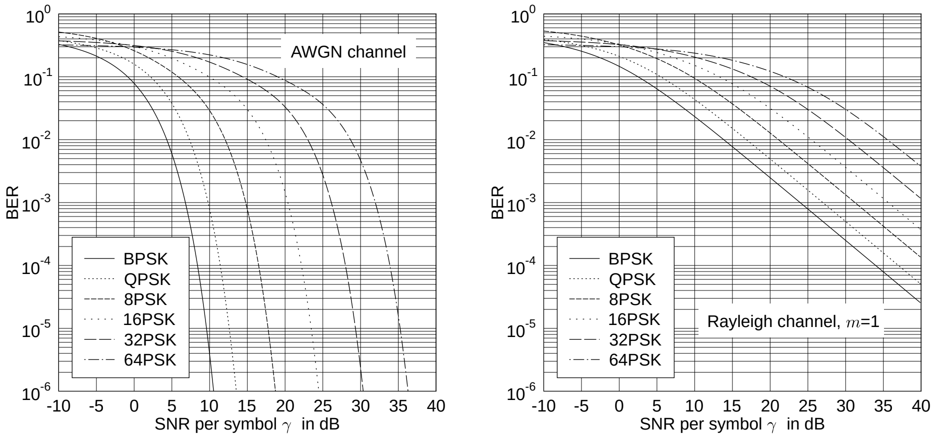

(a) AWGN Channel

(b) Rayleigh Channel, $m = 1$

Figure 22.21: The average BEP of various MPSK modulation schemes.

where μ_i is defined as:

$$\mu_i \triangleq \sqrt{\frac{a_i\bar{\gamma}}{2m + a_i\bar{\gamma}}} . \qquad (22.86)$$

Figure 22.21(b) shows the average BEP of the various MPSK schemes for transmission over a flat Rayleigh channel, where $m = 1$. The BEP of MPSK over the AWGN channel given in (22.80) and that over a Nakagami channel given in (22.85) will be used in comparing the performance of adaptive PSK schemes.

The parameters of our nine-mode adaptive PSK scheme are summarised in Table 22.5 following the definitions of our generic model used for the adaptive modulation schemes developed in Section 22.7.1. The models of other adaptive PSK schemes employing a different number of modes can be readily obtained by increasing or reducing the number of columns in Table 22.5. Since the number of modes is $K = 9$, we have $K + 1 = 10$ mode-switching lev-

k	0	1	2	3	4	5	6	7	8
m_k	0	2	4	8	16	32	64	128	256
b_k	0	1	2	3	4	5	6	7	8
c_k	0	1	1	1	1	1	1	1	1
mode	No Tx	BPSK	QPSK	8PSK	16PSK	32PSK	64PSK	128PSK	256PSK

Table 22.5: Parameters of a nine-mode adaptive PSK scheme following the definitions of the generic adaptive modulation model developed in Section 22.7.1.

els, which are hosted by the vector $\mathbf{s} = \{s_k \mid k = 0, 1, 2, \cdots, 9\}$. Let us assume $s_0 = 0$ and

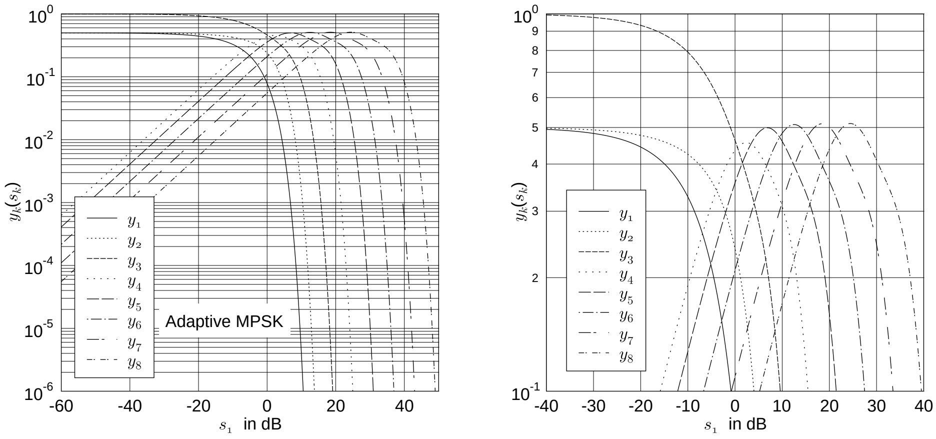

(a) Global Relationship

(b) Near $y_k(s_k) = 0.5$

Figure 22.22: 'Lagrangian-free' functions of (22.61) for a nine-mode adaptive PSK scheme. For a given value of s_1, there exist two solutions for s_k satisfying $y_k(s_k) = y_1(s_1)$. However, only the higher value of s_k satisfies the constraint of $s_{k-1} \leq s_k, \ \forall\, k$.

$s_9 = \infty$. In order to evaluate the performance of the nine-mode adaptive PSK scheme, we have to obtain the optimum switching levels first. Let us evaluate the 'Lagrangian-free' functions defined in (22.61), using the parameters given in Table 22.5 and the BEP expressions given in (22.80). The 'Lagrangian-free' functions of our nine-mode adaptive PSK scheme are depicted in Figure 22.22. We can observe that there exist two solutions for s_k satisfying $y_k(s_k) = y_1(s_1)$ for a given value of s_1, which are given by the crossover points over the horizontal lines at the various coordinate values scaled on the vertical axis. However, only the higher value of s_k satisfies the constraint of $s_{k-1} \leq s_k, \ \forall\, k$. The enlarged view near $y_k(s_k) = 0.5$ seen in Figure 22.22(b) reveals that $y_4(s_4)$ may have no solution of $y_4(s_4) = y_1(s_1)$, when $y_1(s_1) > 0.45$. One option is to use a constant value of $s_4 = 2.37$dB, where $y_4(s_4)$ reaches its peak value. The other option is to set $s_4 = s_3$, effectively eliminating 16PSK from the set of possible modulation modes. It was found that both policies result in the same performance up to four effective decimal digits in terms of the average BPS throughput.

Upon solving $y_k(s_k) = y_1(s_1)$, we arrive at the relationships sought between the first optimum switching level s_1 and the remaining optimum switching levels s_k. Figure 22.23(a) depicts these relationships. All the optimum switching levels, except for s_1 and s_2, approach their asymptotic limit monotonically, as s_1 decreases. A decreased value of s_1 corresponds to an increased value of the average SNR. Figure 22.23(b) illustrates the optimum switching levels of a seven-mode adaptive PSK scheme operating over a Rayleigh channel associated with $m = 1$ at the target BEP of $P_{th} = 10^{-2}$. These switching levels were obtained by solving (22.68). The optimum switching levels show a steady decrease in their values as the average SNR increases, until it reaches the avalanche SNR value of $\bar{\gamma} = 35$dB, beyond which always the highest-order PSK modulation mode, namely 64PSK, is activated.

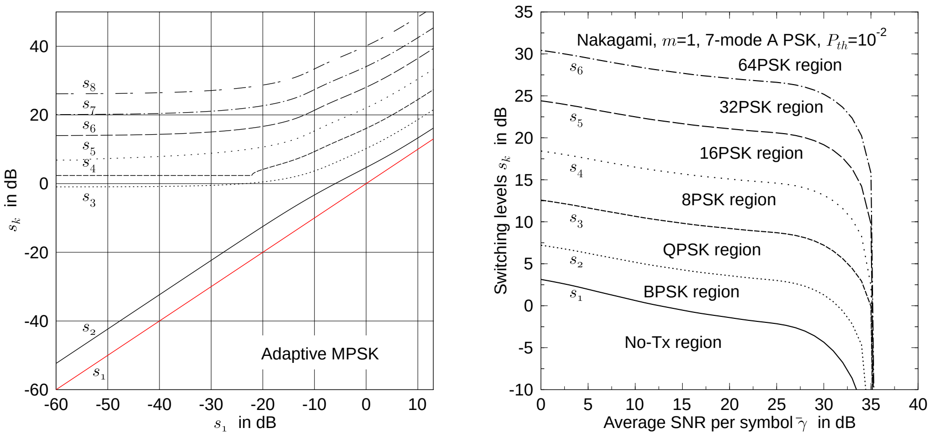

(a) Relationship between the optimum switching levels of a nine-mode PSK scheme

(b) Optimum switching levels of a seven-mode adaptive PSK scheme

Figure 22.23: Optimum switching levels. (a) Relationships between s_k and s_1 in a nine-mode adaptive PSK scheme. (b) Optimum switching levels for 7-mode adaptive PSK scheme operating over a Rayleigh channel at the target BEP of $P_{th} = 10^{-2}$.

Having highlighted the evaluation of the optimum switching levels for an adaptive PSK scheme, let us now consider the associated performance results. We are reminded that the average BEP of our optimised adaptive scheme remains constant at $P_{avg} = P_{th}$, provided that the average SNR is less than the avalanche SNR. Hence, the average BPS throughput and the relative SNR gain of our APSK scheme in comparison to the corresponding fixed-mode modem are our concern.

Let us now consider Figure 22.24, where the average BPS throughput of the various adaptive PSK schemes operating over a Rayleigh channel associated with $m = 1$ are plotted, which were designed for the target BEP of $P_{th} = 10^{-2}$ and $P_{th} = 10^{-3}$. The markers '$\otimes$' and '$\odot$' represent the required SNR of the various fixed-mode PSK schemes, while achieving the same target BER as the adaptive schemes, operating over an AWGN channel and a Rayleigh channel, respectively. It can be observed that introducing an additional constituent mode into an adaptive PSK scheme does not make any impact on the average BPS throughput, when the average SNR is relatively low. For example, when the average SNR $\bar{\gamma}$ is less than 10dB in Figure 22.24(a), employing more than four APSK modes for the adaptive scheme does not improve the average BPS throughput. In comparison to the various fixed-mode PSK modems, the adaptive modem achieved the SNR gains between 4dB and 8dB for the target BEP of $P_{th} = 10^{-2}$ and 10dB to 16dB for the target BEP of $P_{th} = 10^{-3}$ over a Rayleigh channel. Since no adaptive scheme operating over a fading channel can outperform the corresponding fixed-mode counterpart operating over an AWGN channel, it is interesting to investigate the performance differences between these two schemes. Figure 22.24 suggests that the required SNR of our adaptive PSK modem achieving 1BPS for transmission over a Rayleigh channel is approximately 1dB higher, than that of fixed-mode BPSK operating over

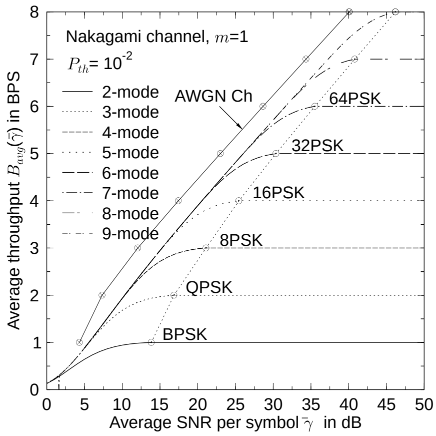

(a) $P_{th} = 10^{-2}$

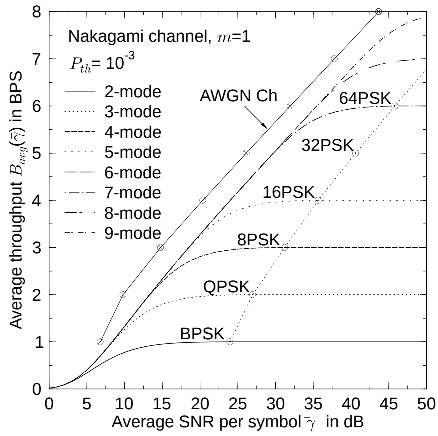

(b) $P_{th} = 10^{-3}$

Figure 22.24: The average BPS throughput of various adaptive PSK schemes operating over a Rayleigh channel ($m = 1$) at the target BEP of (a) $P_{th} = 10^{-2}$ and (b) $P_{th} = 10^{-3}$. The markers '$\otimes$' and '$\odot$' represent the required SNR of the corresponding fixed-mode PSK scheme, while achieving the same target BEP as the adaptive schemes, operating over an AWGN channel and a Rayleigh channel, respectively.

an AWGN channel. Furthermore, this impressive performance can be achieved by employing only three modes, namely No-Tx, BPSK and QPSK for the adaptive PSK modem. For other BPS throughput values, the corresponding SNR differences are in the range of 2dB to 3dB, while maintaining the BEP of $P_{th} = 10^{-2}$ and 4dB for the BEP of $P_{th} = 10^{-3}$.

We observed in Figure 22.24 that the average BPS throughput of the various adaptive PSK schemes is dependent on the target BEP. Hence, let us investigate the BPS performances of the adaptive modems for the various values of target BEPs using the results depicted in Figure 22.25. The average BPS throughputs of a nine-mode adaptive PSK scheme are represented as various types of lines without markers depending on the target average BERs, while those of the corresponding fixed PSK schemes are represented as various types of lines with markers according to the key legend shown in Figure 22.25. We can observe that the difference between the required SNRs of the adaptive schemes and fixed schemes increases, as the target BEP decreases. It is interesting to note that the average BPS curves of the adaptive PSK schemes seem to converge to a set of densely packed curves, as the target BEP decreases to values around $10^{-4} - 10^{-6}$. In other words, the incremental SNR required for achieving the next target BEP, which is an order of magnitude lower, decreases as the target BEP decreases. On the other hand, the incremental SNR for the same scenario of fixed modems seems to remain nearly constant at 10dB. Comparing Figure 22.25(a) and Figure 22.25(b), we find that this seemingly constant incremental SNR of the fixed-mode modems is reduced to about 5dB, as the fading becomes less severe, *i.e.* when the fading parameter becomes $m = 2$.

Let us now investigate the effects of the Nakagami fading parameter m on the average BPS throughput performance of various adaptive PSK schemes by observing Figure 22.26.

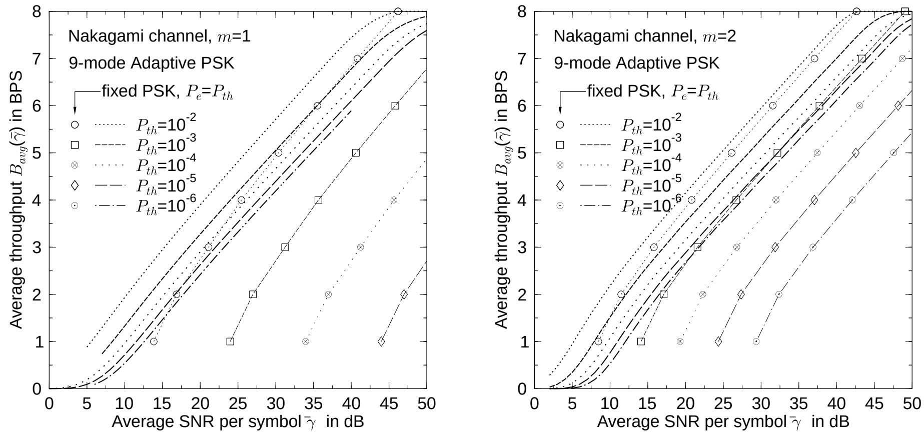

(a) $m = 1$ **(b)** $m = 2$

Figure 22.25: The average BPS throughput of a nine-mode adaptive PSK scheme operating over a Nakagami fading channel (a) $m = 1$ and (b) $m = 2$. The markers represent the SNR required for achieving the same BPS throughput and the same average BEP as the adaptive schemes.

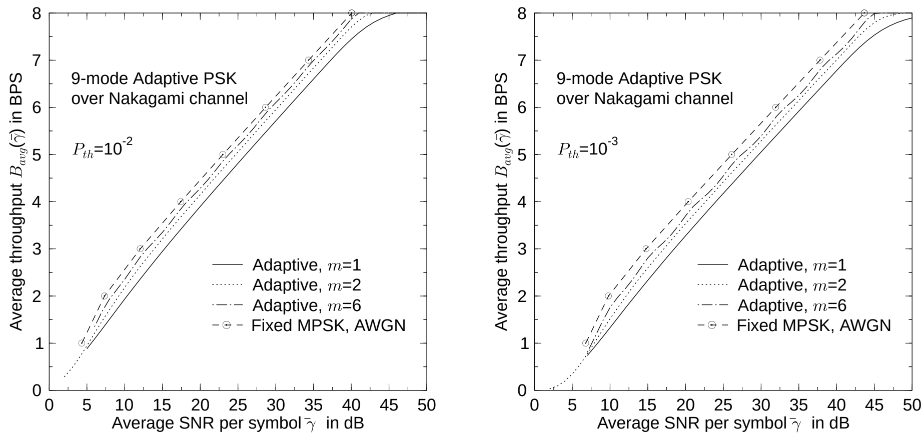

(a) $P_{th} = 10^{-2}$ **(b)** $P_{th} = 10^{-3}$

Figure 22.26: The effects of the Nakagami fading parameter m on the average BPS throughput of a nine-mode adaptive PSK scheme designed for the target BEP of (a) $P_{th} = 10^{-2}$ and (b) $P_{th} = 10^{-3}$. As m increases, the average throughput of the adaptive modem approaches the throughput of fixed PSK modems operating over an AWGN channel.

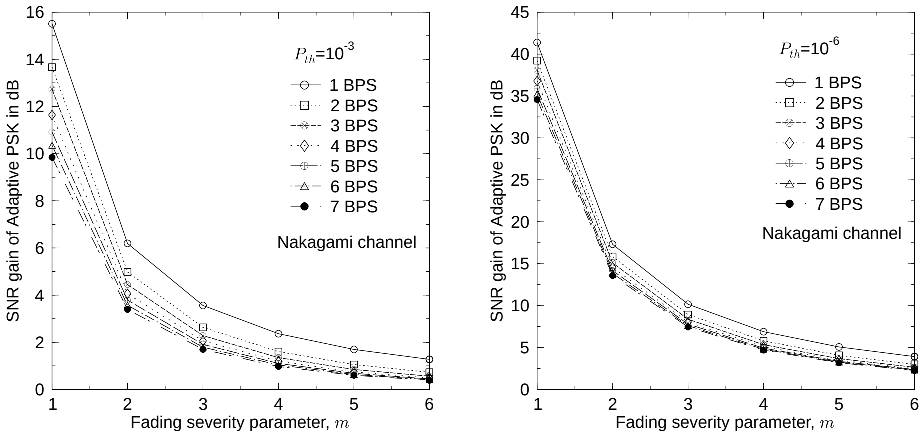

(a) $P_{th} = 10^{-3}$ **(b)** $P_{th} = 10^{-6}$

Figure 22.27: The SNR gain of adaptive PSK schemes in comparison to the corresponding fixed-mode PSK schemes yielding the same BPS throughput for the target BEP of (a) $P_{th} = 10^{-3}$ and (b) $P_{th} = 10^{-6}$. The performance advantage of employing adaptive PSK schemes decreases, as the fading becomes less severe.

The BPS throughput of the various fixed PSK schemes for transmission over an AWGN channel is depicted in Figure 22.26 as the ultimate performance limit achievable by the adaptive schemes operating over Nakagami fading channels. For example, when the channel exhibits Rayleigh fading, *i.e.* when the fading parameter becomes $m = 1$, the adaptive PSK schemes show 3dB to 4dB SNR penalty compared to their fixed-mode counterparts operating over the AWGN channel. Compared to fixed-mode BPSK, the adaptive scheme required only a 1dB higher SNR. As the fading becomes less severe, the average BPS throughput of the adaptive PSK schemes approaches that of fixed-mode PSK operating over the AWGN channel. For the target BEP of $P_{th} = 10^{-3}$, the SNR gap between the BPS throughput curves becomes higher. The adaptive PSK scheme operating over the Rayleigh channel required 4dB to 5dB higher SNR for achieving the same throughput compared to the fixed PSK schemes operating over the AWGN channel.

Figure 22.27 summarises the relative SNR gains of our adaptive PSK schemes over the corresponding fixed PSK schemes. For the target BEP of $P_{th} = 10^{-3}$ the relative SNR gain of the nine-mode adaptive scheme compared to BPSK changes from 15.5dB to 1.3dB, as the Nakagami fading parameter changes from 1 to 6. Observing Figure 22.27(a) and Figure 22.27(b) we conclude that the advantages of employing adaptive PSK schemes are more pronounced when

1) the fading is more severe,

2) the target BEP is lower, and

3) the average BPS throughput is lower.

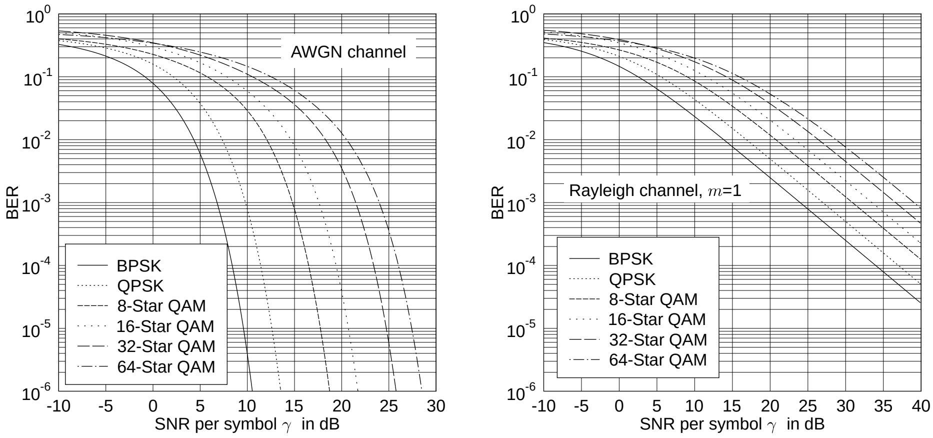

(a) AWGN Channel **(b)** Rayleigh Channel, $m = 1$

Figure 22.28: The average BEP of various SQAM modulation schemes.

Having studied the range of APSK schemes, let us in the next section consider the family of adaptive coherently detected Star-QAM schemes.

22.9.1.2 Adaptive Coherent Star QAM Schemes

In this section, we study the performance of adaptive coherent QAM schemes employing Type-I Star constellations [179]. Even though non-coherent Star QAM (SQAM) schemes are more popular owing to their robustness to fading without requiring pilot symbol assisted channel estimation and Automatic Gain Control (AGC) at the receiver, the results provided in this section can serve as benchmark results for non-coherent Star QAM schemes and the coherent Square QAM schemes.

The BEP of coherent Star QAM over an AWGN channel is derived in Appendix 31.1. It is shown that their BEP can be expressed as:

$$p_{SQAM}(\gamma) \simeq \sum_i A_i \, Q(\sqrt{a_i \gamma}\,), \tag{22.87}$$

where A_i and a_i are given in Appendix 31.1 for 8-Star, 16-Star, 32-Star and 64-Star QAM. The SNR-dependent optimum ring ratios were also derived in Appendix 31.1 for these Star QAM modems. Figure 22.28(a) shows the BEP of BPSK, QPSK, 8-Star QAM, 16-Star QAM, 32-Star QAM and 64-Star QAM employing the optimum ring ratios over the AWGN channel. Comparing Figure 22.21(a) and Figure 22.28(a), we can observe that 16-Star QAM, 32-Star QAM and 64-Star QAM are more power-efficient than 16 PSK, 32 PSK and 64 PSK, respectively. However, the envelope power of the Star QAM signals is not constant, unlike that of the PSK signals. Following an approach similar to that used in (22.84) and (22.85), the average BEP of the various SQAM schemes over a flat Nakagami-m fading channel can be expressed as:

$$P_{SQAM}(\bar{\gamma}) = \sum_i A_i \left[\tfrac{1}{2}(1-\mu_i)\right]^m \sum_{j=0}^{m-1} \binom{m-1+j}{j} \left[\tfrac{1}{2}(1+\mu_i)\right]^j , \qquad (22.88)$$

where μ_i is defined as:

$$\mu_i \triangleq \sqrt{\frac{a_i\bar{\gamma}}{2m + a_i\bar{\gamma}}} \, . \qquad (22.89)$$

Figure 22.28(b) shows the average BEP of various SQAM schemes for transmission over a flat Rayleigh channel, where $m = 1$. It can be observed that the 16-Star, 32-Star and 64-Star QAM schemes exhibit SNR advantages of around 3.5dB, 4dB, and 7dB compared to 16-PSK, 32-PSK and 64-PSK schemes at a BEP of 10^{-2}. The BEP of SQAM for transmission over the AWGN channel given in (22.87) and that over a Nakagami channel given in (22.88) will be used in comparing the performance of the various adaptive SQAM schemes.

k	0	1	2	3	4	5	6
m_k	0	2	4	8	16	32	64
b_k	0	1	2	3	4	5	6
c_k	0	1	1	1	1	1	1
mode	No Tx	BPSK	QPSK	8-Star	16-Star	32-Star	64-Star

Table 22.6: Parameters of a seven-mode adaptive Star QAM scheme following the definitions developed in Section 22.7.1 for the generic adaptive modulation model.

The parameters of a seven-mode adaptive Star QAM scheme are summarised in Table 22.6 following the definitions of the generic model developed in Section 22.7.1 for adaptive modulation schemes. Since the number of modes is $K = 7$, we have $K + 1 = 8$ mode-switching levels hosted by the vector $\mathbf{s} = \{s_k \mid k = 0, 1, 2, \cdots, 7\}$. Let us assume that $s_0 = 0$ and $s_7 = \infty$. Then, we have to determine the optimum values for the remaining six switching levels using the technique developed in Section 22.8.4. The 'Lagrangian-free' functions corresponding to a seven-mode Star QAM scheme are depicted in Figure 22.29 and the relationships obtained for the switching levels are displayed in Figure 22.30(a). We can observe that as seen for APSK in Figure 22.22 there exist two solutions for s_6 satisfying $y_6(s_6) = y_1(s_1)$ for a given value of s_1, when $y_1 \leq 0.382$. However, only the higher value of s_k satisfies the constraint of $s_6 \geq s_5$. When $s_1 \leq 7.9$dB, the optimum value of s_6 should be set to s_5, in order to guarantee $s_6 \geq s_5$. Figure 22.30(b) illustrates the optimum switching levels of a seven-mode adaptive Star QAM scheme operating over a Rayleigh channel at the target BEP of $P_{th} = 10^{-2}$. These switching levels were obtained by solving (22.68). The optimum switching levels show a steady decrease in their values, as the average SNR increases, until they reach the avalanche SNR value of $\bar{\gamma} = 28.5$dB, beyond which always the highest-order modulation mode, namely 64-Star QAM, is activated.

Let us now investigate the associated performance results. We are reminded that the average BEP of our optimised adaptive scheme remains constant at $P_{avg} = P_{th}$, provided

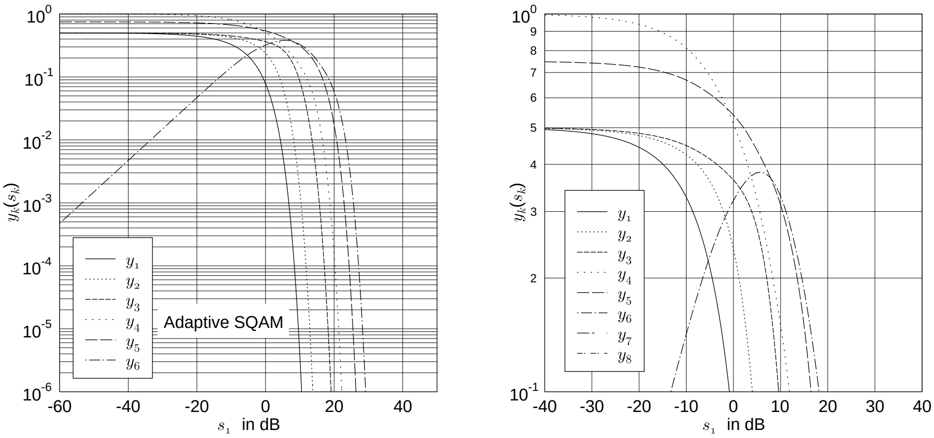

(a) Overall Relationship

(b) Near $y_k(s_k) = 0.5$

Figure 22.29: 'Lagrangian-free' functions of (22.61) for a seven-mode adaptive Star QAM scheme.

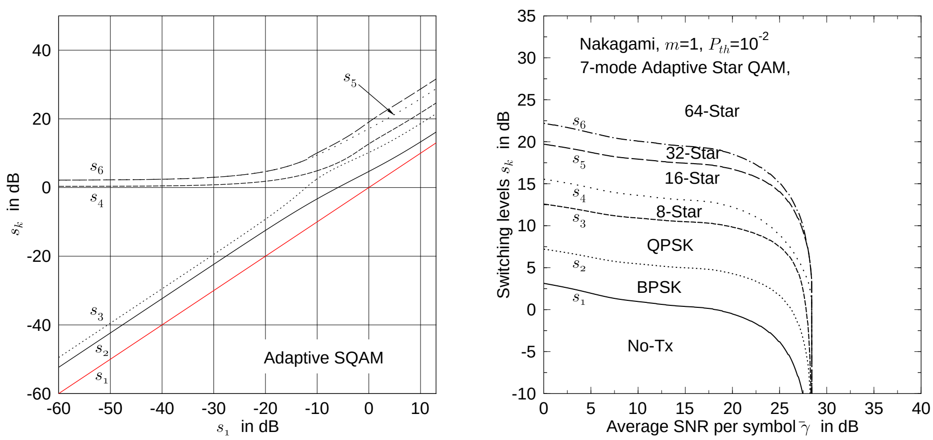

(a) Relationship between the optimum switching levels

(b) Optimum switching levels

Figure 22.30: Optimum switching levels of a seven-mode Adaptive Star QAM scheme. (a) Relationships between s_k and s_1. (b) Optimum switching levels of a seven-mode adaptive Star QAM scheme operating over a Rayleigh channel at the target BEP of $P_{th} = 10^{-2}$.

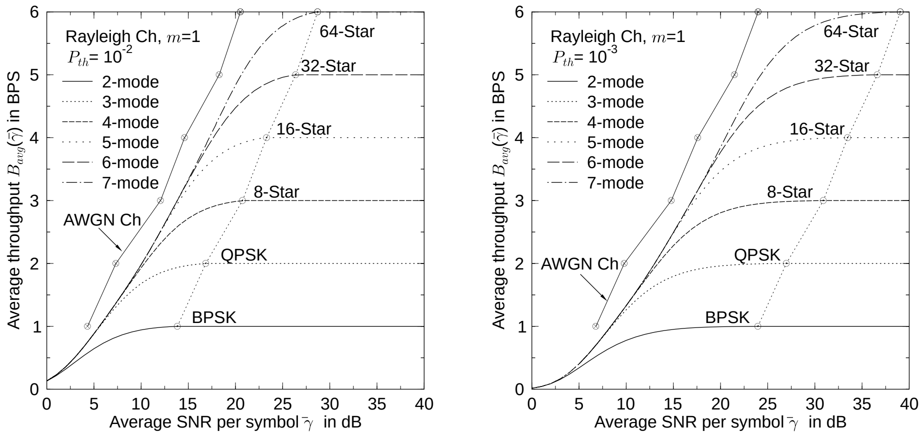

(a) $P_{th} = 10^{-2}$ **(b)** $P_{th} = 10^{-3}$

Figure 22.31: The average BPS throughput of the various adaptive Star QAM schemes operating over a Rayleigh fading channel associated with $m = 1$ at the target BEP of (a) $P_{th} = 10^{-2}$ and (b) $P_{th} = 10^{-3}$. The markers '$\otimes$' and '$\odot$' represent the required SNR of the corresponding fixed-mode Star QAM schemes, while achieving the same target BEP as the adaptive schemes, operating over an AWGN channel and a Rayleigh channel, respectively.

that the average SNR is less than the avalanche SNR. Hence, the average BPS throughput and the SNR gain of our adaptive modem in comparison to the corresponding fixed-mode modems are our concern.

Let us first consider Figure 22.31, where the average BPS throughput of the various adaptive Star QAM schemes operating over a Rayleigh channel associated with $m = 1$ is shown at the target BEP of $P_{th} = 10^{-2}$ and $P_{th} = 10^{-3}$. The markers '$\otimes$' and '$\odot$' represent the required SNR of the corresponding fixed-mode Star QAM schemes, while achieving the same target BEP as the adaptive schemes, operating over an AWGN channel and a Rayleigh channel, respectively. Comparing Figure 22.24(a) and Figure 22.31(a), we find that the tangent of the average BPS curves of the adaptive Star QAM schemes is higher than that of adaptive PSK schemes. Explicitly, the tangent of the Star QAM schemes is around 0.3BPS/dB, whereas that of the APSK schemes was 0.18BPS/dB. This is due to the more power-efficient constellation arrangement of Star QAM in comparison to the single-ring constellations of the PSK modulations schemes. In comparison to the corresponding fixed-mode Star QAM modems, the adaptive modem achieved an SNR gain of 6dB to 8dB for the target BEP of $P_{th} = 10^{-2}$ and 12dB to 16dB for the target BEP of $P_{th} = 10^{-3}$ over a Rayleigh channel. Compared to the fixed-mode Star QAM schemes operating over an AWGN channel, our adaptive schemes approached their performance within about 3dB in terms of the required SNR value, while achieving the same target BEP of $P_{th} = 10^{-2}$ and $P_{th} = 10^{-3}$.

Since Figure 22.31 suggests that the relative SNR gain of the adaptive schemes is dependent on the target BER, let us investigate the effects of the target BEP in more detail.

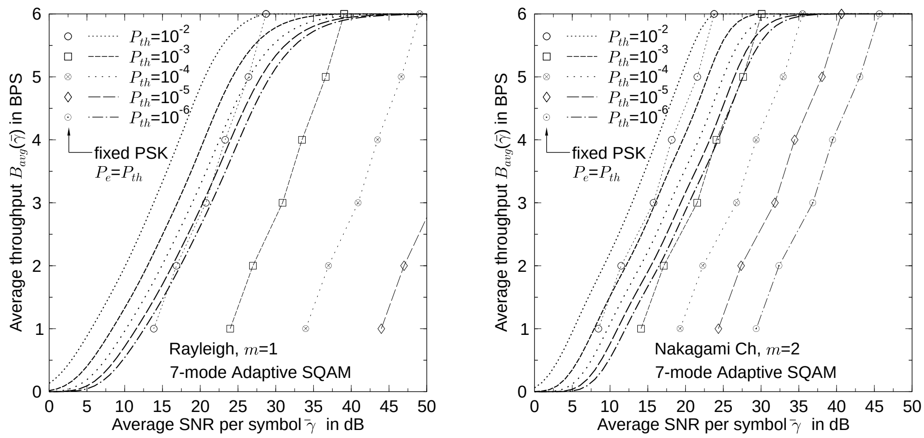

(a) $m = 1$ **(b)** $m = 2$

Figure 22.32: The average BPS throughput of a seven-mode adaptive Star QAM scheme operating over a Nakagami fading channel (a) $m = 1$ and (b) $m = 2$. The markers represent the SNR required by the fixed-mode schemes for achieving the same BPS throughput and the same average BER as the adaptive schemes.

Figure 22.32 shows the BPS throughput of the various adaptive schemes at the target BEP of $P_{th} = 10^{-2}$ to $P_{th} = 10^{-6}$. The average BPS throughput of a seven-mode adaptive Star QAM scheme is represented with the aid of the various line types without markers, depending on the target average BERs, while those of the corresponding fixed-mode Star QAM schemes are represented as various types of lines having markers according to the legends shown in Figure 22.32. We can observe that the difference between the SNRs required for the adaptive schemes and fixed schemes increases, as the target BEP decreases. The fixed-mode Star QAM schemes require additional SNRs of 10dB and 6dB in order to achieve an order of magnitude lower BEP for the Nakagami fading parameters of $m = 1$ and $m = 2$, respectively. However, our adaptive schemes require additional SNRs of only 1dB to 3dB for achieving the same goal.

Let us now investigate the effects of the Nakagami fading parameter m on the average BPS throughput performance of the various adaptive Star QAM schemes by observing Figure 22.33. The BPS throughput of the fixed-mode Star QAM schemes for the transmission over an AWGN channel is depicted in Figure 22.33 as the ultimate performance limit achievable by the adaptive schemes operating over Nakagami fading channels. As the Nakagami fading parameter m increases from 1 to 2 and to 6, the SNR gap between the adaptive schemes operating over a Nakagami fading channel and the fixed-mode schemes decreases. When the average SNR is less than $\bar{\gamma} \leq 6$dB, the average BPS throughput of our adaptive schemes decreases, when the fading parameter m increases. The rationale of this phenomenon is that as the channel becomes more and more like an AWGN channel, the probability of activating the BPSK mode is reduced, resulting in more frequent activation of the No-Tx mode and hence the corresponding average BPS throughput inevitably decreases.

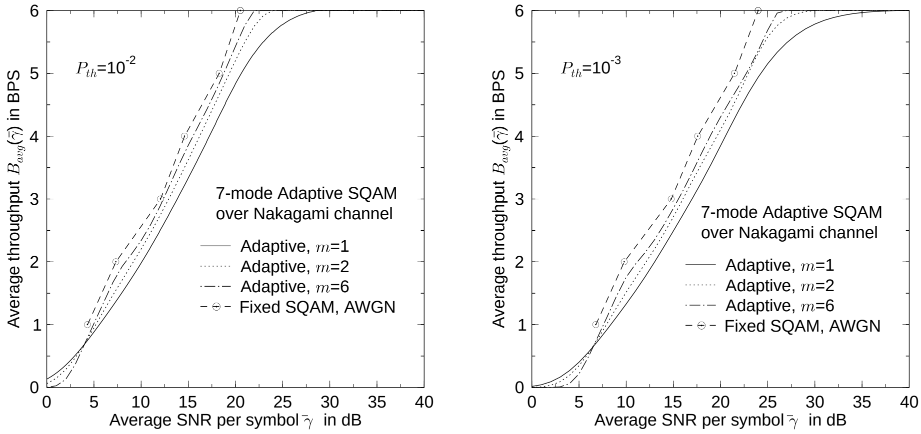

(a) $P_{th} = 10^{-2}$ **(b)** $P_{th} = 10^{-3}$

Figure 22.33: The effects of the Nakagami fading parameter m on the average BPS throughput of a seven-mode adaptive Star QAM scheme at the target BEP of (a) $P_{th} = 10^{-2}$ and (b) $P_{th} = 10^{-3}$. As m increases, the average throughput of the adaptive modem approaches the throughput of the fixed-mode Star QAM modems operating over an AWGN channel.

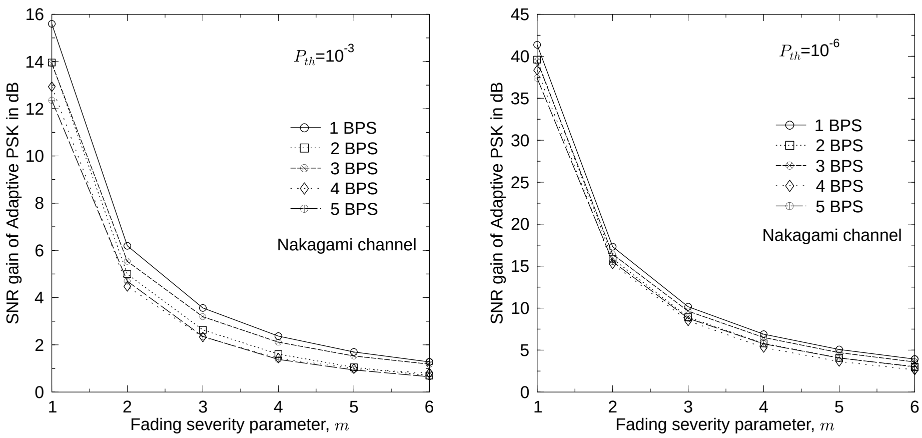

(a) $P_{th} = 10^{-3}$ **(b)** $P_{th} = 10^{-6}$

Figure 22.34: The SNR gain of the various adaptive Star QAM schemes in comparison to the fixed-mode Star QAM schemes yielding the same BPS throughput at the target BEP of (a) $P_{th} = 10^{-3}$ and (b) $P_{th} = 10^{-6}$. The advantage of the adaptive Star QAM schemes decreases, as the fading becomes less severe.

The effects of the Nakagami fading factor m on the SNR gain of our adaptive Star QAM scheme can be observed in Figure 22.34. As expected, the relative SNR gain of the adaptive schemes at a throughput of 1 BPS is the highest among the BPS throughputs considered. However, the order observed in terms of the SNR gain of the adaptive schemes does not strictly follow the increasing BPS order at the target BEP of $P_{th} = 10^{-3}$ and $P_{th} = 10^{-6}$, as it did for the adaptive PSK schemes of Section 22.9.1.1. Even though the adaptive Star QAM schemes exhibit a higher throughput, than the adaptive PSK schemes, the SNR gains compared to their fixed-mode counterparts are more or less the same, showing typically less than 1dB difference, except for the 5 BPS throughput scenario, where the adaptive QAM scheme gained up to 1.3dB more in terms of the required SNR than the adaptive PSK scheme.

Having studied the performance of a range of adaptive Star QAM schemes, in the next section we consider adaptive modulation schemes employing the family of square-shaped QAM constellations.

22.9.1.3 Adaptive Coherent Square QAM Modulation Schemes

Since coherent Square M-ary QAM (MQAM) is the most power-efficient M-ary modulation scheme [179] and the accurate channel estimation becomes possible with the advent of Pilot Symbol Assisted Modulation (PSAM) techniques [138, 139, 177], *Otsuki*, *Sampei* and *Morinaga* proposed to employ coherent square QAM as the constituent modulation modes for an adaptive modulation scheme [178] instead of non-coherent Star QAM modulation [176]. In this section, we study the various aspects of this adaptive square QAM scheme employing the optimum switching levels of Section 22.8.4. The closed form BEP expressions of square QAM over an AWGN channel can be found in (22.2) and that over a Nakagami channel can be expressed using a similar form given in (22.88). The optimum switching levels of adaptive Square QAM were studied in Section 22.8.4 as an example.

The average BEP of our six-mode adaptive Square QAM scheme operating over a flat Rayleigh fading channel is depicted in Figure 22.35(a), which shows that the modem maintains the required constant target BER, until it reaches the BER curve of the specific fixed-mode modulation scheme employing the highest-order modulation mode, namely 256-QAM, and then it follows the BEP curve of the 256-QAM mode. The various grey lines in the figure represent the BEP of the fixed constituent modulation modes for transmission over a flat Rayleigh fading channel. An arbitrarily low target BEP could be maintained at the expense of a reduced throughput.

The average throughput is shown in Figure 22.35(b) together with the estimated channel capacity of the narrow-band Rayleigh channel [180, 181] and with the throughput of several variable-power, variable-rate modems reported in [183]. Specifically, Goldsmith and Chua [183] studied the performance of their variable-power variable-rate adaptive modems based on a BER bound of m-ary Square QAM, rather than using an exact BER expression. Since our adaptive Square QAM schemes do not vary the transmission power, our scheme can be regarded as a sub-optimal policy viewed for their respective [183]. However, the throughput performance of Figure 22.35(b) shows that the SNR degradation is within 2dB in the low-SNR region and within half a dB in the high-SNR region, in comparison to the ideal continuously variable-power adaptive QAM scheme employing a range of hypothetical continuously variable-BPS QAM modes [183], represented as the ‘Goldsmith 1’ scheme in the figure. *Goldsmith* and *Chua* [183] also reported the performance of a variable-power

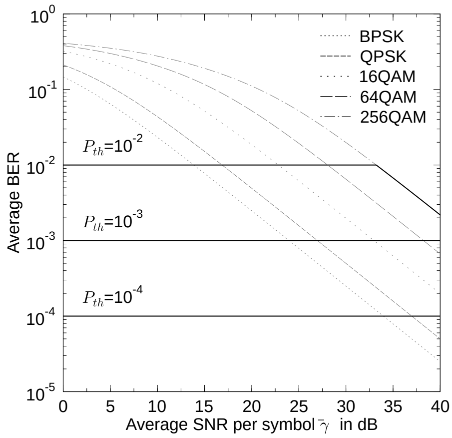

(a) BER

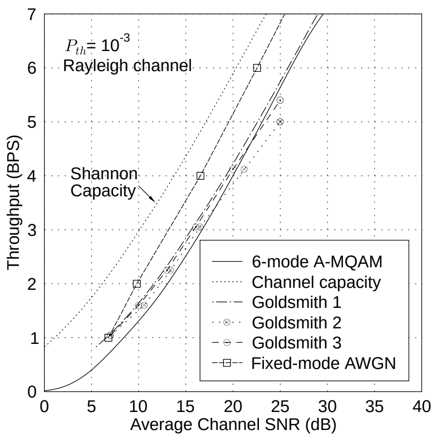

(b) Throughput: $P_t = 10^{-3}$

Figure 22.35: The average BEP and average throughput performance of a six-mode adaptive Square QAM scheme operating over a flat Rayleigh channel ($m = 1$). (a) The constant target average BEP is maintained over the entire range of the average SNR values up to the avalanche SNR. (b) The average BPS throughput of the equivalent constant-power adaptive scheme is compared to *Goldsmith*'s schemes [183]. The 'Goldsmith 1' and 'Goldsmith 2' schemes represent a variable-power adaptive scheme employing hypothetical continuously variable-BPS QAM modulation modes and Square QAM modes, respectively. The 'Goldsmith 3' scheme represents the simulation results associated with a constant-power adaptive Square QAM reported in [183].

discrete-rate and a constant-power discrete-rate scheme, which we represented as the 'Goldsmith 2' and 'Goldsmith 3' scenarios in Figure 22.35(b), respectively. Since their results are based on approximate BER formulas, the average BPS throughput performance of the 'Goldsmith 3' scheme is optimistic, when the average SNR γ is less than 17dB. Considering that our scheme achieves the maximum possible throughput the given average SNR value with the aid of the globally optimised switching levels, the average throughput of the 'Goldsmith 3' scheme is expected to be lower, than that of our scheme, as is the case when the average SNR γ is higher than 17dB.

Figure 22.36(a) depicts the average BPS throughput of our various adaptive Square QAM schemes operating over a Rayleigh channel associated with $m = 1$ at the target BEP of $P_{th} = 10^{-3}$. Figure 22.36(a) shows that even though the constituent modulation modes of our adaptive schemes do not include 3, 5 and 7-BPS constellations, the average BPS throughput steadily increases without undulations. Compared to the fixed-mode Square QAM schemes operating over an AWGN channel, our adaptive schemes require additional SNRs of less than 3.5dB, when the throughput is below 6.5 BPS. The comparison of the average BPS throughputs of the adaptive schemes employing PSK, Star QAM and Square QAM modems, as depicted in Figure 22.36(b), confirms the superiority of Square QAM over the other two schemes in terms of the required average SNR for achieving the same throughput and the

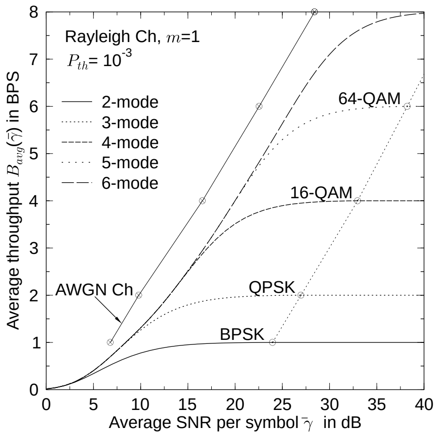

(a) $P_{th} = 10^{-2}$

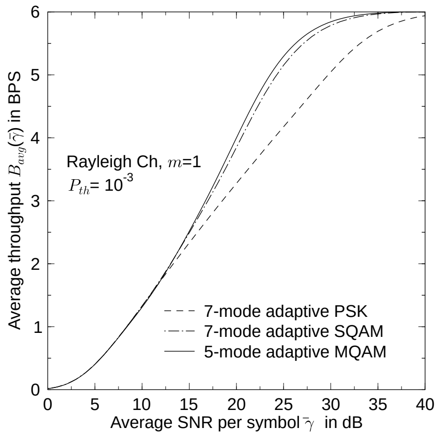

(b) $P_{th} = 10^{-3}$

Figure 22.36: The average BPS throughput of various adaptive Square QAM schemes operating over a Rayleigh channel ($m = 1$) at the target BEP of $P_{th} = 10^{-3}$. (a) The markers '$\otimes$' and '$\odot$' represent the required SNR of the corresponding fixed-mode Square QAM schemes achieving the same target BEP as the adaptive schemes, operating over an AWGN channel and a Rayleigh channel, respectively. (b) The comparison of the various adaptive schemes employing PSK, Star QAM and Square QAM as the constituent modulation modes.

same target average BEP. Since all these three schemes employ BPSK, QPSK as the second and the third constituent modulation modes, their throughput performance shows virtually no difference, when the average throughput is less than or equal to $B_{avg} = 2$ BPS.

Let us now investigate the effects of the Nakagami fading parameter m on the average BPS throughput performance of the adaptive Square QAM schemes observing Figure 22.37. The BPS throughput of the fixed-mode Square QAM schemes over an AWGN channel is depicted in Figure 22.37 as the ultimate performance limit achievable by the adaptive schemes operating over Nakagami fading channels. Similar observations can be made for the adaptive Square QAM scheme, like for the adaptive Star QAM arrangement characterized in Figure 22.33. A specific difference is, however, that the average BPS throughput recorded for the fading parameter of $m = 6$ exhibits an undulating curve. For example, an increased m value results in a limited improvement of the corresponding average BPS throughput near the throughput values of 2.5, 4.5 and 6.5 BPS. This is because our adaptive Square QAM schemes do not use 3-, 5- and 7-BPS constituent modems, unlike the adaptive PSK and adaptive Star QAM schemes. Figure 22.38 depicts the corresponding optimum mode-switching levels for the six-mode adaptive Square QAM scheme. The black lines represent the switching levels, when the Nakagami fading parameter is $m = 6$ and the grey lines when $m = 1$. In general, the lower the switching levels, the higher the average BPS throughput of the adaptive modems. When the Nakagami fading parameter is $m = 1$, the switching levels decrease monotonically, as the average SNR increases. However, when the fading severity parameter is

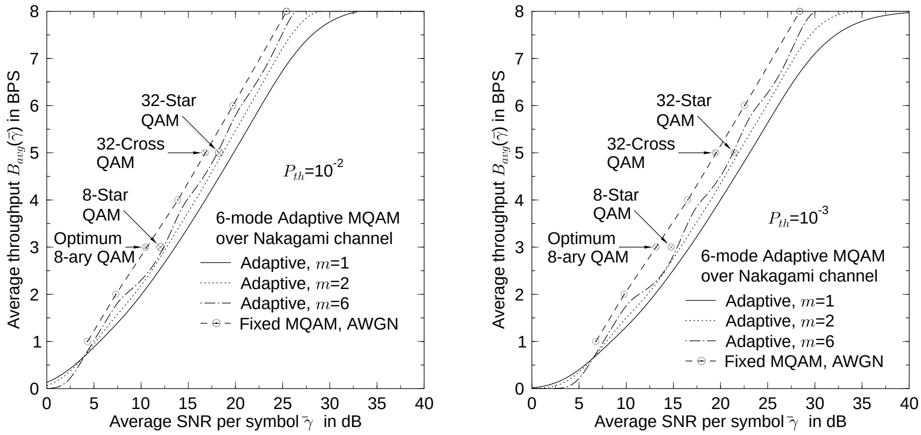

(a) $P_{th} = 10^{-2}$ **(b)** $P_{th} = 10^{-3}$

Figure 22.37: The effects of the Nakagami fading parameter m on the average BPS throughput of a seven-mode adaptive Square QAM scheme at the target BEP of (a) $P_{th} = 10^{-2}$ and (b) $P_{th} = 10^{-3}$. As m increases, the average throughput of the adaptive modem approaches the throughput of the corresponding fixed Square QAM modems operating over an AWGN channel.

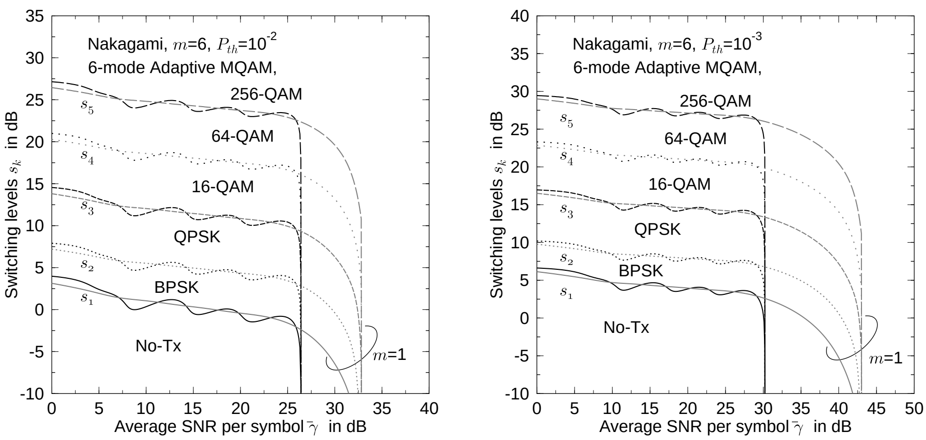

(a) $P_{th} = 10^{-2}$ **(b)** $P_{th} = 10^{-3}$

Figure 22.38: The switching levels of the six-mode adaptive Square QAM scheme operating over Nakagami fading channels at the target BER of (a) $P_{th} = 10^{-2}$ and (b) $P_{th} = 10^{-3}$. The bold lines are used for the fading parameter of $m = 6$ and the grey lines are for $m = 1$.

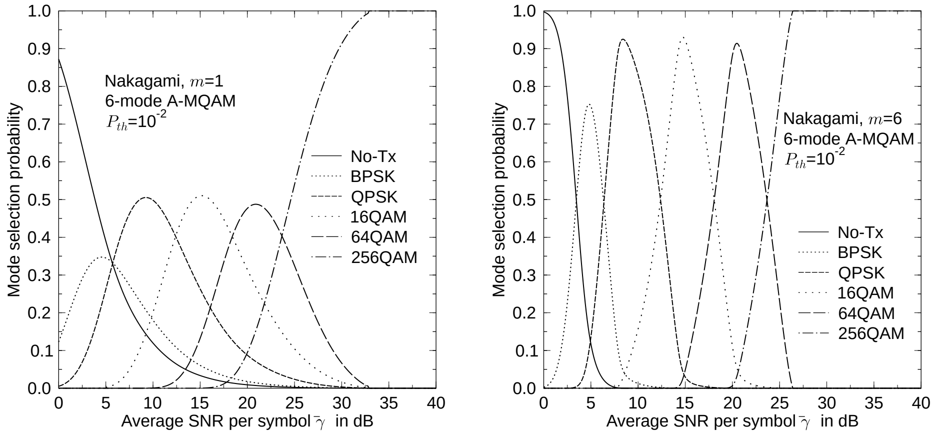

(a) $m = 1$ **(b)** $m = 6$

Figure 22.39: The mode selection probability of a six-mode adaptive Square QAM scheme operating over Nakagami fading channels at the target BEP of $P_{th} = 10^{-2}$. When the fading becomes less severe, the mode selection scheme becomes more 'selective' in comparison to that for $m = 1$.

$m = 6$, the switching levels fluctuate, exhibiting several local minima around 8dB, 15dB and 21dB. In the extreme case of $m \to \infty$, *i.e.* when operating over an AWGN-like channel, the switching levels would be $s_1 = s_2 = 0$ and $s_k = \infty$ for other k values in the SNR range of 7.3dB $< \bar{\gamma} <$ 14dB, $s_1 = s_2 = s_3 = 0$ and $s_4 = s_5 = \infty$ when we have 14dB $< \bar{\gamma} <$ 20dB, $s_k = 0$ except for $s_5 = \infty$ when the SNR is in the range of 20dB $< \bar{\gamma} <$ 25dB and finally, all $s_k = 0$ for $\forall k$, when $\bar{\gamma} >$ 25dB, when considering the fixed-mode Square QAM performance achieved over an AWGN channel represented by markers '$\odot$' in Figure 22.37. Observing Figure 22.39, we find that our adaptive schemes become highly 'selective', when the Nakagami fading parameter becomes $m = 6$, exhibiting narrow triangular shapes. As m increases, the shapes will eventually converge to Kronecker delta functions.

A possible approach to reducing the undulating behaviour of the average BPS throughput curve is the introduction of a 3-BPS and a 5-BPS mode as additional constituent modem modes. The power-efficiency of 8-Star QAM and 32-Star QAM is insufficient for maintaining a linear growth of the average BPS throughput, as we can observe in Figure 22.37. Instead, the most power-efficient 8-ary QAM scheme (see page 279 of [388]) and the so-called 32-ary cross-shaped QAM scheme have a potential of reducing these undulation effects. However, since we observed in Section 22.9.1.1 and Section 22.9.1.2 that the relative SNR advantage of employing adaptive Square QAM rapidly reduces, when the Nakagami fading parameter increases, even though the additional 3-BPS and 5-BPS modes are also used, there seems to be no significant benefit in employing non-square shaped additional constellations.

Again, we can observe in Figure 22.37 that when the average SNR is less than $\bar{\gamma} \leq 6$dB, the average BPS throughput of our adaptive Square QAM scheme decreases, as the Nakagami fading parameter m increases. As we discussed in Section 22.9.1.2, this is due to the less

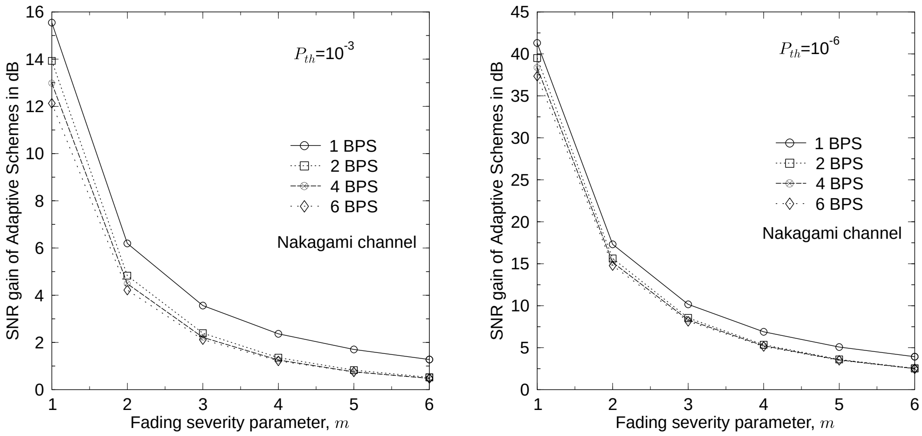

(a) $P_{th} = 10^{-3}$

(b) $P_{th} = 10^{-6}$

Figure 22.40: The SNR gain of the six-mode adaptive Square QAM scheme in comparison to the various fixed-mode Square QAM schemes yielding the same BPS throughput at the target BEP of (a) $P_{th} = 10^{-3}$ and (b) $P_{th} = 10^{-6}$. The performance advantage of the adaptive Square QAM schemes decreases, as the fading becomes less severe.

frequent activation of the BPSK mode in comparison to the 'No-Tx' mode, as the channel variation is reduced.

The effects of the Nakagami fading factor m on the relative SNR gain of our adaptive Square QAM scheme can be observed in Figure 22.40. The less severe the fading, the smaller the relative SNR advantage of employing adaptive Square QAM in comparison to its fixed-mode counterparts. Except for the 1-BPS mode, the SNR gains become less than 0.5dB, when m is increased to 6 at the target BEP of $P_{th} = 10^{-3}$. The trend observed is the same at the target BEP of $P_{th} = 10^{-6}$, showing relatively higher gains in comparison to the $P_{th} = 10^{-3}$ scenario.

22.9.2 Performance over Narrow-band Rayleigh Channels Using Antenna Diversity

In the last section, we observed that the adaptive modulation schemes employing Square QAM modes exhibit the highest BPS throughput among the schemes investigated, when operating over Nakagami fading channels. Hence, in this section we study the performance of the adaptive Square QAM schemes employing antenna diversity operating over independent Rayleigh fading channels. The BEP expression of the fixed-mode coherent BPSK scheme can be found on Page 781 of [388] and those of coherent Square QAM can be readily extended using the equations in (22.2) and (22.3). Furthermore, the antenna diversity scheme operating over independent narrow-band Rayleigh fading channels can be viewed as a special case of the two-dimensional (2D) Rake receiver analysed in Appendices 31.2 and 31.3. The performance of antenna-diversity assisted adaptive Square QAM schemes can be readily

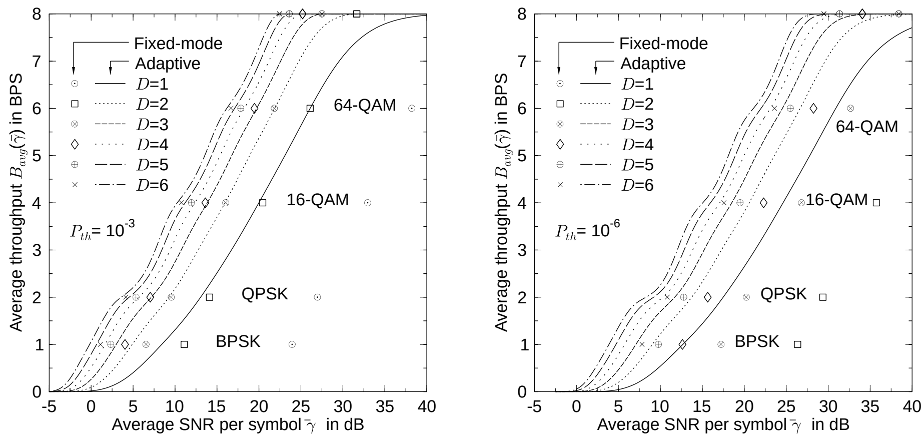

(a) $P_{th} = 10^{-3}$ **(b)** $P_{th} = 10^{-6}$

Figure 22.41: The average BPS throughput of the MRC-aided antenna-diversity assisted adaptive Square QAM scheme operating over independent Rayleigh fading channels at the target average BEP of (a) $P_{th} = 10^{-3}$ and (b) $P_{th} = 10^{-6}$. The markers represent the corresponding fixed-mode Square QAM performances.

analysed using the technique developed in Section 22.8.4.

Figure 22.41 depicts the average BPS throughput performance of our adaptive schemes employing Maximal Ratio Combining (MRC) aided antenna diversity [381] (Chapters 5 and 6) operating over independent Rayleigh fading channels at the target average BEP of $P_{th} = 10^{-3}$ and $P_{th} = 10^{-6}$. The markers represent the performance of the corresponding fixed-mode Square QAM modems in the same scenario. The average SNRs required achieving the target BEP of the fixed-mode schemes and that of the adaptive schemes decrease, as the antenna diversity order increases. However, the differences between the required SNRs of the adaptive schemes and their fixed-mode counterparts also decrease, as the antenna diversity order increases. The SNRs of both schemes required for achieving the target BEPs of $P_{th} = 10^{-3}$ and $P_{th} = 10^{-6}$ are displayed in Figure 22.42, where we can observe that dual antenna diversity is sufficient for the fixed-mode schemes in order to obtain half of the achievable SNR gain of the six-antenna aided diversity scheme, whereas triple-antenna diversity is required for the adaptive schemes operating in the same scenario. The corresponding first switching levels s_1 are depicted in Figure 22.43 for different orders of antenna diversity up to an order of six. As the antenna diversity order increases, the avalanche SNR becomes lower and the switching-threshold undulation effects begin to appear. The required values of the first switching level s_1 are within a range of about 1dB and 0.5dB for the target BEPs of $P_{th} = 10^{-3}$ and $P_{th} = 10^{-6}$, respectively, before the avalanche SNR is reached. This suggests that the optimum mode-switching levels are more dependent on the target BEP, than on the number of diversity antennas.

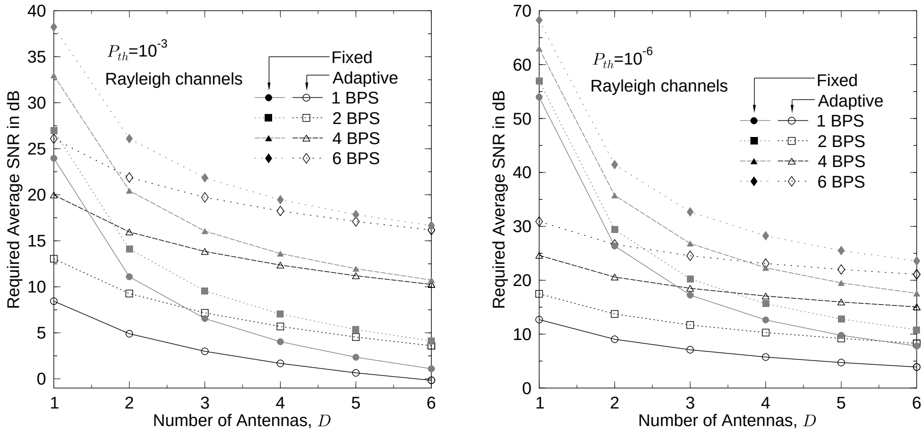

(a) $P_{th} = 10^{-3}$ **(b)** $P_{th} = 10^{-6}$

Figure 22.42: The SNR required for the MRC-aided antenna-diversity assisted adaptive Square QAM schemes and the corresponding fixed-mode modems operating over independent Rayleigh fading channels at the target average BEP of (a) $P_{th} = 10^{-3}$ and (b) $P_{th} = 10^{-6}$.

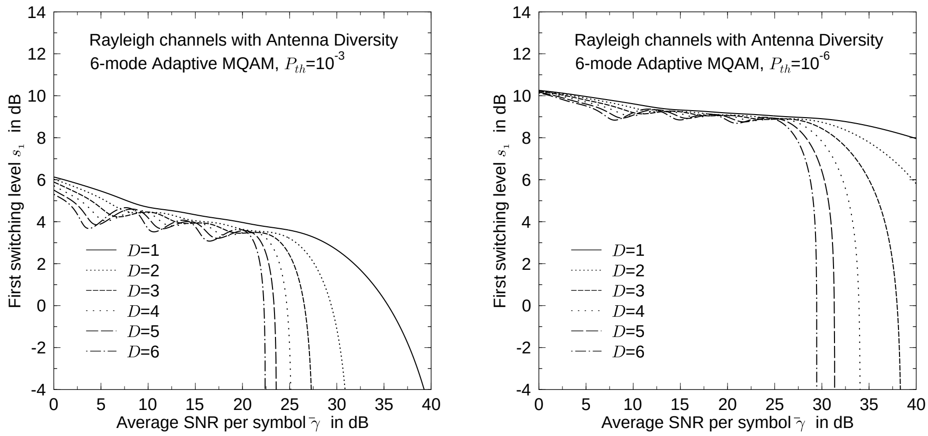

(a) $P_{th} = 10^{-3}$ **(b)** $P_{th} = 10^{-6}$

Figure 22.43: The first switching level s_1 of the MRC-aided antenna-diversity assisted adaptive Square QAM scheme operating over independent Rayleigh fading channels at the target average BEP of (a) $P_{th} = 10^{-3}$ and (b) $P_{th} = 10^{-6}$.

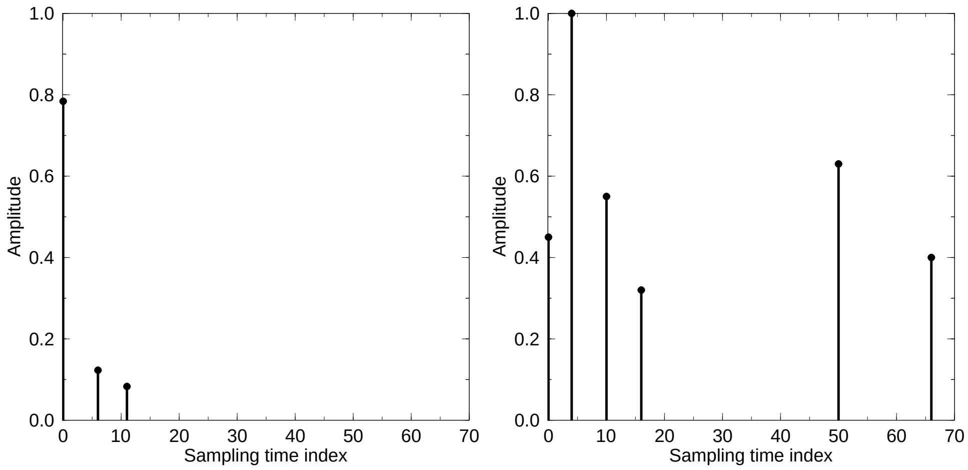

(a) W-ATM Channel **(b)** Bad Urban-A Channel

Figure 22.44: Multi-path Intensity Profiles (MIPs) of the Wireless Asynchronous Transfer Mode (W-ATM) indoor channel of Figure 17.1 and that of the Bad-Urban Reduced-model A (BU-RA) channel [676].

22.9.3 Performance over Wideband Rayleigh Channels using Antenna Diversity

Wideband fading channels are characterized by their multi-path intensity profiles (MIP). In order to study the performance of the various adaptive modulation schemes, we employ two different MIP models in this section, namely the shortened Wireless Asynchronous Transfer Mode (W-ATM) channel of Figure 17.3 for an indoor scenario and a Bad-Urban Reduced-model A (BU-RA) channel [676] for a hilly urban outdoor scenario. Their MIPs are depicted in Figure 22.44. The W-ATM channel exhibits short-range, low-delay multi-path components, while the BU-RA channel exhibits six higher-delay multi-path components. Again, let us assume that our receivers are equipped with MRC Rake receivers [677], employing a sufficiently higher number of Rake fingers, in order to capture all the multi-path components generated by our channel models. Furthermore, we employ antenna diversity [381] (Chapter 5) at the receivers. This combined diversity scheme is often referred to as a two-dimensional (2D) Rake receiver [678] (Page 263). The BEP of the 2D Rake receiver transmission over wide-band independent Rayleigh fading channels is analysed in Appendix 31.2. A closed-form expression for the mode-specific average BEP of a 2D-Rake assisted adaptive Square QAM scheme is also given in Appendix 31.3. Hence, the performance of our 2D-Rake assisted adaptive modulation scheme employing the optimum switching levels can be readily obtained.

The average BPS throughputs of the 2D-Rake assisted adaptive schemes operating over the two different types of wideband channel scenarios are presented in Figure 22.45 at the target BEP of $P_{th} = 10^{-2}$. The throughput performance depicted corresponds to the

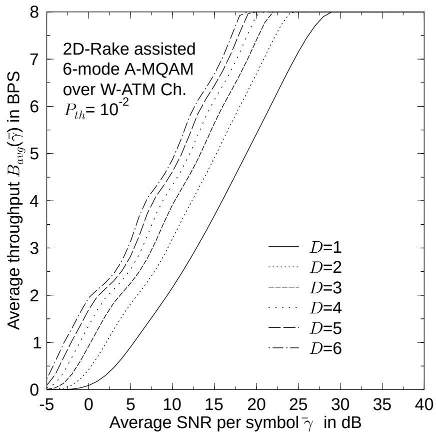

(a) W-ATM Channel

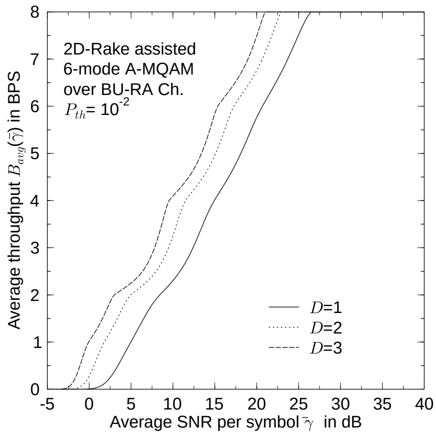

(b) BU-RA Channel

Figure 22.45: The effects of the number of diversity antennas D on the average BPS throughput of the 2D-Rake assisted six-mode adaptive Square QAM scheme operating over the wideband independent Rayleigh fading channels characterized in Figure 22.44 at the target BEP of $P_{th} = 10^{-2}$.

upper-bound performance of Direct-Sequence Code Division Multiple Access (DS-CDMA) or Multi-Carrier CDMA employing Rake receivers and the MRC-aided diversity assisted scheme in the absence of Multiple Access Interference (MAI). We can observe that the BPS throughput curves undulate, when the number of antennas D increases. This effect is more pronounced for transmission over the BU-RA channel, since the BU-RA channel exhibits six multi-path components, increasing the available diversity potential of the system approximately by a factor of two in comparison to that of the W-ATM channel. The performance of our adaptive scheme employing more than three antennas for transmission over the BU-RA channel could not be obtained owing to numerical instability, since the associated curves become similar to a series of step-functions, which is not analytic in mathematical terms. A similar observation can be made in the context of Figure 22.46, where the target BEP is $P_{th} = 10^{-3}$. Comparing Figure 22.45 and Figure 22.46, we observe that the BPS throughput curves corresponding to $P_{th} = 10^{-3}$ are similar to shifted versions of those corresponding to $P_{th} = 10^{-2}$, which are shifted in the direction of increasing SNRs. On the other hand, the BPS throughput curves corresponding to $P_{th} = 10^{-3}$ undulate more dramatically. When the number of antennas is $D = 3$, the BPS throughput curves of the BU-RA channel exhibit a stair-case like shape. The corresponding mode switching levels and mode selection probabilities are shown in Figure 22.47. Again, the switching levels heavily undulate. The mode-selection probability curve of BPSK has a triangular shape, increasing linearly, as the average SNR $\bar{\gamma}$ increases to 2.5dB and decreasing linearly again as $\bar{\gamma}$ increases from 2.5dB. On the other hand, the mode-selection probability curve of QPSK increases linearly and decreases exponentially, since no 3-BPS mode is used. This explains, why the BPS throughput curves increase in a near-linear fashion in the SNR range of 0 to 5dB and in a stair-case fash-

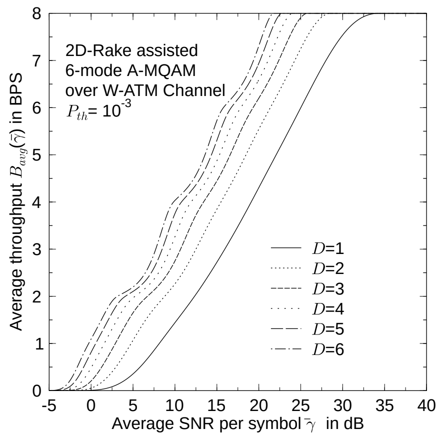

(a) W-ATM Channel **(b)** BU-RA Channel

Figure 22.46: The effects of the number of diversity antennas D on the average BPS throughput of the 2D-Rake assisted six-mode adaptive Square QAM scheme operating over the wideband independently Rayleigh fading channels characterized in Figure 22.44 at the target BEP of $P_{th} = 10^{-3}$.

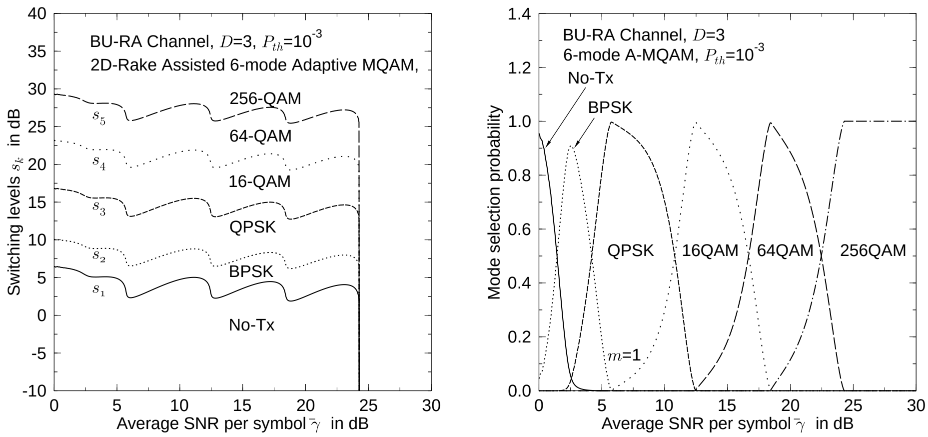

(a) Switching Levels **(b)** Mode Selection Probability

Figure 22.47: The mode switching levels and mode selection probability of the 2D-Rake assisted six-mode adaptive Square QAM scheme using $D = 3$ antennas operating over the BU-RA channel characterized in Figure 22.44(b) at the target BEP of $P_{th} = 10^{-3}$.

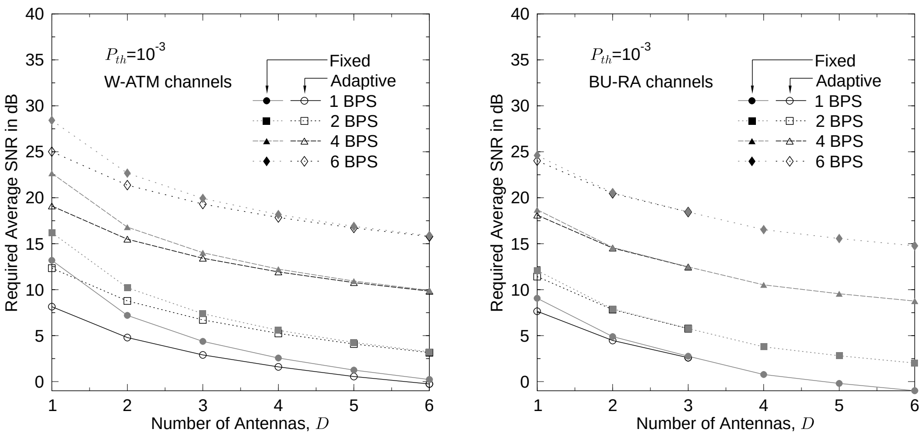

(a) W-ATM Channel

(b) BU-RA Channel

Figure 22.48: The average SNRs required for achieving the target BEP of $P_{th} = 10^{-3}$ by the 2D-Rake assisted adaptive schemes and by the fixed-mode schemes operating over (a) the W-ATM channel and (b) the BU-RA channel.

ion beyond that point. We can conclude that the stair-case like shape in the upper SNR range of SNR is a consequence of the absence of the 3-BPS, 5-BPS and 7-BPS modulation modes in the set of constituent modulation modes employed. As we discussed in Section 22.9.1.3, this problem may be mitigated by introducing power-efficient 8 QAM, 32 QAM and 128 QAM modes.

The average SNRs required achieving the target BEP of $P_{th} = 10^{-3}$ by the 2D-Rake assisted adaptive scheme and the fixed-mode schemes operating over wide-band fading channels are depicted in Figure 22.48. Since the fixed-mode schemes employing Rake receivers are already enjoying the diversity benefit of multi-path fading channels, the SNR advantages of our adaptive schemes are less than 8dB and 2.6dB over the W-ATM channel and over the BU-RA channel, respectively, even when a single antenna is employed. This relatively small SNR gain in comparison to those observed over narrow-band fading channels in Figure 22.42 erodes as the number of antennas increases. For example, when the number of antennas is $D = 6$, the SNR gains of the adaptive schemes operating over the W-ATM channel of Figure 22.44(a) become virtually zero, where the combined channel becomes an AWGN-like channel. On the other hand, $D = 3$ number of antennas is sufficient for the BU-RA channel for exhibiting such a behaviour, since the underlying multi-path diversity provided by the six-path BU-RA channel is higher than that of the tree-path W-ATM channel.

22.9.4 Uncoded Adaptive Multi-Carrier Schemes

The performance of the various adaptive Square QAM schemes has been studied also in the context of multi-carrier systems [179, 644, 679] . The family of Orthogonal Frequency Division Multiplex (OFDM) [593] systems converts frequency selective Rayleigh channels

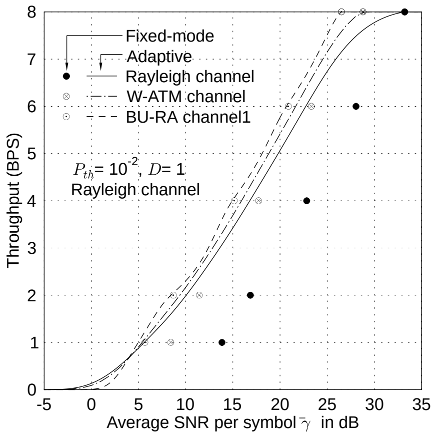

(a) $P_{th} = 10^{-2}$

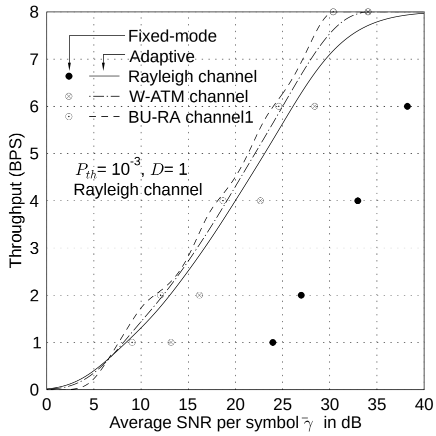

(b) $P_{th} = 10^{-3}$

Figure 22.49: The average BPS throughput of the adaptive schemes and fixed-mod schemes transmission over a narrow-band Rayleigh channel, the W-ATM channel and BU-RA channel of Figure 22.44 at the target BEP of (a) $P_{th} = 10^{-2}$ and (b) $P_{th} = 10^{-3}$.

into frequency non-selective or flat Rayleigh channels for each sub-carrier, provided that the number of sub-carriers is sufficiently high. The power and bit allocation strategy of adaptive OFDM has attracted substantial research interests [179]. OFDM is particularly suitable for combined time-frequency domain processing [644]. Since each sub-carrier of an OFDM system experiences a flat Rayleigh channel, we can apply adaptive modulation for each sub-carrier independently from other sub-carriers. Although a practical scheme would group the sub-carriers into similar-quality sub-bands for the sake of reducing the associated modem mode signalling requirements. The performance of this AQAM assisted OFDM (A-OFDM) scheme is identical to that of the adaptive scheme operating over flat Rayleigh fading channels, characterized in Section 22.9.2.

MC-CDMA [251, 254] receiver can be regarded as a frequency domain Rake-receiver, where the multiple carriers play a similar role to that of the time-domain Rake fingers. Our simulation results showed that the single-user BEP performance of MC-CDMA employing multiple antennas is essentially identical to that of the time-domain Rake receiver using antenna diversity, provided that the spreading factor is higher than the number of resolvable multi-path components in the channel. Hence, the throughput of the Rake-receiver over the three-path W-ATM channel [179] and the six-path BU-RA channel [676] studied in Section 22.9.3 can be used for investigating the upper-bound performance of adaptive MC-CDMA schemes over these channels. Figure 22.49 compares the average BPS throughput performances of these schemes, where the throughput curves of the various adaptive schemes are represented as three different types of lines, depending on the underlying channel scenarios, while the fixed-mode schemes are represented as three different types of markers. The solid line corresponds to the performance of A-OFDM and the marker '•' corresponds to that of the fixed-mode OFDM. On the other hand, the dotted lines correspond to the BPS throughput performance of adaptive MC-CDMA operating over wide-band channels and the markers '$\odot$' and '$\otimes$' to those of the fixed-mode MC-CDMA schemes.

It can be observed that fixed-mode MC-CDMA has a potential to outperform A-OFDM, when the underlying channel provides sufficient diversity due to the high number of resolvable multi-path components. For example, the performance of fixed-mode MC-CDMA operating over the W-ATM channel of Figure 22.44(a) is slightly lower than that of A-OFDM for the BPS range of less than or equal to 6 BPS, owing to the insufficient diversity potential of the wide-band channel. On the other hand, fixed-mode MC-CDMA outperforms A-OFDM, when the channel is characterized by the BU-RA model of Figure 22.44(b). We have to consider several factors, in order to answer, whether fixed-mode MC-CDMA is better than A-OFDM. Firstly, fully loaded MC-CDMA, which can transmit the same number of symbols as OFDM, suffers from multi-code interference and our simulation results showed that the SNR degradation is about 2-4dB at the BEP of 10^{-3}, when the Minimum Mean Square Error Block Decision Feedback Equalizer (MMSE-BDFE) [680] based joint detector is used at the receiver. Considering these SNR degradations, the throughput of fixed-mode MC-CDMA using the MMSE-BDFE joint detection receiver falls just below that of the A-OFDM scheme, when the channel is characterized by the BU-RA model. On the other hand, the adaptive schemes may suffer from inaccurate channel estimation/prediction and modem mode signalling feedback delay [183]. Hence, the preference order of the various schemes may depend on the channel scenario encountered, on the interference effects and other practical issues, such as the aforementioned channel estimation accuracy, feedback delays, etc.

22.9.5 Concatenated Space-Time Block Coded and Turbo Coded Symbol-by-Symbol Adaptive OFDM and Multi-Carrier CDMA[3]

In the previous sections we studied the performance of uncoded adaptive schemes. Since a Forward Error Correction (FEC) code reduces the SNR required for achieving a given target BEP at the expense of a reduced BPS throughput, it is interesting to investigate the performance of adaptive schemes employing FEC techniques. These investigations will allow us to gauge, whether channel coding is capable of increasing the system's effective throughput, when aiming for a specific target BER. Another important question to be answered is whether there are any further potential performance advantages, when we combine adaptive modulation with space-time coding. We note in advance that our related investigations are included here with a view to draw the reader's attention to the associated system design trade-offs, rather than to provide an indepth comparative study of adaptive modulation and space-time coding. Hence for reasons of space economy here we will be unable to elaborate on the philosophy of space-time coding, we will simply refer to the associated literature for background reading [170].

A variety of FEC techniques has been used in the context of adaptive modulation schemes. In their pioneering work on adaptive modulation, Webb and Steele [176] used a set of binary BCH codes. Vucetic [682] employed various punctured convolutional codes in response to the time-variant channel status. On the other hand, various Trellis Coded Modulation (TCM) [495, 496] schemes were used in the context of adaptive modulation by Alamouti and Kallel [683], Goldsmith and Chua [684], as well as Hole, Holm and Øien [208]. Keller,

[3]This section was based on collaborative research with the contents of [681].

Liew and Hanzo studied the performance of Redundant Residue Number System (RRNS) codes in the context of adaptive multi-carrier modulation [685, 686]. Various turbo coded adaptive modulation schemes have been investigated also by Liew, Wong, Yee and Hanzo [202,687,688]. With the advent of space-time (ST) coding techniques [617,619,620], various concatenated coding schemes combining ST coding and FEC coding can be applied in adaptive modulation schemes. In this section, we investigate the performance of various concatenated space-time block-coded and turbo-coded adaptive OFDM and MC-CDMA schemes.

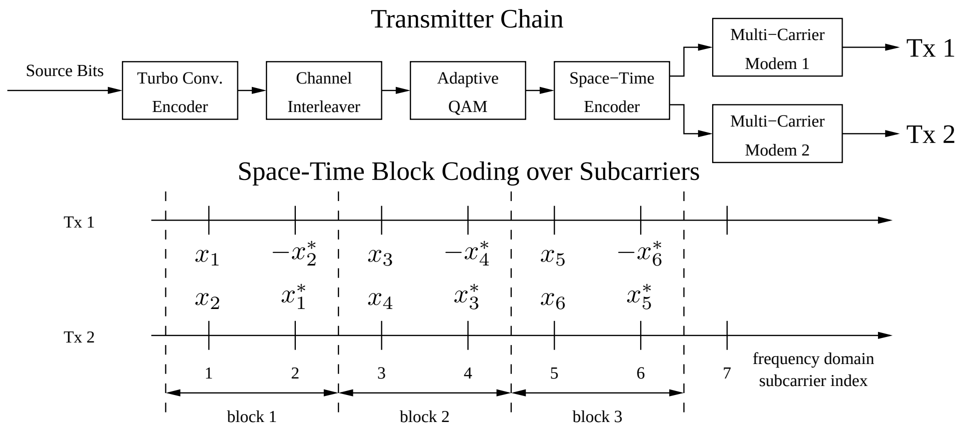

Figure 22.50: Transmitter structure and space-time block encoding scheme

Figure 22.50 portrays the stylised transmitter structure of our system. The source bits are channel coded by a half-rate turbo convolutional encoder [689] using a constraint length of $K = 3$ as well as an interleaver having a memory of $L = 3072$ bits and interleaved by a random block interleaver. Then, the AQAM block selects a modulation mode from the set of no transmission, BPSK, QPSK, 16-QAM and 64-QAM depending on the instantaneous channel quality perceived by the receiver, according to the SNR-dependent optimum switching levels derived in Section 22.8.4. It is assumed that the perfectly estimated channel quality experienced by receiver A is fed back to transmitter B superimposed on the next burst transmitted to receiver B. The modulation mode switching levels of our AQAM scheme determine the average BEP as well as the average throughput.

The modulated symbol is now space-time encoded. As seen at the bottom of Figure 22.50, Alamouti's space-time block code [617] is applied across the frequency domain. A pair of the adjacent sub-carriers belonging to the same space-time encoding block is assumed to have the same channel quality. We employed a Wireless Asynchronous Transfer Mode (W-ATM) channel model of Figure 17.1 transmitting at a carrier frequency of 60GHz, at a sampling rate of 225MHz and employing 512 sub-carriers. Specifically, we used a three-path fading channel model, where the average SNR of each path is given by $\bar{\gamma}_1 = 0.79192\bar{\gamma}$, $\bar{\gamma}_2 = 0.12424\bar{\gamma}$ and $\bar{\gamma}_3 = 0.08384\bar{\gamma}$. The Multi-path Intensity Profile (MIP) of the W-ATM channel is illustrated in Figure 22.44(a) in Section 22.9.3. Each channel associated with a different antenna is assumed to exhibit independent fading.

The simulation results related to our uncoded adaptive modems are presented in Fig-

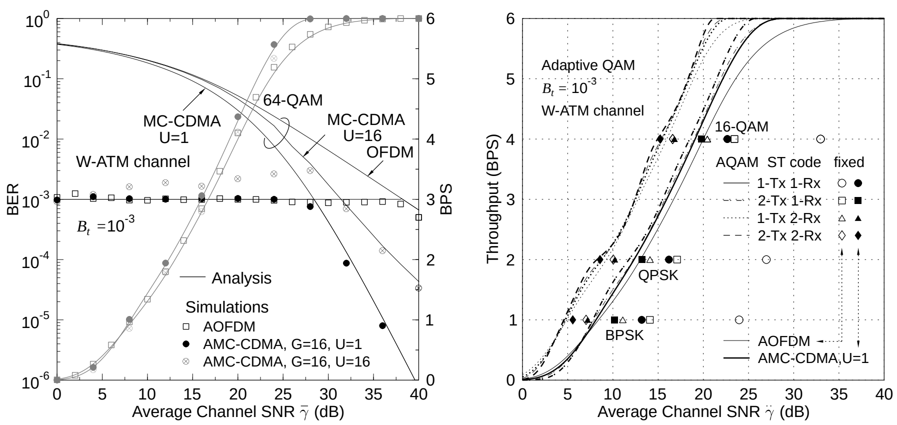

(a) BER and Throughput, No ST coding **(b)** Throughput with ST coding

Figure 22.51: Performance of uncoded five-mode AOFDM and AMC-CDMA. The target BEP is $B_t = 10^{-3}$ when transmitting over the W-ATM channel model of Figurefig:10+420. (a) The constant average BEP is maintained for AOFDM and single user AMC-CDMA, while 'full-user' AMC-CDMA exhibits a slightly higher average BEP due to the residual MUI. (b) The SNR gain of the adaptive modems decreases, as ST coding increases the diversity order. The BPS curves appear in pairs, corresponding to AOFDM and AMC-CDMA - indicated by the thin and thick lines, respectively - for each of the four different ST code configurations. The markers represent the SNRs required by the fixed-mode OFDM and MC-CDMA schemes for maintaining the target BER of 10^{-3} in conjunction with the four ST-coded schemes considered.

ure 22.51. Since we employed the optimum switching levels derived in Section 22.8.4, both our adaptive OFDM (AOFDM) and the adaptive single-user MC-CDMA (AMC-CDMA) modems maintain the constant target BER of 10^{-3} up to the 'avalanche' SNR value, and then follow the BER curve of the 64-QAM mode. However, 'full-user' AMC-CDMA, which is defined as an AMC-CDMA system supporting $U = 16$ users with the aid of a spreading factor of $G = 16$ and employing the MMSE-BDFE Joint Detection (JD) receiver [690], exhibits a slightly higher average BER, than the target of $B_t = 10^{-3}$ due to the residual Multi-User Interference (MUI) of the imperfect joint detector. Since in Section 22.8.4 we derived the optimum switching levels based on a single-user system, the levels are no longer optimum, when residual MUI is present. The average throughputs of the various schemes expressed in terms of BPS steadily increase and at high SNRs reach the throughput of 64-QAM, namely 6 BPS. The throughput degradation of 'full-user' MC-CDMA imposed by the imperfect JD was within a fraction of a dB. Observe in Figure 22.51(a) that the analytical and simulation results are in good agreement, which we denoted by the lines and distinct symbols, respectively.

The effects of ST coding on the average BPS throughput are displayed in Figure 22.51(b). Specifically, the thick lines represent the average BPS throughput of our AMC-CDMA scheme, while the thin lines represent those of our AOFDM modem. The four pairs of hollow and filled markers associated with the four different ST-coded AOFDM and AMC-CDMA scenarios considered represent the BPS throughput versus SNR values associated with fixed-mode OFDM and fixed-mode MMSE-BDFE JD assisted MC-CDMA schemes. Specifically, observe for each of the 1, 2 and 4 BPS fixed-mode schemes that the right most markers, namely the circles, correspond to the 1-Tx / 1-Rx scenario, the squares to the 2-Tx / 1-Rx scheme, the triangles to the 1-Tx / 2-Rx arrangement and the diamonds to the 2-Tx / 2-Rx scenarios. First of all, we can observe that the BPS throughput curves of OFDM and single-user MC-CDMA are close to each other, namely within 1 dB for most of the SNR range. This is surprising, considering that the fixed-mode MMSE-BDFE JD assisted MC-CDMA scheme was reported to exhibit around 10dB SNR gain at a BEP of 10^{-3} and 30dB gain at a BEP of 10^{-6} over OFDM [256]. This is confirmed in Figure 22.51(b) by observing that the SNR difference between the $\circ$ and $\bullet$ markers is around 10dB, regardless whether the 4, 2 or 1 BPS scenario is concerned.

Let us now compare the SNR gains of the adaptive modems over the fixed modems. The SNR difference between the BPS curve of AOFDM and the fixed-mode OFDM represented by the symbol $\circ$ at the same throughput is around 15dB. The corresponding SNR difference between the adaptive and fixed-mode 4, 2 or 1 BPS MC-CDMA modem is around 5dB. More explicitly, since in the context of the W-ATM channel model of Figure 17.1 fixed-mode MC-CDMA appears to exhibit a 10dB SNR gain over fixed-mode OFDM, the additional 5dB SNR gain of AMC-CDMA over its fixed-mode counterpart results in a total SNR gain of 15dB over fixed-mode OFDM. Hence ultimately the performance of AOFDM and AMC-CDMA becomes similar.

Let us now examine the effect of ST block coding. The SNR gain of the fixed-mode schemes due to the introduction of a 2-Tx / 1-Rx ST block code is represented as the SNR difference between the two right most markers, namely circles and squares. These gains are nearly 10dB for fixed-mode OFDM, while they are only 3dB for fixed-mode MC-CDMA modems. However, the corresponding gains are less than 1dB for both adaptive modems, namely for AOFDM and AMC-CDMA. Since the transmitter power is halved due to using two Tx antennas in the ST codec, a 3dB channel SNR penalty was already applied to the curves in Figure 22.51(b). The introduction of a second receive antenna instead of a second transmit antenna eliminates this 3dB penalty, which results in a better performance for the 1-Tx/2-Rx scheme than for the 2-Tx/1-Rx arrangement. Finally, the 2-Tx / 2-Rx system gives around 3-4dB SNR gain in the context of fixed-mode OFDM and a 2-3dB SNR gain for fixed-mode MC-CDMA, in both cases over the 1-Tx / 2-Rx system. By contrast, the SNR gain of the 2-Tx / 2-Rx scheme over the 1-Tx / 2-Rx based adaptive modems was, again, less than 1dB in Figure 22.51(b). More importantly, for the 2-Tx / 2-Rx scenario the advantage of employing adaptive modulation erodes, since the fixed-mode MC-CDMA modem performs as well as the AMC-CDMA modem in this scenario. Moreover, the fixed-mode MC-CDMA modem still outperforms the fixed-mode OFDM modem by about 2dB. We conclude that since the diversity-order increases with the introduction of ST block codes, the channel quality variation becomes sufficiently small for the performance advantage of adaptive modems to erode. This is achieved at the price of a higher complexity due to employing two transmitters and two receivers in the ST coded system.

When channel coding is employed in the fixed-mode multi-carrier systems, it is expected that OFDM benefits more substantially from the frequency domain diversity than MC-CDMA, which benefited more than OFDM without channel coding. The simulation

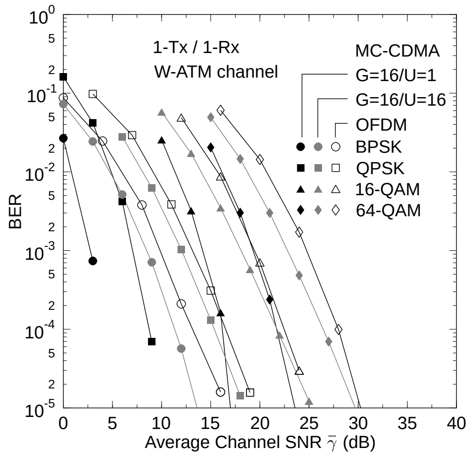

Figure 22.52: Performance of turbo convolutional coded fixed-mode OFDM and MC-CDMA for transmission over the W-ATM channel of Figure 17.1, indicating that JD MC-CDMA still outperforms OFDM. However, the SNR gain of JD MC-CDMA over OFDM is reduced to 1-2dB at a BEP of 10^{-4}.

results depicted in Figure 22.52 show that the various turbo-coded fixed-mode MC-CDMA systems consistently outperform OFDM. However, the SNR differences between the turbo-coded BER curves of OFDM and MC-CDMA are reduced considerably.

The performance of the concatenated ST block coded and turbo convolutional coded adaptive modems is depicted in Figure 22.53. We applied the optimum set of switching levels designed in Section 22.8.4 for achieving an uncoded BEP of 3×10^{-2}. This uncoded target BEP was stipulated after observing that it is reduced by half-rate, $K = 3$ turbo convolutional coding to a BEP below 10^{-7}, when transmitting over AWGN channels. However, our simulation results yielded zero bit errors, when transmitting 10^9 bits, except for some SNRs, when employing only a single antenna.

Figure 22.53(a) shows the BEP of our turbo coded adaptive modems, when a single antenna is used. We observe in the figure that the BEP reaches its highest value around the 'avalanche' SNR point, where the adaptive modulation scheme consistently activates 64-QAM. The system is most vulnerable around this point. In order to interpret this phenomenon, let us briefly consider the associated interleaving aspects. For practical reasons we have used a fixed interleaver length of $L = 3072$ bits. When the instantaneous channel quality was high, the $L = 3072$ bits were spanning a shorter time-duration during their passage over the fading channel, since the effective BPS throughput was high. Hence the channel errors appeared more bursty, than in the lower-throughput AQAM modes, which conveyed the $L = 3072$ bits over a longer time duration, hence dispersing the error bursts over a longer duration of time. The uniform dispersion of erroneous bits versus time enhances the error correction power of the turbo code. On the other hand, in the SNR region beyond the 'avalanche' SNR point seen in Figure 22.53(a) the system exhibited a lower uncoded BER, reducing the coded BEP even further. This observation suggests that further research ought to determine the set of switching thresholds directly for a coded adaptive system, rather than by simply

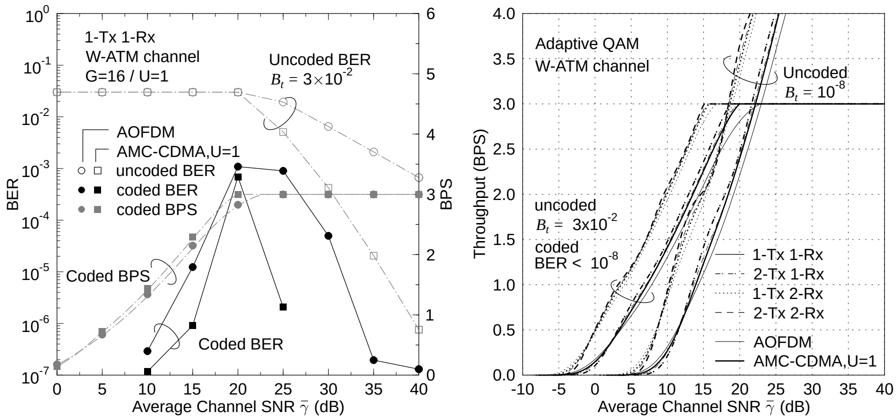

(a) BER **(b)** Throughput

Figure 22.53: Performance of the concatenated ST block coded and turbo convolutional coded adaptive OFDM and MC-CDMA systems communicating over the W-ATM channel of Figure 17.1. The uncoded target BEP is 3×10^{-2}. The coded BEP was less than 10^{-8} for most of the SNR range, resulting in virtually error free transmission. (a) The coded BEP becomes higher near the 'avalanche' SNR point, when a single antenna was used. (b) The coded adaptive modems have SNR gains up to 7dB compared to their uncoded counterparts achieving a comparable average BER.

estimating the uncoded BER, which is expected to result in near-error-free transmission.

We can also observe that the turbo coded BEP of AOFDM is higher than that of AMC-CDMA in the SNR range of 10-20dB, even though the uncoded BER is the same. This appears to be the effect of the limited exploitation of frequency domain diversity of coded OFDM, compared to MC-CDMA, which leads to a more bursty uncoded error distribution, hence degrading the turbo coded performance. The fact that ST block coding aided multiple antenna systems show virtually error free performance corroborates our argument.

Figure 22.53(b) compares the throughputs of the coded adaptive modems and the uncoded adaptive modems exhibiting a comparable average BER. The SNR gains due to channel coding were in the range of 0dB to 8dB, depending on the SNR region and on the scenarios employed. Each bundle of throughput curves corresponds to the scenarios of 1-Tx/1-Rx OFDM, 1-Tx/1-Rx MC-CDMA, 2-Tx/1-Rx OFDM, 2-Tx/1-Rx MC-CDMA, 1-Tx/2-Rx OFDM, 1-Tx/2-Rx MC-CDMA, 2-Tx/2-Rx OFDM and 2-Tx/2-Rx MC-CDMA starting from the far right curve, when viewed for throughput values higher than 0.5 BPS. The SNR difference between the throughput curves of the ST and turbo coded AOFDM and those of the corresponding AMC-CDMA schemes was reduced compared to the uncoded performance curves of Figure 22.51(b). The SNR gain owing to ST block coding assisted transmit diversity in the context of AOFDM and AMC-CDMA was within 1dB due to the halved transmitter power. Therefore, again, ST block coding appears to be less effective in conjunction with adaptive modems.

In conclusion, the performance of ST block coded constant-power adaptive multi-carrier modems employing optimum SNR-dependent modem mode switching levels were investigated in this section. The adaptive modems maintained the constant target BEP stipulated, whilst maximizing the average throughput. As expected, it was found that ST block coding reduces the relative performance advantage of adaptive modulation, since it increases the diversity order and eventually reduces the channel quality variations. When turbo convolutional coding was concatenated to the ST block codes, near-error-free transmission was achieved at the expense of halving the average throughput. Compared to the uncoded system, the turbo coded system was capable of achieving a higher throughput in the low SNR region at the cost of a higher complexity. The study of the relationship between the uncoded BEP and the corresponding coded BEP showed that adaptive modems obtain higher coding gains, than that of fixed modems. This was due to the fact that the adaptive modem avoids burst errors even in deep channel fades by reducing the number of bits per modulated symbol eventually to zero.

22.10 Summary

Following a brief introduction to several fading counter-measures, a general model was used to describe several adaptive modulation schemes employing various constituent modulation modes, such as PSK, Star QAM and Square QAM, as one of the attractive fading counter-measures. In Section 22.7.3.1, the closed form expressions were derived for the average BER, the average BPS throughput and the mode selection probability of the adaptive modulation schemes, which were shown to be dependent on the mode-switching levels as well as on the average SNR. After reviewing in Section 22.8.1, 22.8.2 and 22.8.3 the existing techniques devised for determining the mode-switching levels, in Section 22.8.4 the optimum switching levels achieving the highest possible BPS throughput while maintaining the average target BEP were developed based on the Lagrangian optimization method.

Then, in Section 22.9.1 the performance of uncoded adaptive PSK, Star QAM and Square QAM was characterized, when the underlying channel was a Nakagami fading channel. It was found that an adaptive scheme employing a k-BPS fixed-mode as the highest throughput constituent modulation mode was sufficient for attaining all the benefits of adaptive modulation, while achieving an average throughput of up to $(k-1)$ BPS. For example, a three-mode adaptive PSK scheme employing No-Tx, 1-BPS BPSK and 2-BPS QPSK modes attained the maximum possible average BPS throughput of 1 BPS and hence adding higher-throughput modes, such as 3-BPS 8-PSK to the three-mode adaptive PSK scheme resulting in a four-mode adaptive PSK scheme did not achieve a better performance across the 1 BPS throughput range. Instead, this four-mode adaptive PSK scheme extended the maximal achievable BPS throughput by any adaptive PSK scheme to 2 BPS, while asymptotically achieving a throughput of 3 BPS as the average SNR increases.

On the other hand, the relative SNR advantage of adaptive schemes in comparison to fixed-mode schemes increased as the target average BER became lower and decreased as the fading became less severe. More explicitly, less severe fading corresponds to an increased Nakagami fading parameter m, to an increased number of diversity antennas, or to an increased number of multi-path components encountered in wide-band fading channels. As the fading becomes less severe, the average BPS throughput curves of our adaptive Square QAM schemes exhibit undulations owing to the absence of 3-BPS, 5-BPS and 7-BPS square QAM modes.

The comparisons between fixed-mode MC-CDMA and adaptive OFDM (AOFDM) were made based on different channel models. In Section 22.9.4 it was found that fixed-mode MC-CDMA might outperform adaptive OFDM, when the underlying channel provides sufficient diversity. However, a definite conclusion could not be drawn since in practice MC-CDMA might suffer from MUI and AOFDM might suffer from imperfect channel quality estimation and feedback delays.

Concatenated space-time block coded and turbo convolutional-coded adaptive multi-carrier systems were investigated in Section 22.9.5. The coded schemes reduced the required average SNR by about 6dB-7dB at throughput of 1 BPS achieving near error-free transmission. It was also observed in Section 22.9.5 that increasing the number of transmit antennas in adaptive schemes was not very effective, achieving less than 1dB SNR gain, due to the fact that the transmit power per antenna had to be reduced in order to limit the total transmit power for the sake of fair comparison.

Part IV

Advanced QAM: Turbo-Equalised Adaptive TCM, TTCM, BICM, BICM-ID and Space-Time Coding Assisted OFDM and CDMA Systems

Chapter 23

Capacity and Cutoff Rate of Gaussian and Rayleigh Channels

23.1 Introduction

An important accomplishment of information theory is the determination of the channel capacity, C, which quantifies the maximum achievable transmission rate, C^*, of a system communicating over a bandlimited channel, while maintaining an arbitrarily low probability of error. Given the fact that the available bandwidth of all transmission media is limited, it is desirable to transmit information as bandwidth-efficiently, as possible. This implies transmitting as many bits per Hertz, as possible. In recent years the available wireless communications frequency bands have been auctioned by the American, British, German and by other goverments to service provider companies at a high price and therefore its is of high commercial interest to exploit the available bandwidth as best as possible. Quantifying these information theoretic limits is the objective of this chapter. Given these limits, in the rest of the book we will aim for quantifying the various system's ability to perform as close to the limits as possible. This issue was first discussed in a rudimentary fashion in the context of Figure 2.4 and here we will considerably deepen our approach.

The units of the channel capacity C and relative or normalised channel capacity $C^* = C/T$ are bit per symbol and bit per second, respectively, where T is the symbol period. The capacity of a Single-Input Single-Output (SISO) AWGN channel was quantified by Shannon in 1948 [551]. Since then, substantial research efforts have been invested in finding channel codes that would produce an arbitrarily low probability of error at a transmission rate close to C^*. Normalising the channel capacity with respect to the bandwidth occupied yields another useful parameter, namely the bandwidth efficiency η. A lower bound to the channel capacity referred to as the channel's cutoff rate is another useful parameter. The cutoff rate, R_0, has been also referred to as the "practically achievable capacity", since the complexity of a coded system becomes substantially higher, when communicating near R_0, in comparison to transmissions at rates below R_0 [494, 502, 691].

23.2 Channel Capacity

Let the input and output of the Discrete Memoryless Channel (DMC) [388] be X and Y, respectively, where X may assume one of K discrete-amplitude values, while Y can be one of J legitimate discrete-amplitude values. The assignment of $x = a_k$ and $y = b_j$ corresponds to encountering two specific $events$. Let the probability of encountering each event be denoted as:

$$p(k) = P(x = a_k), \tag{23.1}$$

$$p(j) = P(y = b_j), \tag{23.2}$$

while the conditional probability of receiving $y = b_j$, given that $x = a_k$ was transmitted be denoted as:

$$p(j|k) \quad = \quad P(y = b_j|x = a_k). \tag{23.3}$$

Mutual information is by definition a measure of "information about the event $x = a_k$ provided by the occurrence of the event $y = b_j$", which is defined as [692]:

$$I_{X;Y}(a_k; b_j) \quad = \quad \log_2 \left[\frac{p(k|j)}{p(k)}\right] \text{ [bit]}, \tag{23.4}$$

where the base of the logarithm is 2 and hence the units of mutual information are bits. The average mutual information, $I(X;Y)$, is the expectation of $I_{X;Y}(a_k; b_j)$ expressed in Equation 23.4, which yields:

$$I(X;Y) \quad = \quad \sum_{k=1}^{K}\sum_{j=1}^{J} p(k,j) \log_2 \left[\frac{p(k|j)}{p(k)}\right] \text{ [bit/symbol]}, \tag{23.5}$$

where the unit of bit/symbol is used for indicating the number of bits conveyed per transmitted symbol. By using the probability identities [672] of $p(x|y) = \frac{p(y|x)p(x)}{p(y)}$ and $p(x,y) = p(y|x)p(x)$, derived from Bayes' rule, the average mutual information is rewritten as:

$$I(X;Y) \quad = \quad \sum_{k=1}^{K}\sum_{j=1}^{J} p(j|k)p(k) \log_2 \left[\frac{p(j|k)}{p(j)}\right] \text{ [bit/symbol]}. \tag{23.6}$$

The channel capacity is defined as the highest possible average mutual information obtained by finding the specific set of input symbol probability assignments, $\{p(k); k = 1, \ldots, K\}$, which maximises $I(X;Y)$. The DMC capacity, C_{DMC}, may be written as [692, p. 74]:

$$C_{\text{DMC}} \quad = \quad \max_{\{p(k);k=1,\ldots,K\}} \sum_{k=1}^{K}\sum_{j=1}^{J} p(j|k)p(k) \log_2 \left[\frac{p(j|k)}{p(j)}\right] \text{ [bit/symbol]}. \tag{23.7}$$

Naturally, in practise we do not have control over the probability of the channel's input symbols and hence depending on the specific probabilities of the channel input symbols we may not be able to approach the capacity of the channel.

23.2.1 Vector Channel Model

It was argued in [503, pp. 348-351] that bandlimited signals having a finite energy may be described as vectors having a dimensionality of:

$$N = 2WT, \tag{23.8}$$

provided that the following assumptions are satisfied:

1) the waveform is constrained to an ideal lowpass or bandpass bandwidth, W; and

2) the waveform is limited to the time interval, $0 \leq t \leq T$.

Strictly speaking assumptions 1 and 2 cannot be fulfilled simultaneously, because according to the properties of the Fourier transform a finite-bandwidth signal has an infinite time-domain support and vice-versa. Let us however briefly consider a full-response Minimum Shift Keying (MSK) [388] modulator, where the modulated signal's spectrum has a sinc-function shape. The first and highest spectral side-lobe of the sinc-shaped spectrum is about 20 dB lower than the main spectral lobe, as seen for example in Figure 13.15 of [369]. Hence we may argue that although the time-domain signalling pulse is time-limited, the corresponding spectrum has a low energy outside the main spectral lobe. This line of argument may be continued by considering for example partial-response Gaussian MSK (GMSK) signalling, which results in substantially lower spectral side-lobes, than MSK, again as seen for example in Figure 13.15 of [369]. In fact the time-domain Gaussian pulse is known to have the smoothest possible time-domain signalling pulse evolution, resulting in the most compact spectral-domain representation and a more-or-less bandlimited spectrum. Hence loosely speaking we may argue that although according to the Fourier transform the spectral-domain support of a finite-duration signal is infinite, for practical reasons the signal may be considered both time- and band-limited. Similar arguments are also valid in case of full-response Nyquist signalling based system such as those considered in this monograph.

A set of functions is said to be orthonormal, if the functions are orthogonal to each other and they are also normalised to unit energy within a common interval of $T = T_2 - T_1$, yielding [693, p. 153]:

$$\int_{T_1}^{T_2} \phi_i(t)\phi_j(t)\, dt = \begin{cases} 1, & i = j, \\ 0, & i \neq j. \end{cases} \tag{23.9}$$

Orthonormal functions $\{\phi_n(t)\}$ can be generated using a variety of different methods, such as the Fourier series and Gram-Schmidt procedures [388, pp. 167-173]. However, the dimensionality of the signal space remains $N = 2WT$, as long as the signals are being time and bandlimited in the sense as argued above. Specifically, a bandlimited continuous-time signalling waveform, $x(t)$, can be expressed as a linear combination of orthonormal functions,

$\{\phi_n(t)\}$, as:

$$x(t) = \sum_{n=1}^{N} x[n]\phi_n(t), \tag{23.10}$$

which is sufficiently accurately defined by $N = 2WT$ number of coefficients, when $x(t)$ is sufficiently close zero outside the interval T. Furthermore, the coefficients, $x[n]$, can be obtained from:

$$x[n] = \int_{t=0}^{T} x(t)\phi_n(t)\, dt \tag{23.11}$$

for all n, where the integration is over the signalling period T. Let us now represent the channel's input $\mathbf{x} = (x[1], \ldots, x[N])$ and output $\mathbf{y} = (y[1], \ldots, y[N])$ as N-component, i.e. N-dimensional real-valued vectors. Note that $\mathbf{x}$ and $\mathbf{y}$ may be discrete-valued or continuous-valued, depending on the channel encountered.

A relative of the DMC is the Continuous-Input Continuous-Output Memoryless Channel (CCMC) [388], where the corresponding coefficients of $\mathbf{x}$ and $\mathbf{y}$ are continuous-valued as indicated below:

$$x[n] \in [-\infty, +\infty], \tag{23.12}$$
$$y[n] \in [-\infty, +\infty],\ n = 1, \ldots, N. \tag{23.13}$$

This model is applicable to a scenario employing an analogue modulation scheme, such as amplitude, phase or frequency modulation. The channel capacity of the DMC in Equation 23.7 can be extended for the CCMC as [692]:

$$C_{\text{CCMC}} = \max_{p(\mathbf{x})} \underbrace{\int_{-\infty}^{\infty} \cdots \int_{-\infty}^{\infty}}_{\text{2N-fold}} p(\mathbf{y}|\mathbf{x})p(\mathbf{x}) \log_2 \left[\frac{p(\mathbf{y}|\mathbf{x})}{p(\mathbf{y})}\right] d\mathbf{x}\, d\mathbf{y} \text{ [bit/symbol]}, \tag{23.14}$$

where again, $\mathbf{x} = (x[1], \ldots, x[N])$ and $\mathbf{y} = (y[1], \ldots, y[N])$ are N-dimensional signals at the channel input and output, respectively.

Another relative of the DMC is the Discrete-Input Continuous-Output Memoryless Channel (DCMC) [388], where the channel input belongs to the discrete set of M-ary values:

$$\mathbf{x} \in \{\mathbf{x}_m : m = 1, \ldots, M\}. \tag{23.15}$$

More explicitly, the channel input $\mathbf{x}_m = (x_m[1], \ldots, x_m[N])$ is a $\log_2(M)$-bit symbol having N discrete-valued coefficients. By contrast, the channel output $\mathbf{y}$ has continuous-valued coefficients:

$$y[n] \in [-\infty, +\infty],\ n = 1, \ldots, N. \tag{23.16}$$

The channel capacity for the DCMC can also be derived from Equation 23.7 as [694]:

$$C_{\text{DCMC}} = \max_{p(\mathbf{x}_1)\ldots p(\mathbf{x}_M)} \sum_{m=1}^{M} \underbrace{\int_{-\infty}^{\infty} \cdots \int_{-\infty}^{\infty}}_{\text{N-fold}} p(\mathbf{y}|\mathbf{x}_m) p(\mathbf{x}_m) \log_2 \left[\frac{p(\mathbf{y}|\mathbf{x}_m)}{p(\mathbf{y})} \right] d\mathbf{y} \text{ [bit/symbol]}, \quad (23.17)$$

where again $\mathbf{x}_m = (x_m[1], \ldots, x_m[N])$ is the N-dimensional M-ary symbol at the channel's input while $\mathbf{y} = (y[1], \ldots, y[N]$ is the N-dimensional signal at the channel's output.

23.2.2 The Capacity of AWGN Channels

The Shannon bound of an AWGN channel is obtained by finding the capacity of a continuous-input continuous-output AWGN channel, where the modulated signal itself, $x(t)$, may be modelled by bandlimited Gaussian noise [1] at the channel input, which is contaminated by the AWGN channel noise $n(t)$. After bandlimiting, the samples of both noise sources are taken at the Nyquist rate. These samples are independent identical distributed (iid) Gaussian random variables with zero mean having a variance of σ^2 for $x(t)$ and $N_0/2$ for $n(t)$. The resultant sampled waveforms can be described as vectors of N discrete-time but continuous-valued samples, where $N = 2WT$ is the signal dimensionality defined in Equation 23.8. Upon exploiting that the Probability Density Functions (PDFs) of $p(\mathbf{x})$, $p(\mathbf{y})$ and $p(\mathbf{y}|\mathbf{x})$ are Gaussian, the Shannon bound can be derived from Equation 23.14 as [551, 695]:

$$\begin{aligned} C_{\text{CCMC}}^{\text{AWGN}} &= WT \log_2(1+\gamma) \text{ [bit/symbol]}, \\ &= \frac{N}{2} \log_2(1+\gamma) \text{ [bit/symbol]}, \end{aligned} \quad (23.18)$$

where γ is the Signal to Noise ratio (SNR). Note that when the channel input is a continuous-valued variable corresponding to an analogue modulation scheme, the capacity is only restricted either by the signalling energy and hence γ or by the bandwidth W [388]. Therefore we will refer to the capacity of the CCMC as the **unrestricted bound**.

Let us now consider the achievable capacity of DCMC, when transmitting the N-dimensional M-ary signals using Equation 23.17. Assuming equiprobable M-ary input symbols conveying $\log_2(M)$ bit/symbol information, we have:

$$p(\mathbf{x}_m) = \frac{1}{M}, \; m = 1, \ldots, M. \quad (23.19)$$

The conditional probability of receiving $\mathbf{y}$ given that $\mathbf{x}$ was transmitted when communicating over an AWGN channel is determined by the PDF of the noise, yielding:

$$p(\mathbf{y}|\mathbf{x}_m) = \prod_{n=1}^{N} \frac{1}{\sqrt{\pi N_0}} \exp\left(\frac{-(y_n - x_{mn})^2}{N_0} \right), \quad (23.20)$$

where $N_0/2$ is the channel's noise variance. Note that $p(\mathbf{y}|\mathbf{x}_m)$ is also referred to as the chan-

[1] Naturally, the information to be transmitted is not an AWGN process. However, it was shown by Shannon [551] that it is beneficial to render the modulated signal input to the channel as 'AWGN-like' as possible.

nel's transition probability. By substituting Equations 23.19 and 23.20 into Equation 23.17, the capacity expression of the DCMC can be simplified to [695, 696]:

$$C_{\text{DCMC}}^{\text{AWGN}} = \log_2(M) - \frac{1}{M(\sqrt{\pi})^N} \cdot \sum_{m=1}^{M} \underbrace{\int_{-\infty}^{\infty} \cdots \int_{-\infty}^{\infty}}_{\text{N-fold}} \exp\left(-|\mathbf{t}|^2\right) \log_2 \left[\sum_{i=1}^{M} \exp\left(-2\mathbf{t}\cdot\mathbf{d}_{mi} - |\mathbf{d}_{mi}|^2\right)\right] d\mathbf{t} \text{ [bit/symbol]} \quad (23.21)$$

where $\mathbf{d}_{mi} = (\mathbf{x}_m - \mathbf{x}_i)/\sqrt{N_0}$ and $\mathbf{t} = (t[1], \ldots, t[N])$ is an integration variable. The DCMC capacity given by Equation 23.21 can be determined using numerical integration. More specifically, the integration can be approximated using the Gauss-Hermite Quadrature method [294, 695]. Let us also represent the effect of the AWGN channel as an N-dimensional additive noise vector given by $\mathbf{n} = (n[1], \ldots, n[N])$. The average SNR can be determined from [496, 695] as:

$$\begin{aligned} \gamma &= \frac{\mathrm{E}[x_m^2(t)]}{\mathrm{E}[n^2(t)]}, \\ &= \frac{\frac{1}{M}\sum_{m=1}^{M} |\mathbf{x}_m|^2}{\sum_{n=1}^{N} \mathrm{E}[n^2[n]]}, \\ &= \frac{E_s}{NN_0/2}, \end{aligned} \quad (23.22)$$

where E_s is the average energy of the N-dimensional M-ary symbol $\mathbf{x}_m$ and $N\frac{N_0}{2}$ is the average energy of the N-dimensional AWGN $\mathbf{n}$. Hence, if E_s is normalised to unity, from Equation 23.22 we have $N_0 = 2/(N\gamma)$.

On the other hand, it was shown in [496] that the channel capacity of the DCMC for $N = 2$-dimensional M-ary signalling can also be obtained using:

$$C_{\text{DCMC}}^{\text{AWGN}} = \log_2(M) - \frac{1}{M}\sum_{m=1}^{M} \mathrm{E}\left[\log_2 \sum_{i=1}^{M} \exp\left(\frac{-|\mathbf{x}_m + \mathbf{n} - \mathbf{x}_i|^2 + |\mathbf{n}|^2}{N_0}\right)\right] \text{ [bit/symbol]} \quad (23.23)$$

where $\mathbf{n}$ is the complex AWGN having a variance of $N_0/2$ per dimension. The expectation E[.] in Equation 23.23 is taken over $\mathbf{n}$ and it can be determined using the Monte Carlo averaging method.

23.2.3 The Capacity of Uncorrelated Rayleigh Fading Channels

Let us define $\mathbf{h} = h_i + jh_q$ as the *complex* uncorrelated Rayleigh fading coefficient, where h_i and h_q are the in-phase and quadrature-phase coefficients, respectively. Specifically, h_i and h_q are zero mean iid Gaussian random variables, each having a variance of $\sigma_r^2 = 1/2$. Note that σ_r^2 is normalised to $1/2$ so that the average energy of $|\mathbf{h}|^2$ is unity. Furthermore the coefficient $\chi_2^2 = |\mathbf{h}|^2 = h_i^2 + h_q^2$ of the Rayleigh fading channel is a chi-squared distributed random variable with two degrees of freedom. The corresponding PDF is given by [388]:

$$p(\chi_2^2) = \frac{1}{2\sigma_r^2} \exp\left(-\frac{\chi_2^2}{2\sigma_r^2}\right). \tag{23.24}$$

The capacity of continuous-input continuous-output uncorrelated (memoryless) Rayleigh fading channels can be evaluated based on the capacity formula of the Gaussian channel given in Equation 23.18 by simply weighting the SNR γ of the Gaussian channel by the probability of encountering the specific SNR determined by the Rayleigh fading magnitude χ_2^2, i.e. $\chi_2^2\gamma$. Then the resultant capacity value must be averaged, either by integration or summation over the legitimate range of the SNR given by $\chi_2^2\gamma$, yielding [179, 697]:

$$C_{\text{CCMC}}^{\text{RAY}} = \text{E}\left[\frac{N}{2}\log_2(1+\chi_2^2\gamma)\right] \text{ [bit/symbol]}, \tag{23.25}$$

where the expectation is taken over χ_2^2.

The capacity of the DCMC for $N = 2$-dimensional M-ary $complex$ signals, such as the classic PSK [388], can be derived from Equation 23.23 as follows:

$$C_{\text{DCMC}}^{\text{RAY}} = \log_2(M) - \frac{1}{M}\sum_{m=1}^{M} \text{E}\left[\log_2 \sum_{i=1}^{M} \exp(\Phi_i^m)\right] \text{ [bit/symbol]}, \tag{23.26}$$

where we have:

$$\begin{aligned}\Phi_i^m &= \frac{-|\mathbf{h}(\mathbf{x}_m - \mathbf{x}_i) + \mathbf{n}|^2 + |\mathbf{n}|^2}{N_0}, \\ &= \frac{-|\chi_2^2(\mathbf{x}_m - \mathbf{x}_i) + \mathbf{\Omega}|^2 + |\mathbf{\Omega}|^2}{\chi_2^2 N_0}.\end{aligned} \tag{23.27}$$

More explicitly the capacity of DCMC depends on M, $\mathbf{x}_m$, $\mathbf{x}_i$, χ_2^2 and $\mathbf{\Omega} = \mathbf{h}^*\mathbf{n}$, which is the effective AWGN having a zero mean and a variance of $\chi_2^2 N_0/2$ per dimension. The expectation in Equation 23.26 is taken over the Rayleigh-faded magnitude χ_2^2 and the effective AWGN $\mathbf{\Omega}$. The expectation can be estimated using the Monte Carlo averaging method.

For the general case of M-ary $complex$ signals having $N \geq 2$ dimensions, such as L-orthogonal PSK signalling [698, 699] of Section 23.5.5, we have:

$$\Phi_i^m = \sum_{n=1}^{N} \frac{-|\chi_2^2[n](x_m[n] - x_i[n]) + \Omega[n]|^2 + |\Omega[n]|^2}{\chi_2^2[n] N_0}, \tag{23.28}$$

where $\chi_2^2[j] = \chi_2^2[j+1]$ for $j \in \{1, 3, 5 \ldots\}$ since a $complex$ channel has two dimensions and $\Omega[n]$ is the dth dimension of the N-dimensional AWGN having a zero mean and a variance of $\chi_2^2[n]N_0/2$ per each of the N dimensions. In this case, the expectation in Equation 23.26 is taken over $\chi_2^2[n]$ and $\Omega[n]$. Note that the relationship between Equations 23.27 and 23.28 for $N = 2$ complex signals is that we have $\mathbf{x}_k = x_k[1] + jx_k[2]$ for $k \in \{1, \ldots, M\}$, $\chi_2^2 = \chi_2^2[1] = \chi_2^2[2]$ and $\mathbf{\Omega} = \Omega[1] + j\Omega[2]$.

Note that when the channel is $real$, where only the in-phase coefficient h_i is considered, the uncorrelated Rayleigh fading coefficient is given by $h = h_i$. Explicitly, h_i is a zero mean iid Gaussian random variable having a variance of $\sigma_r^2 = 1$. We also have $\chi_1^2 = h^2$, which is a chi-squared distributed random variable with one degree of freedom. Hence, for the case of N-dimensional M-ary *real* signals, such as M-ary orthogonal signalling [388] having $N = M$ or for pulse amplitude modulation schemes [388] having $N = 1$, we have:

$$\Phi_i^m = \sum_{n=1}^{N} \frac{-|\chi_1^2[n](x_m[n] - x_i[n]) + \Omega[n]|^2 + |\Omega[n]|^2}{\chi_1^2[n]N_0}, \tag{23.29}$$

where $\Omega[n]$ is the dth dimension of the N-dimensional AWGN having a zero mean and a variance of $\chi_1^2[n]N_0/2$ per dimension. In this case, the expectation in Equation 23.26 is taken over $\chi_1^2[n]$ and $\Omega[n]$.

23.3 Channel Cutoff Rate

The cutoff rate R_0 of the channel is defined as a channel capacity related quantity such that for any $R < R_0$, it is possible to construct a channel code having a block length n and coding rate of at least R capable of maintaining an average error probability that obeys $P_e \leq 2^{-n(R_0-R)}$ [388]. As mentioned before, R_0 has also been referred to as the "practically achievable capacity" of channel coded systems, where communication at rates above R_0 is typically far more complex to implement, than at rates below R_0 [494,502,691]. For example, as soon as the coding rate reaches R_0, the expected number of computation per nodes in the context of sequential decoding [502] tends to infinity. Although it is maintained that turbo codes are indeed capable of operating at rates above R_0, their decoding does get substantially more complex, as R exceeds R_0.

Apart from the above complexity-related context, R_0 is also used as an analytical bound limiting the bit error ratio performance of various classes of random codes designed for specific channels [365, 700]. Furthermore, R_0 constitutes a lower bound of the channel capacity and it is more straightforward to compute compared to the channel capacity. In general, the cutoff rate associated with M-ary QAM/PSK signalling and a Rician fading channel in the presence of perfect channel magnitude and phase estimates is given by [701–703]:

$$\mathrm{R}_0 = 2\log_2(M) - \log_2\left(\sum_{m=1}^{M}\sum_{i=1}^{M} C(\mathbf{x}_m, \mathbf{x}_i)\right) \text{ [bit/symbol]}, \tag{23.30}$$

where $C(\mathbf{x}_m, \mathbf{x}_i)$ is the Chernoff bound on the pairwise error probability expressed as [701, 703, 704]:

$$C(\mathbf{x}_m, \mathbf{x}_i) = \frac{1+K}{1+K+\frac{1}{4}\left|\mathbf{d}_{mi}\right|^2} \times \exp\left(-\frac{K\frac{1}{4}\left|\mathbf{d}_{mi}\right|^2}{1+K+\frac{1}{4}\left|\mathbf{d}_{mi}\right|^2}\right), \tag{23.31}$$

where we have $\left|\mathbf{d}_{mi}\right|^2 = \left|\mathbf{x}_m - \mathbf{x}_i\right|^2/N_0$ and K is the Rician factor. For an AWGN channel having a Rician factor of $K = \infty$ we have:

$$C(\mathbf{x}_m, \mathbf{x}_i) = \exp\left(-\frac{1}{4}|\mathbf{d}_{mi}|^2\right). \tag{23.32}$$

By contrast, for the other extreme scenario of encountering a Rayleigh fading channel, where $K = 0$, we have:

$$C(\mathbf{x}_m, \mathbf{x}_i) = \frac{1}{1+\frac{1}{4}|\mathbf{d}_{mi}|^2}. \tag{23.33}$$

Note that we will apply Equations 23.30, 23.32 and 23.33 in Section 23.5 for the computation of the cutoff rate for a range of M-ary digital signalling sets, when communicating over AWGN and Rayleigh fading channels.

23.4 Bandwidth Efficiency

The capacity analysis of the CCMC and DCMC provided in Section 23.2 determines the maximum number of information bits conveyed per transmitted symbol, as a function of the SNR. The system's bandwidth efficiency may be expressed as the capacity C normalised by the product of the bandwidth W occupied and the symbol period T, given by:

$$\eta = \frac{C}{WT} = \frac{C}{N/2} \text{ [bit/s/Hz]}, \tag{23.34}$$

where the associated unit is bit/s/Hz. The bandwidth efficiency of the CCMC may be expressed as:

$$\begin{aligned} \eta_{\text{CCMC}} &= \frac{C_{\text{CCMC}}}{WT} \\ &= \begin{cases} \log_2(1+\gamma) \text{ [bit/s/Hz]}, & \text{AWGN Channel}, \\ \text{E}\left[\log_2(1+\chi_2^2\gamma)\right] \text{ [bit/s/Hz]}, & \text{Rayleigh channel}. \end{cases} \end{aligned} \tag{23.35}$$

We will refer to the bandwidth efficiency of CCMC as the normalised unrestricted bound. The bandwidth efficiency curve may be plotted as a function of the bit energy to noise spectral density ratio (E_b/N_0), which can be determined from the SNR γ as:

$$\frac{E_b}{N_0} = \frac{\gamma}{\eta}. \tag{23.36}$$

Note that the bandwidth efficiency of the CCMC may be directly computed using Equations 23.18, 23.34 and 23.36, yielding:

$$\begin{aligned} \eta &= \log_2\left(1+\eta\frac{E_b}{N_0}\right), \\ \frac{E_b}{N_0} &= \frac{2^\eta - 1}{\eta}. \end{aligned} \tag{23.37}$$

It is interesting to note that as the bandwidth efficiency η of the CCMC tends to zero, by using L'Hôpital's rule [672], we arrive at:

$$\begin{aligned}\lim_{\eta\to 0}\frac{E_b}{N_0} &= \lim_{\eta\to 0}\frac{2^{\eta}-1}{\eta},\\ &= \lim_{\eta\to 0} 2^{\eta}\ln(2),\\ &= \ln(2),\\ &\approx -1.59 \text{ [dB]}.\end{aligned} \tag{23.38}$$

More explicitly, Equation 23.38 suggests that as E_b/N_0 approaches -1.59 dB, the bandwidth efficiency of the CCMC approaches zero.

It is also useful to normalise the cutoff rate R_0 with respect to the product of the bandwidth W occupied and the symbol period T, yielding:

$$R_{0,\eta} = \frac{R_0}{WT} = \frac{R_0}{N/2} \text{ [bit/s/Hz]}, \tag{23.39}$$

where the associated unit is bit/s/Hz. The normalised cutoff rate of the channel $R_{0,\eta}$ may be used for direct comparison with η of Equation 23.34.

23.5 Channel Capacity and Cutoff Rate of M-ary Modulation

In this section we will quantify the capacity, cutoff rate, bandwidth efficiency and normalised cutoff rate of the AWGN and the uncorrelated Rayleigh fading channels for a range of M-ary signalling sets based on the DCMC model. The unrestricted bounds of the AWGN and uncorrelated Rayleigh fading channels based on the CCMC model are also plotted for comparisons. Explicitly, the capacity of the AWGN CCMC and DCMC is computed using Equation 23.18 and Equation 23.21, respectively. By contrast, the capacity of the uncorrelated Rayleigh fading CCMC may be computed using Equation 23.25, while that of the DCMC is quantified using Equations 23.26, 23.28 and 23.29. On the other hand, the cutoff rate of the channel is determined using Equation 23.30 as well as Equations 23.32 and 23.33 for the AWGN and Rayleigh fading channels, respectively. Finally, the bandwidth efficiency curves of the DCMC and CCMC are evaluated using Equations 23.34 and 23.35, while the normalised cutoff rate of the DCMC is computed using Equation 23.39.

23.5.1 Introduction

An M-ary modulator is a device that maps each of the discrete-time symbols belonging to a set of M alphabets into one of the M continuous-time analogue waveforms suitable for transmission over the physical channel. There are many types of modulation techniques, differing in the way they manipulate an electromagnetic signal. Such manipulations include changing the amplitude, frequency or phase angle of a sinusoidal signal, the polarisation of the electromagnetic radiation or the pulse position within a modulation interval.

There are several different signalling pulse shaping functions. Most often, pulse shaping is carried out in the frequency-domain by designing a Nyquist filter having a certain roll-off factor α, as shown in Figure 4.6. Alternatively, pulse shaping may be implemented in the time-domain, as seen in Figure 4.15. The choice of the pulse shaping function influences the spectrum of the transmitted signal. More specifically, rectangular signalling pulses give rise to an infinite bandwidth requirement. By contrast, the raised cosine time-domain pulse shaping principle of Figure 4.6 results in a more compact spectrum. On one hand, the half-cycle sinusoidal time-domain pulse shaping function was utilised in the Minimum Shift Keying (MSK) scheme of [388, pp. 197-199]. On the other hand, the Q^2PSK and Q^2AM schemes outlined in Chapter 13 employ both sinusoidal and cosinusoidal pulse shaping functions. For the sake of simplicity, we will employ the rectangular time-domain pulse shaping function for illustrating the implementation of M-ary modulation techniques. We define the signalling pulse duration as T_p and the modulated symbol duration as T_s. As seen in Figure 4.5 for example, the baseband equivalent filter response of a rectangular frequency-domain Nyquist filter associated with $\alpha = 0$ spans from $-f_N = -1/2T_p$ to $f_N = 1/2T_p$. Hence the bandwidth required is given by $W = 2f_N = 1/T_p$ and the number of signal dimensions is given by Equation 23.8 as $N = 2WT_s$, when obeying the assumptions made in Section 23.2.1.

As explained in Section 13.2, we note that the MSK scheme exploits only two out of the four possible signalling dimensions available. On the other hand, when the channel is strictly bandlimited, the Q^2PSK and Q^2AM signalling schemes outlined in Chapter 13 have an identical bandwidth efficiency to their classic QPSK and QAM counterparts, despite being more difficult to implement. Furthermore, the MSK, Q^2PSK and Q^2AM signalling schemes require two different carrier frequencies as we have shown briefly in Equations 13.4 and 13.9 of Chapter 13. Therefore, we do not study the family of MSK, Q^2PSK and Q^2AM signalling schemes in this chapter.

23.5.2 M-ary Phase Shift Keying

M-ary Phase Shift Keying (PSK) constitutes a signalling scheme, where the $\log_2(M)$-bit information to be transmitted is mapped to M number of phases of the transmitted carrier. The modulated signalling waveforms may be expressed as:

$$\begin{aligned} x_m(t) &= \sqrt{\frac{2E_s}{T}} \cos\left(w_0 t - \frac{2\pi m}{M}\right), \;\; m = 1, \ldots, M, \;\; 0 \le t \le T, && (23.40) \\ &= x_m[1]\phi_1(t) + x_m[2]\phi_2(t), \;\; m = 1, \ldots, M, \;\; 0 \le t \le T, && (23.41) \end{aligned}$$

where w_0 is the carrier frequency in radians per second and the orthonormal basis functions are given by:

$$\begin{aligned} \phi_1(t) &= \sqrt{\frac{2}{T}} \cos(w_0 t), \;\; 0 \le t \le T, && (23.42) \\ \phi_2(t) &= \sqrt{\frac{2}{T}} \sin(w_0 t), \;\; 0 \le t \le T, && (23.43) \end{aligned}$$

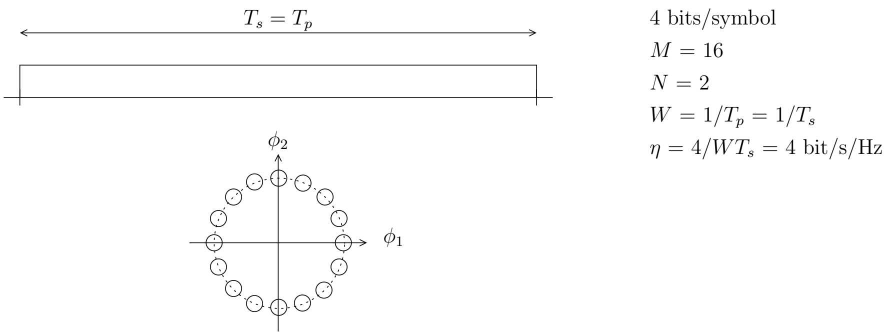

Figure 23.1: A PSK signalling example conveying 4 information bits per symbol.

while the coefficients of the signalling vector, $\mathbf{x}_m = x_m[1] + jx_m[2] = (x_m[1], x_m[2])$, are given by:

$$x_m[1] = \sqrt{E_s}\cos(\frac{2\pi m}{M}), \ \ 1 \leq m \leq M, \tag{23.44}$$

$$x_m[2] = \sqrt{E_s}\sin(\frac{2\pi m}{M}), \ \ 1 \leq m \leq M. \tag{23.45}$$

Specifically, each phasor $\mathbf{x}_m$ of the PSK signalling set has an equal energy and its signalling phasor constellation is mapped to a circle of radius $\sqrt{E_s}$. Figure 23.1 depicts an example of PSK signalling having $M = 16$ for the sake of conveying 4 information bits per symbol. In the context of classic M-ary PSK signalling, the duration of the rectangular signalling pulse T_p equals the modulated symbol duration T_s, as illustrated in Figure 23.1. Therefore, the bandwidth required is $W = 1/T_p = 1/T_s$ Hz and the number of dimensions offered by the signal space is $N = 2WT_s = 2$. During a symbol duration T_s, a phasor $\mathbf{x}_m$ chosen from the M legitimate phasors in the constellation is transmitted. Since we have $WT_s = N/2 = 1$, the asymptotic value of the bandwidth efficiency is similar to that of the achievable capacity of the classic PSK signalling sets. Note that when we have $M = 2$, 2-PSK signalling utilises only 1 out of the 2 possible signalling dimensions.

We may conclude that PSK signalling does not constitute an efficient scheme, since it has to obey the *PSK limit* [705], which is significantly lower than the unrestricted bound of Equation 23.18. The PSK limit for AWGN channels is given by [705, pp. 276-279]:

$$C^{\text{AWGN}}_{\text{PSK LIMIT}} = \log_2 \sqrt{\frac{4\pi}{e}\frac{E_s}{N_0}} \text{ [bit/symbol]}, \tag{23.46}$$

where we have $\frac{E_s}{N_0} = \gamma$ according to Equation 23.22, since the signalling dimensionality is $N = 2$. On other hand, the PSK limit valid for the Rayleigh fading channel may be derived from Equation 23.46 by weighting the SNR γ of the Gaussian channel by its probability of occurrence given by the Rayleigh-faded magnitude χ^2_2, which was defined in Section 23.2.3,

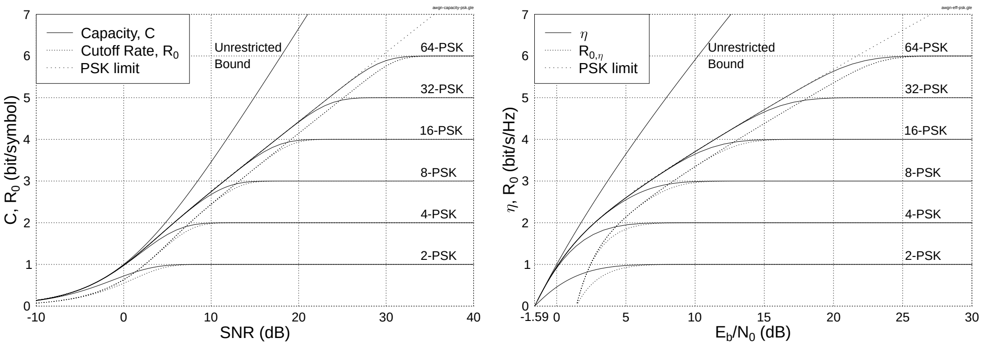

(a) The capacity C and cutoff rate R_0 are computed using Equations 23.18, 23.21, 23.30 and 23.32.

(b) The bandwidth efficiency η and normalised cutoff rate $R_{0,\eta}$ are determined using Equations 23.34 and 23.39.

Figure 23.2: M-ary PSK characteristics for M = 2, 4, 8, 16, 32 and 64 when communicating over an AWGN channel.

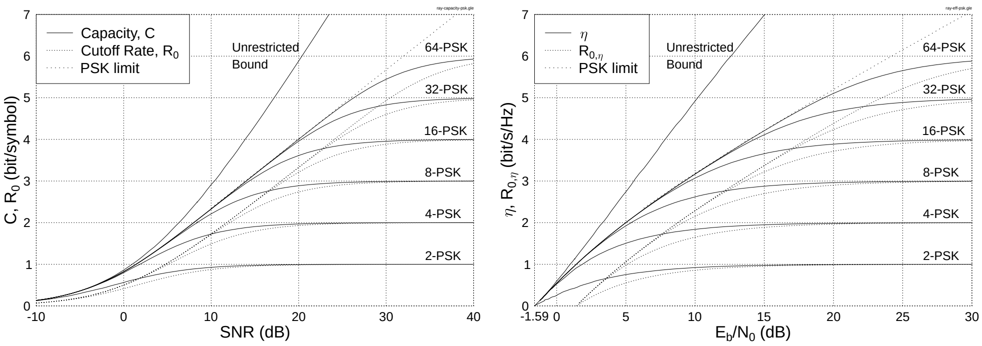

(a) The capacity C and cutoff rate R_0 are computed using Equations 23.25, 23.26, 23.28, 23.30 and 23.33.

(b) The bandwidth efficiency η and normalised cutoff rate $R_{0,\eta}$ are determined using Equations 23.34 and 23.39.

Figure 23.3: M-ary PSK characteristics for M = 2, 4, 8, 16, 32 and 64 when communicating over a Rayleigh fading channel.

and then averaging it over χ_2^2 yielding:

$$C_{\text{PSK LIMIT}}^{\text{RAY}} = \mathrm{E}\left[\log_2 \sqrt{\frac{4\pi}{e}\chi_2^2 \frac{E_s}{N_0}}\right] \text{ [bit/symbol]}, \tag{23.47}$$

where the expectation is evaluated with respect to χ_2^2. Note that the $\frac{E_b}{N_0}$ value of the PSK limit curve is given by $\frac{\gamma}{C_{\text{PSK LIMIT}}}$ and the normalised PSK limit is given by:

$$\eta_{\text{PSK LIMIT}} = \frac{C_{\text{PSK LIMIT}}}{N/2} \text{ [bit/s/Hz]}. \tag{23.48}$$

Figures 23.2 and 23.3 show the capacity, cutoff rate, bandwidth efficiency, normalised cutoff rate and PSK limit of the M-ary PSK signals, when communicating over AWGN and Rayleigh fading channels, respectively. As we can observe from Figure 23.2(a), at a capacity of $b = 3$ bit/symbol the SNR performance of the $2^{b+1} = 16$-PSK scheme is about 3 dB better than that of the $2^b = 8$-PSK scheme, when communicating over an AWGN channel. Even more significantly, when communicating over a Rayleigh fading channel, the SNR performance of the 16-PSK scheme is about 13 dB better than that of the 8-PSK scheme at a capacity of 3 bit/symbol, as it is shown in Figure 23.3(a). However, at a capacity of $b = 3$ bit/symbol, the PSK schemes having $M > 2^{b+1}$ yield very little additional SNR gain in comparison to 16-PSK. More explicitly, all PSK signalling schemes having $M > 16$ perform virtually identically to 16-PSK at a capacity of $b = 3$ bit/symbol, when communicating over AWGN channels, as evidenced by Figure 23.2(a). When communicating over uncorrelated Rayleigh fading channels, an SNR gain of less than 0.5 dB is obtained by a PSK signalling schemes having $M > 16$ in comparison to 16-PSK at a capacity of $b = 3$ bit/symbol, as it is shown in Figure 23.3(a). Similar observations are also true for $b \in \{1, 2, \ldots, 6\}$, as it is evidenced by Figures 23.2 and 23.3. Therefore, in order to approach the achievable capacity of b bit/symbol, it is better to employ 2^{b+1}-PSK, rather than 2^b-PSK. At first sight this statement may seem inplausible, however, we will show in Chapter 24 that this is exactly the motivation of Ungerböck's Trellis Coded Modulation (TCM) scheme, where the modulation constellation size is doubled for the sake of accommodating an extra bit. This extra bit is used in TCM for error correction, potentially allowing us to operate without errors at the cost of a higher complexity but at a lower SNR, i.e. to approach the capacity limit more closely. As a further observation, by doubling M from 2^b to 2^{b+1} most of the total achievable gain can be obtained, when aiming for a capacity of $C = b$ bit/symbol and any further expansion of the modulation constellation is only likely to yield marginal SNR benefits.

By comparing Figures 23.2 and 23.3, we notice that the SNR or E_b/N_0 gap between the capacity and cutoff rate of the uncorrelated Rayleigh fading channel is wider than that observed for the AWGN channel. For example, at a capacity of 3 bit/symbol the SNR gap between the capacity curve and cutoff rate curve of 16-PSK communicating over AWGN channels and uncorrelated Rayleigh fading channels is about 1 dB (as shown in Figure 23.2(a)) and 4 dB (as shown in Figure 23.3(a)), respectively. This implies that it is harder to reach the capacity of the uncorrelated Rayleigh fading channel compared to that of the AWGN channel. Additionally, the SNR gap between the capacity of M-ary PSK and the unrestricted bound becomes larger for increasing values of M at a capacity of $(\log_2(M) - 1)$ bit/symbol. For example, when communicating over uncorrelated Rayleigh fading channels, the SNR gap between the capacity curve of 4-PSK and the unrestricted bound at 1 bit/symbol is only about 1 dB. By contrast, the SNR gap between the capacity curve of 64-PSK and the unrestricted bound is approximately 10 dB, as we can observe from Figure 23.3(a). This is a consequence of the convergence of the PSK curves to the ultimate PSK limit mentioned earlier.

23.5.3 M-ary Quadrature Amplitude Modulation

M-ary Quadrature Amplitude Modulation (QAM) may be viewed as a combination of two independent Pulse Amplitude Modulation (PAM) schemes. The modulated signalling waveforms may be expressed as in Equation 23.41 and the two orthonormal basis functions are similar to that of PSK, which are given by Equations 23.42 and 23.43. Specifically, the QAM signalling set maps each message block onto a rectangular phasor constellation based on the

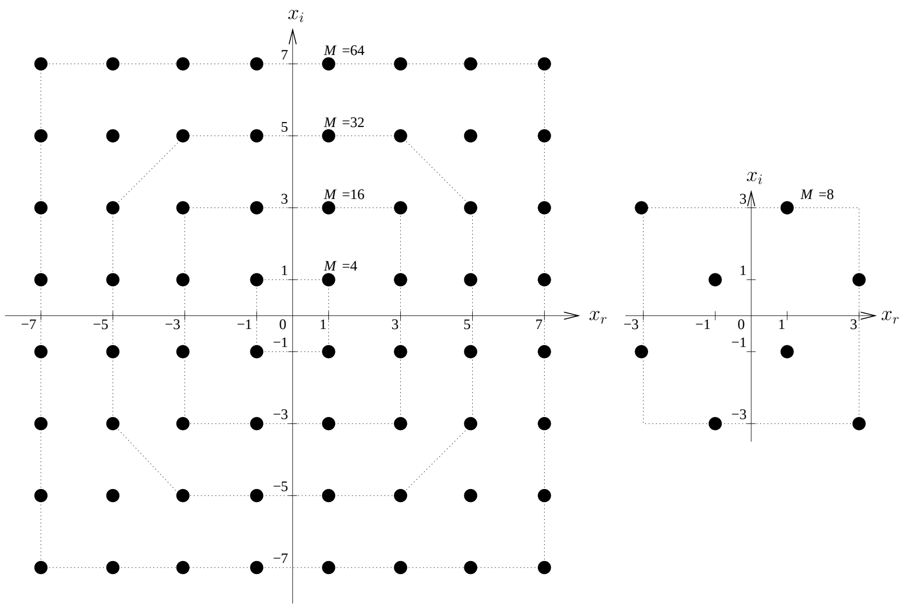

Figure 23.4: QAM constellations for M = 4, 8, 16, 32 and 64.

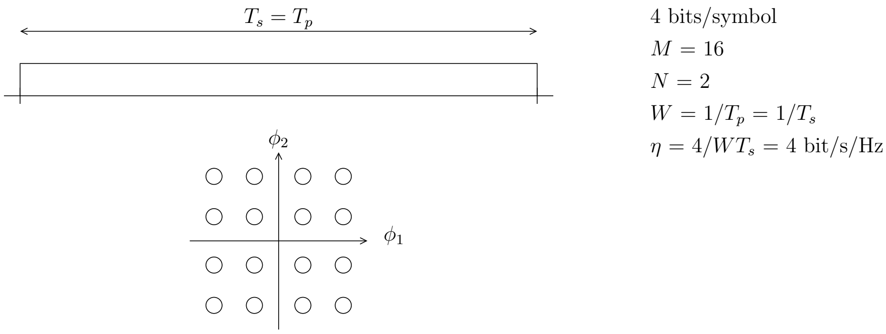

Figure 23.5: A QAM signalling example conveying 4 information bits per symbol.

coefficients of $\mathbf{x}_m$ as follows:

$$\mathbf{x}_m = x_m[1] + jx_m[2], \;\; x_m[1] \in x_r, \;\; x_m[2] \in x_i, \;\; m = 1, \ldots, M, \quad (23.49)$$

where x_r and x_i are the values of $\mathbf{x}_m$ mapped to the real and imaginary axis of the signal constellation. The QAM signalling set may also be viewed as a combined amplitude and phase modulation scheme. The signal space diagrams of QAM constellations used in this chapter are shown in Figure 23.4. Note that the 8-QAM constellation seen in Figure 23.4, which was originally proposed in [496], exhibits a higher minimum Euclidean distance compared to the rectangular 8-QAM of [388, p. 180], although its peak-to-mean envelope and its phase-jitter resilience defined in Section 4.1 are inferior.

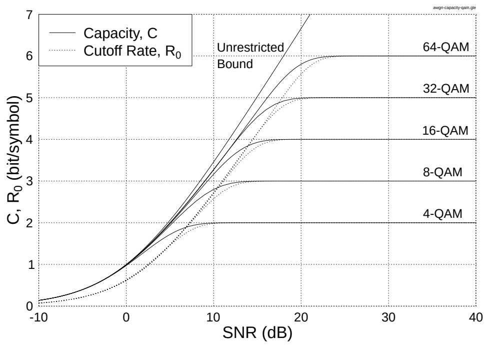

(a) The capacity C and cutoff rate R_0 are computed using Equations 23.18, 23.21, 23.30 and 23.32.

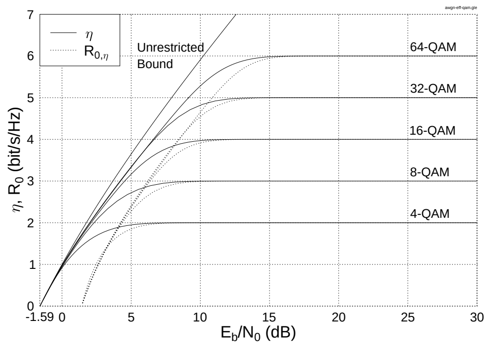

(b) The bandwidth efficiency η and normalised cutoff rate $R_{0,\eta}$ are determined using Equations 23.34 and 23.39.

Figure 23.6: M-ary QAM characteristics for M = 4, 8, 16, 32 and 64 when communicating over AWGN channel.

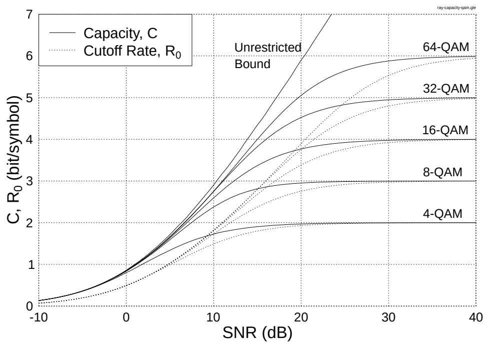

(a) The capacity C and cutoff rate R_0 are computed using Equations 23.25, 23.26, 23.28, 23.30 and 23.33.

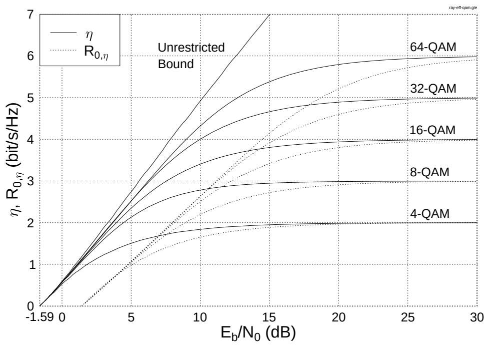

(b) The bandwidth efficiency η and normalised cutoff rate $R_{0,\eta}$ are determined using Equations 23.34 and 23.39.

Figure 23.7: M-ary QAM characteristics for M = 4, 8, 16, 32 and 64 when communicating over a Rayleigh fading channel.

Figure 23.5 characterises QAM signalling having $M = 16$ for the sake of conveying 4 information bits per symbol. Specifically, in the 16-QAM scheme, we have $x_r = -3, -1, 1, 3$ and $x_i = -3, -1, 1, 3$. In the classic M-ary QAM signalling scheme, the duration of the rectangular signalling pulse T_p equals the modulated symbol duration T_s, as depicted in Figure 23.5. Therefore, the bandwidth required is $W = 1/T_p = 1/T_s$ Hz and the number of dimensions of the signalling space is $N = 2WT_s = 2$. During a symbol duration T_s, a phasor $\mathbf{x}_m$ chosen from the M legitimate phasors of the constellation is transmitted. Since we have $WT_s = N/2 = 1$, the asymptotic value of the bandwidth efficiency is similar to that of the achievable capacity of the classic QAM signalling sets.

Figures 23.6 and 23.7 show the achievable capacity, cutoff rate, bandwidth efficiency and normalised cutoff rate of the family of M-ary QAM signals, when communicating over AWGN and Rayleigh fading channels, respectively. Similar to our finding in the context of the M-ary PSK results of Section 23.5.2, in order to achieve a capacity of b bit/symbol, it is better to employ 2^{b+1}-ary QAM, rather than the QAM scheme having $M = 2^b$ or $M > 2^{b+1}$. Explicitly, by doubling M from 2^b to 2^{b+1} most of the achievable capacity gain may be obtained when aiming for a capacity of $C = b$ bit/symbol. For example, as evidenced in Figure 23.7(a), the SNR required for 8-QAM, 16-QAM, 32-QAM and 64-QAM is about 28 dB, 12 dB, 11 dB and 11 dB, respectively, when communicating over uncorrelated Rayleigh fading channels at a capacity of $b = 3$ bit/symbol. It is also harder to approach the capacity of the Rayleigh fading channel compared to the AWGN channel in the context of QAM, as a consequence of having a wider SNR gap between the capacity and cutoff rate of Rayleigh fading channels compared to that of the AWGN channels. For example, at a capacity of 3 bit/symbol the SNR gap between the capacity curve and cutoff rate curve of 16-QAM when communicating over AWGN channels and uncorrelated Rayleigh fading channels is about 2 dB (as shown in Figure 23.6(a)) and 5 dB (as shown in Figure 23.7(a)), respectively. However, as seen by comparing Figures 23.3(a) and 23.7(a), the SNR performance difference between the unrestricted bound and the capacity of M-ary QAM is significantly smaller than that of the M-ary PSK scheme of Section 23.5.2. As we can see from Figures 23.3(a) and 23.7(a), the SNR requirement of 5 bit/symbol signalling at the unrestricted bound as well as when using 64-QAM and 64-PSK communicating over uncorrelated Rayleigh fading channels is approximately 17 dB, as well as 20 dB and 26 dB, respectively. This indicates that QAM is potentially more bandwidth efficient than PSK. Again, a practical manifestation of this statement will be detailed in the context of TCM in Chapter 24, where the expanded signalling constellation accommodates an error correction code, potentially allowing the expanded phasor constellation to approach the capacity more closely owing to its better error resilience, despite its reduced minimum distance amongst the constellation points.

23.5.4 M-ary Orthogonal Signalling

M-ary orthogonal signalling constitutes a transmission scheme, where $\log_2(M)$ number of bits are mapped to M orthogonal waveforms, as for example in the IS-95 CDMA standard, which is also known as cdmaOne [706]. The bandwidth requirement of M-ary orthogonal signalling is given by [388, p. 283]:

$$W = \frac{M}{2T_s}, \tag{23.50}$$

where T_s is the symbol duration and hence this signalling scheme may also be interpreted as a collection of phasor points in the $N = 2WT_s = M$-dimensional phasor space, where only one phasor point is located on each of the M coordinate axes. The M-dimensional signalling vectors can be represented as [388, 695]:

$$\begin{aligned}
\mathbf{x}_1 &= \sqrt{E_s}(1, 0, \ldots, 0) = \sqrt{E_s}\phi_1, \\
\mathbf{x}_2 &= \sqrt{E_s}(0, 1, \ldots, 0) = \sqrt{E_s}\phi_2, \\
&\vdots \\
\mathbf{x}_M &= \sqrt{E_s}(0, 0, \ldots, 1) = \sqrt{E_s}\phi_M,
\end{aligned} \tag{23.51}$$

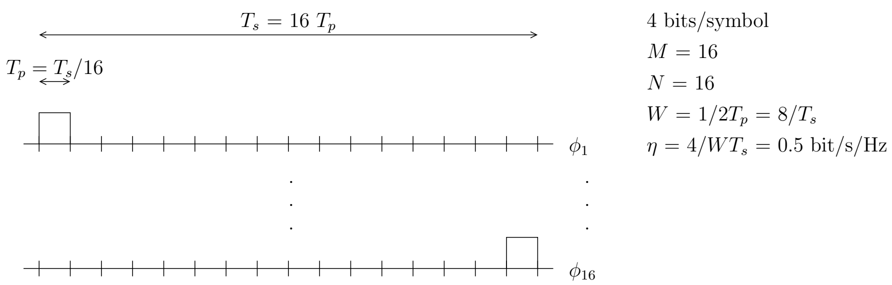

Figure 23.8: An orthogonal signalling example conveying 4 information bits per symbol.

where each $\mathbf{x}_m$, $m \in \{1, \ldots, M\}$, in the M-dimensional space is located at a distance of $\sqrt{E_s}$ from the origin. The orthonormal basis function ϕ_m is M-dimensional:

$$\phi_m = (\phi_m[1], \phi_m[2], \ldots, \phi_m[M]), \tag{23.52}$$

which may be constructed from non-overlapping signalling pulses as follows:

$$\phi_m[i] = \begin{cases} 1, & i = m, \\ 0, & i \neq m. \end{cases} \tag{23.53}$$

Note that M-ary orthogonal signalling is more power-efficient and more error-resilient, but less bandwidth efficient compared to classic M-ary PSK and QAM [388, p. 284]. Figure 23.8 depicts an example of the M-ary orthogonal signalling scheme having $M = N = 16$ for the sake of conveying 4 information bits per symbol. In M-ary orthogonal signalling, the duration of the rectangular pulse is given by $T_p = T_s/M$, as seen in Figure 23.8. However, the bandwidth required is given by Equation 23.50 as $W = \frac{M}{2T_s} = 1/2T_p$ Hz, which is different from that of the QAM and PSK schemes. The number of dimensions of the signalling space is $N = 2WT_s = M$. During a symbol duration T_s, only one pulse duration is active, while the rest are inactive, when the orthonormal basis functions are constructed as non-overlapping pulses according to Equation 23.53. Since we have $WT_s = N/2 = M/2$, the asymptotic value of bandwidth efficiency is different from that of the capacity of the M-ary orthogonal signalling sets for values of $M > 2$.

Figures 23.9 and 23.10 show the capacity, cutoff rate, bandwidth efficiency and normalised cutoff rate of M-ary orthogonal signalling, when communicating over AWGN and Rayleigh fading channels, respectively. Note that the unrestricted bound of Equation 23.18 is dependent on $WT = N/2$, hence it is different for different dimensionality values N. However, the normalised unrestricted bound expressed in Equation 23.35 is independent of $WT = N/2$. As shown in Figures 23.9(a) and 23.10(a), the channel capacity curves reach the asymptotic performance of $\log_2(M)$ bit/symbol at low SNRs, when increasing the value of M. This trend is different from the channel capacity curves recorded for classic PSK and QAM. As depicted in Figures 23.9(b) and 23.10(b), unlike for classic PSK and QAM signals, the bandwidth efficiency of M-ary orthogonal signalling is farther away from the unrestricted bound at low E_b/N_0 values as M decreases. This phenomenon is a consequence of having non-zero centre of gravity or mean in M-ary orthogonal signalling, which is given

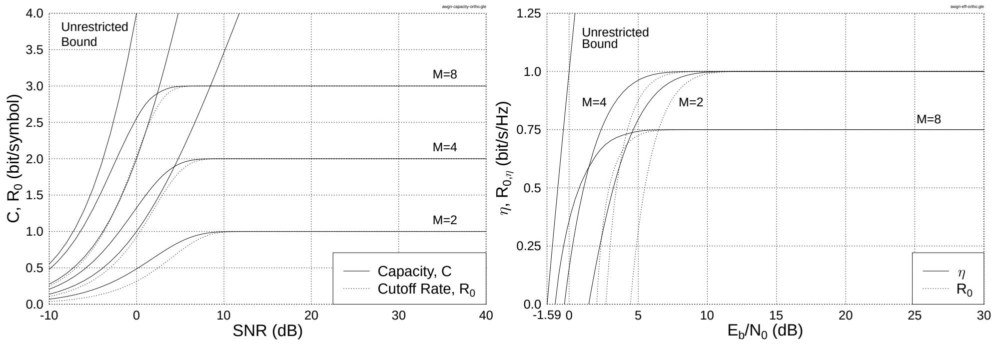

(a) The capacity C and cutoff rate R_0 are computed using Equations 23.18, 23.21, 23.30 and 23.32.

(b) The bandwidth efficiency η and normalised cutoff rate $R_{0,\eta}$ are determined using Equations 23.34 and 23.39.

Figure 23.9: M-ary orthogonal characteristics for M = 2, 4 and 8 when communicating over an AWGN channel.

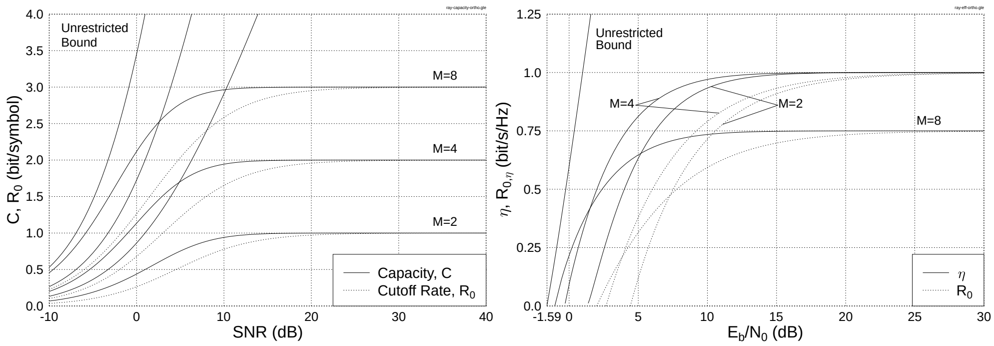

(a) The capacity C and cutoff rate R_0 are computed using Equations 23.25, 23.26, 23.29, 23.30 and 23.33.

(b) The bandwidth efficiency η and normalised cutoff rate $R_{0,\eta}$ are determined using Equations 23.34 and 23.39.

Figure 23.10: M-ary orthogonal characteristics for M = 2, 4 and 8 when communicating over a Rayleigh fading channel.

by [707, p. 245]:

$$\bar{\mathbf{x}} \quad = \quad \frac{1}{M}\sum_{m=1}^{M}\mathbf{x}_m = \frac{\sqrt{E_s}}{M}\sum_{m=1}^{M}\phi_m, \tag{23.54}$$

and the energy of $\bar{\mathbf{x}}$ is:

$$|\bar{\mathbf{x}}|^2 \quad = \quad \frac{E_s}{M^2}\sum_{m=1}^{M}|\phi_m|^2 = \frac{E_s}{M}. \tag{23.55}$$

Therefore, the actual transmitted power used for conveying information is $E_s - |\bar{\mathbf{x}}|^2 =$

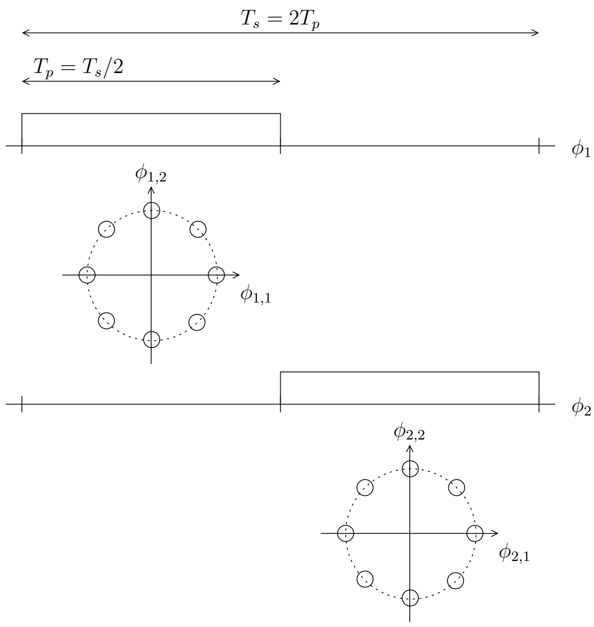

4 bits/symbol
$V = 2$
$L = 8$
$M = VL = 16$
$N = 2V = 4$
$W = 1/T_p = 2/T_s$
$\eta = 4/WT_s = 2$ bit/s/Hz

Figure 23.11: An L-orthogonal PSK signalling example conveying 4 bits per symbol.

$E_s(\frac{M-1}{M})$, which is lower than the total transmitted power of E_s. The corresponding E_b/N_0 value at 0 bit/s/Hz may be calculated as: $E_b/N_0 = -1.59 - 10\log_{10}\left(\frac{M-1}{M}\right)$ dB. Hence, as M increases, the bandwidth efficiency curves converge more closely to the Shannon bound. However, since we have $WT = M/2 > 1$ for $M > 2$, the asymptotic value of the bandwidth efficiency is a factor of $M/2$ lower than that of the capacity of the M-ary orthogonal signalling set. Therefore, as $M \to \infty$, we have $\eta = \frac{C}{M/2} \to 0$, which implies having a zero bandwidth efficiency. Similar to the related findings for classic PSK and QAM, the SNR gap between the capacity and cutoff rate of the uncorrelated Rayleigh fading channel is wider than that of the AWGN channel. For example, at a capacity of 2 bit/symbol the SNR gap between the capacity curve and cutoff rate curve of 8-orthogonal signalling communicating over AWGN channels and uncorrelated Rayleigh fading channels is about 2 dB (as shown in Figure 23.9(a)) and 5.5 dB (as shown in Figure 23.10(a)), respectively. This indicates that it is harder to reach the capacity of the uncorrelated Rayleigh fading channel compared to that of the AWGN channel.

23.5.5 L-Orthogonal PSK Signalling

L-orthogonal PSK signalling constitutes a hybrid form of M-ary orthogonal and classic PSK signalling [698, 699], comprised of V number of independent L-ary PSK subsets. Therefore, the total number of available signalling waveforms is $M = VL$ and hence the number of bits transmitted per signalling symbol is $\log_2(VL)$. The total number of dimensions is $N = 2V$.

The vector representation of L-orthogonal PSK signalling may be formulated as:

$$\mathbf{x}_m = \mathbf{x}_l^{LPSK}\phi_v, \;\; m = 1, \ldots, M, \;\; l = m\%L, \;\; v = \left(\frac{m-l}{V}+1\right), \quad (23.56)$$

where $m\%L$ is the remainer of m/L and $\mathbf{x}_l^{LPSK}$ is the classic 2-dimensional L-ary PSK signal vector, which obeys the form of Equations 23.44 and 23.45, yielding:

$$\mathbf{x}_l^{LPSK} = \left(x_l^{LPSK}[1], x_l^{LPSK}[2]\right), \;\; l = 1, \ldots, L. \quad (23.57)$$

Furthermore, the orthonormal basis function $\phi_v = (\phi_v[1], \phi_v[2], \ldots, \phi_v[V])$ is a vector of V elements, which may be constructed as a set of non-overlapping pulses defined in Equation 23.53.

Specifically, the vector of an L-orthogonal PSK signalling set having $L = 8$ and $V = 2$ may be formulated as:

$$\begin{aligned}
\mathbf{x}_1 &= \mathbf{x}_1^{8PSK}(1,0) = \left(x_1^{8PSK}[1], x_1^{8PSK}[2], 0, 0\right), \\
\mathbf{x}_2 &= \mathbf{x}_2^{8PSK}(1,0) = \left(x_2^{8PSK}[1], x_2^{8PSK}[2], 0, 0\right), \\
&\vdots \\
\mathbf{x}_8 &= \mathbf{x}_8^{8PSK}(1,0) = \left(x_8^{8PSK}[1], x_8^{8PSK}[2], 0, 0\right), \\
\mathbf{x}_9 &= \mathbf{x}_1^{8PSK}(0,1) = \left(0, 0, x_1^{8PSK}[1], x_1^{8PSK}[2]\right), \\
\mathbf{x}_{10} &= \mathbf{x}_2^{8PSK}(0,1) = \left(0, 0, x_2^{8PSK}[1], x_2^{8PSK}[2]\right), \\
&\vdots \\
\mathbf{x}_{16} &= \mathbf{x}_8^{8PSK}(0,1) = \left(0, 0, x_8^{8PSK}[1], x_8^{8PSK}[2]\right),
\end{aligned} \quad (23.58)$$

where the total number of legitimate waveforms is $M = VL = 16$ and hence the number of bits per symbol is $\log_2(M) = 4$. Explicitly, the L-orthogonal PSK signalling set having $L = 8$ and $V = 2$ is illustrated in Figure 23.11. As we can see from Figure 23.11, the duration of the rectangular pulse is given by $T_p = T_s/V$ and during a modulated symbol duration T_s, only one signalling pulse of duration T_p is active, while the rest of them inactive when the orthonormal basis functions are constructed as non-overlapping pulses according to Equation 23.53. A phasor $\mathbf{x}_m$ chosen from the $L = 8$ legitimate phasors in the 8-PSK constellation is transmitted, when the corresponding pulse-slot is active. The bandwidth required is $W = 1/T_p = V/T_s$, hence the number of dimensions of the signal space is $N = 2WT_s = 2V$. Therefore, we have:

$$V = WT_s = \frac{N}{2}. \quad (23.59)$$

Since we have $WT_s = N/2 = V$, the asymptotic value of bandwidth efficiency is a factor of V lower than the capacity. When $V = 1$, we have $L = M$ and hence L-orthogonal PSK signalling becomes analogous to classic M-ary PSK signalling. Note that L-orthogonal PSK signalling requires only $V = N/2$ number of timeslots for conveying a symbol, whereas the M-ary orthogonal signalling waveforms of Section 23.5.4 require N number of timeslots for

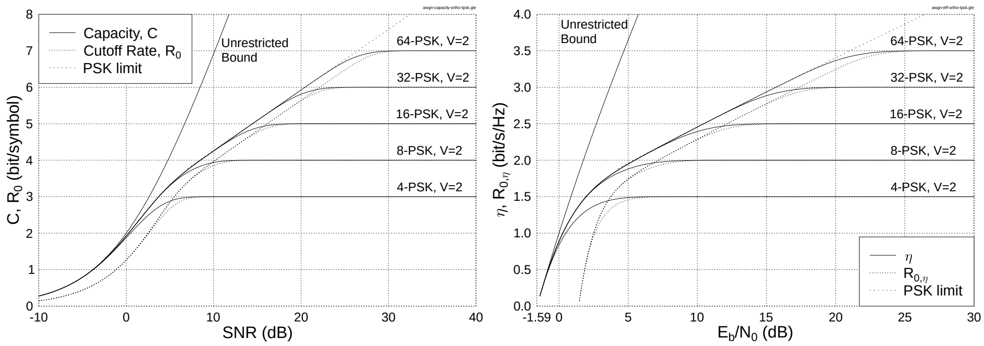

(a) The capacity C and cutoff rate R_0 are computed using Equations 23.18, 23.21, 23.30 and 23.32.

(b) The bandwidth efficiency η and normalised cutoff rate $R_{0,\eta}$ are determined using Equations 23.34 and 23.39.

Figure 23.12: L-orthogonal PSK characteristics for $V = 2$ and L = 4, 8, 16, 32 and 64 when communicating over AWGN channel.

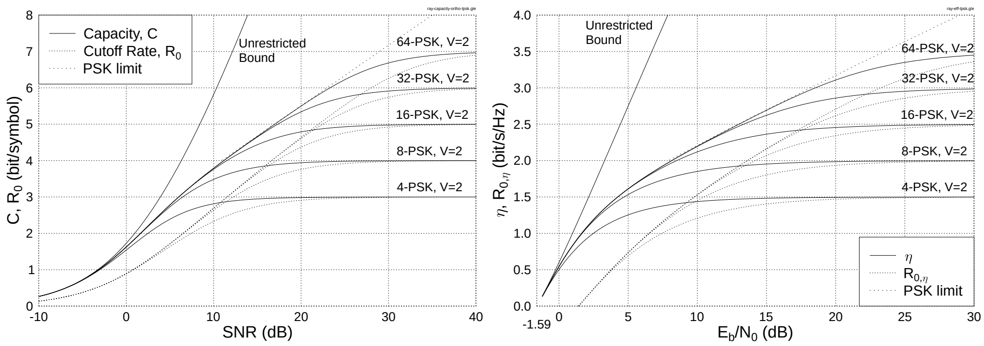

(a) The capacity C and cutoff rate R_0 are computed using Equations 23.25, 23.26, 23.28, 23.30 and 23.33.

(b) The bandwidth efficiency η and normalised cutoff rate $R_{0,\eta}$ are determined using Equations 23.34 and 23.39.

Figure 23.13: L-orthogonal PSK, $V = 2$ and L = 4, 8, 16, 32 and 64 when communicating over a Rayleigh fading channel.

conveying a symbol. Hence, for a given number of dimensions N, the achievable transmission rate of L-orthogonal PSK signalling is a factor of two higher than that of M-ary orthogonal signalling. Furthermore, at a given dimensionality N there are $M = VL = NL/2$ number of waveforms in the context of L-orthogonal PSK signalling, which is a factor of $L/2$ times higher than that of classic M-ary orthogonal signalling. However, at a given value of M, L-orthogonal PSK signalling is $V = M/L$ times less bandwidth efficient, than the classic M-ary PSK signalling scheme.

Figures 23.12 and 23.13 portray the capacity, cutoff rate, bandwidth efficiency and normalised cutoff rate of L-orthogonal PSK signalling schemes having $V = 2$, when communicating over AWGN and uncorrelated Rayleigh fading channels, respectively. Similar to classic PSK signalling, most of the achievable gain has already been attained by doubling the value of L and very little additional gain may be achieved, if L is further increased. More explicitly, as we can observe from Figure 23.13(a), the 16-orthogonal PSK having $V = 2$ is approximately 14 dBs better than the 8-orthogonal PSK having $V = 2$ at a capacity of 4 bit/symbol. It is also harder to approach the capacity of the uncoded Rayleigh fading channel compared to the AWGN channel, since there is a wider SNR gap between the capacity and cutoff rate of the Rayleigh fading channel compared to that of the AWGN channel.

Since we have $M = VL$ for the L-orthogonal PSK signalling, the capacity of L-orthogonal PSK signalling is $\log_2\left(\frac{VL}{L}\right) = \log_2(V)$ bit higher than that of the classic L-ary PSK subset. However, the bandwidth efficiency of L-orthogonal PSK signalling is $\frac{V\log_2(L)}{\log_2(VL)}$ times lower than that of its L-ary PSK subset. For example, 16-PSK signalling has a capacity of $C = 4$ bit/symbol and bandwidth efficiency of $\eta = 4$ bit/s/Hz. By contrast, the L-orthogonal PSK signalling employing $V = 2$ number of 16-PSK subsets has $C = 5$ and $\eta = 2.5$. Therefore, L-orthogonal PSK signalling having $V = 2$ and $L = 16$ is $5 - 4 = 1$ bit higher than 16-PSK in terms of capacity, but it is $4/2.5 = 1.6$ times lower than 16-PSK in terms of bandwidth efficiency, where $\log_2(V) = 1$ and $\frac{V\log_2(L)}{\log_2(VL)} = 1.6$.

As we can see from Figures 23.12 and 23.13, L-orthogonal PSK signalling also exhibits an PSK limit. In general, the ultimate limit of L-orthogonal PSK signalling when communicating over AWGN channels may be derived from Equation 23.46 as:

$$C^{\text{AWGN}}_{L\text{-ORTHO PSK LIMIT}} = \log_2\left(V \cdot \sqrt{\frac{4\pi}{e}\frac{E_s}{N_0}}\right) \text{ [bit/symbol]}, \tag{23.60}$$

where $\frac{E_s}{N_0} = V\gamma$ according to Equation 23.22, since we have $V = N/2$ and γ is the SNR. Therefore, Equation 23.60 can be further simplified to:

$$\begin{aligned} C^{\text{AWGN}}_{L\text{-ORTHO PSK LIMIT}} &= \log_2\left(V^{3/2}\sqrt{\frac{4\pi}{e}\gamma}\right) \text{ [bit/symbol]}, \\ &= \log_2\left(\sqrt{\frac{4\pi}{e}\gamma}\right) + \frac{3}{2}\log_2(V) \text{ [bit/symbol]}, \qquad (23.61) \\ &= C^{\text{AWGN}}_{\text{PSK LIMIT}} + \frac{3}{2}\log_2(V) \text{ [bit/symbol]}, \qquad (23.62) \end{aligned}$$

where $C^{\text{AWGN}}_{\text{PSK LIMIT}}$ is the ultimate limit of PSK signalling ($V = 1$) given by Equation 23.46. Similar to Equation 23.62, the ultimate limit for L-orthogonal PSK signalling, when communicating over uncorrelated Rayleigh fading channels can be expressed as:

$$C^{\text{RAY}}_{L\text{-ORTHO PSK LIMIT}} = C^{\text{RAY}}_{\text{PSK LIMIT}} + \frac{3}{2}\log_2(V) \text{ [bit/symbol]}, \tag{23.63}$$

where $C^{\text{RAY}}_{\text{PSK LIMIT}}$ was given by Equation 23.47. Hence, when V varies, the curve of L-orthogonal PSK limit is shifted by a constant of $\frac{3}{2}\log_2 V$, but the slope of the curve remains unchanged. The L-orthogonal PSK limit curves calculated for V = 1, 2, 4 and 8 are illustrated in Figures 23.14(a) and 23.15(a). In terms of the achievable bandwidth efficiency, according to Equations 23.34 and 23.59, we may express the normalised L-orthogonal PSK

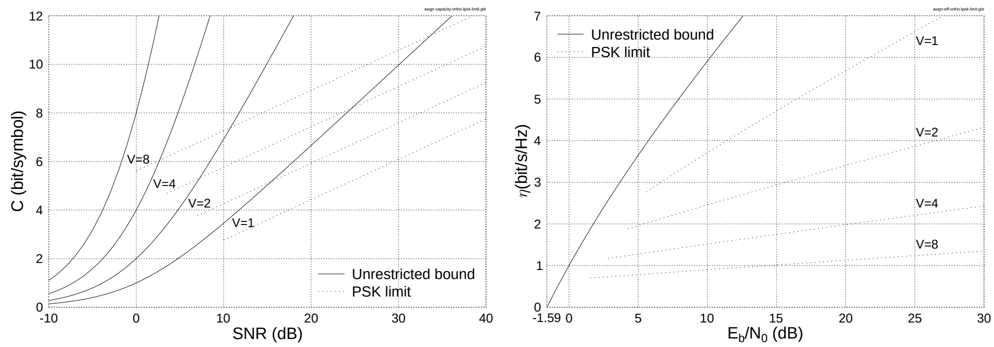

(a) The unrestricted bound and PSK limit are computed using Equations 23.18 and 23.62.

(b) The unrestricted bound and PSK limit normalised to WT are determined using Equations 23.34 and 23.64.

Figure 23.14: L-orthogonal PSK characteristics for V = 1, 2, 4, and 8 when communicating over an AWGN channel.

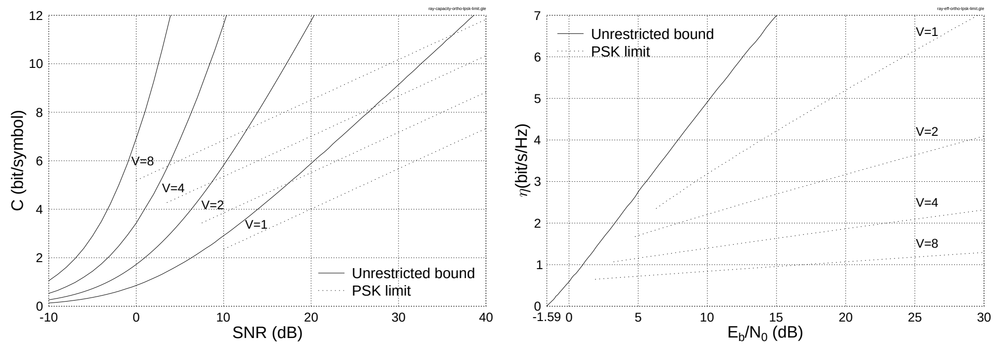

(a) The unrestricted bound and PSK limit are computed using Equations 23.25 and 23.63.

(b) The unrestricted bound and PSK limit normalised to WT are determined using Equations 23.34 and 23.64.

Figure 23.15: L-orthogonal PSK characteristics for V = 1, 2, 4, and 8 when communicating over a Rayleigh fading channel.

limit as:

$$\eta_{L\text{-ORTHO PSK LIMIT}} = \frac{C_{L\text{-ORTHO PSK LIMIT}}}{V} \text{ [bit/s/Hz]}. \quad (23.64)$$

Therefore, the gradient of the normalised L-orthogonal PSK limit is reduced by a factor of V, as portrayed in Figures 23.14(b) and 23.15(b). From Figures 23.12, 23.13, 23.14 and 23.15, we can see that L-orthogonal PSK signalling becomes inefficient for a large value of L and V. For example, when communicating over uncorrelated Rayleigh fading channels, the SNR gap between the capacity curve of 4-orthogonal PSK and the unrestricted bound at 2 bit/symbol is only about 1.5 dB. By contrast, the SNR gap between the capacity curve of 64-orthogonal PSK and the unrestricted bound is approximately 13.5 dB, as we can observe from Figure 23.13(a), when we have $V = 2$. Furthermore, the L-orthogonal PSK limit curves is farther away from the unrestricted bound for higher values of V, as we can observe from Figure 23.15(b). More specifically, at a bandwidth efficiency of $\eta = 2$ bit/s/Hz the E_b/N_0 gap between the unrestricted bound and L-orthogonal PSK limit curves plotted for $V = 2$ and $V = 4$ is about 4.5 dB and 19.5 dB, respectively, as it is evidenced by Figure 23.15(b).

23.5.6 L-Orthogonal QAM Signalling

The novel message of this section is that L-orthogonal signalling may also incorporate QAM subsets instead of the PSK subsets, which have to obey the ultimate PSK limit. Explicitly, L-orthogonal QAM signalling constitutes a hybrid form of M-ary orthogonal and QAM signalling. Similar to L-orthogonal PSK, it comprised of V independent L-ary QAM subsets. The total number of legitimate waveforms is $M = VL$ and the number of transmitted bits per symbol is $\log_2(VL)$. The total number of dimensions is $N = 2V$. The vector representation of L-orthogonal QAM signalling may be formulated as:

$$\mathbf{x}_m = \mathbf{x}_l^{LQAM}\phi_v, \ \ m = 1, \ldots, M, \ \ l = m\%L, \ \ v = \left(\frac{m-l}{V} + 1\right), \quad (23.65)$$

where $\mathbf{x}_l^{LQAM}$ is the classic 2-dimensional L-ary QAM signal vector given by Equation 23.49. The orthonormal basis function ϕ_v may be constructed as a set of non-overlapping pulses outlined in Equation 23.53 similar to that of the L-orthogonal PSK signalling characterised in Equation 23.56.

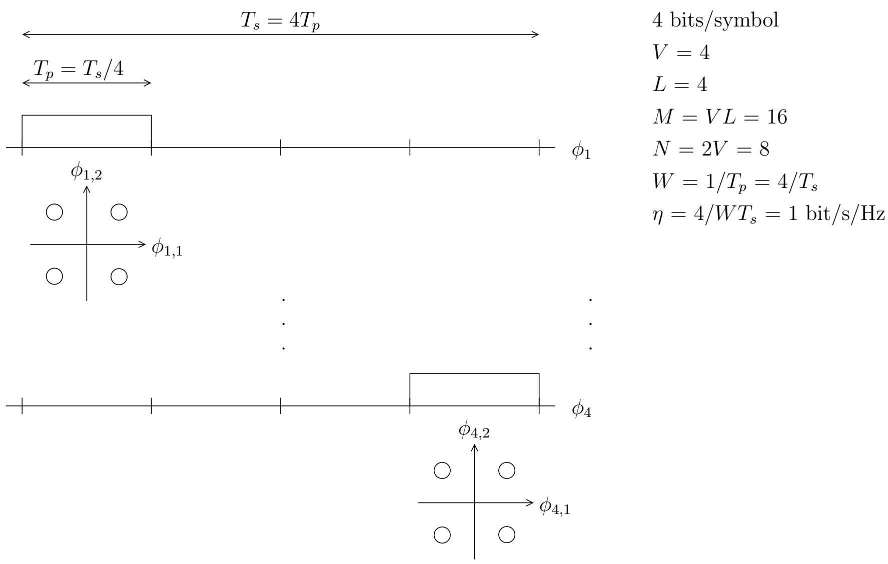

Figure 23.16: An L-orthogonal QAM signalling example conveying 4 bits per symbol.

Figure 23.16 depicts an example of the L-orthogonal QAM signalling scheme having $L = 4$ and $V = 4$, which conveys 4 information bits per symbol. In the L-orthogonal QAM signalling scheme, the duration of the rectangular signalling pulse is given by $T_p = T_s/V$, as it was shown in Figure 23.5. Therefore, the bandwidth required is $W = 1/T_p = V/T_s$ Hz and the number of dimensions of the signalling space is $N = 2WT_s = 2V$. A phasor $\mathbf{x}_m$ chosen from the L legitimate phasors in the 4-QAM constellation is transmitted for a signalling pulse duration of T_p, followed by silence for the rest of the $(V-1)$ timeslots, since the orthonormal basis functions are constructed as non-overlapping pulses according to Equation 23.53. Since we have $WT_s = N/2 = V$, the asymptotic value of the bandwidth efficiency of L-orthogonal QAM signalling is a factor of V lower than the capacity. More explicitly, the vector of an L-orthogonal QAM signalling set having $L = 4$ and $V = 4$ may be expressed as:

$$
\begin{aligned}
\mathbf{x}_1 &= \mathbf{x}_1^{4QAM}(1,0,0,0) = \left(x_1^{4QAM}[1], x_1^{4QAM}[2], 0,0,0,0,0,0\right), \\
\mathbf{x}_2 &= \mathbf{x}_2^{4QAM}(1,0,0,0) = \left(x_2^{4QAM}[1], x_2^{4QAM}[2], 0,0,0,0,0,0\right), \\
\mathbf{x}_3 &= \mathbf{x}_3^{4QAM}(1,0,0,0) = \left(x_3^{4QAM}[1], x_3^{4QAM}[2], 0,0,0,0,0,0\right), \\
\mathbf{x}_4 &= \mathbf{x}_4^{4QAM}(1,0,0,0) = \left(x_4^{4QAM}[1], x_4^{4QAM}[2], 0,0,0,0,0,0\right), \\
&\vdots \\
\mathbf{x}_{13} &= \mathbf{x}_1^{4QAM}(0,0,0,1) = \left(0,0,0,0,0,0, x_1^{4QAM}[1], x_1^{4QAM}[2]\right), \\
\mathbf{x}_{14} &= \mathbf{x}_2^{4QAM}(0,0,0,1) = \left(0,0,0,0,0,0, x_2^{4QAM}[1], x_2^{4QAM}[2]\right), \\
\mathbf{x}_{15} &= \mathbf{x}_3^{4QAM}(0,0,0,1) = \left(0,0,0,0,0,0, x_3^{4QAM}[1], x_3^{4QAM}[2]\right), \\
\mathbf{x}_{16} &= \mathbf{x}_4^{4QAM}(0,0,0,1) = \left(0,0,0,0,0,0, x_4^{4QAM}[1], x_4^{4QAM}[2]\right), \qquad (23.66)
\end{aligned}
$$

where the number of signalling waveforms is $M = VL = 16$ and the number of signalling dimensions is $N = 2V = 8$. Again, when we have $V = 1$, the L-orthogonal QAM scheme becomes a classic QAM signalling scheme. We can expect the L-orthogonal QAM scheme to exhibit a better performance, in terms of bandwidth efficiency versus E_b/N_0 and capacity versus SNR, than that of L-orthogonal PSK, since the performance of QAM studied in Section 23.5.3 was shown to be better than that of PSK studied in Section 23.5.2.

Figures 23.17 and 23.18 characterise the capacity, cutoff rate, bandwidth efficiency and normalised cutoff rate of L-orthogonal QAM signalling schemes, when communicating over both AWGN and uncorrelated Rayleigh fading channels, respectively. Similar to classic QAM signalling, most of the achievable gain are already attained by doubling the modulation levels M from L to $2L$, when aiming for a capacity of $\log_2(VL)$ bit/symbol. More explicitly, as we can observe from Figure 23.18(a), the 16-orthogonal QAM having $V = 2$ is approximately 18 dBs better than the 8-orthogonal QAM having $V = 2$ at a capacity of 4 bit/symbol. Again, the SNR gap between the capacity and cutoff rate of the uncorrelated Rayleigh fading channel is wider than that of the AWGN channel. Specifically, the SNR gap between the capacity and cutoff rate of the uncorrelated Rayleigh fading channel is approximately 6 dBs at a capacity of 4 bit/symbol, in the context of 16-orthogonal QAM having $V = 2$ as shown in Figure 23.18(a). By contrast, as we can see from Figure 23.17(a), the corresponding SNR gap between the capacity and cutoff rate of AWGN is only about

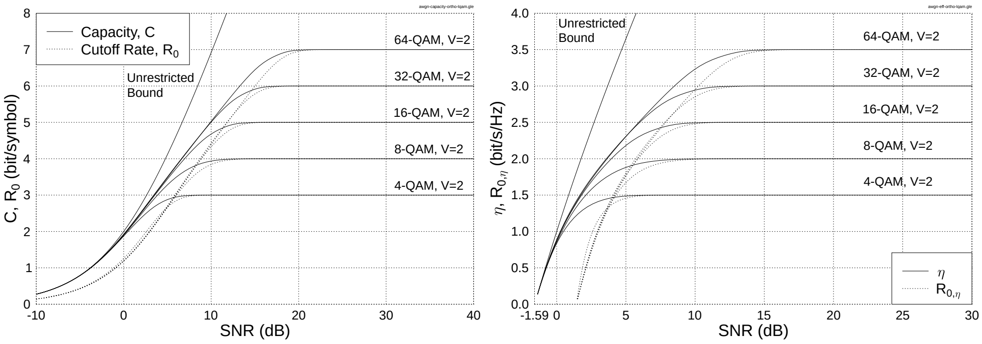

(a) The capacity C and cutoff rate R_0 are computed using Equations 23.18, 23.21, 23.30 and 23.32.

(b) The bandwidth efficiency η and normalised cutoff rate $R_{0,\eta}$ are determined using Equations 23.34 and 23.39.

Figure 23.17: L-orthogonal QAM, $V = 2$ and L = 4, 8, 16, 32 and 64 for AWGN channel.

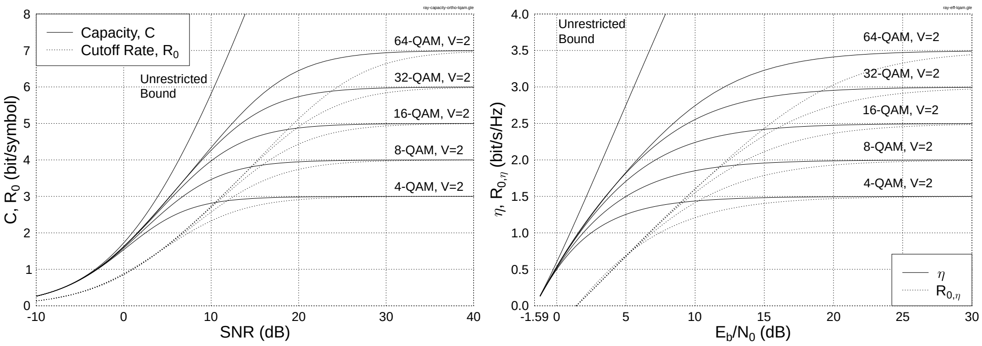

(a) The capacity C and cutoff rate R_0 are computed using Equations 23.25, 23.26, 23.28, 23.30 and 23.33.

(b) The bandwidth efficiency η and normalised cutoff rate $R_{0,\eta}$ are determined using Equations 23.34 and 23.39.

Figure 23.18: L-orthogonal QAM, $V = 2$ and L = 4, 8, 16, 32 and 64 for Rayleigh fading channel.

2 dBs. Hence it is harder to approach the capacity of the uncorrelated Rayleigh fading channel compared to the AWGN channel for the L-orthogonal QAM signalling scheme. Similar to the L-orthogonal QAM signalling, the L-orthogonal QAM signalling is capable of achieving $\log_2(V)$ bits higher throughput than that of the classic L-ary QAM subset, at a cost of $\frac{V \log_2(L)}{\log_2(VL)}$ times lower bandwidth efficiency than that of the L-ary QAM subset. Although the SNR gap between L-orthogonal QAM signalling and the unrestricted bound becomes wider upon increasing L and V, yet this gap is significantly narrower than that of L-orthogonal PSK signalling. For example, the L-orthogonal QAM scheme outperforms the L-orthogonal PSK scheme by an SNR gain of 7 dB, when employing $L = 64$ and $V = 2$ at a capacity of 6 bit/symbol, as evidenced by Figures 23.13(a) and 23.18(a). Since we have $WT_s = V$, the asymptotic value of the bandwidth efficiency is V times lower than that of the capacity, as shown in Figures 23.17 and 23.18.

Note that both L-orthogonal PSK signalling and L-orthogonal QAM signalling schemes have twice the bandwidth efficiency compared to the M-ary orthogonal signalling scheme at a given number of modulation levels M. For instance, the $M = 8$-orthogonal signalling scheme can only achieve a throughput of 0.75 bit/s/Hz, as seen in Figure 23.10(b). However, both L-orthogonal PSK signalling and L-orthogonal QAM signalling having $M = VL = 2 \times 4 = 8$ may achieve a throughput of 1.5 bit/s/Hz, as seen in Figures 23.13(b) and 23.18(b). Furthermore, it was shown in [388] that orthogonal signalling schemes, such as M-ary orthogonal signalling is more error resilient than non-orthogonal signalling schemes, such as the classic QAM arrangement. Hence we can expect the L-orthogonal QAM signalling scheme to be more error resilient than the classic QAM signalling arrangement.

23.6 Summary

In this chapter, we have studied the capacity C, cutoff rate R_0, bandwidth efficiency η and the normalised cutoff rate $R_{0,\eta}$ of M-ary PSK, M-ary QAM, M-ary orthogonal signalling as well as the hybrid of PSK/QAM and orthogonal signalling schemes. The novel contributions of this chapter are:

- the introduction of Equation 23.28 for evaluating the performance of N-dimensional M-ary signalling schemes communicating over uncorrelated Rayleigh fading channels;
- the introduction of Equation 23.47, which quantifies the ultimate PSK limit for transmission over uncorrelated Rayleigh fading channels;
- the introduction of L-orthogonal QAM signalling, as an extension of L-orthogonal PSK signalling;
- the introduction of Equations 23.56 and 23.65 for representing L-orthogonal signalling employing PSK and QAM subsets, respectively, and
- the introduction of Equations 23.62 and 23.63 for quantifying the ultimate limits of L-orthogonal PSK signalling.

This study quantified the maximum achievable capacity for a range of M-ary digital signalling set for transmission over both AWGN and Rayleigh fading channels, in the quest for more error-resilient, power-efficient and bandwidth-efficient channel coding schemes.

As we have seen in Section 23.5 that it is beneficial to double the number of modulation levels M from 2^b to 2^{b+1}, when aiming for a capacity of b bit/symbol in all the M-ary signalling schemes studied. In the forthcoming chapters, we will study a range of bandwidth efficient coded modulation schemes based on both M-ary PSK and QAM signalling, where the number of modulation levels is increased by introducing an extra parity bit in each of the original b-bit information symbol. Since the L-orthogonal QAM signalling scheme was shown in Section 23.5.6 to be more bandwidth efficient compared to the M-ary orthogonal signalling and L-orthogonal PSK signalling schemes, as well as being more error-resilient than the classic PSK and QAM schemes, future research might show the benefits of designing coded modulation schemes based on the family of L-orthogonal QAM signalling scheme.

Chapter 24

Coded Modulation Theory

24.1 Motivation

The objective of channel coding is to combat the effects of channel impairment and thereby aid the receiver in its decision making process. The design of a good channel coding and modulation scheme depends on a range of contradictory factors, some of which are portrayed in Figure 24.1. Specifically, given a certain transmission channel, it is always feasible to design a coding and modulation system which is capable of further reducing the Bit Error Ratio (BER) and/or Frame Error Ratio (FER) achieved. The gain quantified in terms of the bit energy reduction at a certain BER/FER, achieved by the employment of channel coding with respect to the uncoded system is termed the coding gain. However, this implies further investments in terms of the required implementational complexity and coding/interleaving delay as well as reducing the effective throughput. Different solutions accrue, when designing a coding and modulation scheme, which aim for optimising different features. For example, in a power-limited scenario, the system's bandwidth can be extended for the sake of accommodating a low rate code. By contrast, the effective throughput of the system can be reduced for

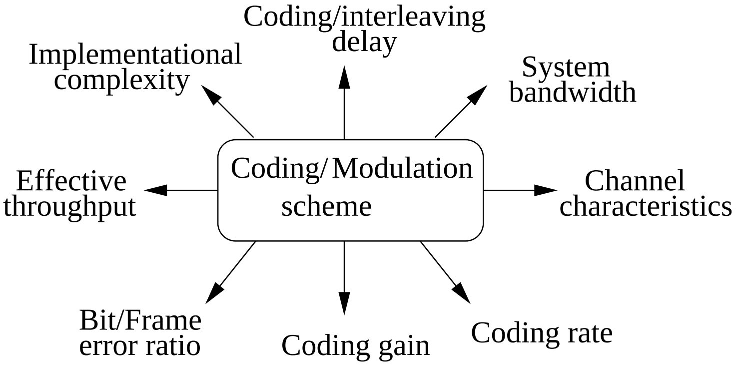

Figure 24.1: Factors affecting the design of channel coding and modulation scheme.

the sake of absorbing more parity information. To elaborate further, in a bandwidth-limited and power-limited scenario a more complex, but a higher coding gain code can be employed. The system's effective throughput can be increased by increasing the coding rate at the cost of sacrificing the achievable transmission integrity. The coding and modulation scheme's design also depends on the channel's characteristics. More specifically, the associated bit and frame error statistics change, when the channel exhibits different statistical characteristics.

On the other hand, a joint channel coding and modulation scheme can be designed by employing high rate channel coding schemes in conjunction with multidimensional or high level modulation schemes. In this coded modulation scheme a coding gain may be achieved without bandwidth expansion. In this part of the book a variety of coded modulation assisted systems will be proposed and investigated in mobile wireless propagation environments.

24.2 A Historical Perspective on Coded Modulation

The history of channel coding or Forward Error Correction (FEC) coding dates back to Shannon's pioneering work [356] in 1948, in which he showed that it is possible to design a communication system with any desired small probability of error, whenever the rate of transmission is smaller than the capacity of the channel. While Shannon outlined the theory that explained the fundamental limits imposed on the efficiency of communications systems, he provided no insights into how to actually approach these limits. This motivated the search for codes that would produce arbitrarily small probability of error. Specifically, Hamming [357] and Golay [358] were the first to develop practical error control schemes. Convolutional codes [359] were later introduced by Elias in 1955, while Viterbi [360] invented a maximum likelihood sequence estimation algorithm in 1967 for efficiently decoding convolutional codes. In 1974, Bahl proposed the more complex Maximum A-Posteriori (MAP) algorithm, which is capable of achieving the minimum achievable BER.

The first successful application of channel coding was the employment of convolutional codes [359] in deep-space probes in the 1970s. However, for years to come, error control coding was considered to have limited applicability, apart from deep-space communications. Specifically, this is a power-limited scenario, which has no strict bandwidth limitation. By contrast mobile communications systems constitute a power- and bandwidth-limited scenario. In 1987, a bandwidth efficient Trellis Coded Modulation (TCM) [361] scheme employing symbol-based channel interleaving in conjunction with Set-Partitioning (SP) [362] assisted signal labelling was proposed by Ungerböck. Specifically, the TCM scheme, which is based on combining convolutional codes with multidimensional signal sets, constitutes a bandwidth efficient scheme that has been widely recognised as an efficient error control technique suitable for applications in mobile communications [363]. Another powerful coded modulation scheme utilising bit-based channel interleaving in conjunction with Gray signal labelling, which is referred to as Bit-Interleaved Coded Modulation (BICM), was proposed by Zehavi [364] as well as by Caire, Taricco and Biglieri [365]. Another breakthrough in the history of error control coding is the invention of turbo codes by Berrou, Glavieux and Thitimajshima [366] in 1993. Convolutional codes were used as the component codes and decoders based on the MAP algorithm were employed. The results proved that a performance close to the Shannon limit can be achieved in practice with the aid of binary codes. The attractive properties of turbo codes have attracted intensive research in this area [367–369].

As a result, turbo coding has reached a state of maturity within just a few years and was standardised in the recently ratified third-generation (3G) mobile radio systems [370].

However, turbo codes often have a low coding rate and hence require considerable bandwidth expansion. Therefore, one of the objectives of turbo coding research is the design of bandwidth-efficient turbo codes. In order to equip the family of binary turbo codes with a higher spectral efficiency, BICM-based Turbo Coded Modulation (TuCM) [371] was proposed in 1994. Specifically, TuCM uses a binary turbo encoder, which is linked to a signal mapper, after its output bits were suitably punctured and multiplexed for the sake of transmitting the desired number of information bits per transmitted symbol. In the TuCM scheme of [371] Gray-coding based signal labelling was utilised. For example, two 1/2-rate Recursive Systematic Convolutional (RSC) codes are used for generating a total of four turbo coded bits and this bit stream may be punctured for generating three bits, which are mapped to an 8PSK modulation scheme. By contrast, in separate coding and modulation scheme, any modulation schemes for example BPSK, may be used for transmitting the channel coded bits. Finally, without puncturing, 16QAM transmission would have to be used for maintaining the original transmission bandwidth. Turbo Trellis Coded Modulation (TTCM) [372] is a more recently proposed channel coding scheme that has a structure similar to that of the family of turbo codes, but employs TCM schemes as its component codes. The TTCM symbols are transmitted alternatively from the first and the second constituent TCM encoders and symbol-based interleavers are utilised for turbo interleaving and channel interleaving. It was shown in [372] that TTCM performs better than the TCM and TuCM schemes at a comparable complexity. In 1998, iterative joint decoding and demodulation assisted BICM referred to as BICM-ID was proposed in [373, 374], which uses SP based signal labelling. The aim of BICM-ID is to increase the Euclidean distance of BICM and hence to exploit the full advantage of bit interleaving with the aid of soft-decision feedback based iterative decoding [374]. Many other bandwidth efficient schemes using turbo codes have been proposed in the literature [368], but we will focus our study on TCM, BICM, TTCM and BICM-ID schemes in the context of wireless channels in this part of the book.

The radio spectrum is a scarce resource. Therefore, one of the most important objectives in the design of digital cellular systems is the efficient exploitation of the available spectrum, in order to accommodate the ever-increasing traffic demands. Trellis-Coded Modulation (TCM) [496], which will be detailed in Section 24.3, was proposed originally for Gaussian channels, but it was further developed for applications in mobile communications [362, 708]. Turbo Trellis-Coded Modulation (TTCM) [709], which will be augmented in Section 24.5, is a more recent joint coding and modulation scheme that has a structure similar to that of the family of power-efficient binary turbo codes [366, 367], but employs TCM schemes as component codes. TTCM [709] requires approximately 0.5 dB lower Signal-to-Noise Ratio (SNR) at a Bit Error Ratio (BER) of 10^{-4} than binary turbo codes when communicating using 8PSK over Additive White Gaussian Noise (AWGN) channels. TCM and TTCM invoked Set Partitioning (SP) based signal labelling, as will be discussed in the context of Figure 24.8 in order to achieve a higher Euclidean distance between the unprotected bits of the constellation, as we will show during our further discourse. It was shown in [496] that parallel trellis transitions can be associated with the unprotected information bits; as we will augment in Figure 24.3(b), this reduced the decoding complexity. Furthermore, in our TCM and TTCM oriented investigations random symbol interleavers, rather than bit interleavers, were utilised, since these schemes operate on the basis of symbol, rather than bit, decisions.

Another coded modulation scheme distinguishing itself by utilising bit-based interleaving in conjunction with Gray signal constellation labelling is referred to as Bit-Interleaved Coded Modulation (BICM) [364]. More explicitly, BICM combines conventional convolutional codes with several independent bit interleavers, in order to increase the achievable diversity order to the binary Hamming distance of a code for transmission over fading channels [364], as will be shown in Section 24.6.1. The number of parallel bit interleavers equals the number of coded bits in a symbol for the BICM scheme proposed in [364]. The performance of BICM is better than that of TCM over uncorrelated or perfectly interleaved narrowband Rayleigh fading channels, but worse than that of TCM in Gaussian channels owing to the reduced Euclidean distance of the bit-interleaved scheme [364], as will be demonstrated in Section 24.6.1. Recently iterative joint decoding and demodulation assisted BICM (BICM-ID) was proposed in an effort to further increase the achievable performance [211, 373, 710–713], which uses SP-based signal labelling. The approach of BICM-ID is to increase the Euclidean distance of BICM, as will be shown in Section 24.7, and hence to exploit the full advantage of bit interleaving with the aid of soft-decision feedback-based iterative decoding [374].

In this chapter we embark on studying the properties of the above-mentioned TCM, TTCM, BICM and BICM-ID schemes in the context of Phase Shift Keying (PSK) and Quadrature Amplitude Modulation (QAM) schemes. Specifically, the code generator polynomials of 4-level QAM (4QAM) or Quadrature PSK (QPSK), 8-level PSK (8PSK), 16-level QAM (16QAM) and 64-level QAM (64QAM) will be given in Tables 24.1, 24.2, 24.3 and 24.4.

24.3 Trellis-Coded Modulation

The basic idea of TCM is that instead of sending a symbol formed by $\bar{\mathsf{m}}$ information bits, for example two information bits for 4PSK, we introduce a parity bit, while maintaining the same effective throughput of 2 bits/symbol by doubling the number of constellation points in the original constellation to eight, i.e. by extending it to 8PSK. As a consequence, the redundant bit can be absorbed by the expansion of the signal constellation, instead of accepting a 50% increase in the signalling rate, i.e. bandwidth. A positive coding gain is achieved when the detrimental effect of decreasing the Euclidean distance of the neighbouring phasors is outweighted by the coding gain of the convolutional coding incorporated.

has written an excellent tutorial paper [361], which fully describes TCM, and which this section is based upon. TCM schemes employ redundant non-binary modulation in combination with a finite state Forward Error Control (FEC) encoder, which governs the selection of the coded signal sequences. Essentially the expansion of the original symbol set absorbs more bits per symbol than required by the data rate, and these extra bit(s) are used by a convolutional encoder which restricts the possible state transitions amongst consecutive phasors to certain legitimate constellations. In the receiver, the noisy signals are decoded by a trellis-based soft-decision maximum likelihood sequence decoder. This takes the incoming data stream and attempts to map it onto each of the legitimate phasor sequences allowed by the constraints imposed by the encoder. The best fitting symbol sequence having the minimum Euclidean distance from the received sequence is used as the most likely estimate of the transmitted sequence.

Simple four-state TCM schemes, where the four-state adjective refers to the number of possible states that the encoder can be in, are capable of improving the robustness of 8PSK-based TCM transmission against additive noise in terms of the required SNR by 3dB compared to conventional uncoded 4PSK modulation. With the aid of more complex TCM schemes the coding gain can reach 6 dB [361]. As opposed to traditional error correction schemes, these gains are obtained without bandwidth expansion, or without the reduction of the effective information rate. Again, this is because the FEC encoder's parity bits are absorbed by expanding the signal constellation in order to transmit a higher number of bits per symbol. The term 'trellis' is used, because these schemes can be described by a state transition diagram similar to the trellis diagrams of binary convolutional codes [714]. The difference is that in the TCM scheme the trellis branches are labelled with redundant non-binary modulation phasors, rather than with binary code symbols.

24.3.1 TCM Principle

We now illustrate the principle of TCM using the example of a four-state trellis code for 8PSK modulation, since this relatively simple case assists us in understanding the principles involved.

The partitioned signal set proposed by [361, 496] is shown in Figure 24.2, where the binary phasor identifiers are now not Gray encoded. Observe in the figure that the Euclidean distance amongst constellation points is increased at every partitioning step. The underlined last two bits, namely bit 0 and bit 1, are used for identifying one of the four partitioned sets, while bit 2 finally pinpoints a specific phasor in each partitioned set.

The signal sets and state transition diagrams for (a) uncoded 4PSK modulation and (b) coded 8PSK modulation using four trellis states are given in Figure 24.3, while the corresponding four-state encoder-based modulator structure is shown in Figure 24.4. Observe that after differential encoding bit 2 is fed directly to the 8PSK signal mapper, whilst bit 1 is half-rate convolutionally encoded by a two-stage four-state linear circuit. The convolutional encoder adds the parity bit, bit 0, to the sequence, and again these two protected bits are used for identifying which constellation subset the bits will be assigned to, whilst the more widely spaced constellation points will be selected according to the unprotected bit 2.

The trellis diagram for 4PSK is a trivial one-state trellis, which portrays uncoded 4PSK from the viewpoint of TCM. Every connected path through the trellis represents a legitimate signal sequence where no redundancy-related transition constraints apply. In both systems, starting from any state, four transitions can occur, as required for encoding two bits/symbol. The four parallel transitions in the state trellis diagram of Figure 24.3(a) do not restrict the sequence of 4PSK symbols that can be transmitted, since there is no channel coding and therefore all trellis paths are legitimate. Hence the optimum detector can only make nearest-phasor-based decisions for each individual symbol received. The smallest distance between the 4PSK phasors is $\sqrt{2}$, denoted as d_0, and this is termed the free distance of the uncoded 4PSK constellation. Each 4PSK symbol has two nearest neighbours at this distance. Each phasor is represented by a two-bit symbol and transitions from any state to any other state are legitimate.

The situation for 8PSK TCM is a little less simplistic. The trellis diagram of Figure 24.3(b) is constituted by four states according to the four possible states of the shift-register encoder of Figure 24.4, which we represent by the four vertically stacked bold nodes. Following the elapse of a symbol period a new two-bit input symbol arrives and the convo-

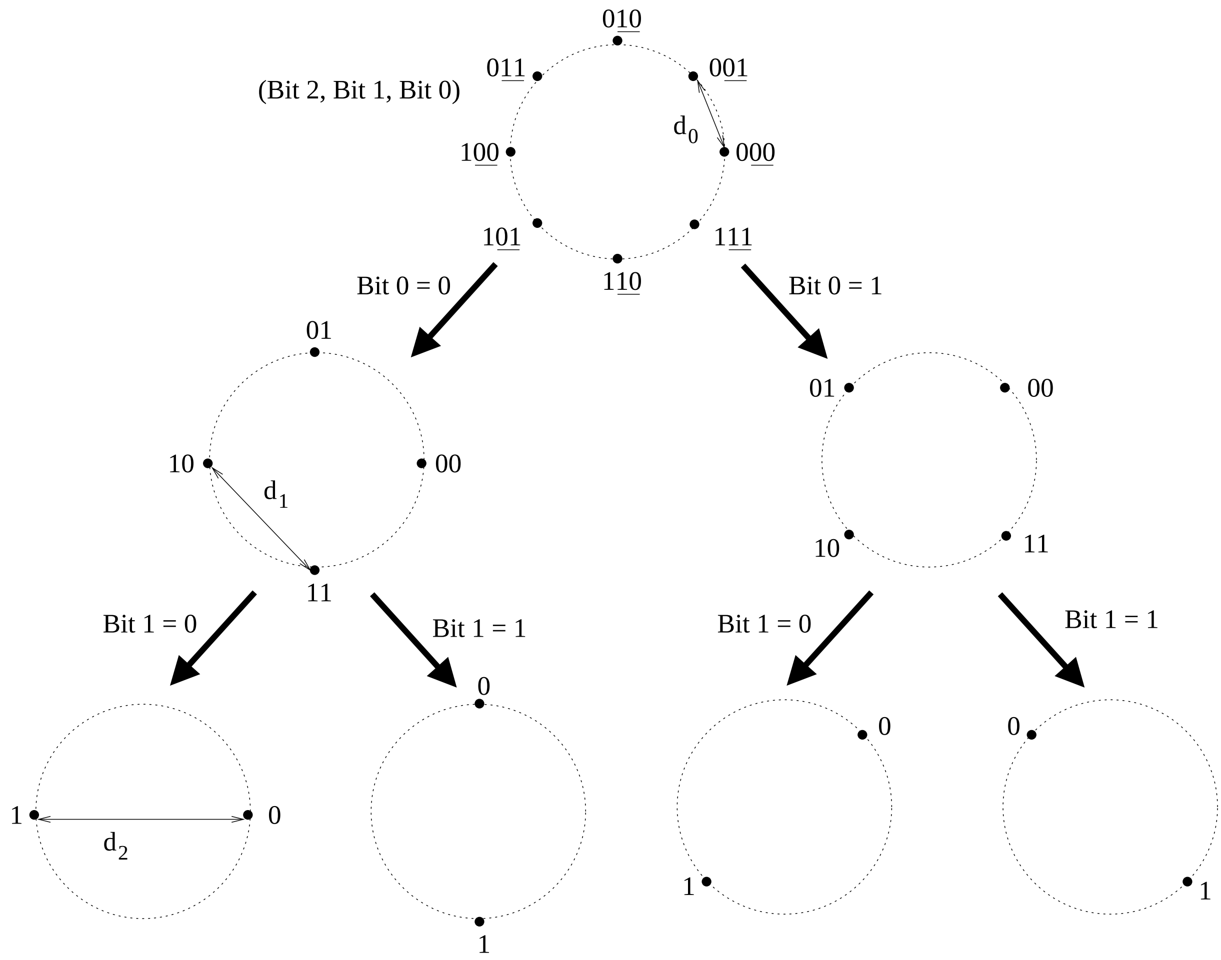

Figure 24.2: 8PSK set partitioning [496] ©IEEE, 1982, Ungerböck.

lutional encoder's shift register is clocked. This event is characterised by a transition in the trellis from state S_n to state S_{n+1}, tracking one of the four possible paths corresponding to the four possible input symbols.

In the four-state trellis of Figure 24.3(b) associated with the 8PSK TCM scheme, the trellis transitions occur in pairs and the states corresponding to the bold nodes are represented by the shift-register states S_n^0 and S_n^1 in Figure 24.4. Owing to the limitations imposed by the convolutional encoder of Figure 24.4 on the legitimate set of consecutive symbols only a limited set of state transitions associated with certain phasor sequence is possible. These limitations allow us to detect and to reject illegitimate symbol sequences, namely those which were not legitimately produced by the encoder, but rather produced by the error-prone channel. For example, when the shift register of Figure 24.4 is in state (0,0), only the transitions to the phasor points (0,2,4,6) are legitimate, whilst those to phasor points (1,3,5,7) are illegitimate. This is readily seen, because the linear encoder circuit of Figure 24.4 cannot produce

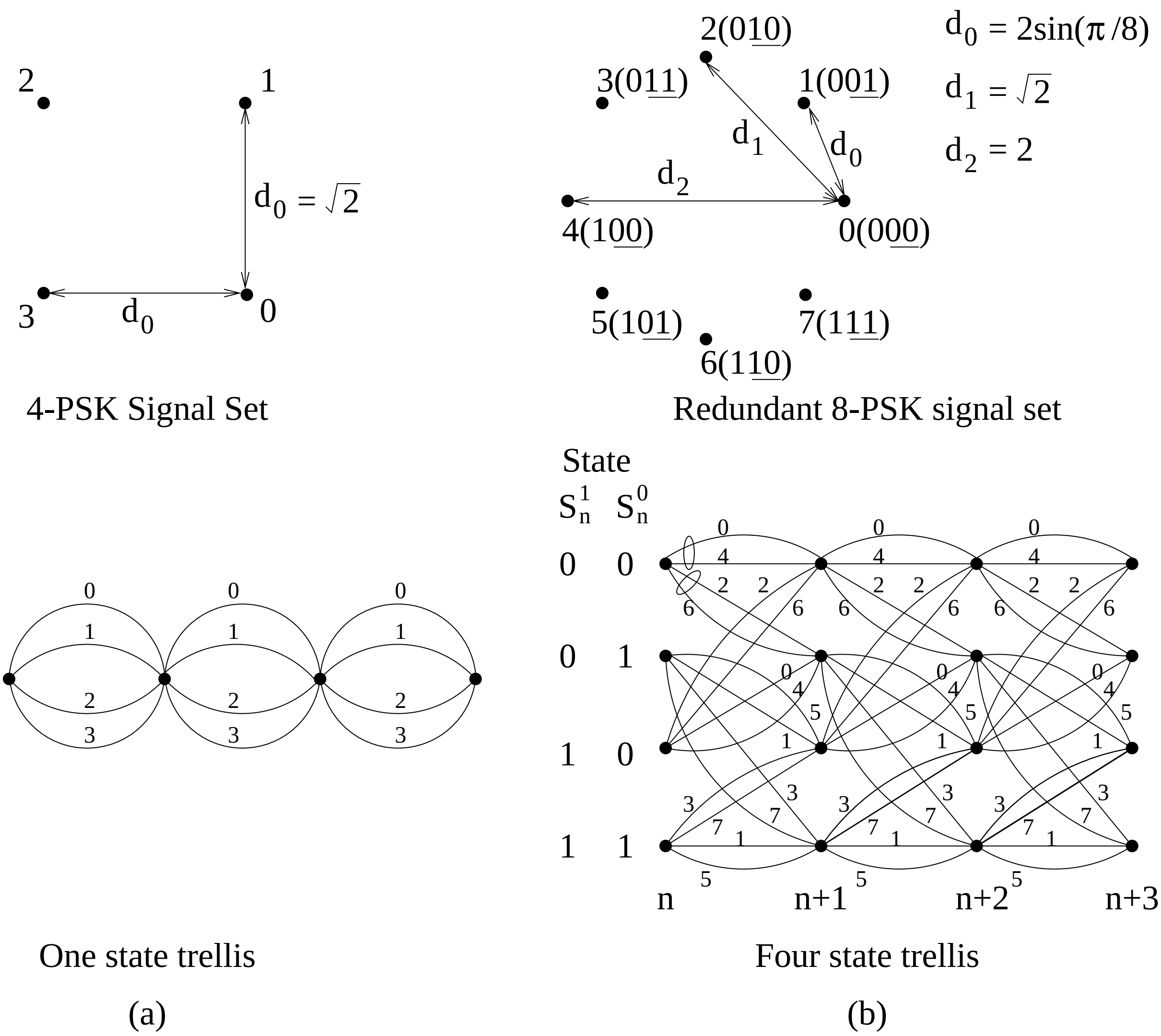

Figure 24.3: Constellation and trellis for 4- and 8PSK [361] ©IEEE, 1982, Ungerböck.

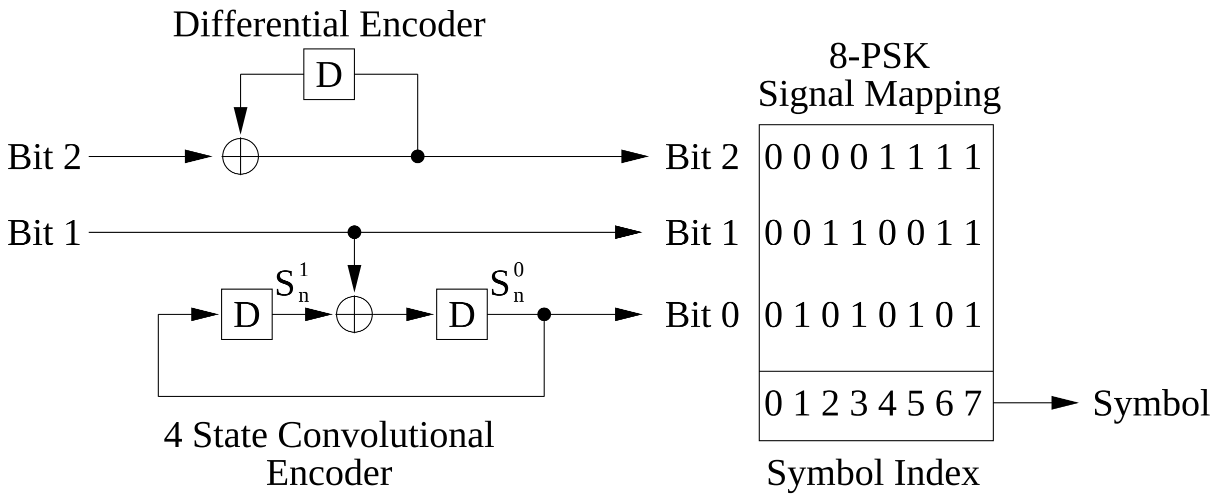

Figure 24.4: Encoder for the four-state 8PSK trellis [361] ©IEEE, 1982, Ungerböck.

a non-zero parity bit from the zero-valued input bits and hence the symbols (1,3,5,7) cannot be produced when the encoder is in the all-zero state. Observe in the 8PSK constellation of Figure 24.3(b) that the underlined bit 1 and bit 0 identify four twin-phasor subsets, where the phasors are opposite to each other in the constellation and hence have a high intra-subset separation. The unprotected bit 2 is then invoked for selecting the required phasor point within the subset. Since the redundant bit 0 constitutes also one of the shift-register state bits, namely S_n^0, from the initial states of (S_n^1,S_n^0) = (0,0) or (1,0) only the even-valued phasors (0,2,4,6) having $S_n^0 = 0$ can emerge, as also seen in Figure 24.3(b). Similarly, if we have (S_n^1,S_n^0) = (0,1) or (1,1) associated with $S_n^0 = 1$ then the branches emerging from these lower two states of the trellis in Figure 24.3(b) can only be associated with the odd-valued phasors of (1,3,5,7).

There are other possible codes, which would result in for example four distinct transitions from each state to all possible successor states, but the one selected here proved to be the most effective [361]. Within the 8PSK constellation we have the following distances: $d_0 = 2\sin(\pi/8)$, $d_1 = \sqrt{2}$ and $d_2 = 2$. The 8PSK signals are assigned to the transitions in the four-state trellis in accordance with the following rules:

1) Parallel trellis transitions are associated with phasors having the maximum possible distance, namely (d_2), between them, which is characteristic of phasor points in the subsets (0,4), (1,5), (2,6) and (3,7). Since these parallel transitions belong to the same subset of Figure 24.3(b) and are controlled by the unprotected bit 2, symbols associated with them should be as far apart as possible.

2) All four-state transitions originating from, or merging into, any one of the states are labelled with phasors having a distance of *at least* $d_1 = \sqrt{2}$ between them. These are the phasors belonging to subsets (0,2,4,6) or (1,3,5,7).

3) All 8PSK signals are used in the trellis diagram with equal probability.

Observe that the assignment of bits to the 8PSK constellation of Figure 24.3(b) does not obey Gray coding and hence adjacent phasors can have arbitrary Hamming distances between them. The bit mapping and encoding process employed was rather designed for exploiting the high Euclidean distances between sets of points in the constellation. The underlined bit 1 and bit 0 of Figure 24.3(b) representing the convolutional codec's output are identical for all parallel branches of the trellis. For example, the branches labelled with phasors 0 and 4 between the identical consecutive states of (0,0) and (0,0) are associated with (bit 1)=0 and (bit 0)=0, while the uncoded bit 2 can be either '0' or '1', yielding the phasors 0 and 4, respectively. However, owing to appropriate code design this unprotected bit has the maximum protection distance, namely $d_2 = 2$, requiring the corruption of phasor 0 into phasor 4, in order to inflict a single bit error in the position of bit 2.

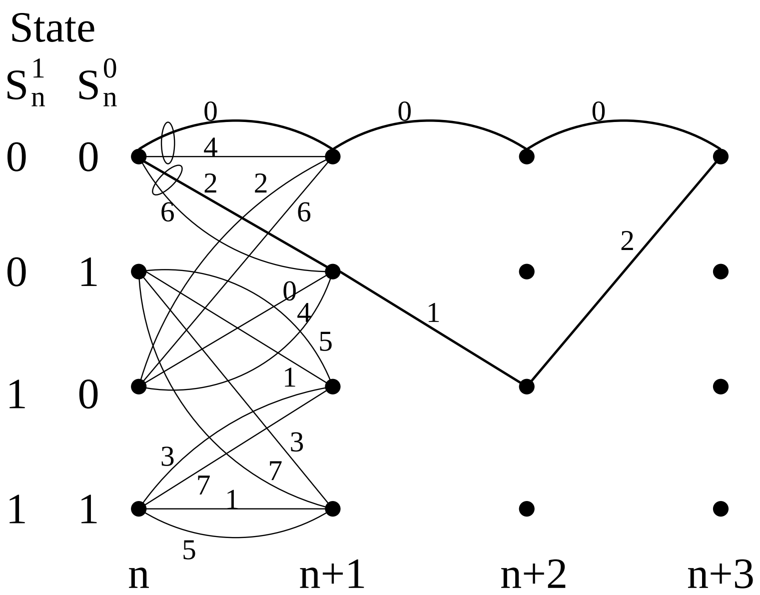

Figure 24.5: Diverging trellis paths for the computation of d_{free}. The parallel paths labelled by the symbols 0 and 4 are associated with the uncoded bits '0' and '1', respectively, as well as with the farthest phasors in the constellation of Figure 24.3(b).

The effect of channel errors exhibits itself at the decoder by diverging from the trellis path encountered in the encoder. Let us consider the example of Figure 24.5, where the encoder generated the phasors 0-0-0 commencing from state (0,0), but owing to channel errors the decoder's trellis path was different from this, since the phasor sequence 2-1-2 was encountered. The so-called free distance of a TCM scheme can be computed as the lower one of two distances. Namely, the Euclidean distances between the phasors labelling the parallel branches in the trellis of Figure 24.3(b) associated with the uncoded bit(s), which is $d_2 = 2$ in our example, as well as the distances between trellis paths diverging and remerging after a number of consecutive trellis transitions, as seen in Figure 24.5 in the first and last of the four consecutive (0,0) states. The lower one of these two distances characterises the error resilience of the underlying TCM scheme, since the error event associated with it will be the one most frequently encountered owing to channel effects. Specifically, if the received phasors are at a Euclidean distance higher than half of the code's free distance from the transmitted phasor, an erroneous decision will be made. It is essential to ensure that by using an appropriate code design the number of decoded bit errors is minimised in the most likely error events, and this is akin to the philosophy of using Gray coding in a non-trellis-coded constellation.

The Euclidean distance between the phasors of Figure 24.3(b) associated with the parallel branches is $d_2 = 2$ in our example. The distance between the diverging trellis paths of Figure 24.3(b) labelled by the phasor sequences of 0-0-0 and 2-1-2 following the states $\{$(0,0),(0,0),(0,0),(0,0)$\}$ and $\{$(0,0),(0,1),(1,0),(0,0)$\}$ respectively, portrayed in Figure 24.5, is inferred from Figure 24.3(b) as d_1-d_0-d_1. By inspecting all the remerging paths of the trellis in Figure 24.3(b) we infer that this diverging path has the shortest accumulated Free Euclidean Distance (FED) that can be found, since all other diverging paths have higher accumulated FED from the error-free 0-0-0 path. Furthermore, this is the only path having the minimum free distance of $\sqrt{d_1^2 + d_0^2 + d_1^2}$. More specifically, the free distance of this TCM sequence is given by:

$$\begin{aligned} d_{free} &= min\{d_2; \sqrt{d_1^2 + d_0^2 + d_1^2}\} \\ &= min\{2; \sqrt{2 + (2.\sin\frac{\pi}{8})^2 + 2}\}. \end{aligned} \tag{24.1}$$

Explicitly, since the term under the square root in Equation 24.1 is higher than $d_2 = 2$, the free distance of this TCM scheme is given ultimately by the Euclidean distance between the parallel trellis branches associated with the uncoded bit 2, i.e.:

$$d_{free} = 2. \tag{24.2}$$

The free distance of the uncoded 4PSK constellation of Figure 24.3(a) was $d_0 = \sqrt{2}$ and hence the employment of TCM has increased the minimum distance between the constellation points by a factor of $g = \frac{d_{free}^2}{d_0^2} = \frac{2^2}{(\sqrt{2})^2} = 2$, which corresponds to 3 dB. There is only one nearest-neighbour phasor at $d_{free} = 2$, corresponding to the π-rotated phasor in Figure 24.3(b). Consequently the phasor arrangement can be rotated by π, whilst retaining all of its properties, but other rotations are not admissible.

The number of erroneous decoded bits induced by the diverging path 2-1-2 is seen from the phasor constellation of Figure 24.3(b) to be 1-1-1, yielding a total of three bit errors. The more likely event of a bit 2 error, which is associated with a Euclidean distance of $d_2 = 2$, yields only a single bit error.

Soft-decision-based decoding can be accomplished in two steps. The first step is known as subset decoding, where within each phasor subset assigned to parallel transitions, i.e. to the uncoded bit(s), the phasor closest to the received channel output in terms of Euclidean distance is determined. Having resolved which of the parallel paths was more likely to have been encountered by the encoder, we can remove the parallel transitions, hence arriving at a conventional trellis. In the second step the Viterbi algorithm is used for finding the most likely signal path through the trellis with the minimum sum of squared Euclidean distances from the sequence of noisy channel outputs received. Only the signals already selected by the subset decoding are considered. For a description of the Viterbi algorithm the reader is referred to references [505, 715].

24.3.2 Optimum TCM Codes

Ungerböck's TCM encoder is a specific convolutional encoder selected from the family of Recursive Systematic Convolutional (RSC) codes [496], which attaches one parity bit to each information symbol. Only $\tilde{\mathsf{m}}$ out of $\bar{\mathsf{m}}$ information bits are RSC encoded and hence only $2^{\tilde{\mathsf{m}}}$ branches will diverge from and merge into each trellis state. When not all information bits are RSC encoded, i.e. $\tilde{\mathsf{m}} < \bar{\mathsf{m}}$, $2^{\bar{\mathsf{m}}-\tilde{\mathsf{m}}}$ parallel transitions are associated with each of the $2^{\tilde{\mathsf{m}}}$ branches. Therefore a total of $2^{\tilde{\mathsf{m}}} \times 2^{\bar{\mathsf{m}}-\tilde{\mathsf{m}}} = 2^{\bar{\mathsf{m}}}$ transitions occur at each trellis stage. The memory length ν of a code defines the number of shift-register stages in the encoder. Figure 24.6 shows the TCM encoder using an eight-state Ungerböck code [496],

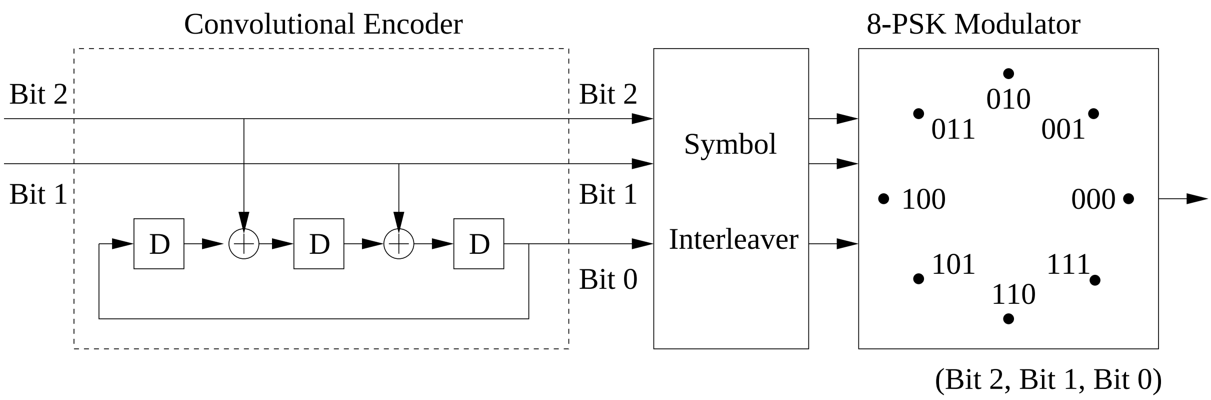

Figure 24.6: Ungerböck's RSC encoder and modulator forming the TCM encoder. The SP-based mapping of bits to the constellation points was highlighted in Figure 24.2.

which has a high FED for the sake of attaining a high performance over AWGN channels. It is a systematic encoder, which attaches an extra parity bit to the original 2-bit information word. The resulting 3-bit codewords generated by the 2-bit input binary sequence are then interleaved by a symbol interleaver in order to disperse the bursty symbol errors induced by the fading channel. Then, these 3-bit codewords are modulated onto one of the $2^3 = 8$ possible constellation points of an 8PSK modulator.

The connections between the information bits and the modulo-2 adders, as shown in Figure 24.6, are given by the generator polynomials. The coefficients of these polynomials are defined as:

$$H^j(D) := h^j_\nu . D^\nu + h^j_{\nu-1} . D^{\nu-1} + \ldots + h^j_1 . D + h^j_0, \tag{24.3}$$

where D represents the delay due to one register stage. The coefficient h^j_i takes the value of '1', if there is a connection at a specific encoder stage or '0', if there is no connection. The polynomial $H^0(D)$ is the feedback generator polynomial and $H^j(D)$ for $j \geq 1$ is the generator polynomial associated with the jth information bit. Hence, the generator polynomial of

Code	State, ν	$\tilde{\mathsf{m}}$	$H^0(D)$	$H^1(D)$	$H^2(D)$
4QAM	8, 3	1	13	06	-
4QAM	64, 6	1	117	26	-
8PSK	8, 3	2	11	02	04
8PSK	32, 5	2	45	16	34
8PSK	64, 6	2	103	30	66
8PSK	128, 7	2	277	54	122
8PSK	256, 8	2	435	72	130
16QAM	64, 6	2	101	16	64

Table 24.1: Ungerböck's TCM codes [361, 496, 716, 717], where ν denotes the code memory and octal format is used for representing the generator polynomial coefficients.

the encoder in Figure 24.6 can be described in binary format as:

$$\begin{aligned} H^0(D) &= 1001 \\ H^1(D) &= 0010 \\ H^2(D) &= 0100, \end{aligned}$$

or equivalently in octal format as:

$$\begin{aligned} \mathbf{H}(\mathbf{D}) &= \left[\begin{array}{ccc} H^0(D) & H^1(D) & H^2(D) \end{array} \right] \\ &= \left[\begin{array}{ccc} 11 & 02 & 04 \end{array} \right]. \end{aligned} \tag{24.4}$$

Ungerböck suggested [496] that all feedback polynomials should have coefficients $h^0_\nu = h^0_0 = 1$. This guarantees the realisability of the encoders shown in Figures 24.4 and 24.6. Furthermore, all generator polynomials should also have coefficients $h^j_\nu = h^j_0 = 0$ for $j > 0$. This ensures that at time n the input bits of the TCM encoder have no influence on the parity bit to be generated, nor on the input of the first binary storage element in the encoder. Therefore, whenever two paths diverge from or merge into a common state in the trellis, the parity bit must be the same for these transitions, whereas the other bits differ in at least one bit [496]. Phasors associated with diverging and merging transitions therefore have at least a distance of d_1 between them, as we can see from Figure 24.3(b). Table 24.1 summarises the generator polynomials of some TCM codes, which were obtained with the aid of an exhaustive computer search conducted by Ungerböck [361], where $\tilde{\mathsf{m}}$ ($\leq \bar{\mathsf{m}}$) indicates the number of information bits to be encoded, out of the $\bar{\mathsf{m}}$ information bits in a symbol.

24.3.3 TCM Code Design for Fading Channels

It was shown in Section 24.3.1 that the design of TCM for transmission over AWGN channels is motivated by the maximisation of the FED, d_{free}. By contrast, the design of TCM concerned for transmission over fading channels is motivated by minimising the length of the shortest error event path and the product of the branch distances along that particular path [708].

The average bit error probability of TCM using M-ary PSK (MPSK) [496] for transmission over Rician channels at high SNRs is given by [708]:

$$P_b \cong \frac{1}{B} C \left(\frac{(1+\bar{K})e^{-\bar{K}}}{E_s/N_0} \right)^{\mathsf{L}} ; E_s/N_0 \gg \bar{K} \tag{24.5}$$

where C is a constant that depends on the weight distribution of the code, which quantifies the number of trellises associated with all possible Hamming distances measured with respect to the all-zero path [370]. The variable B in Equation 24.5 is the number of binary input bits of the TCM encoder during each transmission interval, i.e the information bits per symbol, while $\bar{K}$ is the Rician fading parameter [370] and E_s/N_0 is the channel's symbol energy to noise spectral density ratio. Furthermore, L is defined as the 'length' of the shortest error event path in [718] or as the Effective Code Length (ECL) in [701,719] or as the code's diversity in [708]. Explicity, L is expressed as the number of erroneously decoded TCM symbols asociated with the shortest error event path. Note that, in conventional TCM each trellis branch is labelled by one TCM symbol. Therefore, L can be expressed as the number of trellis branches having erroneously decoded symbol, in the shortest error event path. Most of the time, L is equal to the number of trellis branches on this path. It is clear from Equation 24.5 that P_b varies inversely proportionally with $(E_s/N_0)^{\mathsf{L}}$ and this ratio can be increased by increasing the code's diversity [708]. More specifically, in [718], the authors pointed out that the shortest error event paths are not necessarily associated with the minimum accumulated FED error events. For example, let the all-zero path be the correct path. Then the code characterised by the trellis seen in Figure 24.7 exhibits a minimum squared FED of:

$$\begin{aligned} d^2_{free} &= d^2_1 + d^2_0 + d^2_1 \\ &= 4.585, \end{aligned} \tag{24.6}$$

from the 0-0-0 path associated with the transmission of three consecutive 0 symbols from the path labelled with the transmitted symbols of 6-7-6. However, this is not the shortest error event path, since its length is $\mathsf{L} = 3$, which is longer than the path labelled with transmitted symbols of 2-4, which has a length of $\mathsf{L} = 2$ and a FED of $d^2_{free} = d^2_1 + d^2_2 = 6$. Hence, the 'length' of the shortest error event path is $\mathsf{L} = 2$ for this code, which, again, has a squared Euclidean distance of 6. In summary, the number of bit errors associated with the above $\mathsf{L} = 3$ and $\mathsf{L} = 2$ shortest error event paths is seven and two, respectively, clearly favouring the $\mathsf{L} = 2$ path, which had a higher accumulated FED of 6 than that of the 4.585 FED of the $\mathsf{L} = 3$ path. Hence, it is worth noting that if the code was designed based on the minimum FED, it may not minimise the number of bit errors. Hence, as an alternative design approach, in Section 24.6 we will study BICM, which relies on the shortest error event path L or the bit-based Hamming distance of the code and hence minimises the BER.

The design of coded modulation schemes is affected by a variety of factors. A high squared FED is desired for AWGN channels, while a high ECL and a high minimum product distance are desired for fading channels [708]. In general, a code's diversity or ECL is quantified in terms of the length of the shortest error event path L, which may be increased for example by simple repetition coding, although at the cost of reducing the effective data rate proportionately. Alternatively, space-time-coded multiple transmitter/receiver structures can be used, which increase the scheme's cost and complexity. Finally, simple interleaving can be invoked, which induces latency. In our approach, symbol-based interleaving is employed

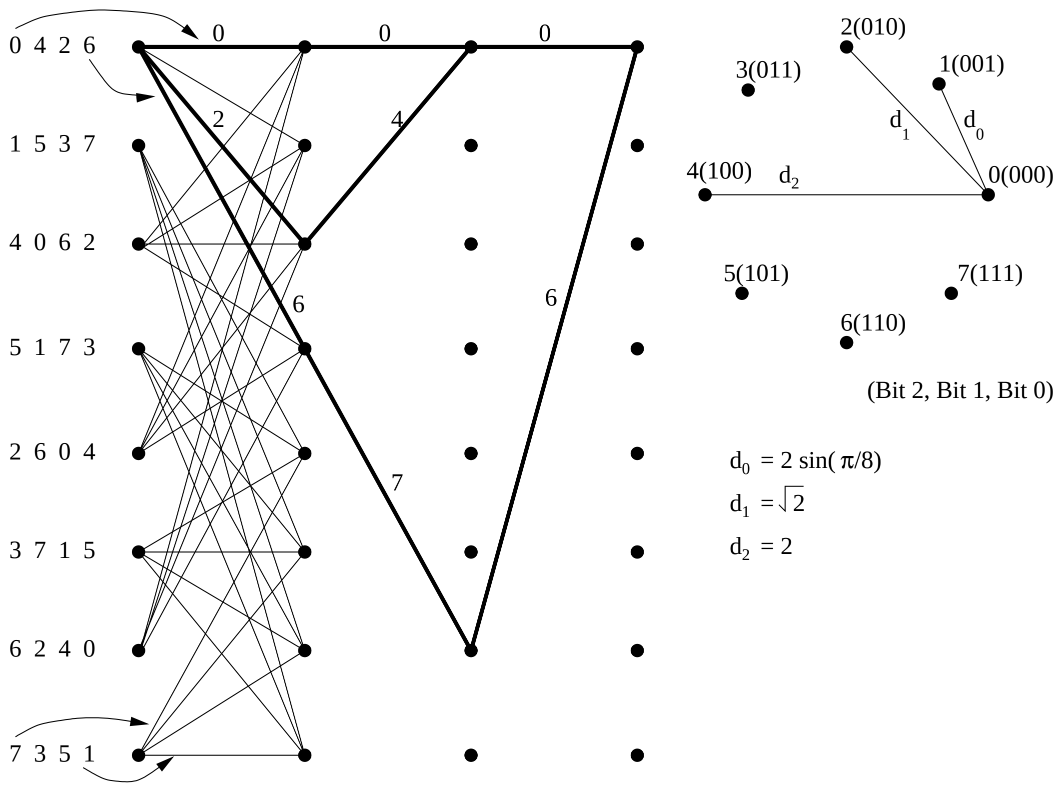

Figure 24.7: Ungerböck's 8-state 8PSK code.

in order to increase the code's diversity.

24.3.4 Set Partitioning

As we have seen in Figure 24.5, if higher-order modulation schemes, such as 16QAM or 64QAM, are used, parallel transitions may appear in the trellis diagram of the TCM scheme, when not all information bits are convolutional channel encoded or when the number of states in the convolutional encoder has to be kept low for complexity reasons. As noted before, in order to avoid encountering high error probabilities, the parallel transitions should be assigned to constellation points exhibiting a high Euclidean distance. Ungerböck solved this problem by introducing the set partitioning technique. Specifically, the signal set is split into a number of subsets, such that the minimum Euclidean distance of the signal points in the new subset is increased at every partitioning step.

In order to elaborate a little further, Figure 24.8 illustrates the set partitioning of 16QAM. Here we used the $R = \frac{3}{4}$-rate code of Table 24.1. This is a relatively high-rate code, which would not be sufficiently powerful if we employed it for protecting all three original information bits. Moreover, if we protect for example two out of the three information bits, we can use a more potent $\frac{2}{3}$-rate code for the protection of the more vulnerable two informa-

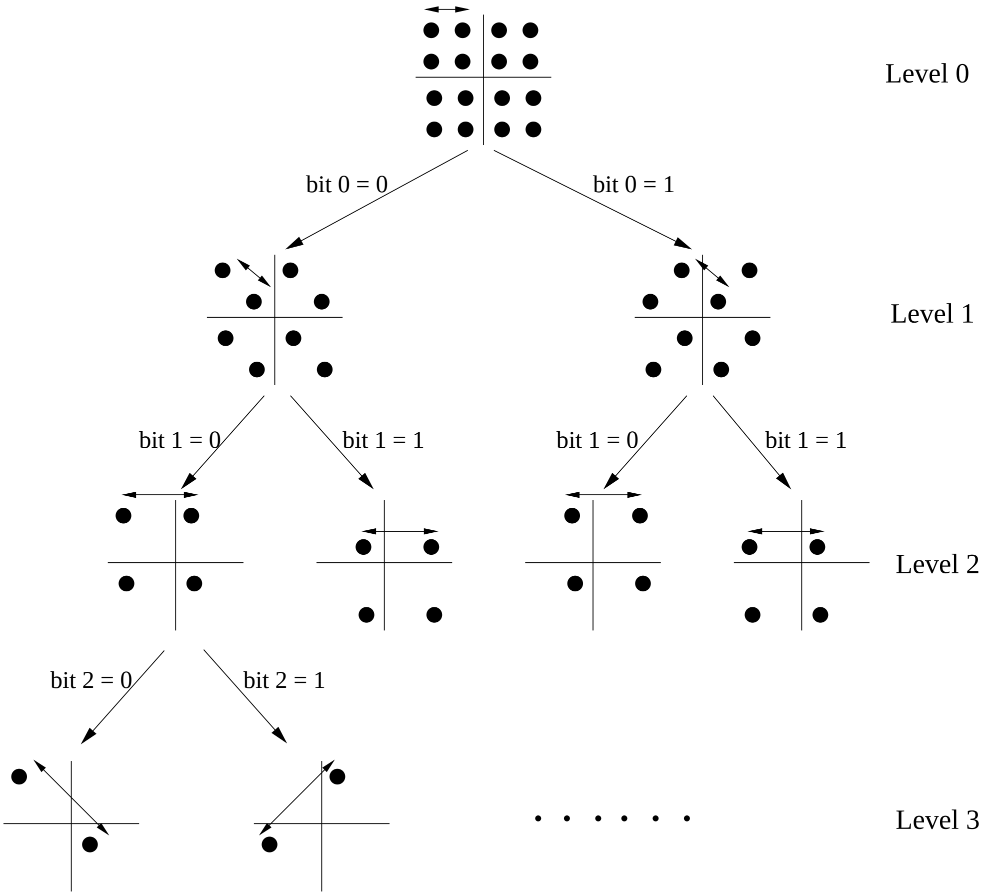

Figure 24.8: Set partitioning of a 16QAM signal constellation. The minimum Euclidean distance at a partition level is denoted by the line between the signal points [496] ©IEEE, 1982, Ungerböck.

tion bits and leave the most error-resilient bit of the 4-bit constellation unprotected. This is justifiable, since we can observe in Figure 24.8 that the minimum Euclidean distance of the constellation points increases from Level 0 to Level 3 of the constellation partitioning tree. This indicates that the bits labelling or identifying the specific partitions have to be protected by the RSC code, since they label phasors that have a low Euclidean distance. By contrast, the intra-set distance at Level 3 is the highest, suggesting a low probability of corruption. Hence the corresponding bit, bit 3, can be left unprotected. The partitioning in Figure 24.8 can be continued, until there is only one phasor or constellation point left in each subset. The intra-subset distance increases as we traverse down the partition tree. The first partition level, $Level\ 0$, is labelled by the parity bit, and the next two levels by the coded bits. Finally, the uncoded bit labels the lowest level, $Level\ 3$, in the constellation, which has the largest minimum Euclidean distance.

Conventional TCM schemes are typically decoded/demodulated with the aid of the appropriately modified Viterbi Algorithm (VA) [720]. Furthermore, the VA is a maximum likelihood sequence estimation algorithm, which does not guarantee that the Symbol Error Ratio (SER) is minimised, although it achieves a performance near the minimum SER. By contrast, the symbol-based MAP algorithm [709] guarantees the minimum SER, albeit at the cost of a significantly increased complexity. Hence the symbol-based MAP algorithm has been used for the decoding of TCM sequences. We will, however, in Section 24.5, also consider Turbo TCM (TTCM), where instead of the VA-based sequence estimation, symbol-by-symbol-based soft information has to be exchanged between the TCM decoders of the TTCM scheme. Hence in the next section we will present the symbol-based MAP algorithm.

24.4 The Symbol-based MAP Algorithm

In this section, the non-binary or symbol-based Maximum-A-Posteriori (MAP) decoding algorithm will be presented. The binary MAP algorithm was first presented in [583], while the non-binary MAP algorithm was proposed in [709]. A reduced-complexity version of the MAP algorithm, operating in the logarithmic domain (log-domain) after transforming the operands and the operations to this domain will also be presented. In our forthcoming discourse we use $p(x)$ to denote the probability of the event x, and, given a symbol sequence y_k, we denote by y_a^b the sequence of symbols given by $y_a, y_{a+1}, \ldots, y_b$.

24.4.1 Problem Description

The problem that the MAP algorithm has to solve is presented in Figure 24.9. An information source produces a sequence of N information symbols u_k, $k = 1, 2, \ldots, N$. Each information symbol can assume M different values, i.e. $u_k \in \{0, 1, \ldots, M-1\}$, where M is typically a power of two, so that each information symbol carries $\bar{\mathsf{m}} = log_2 M$ information bits. We assume here that the symbols are to be transmitted over an AWGN channel. To this end, the $\bar{\mathsf{m}}$-bit symbols are first fed into an encoder for generating a sequence of N channel symbols $x_k \in X$, where X denotes the set of complex values belonging to some phasor constellations such as an increased-order QAM or PSK constellation, having M possible values carrying $\mathsf{m} = log_2 \mathsf{M}$ bits. Again, the channel symbols are transmitted over an AWGN channel and the received symbols are:

$$y_k = x_k + n_k, \tag{24.7}$$

where n_k represents the complex AWGN samples. The received symbols are fed to the decoder, which has the task of producing an estimate $\hat{u}_k$ of the $2^{\bar{\mathsf{m}}}$-ary information sequence, based on the 2^{m}-ary received sequence, where $\mathsf{m} > \bar{\mathsf{m}}$. If the goal of the decoder is that of minimising the number of symbol errors, where a symbol error occurs when $u_k \neq \hat{u}_k$, then the best decoder is the MAP decoder [583]. This decoder computes the A Posteriori Probability (APP) $A_{k,m}$ for every $2^{\bar{\mathsf{m}}}$-ary information symbol u_k that the information symbol value was m given the received sequence, i.e. computes $A_{k,m} = p(u_k = m|y_1^N)$, for $m = 0, 1, \ldots, M-1$, $k = 1, 2, \ldots, N$. Then it decides that the information symbol was the one having the highest probability, i.e. $\hat{u}_k = m$ if $A_{k,m} \geq A_{k,i}$ for $i = 0 \ldots M-1$. In order to realise a MAP decoder one has to devise a suitable algorithm for computing the APP.

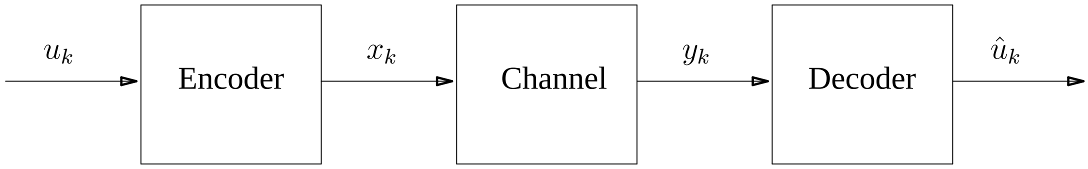

Figure 24.9: The transmission system.

In order to compute the APP, we must specify how the encoder operates. We consider a trellis encoder. The operation of a trellis encoder can be described by its trellis. The trellis seen in Figure 24.10, is constituted by $(N+1) \cdot S$ nodes arranged in $(N+1)$ columns of S nodes. There are M branches emerging from each node, which arrive at nodes in the immediately following column. The trellis structure repeats itself identically between each pair of columns.

It is possible to identify a set of paths originating from the nodes in the first column and terminating in a node of the last column. Each path will comprise exactly N branches. When employing a trellis-encoder, the input sequence unambiguously determines a single path in the trellis. This path is identified by labelling the M branches emerging from each node by the M possible values of the original information symbols, although only the labelling of the first branch at $m = 0$ and the last branch at $m = M - 1$ are shown in Figure 24.10 due to space limitations. Then, commencing from a specified node in the first column, we use the first input symbol, u_1, to decide which branch is to be chosen. If $u_1 = m$, we choose the branch labeled with m, and move to the corresponding node in the second column that this branch leads to. In this node we use the second information symbol, u_2, for selecting a further branch and so on. In this way the information sequence identifies a path in the trellis. In order to complete the encoding operation, we have to produce the symbols to be transmitted over the channel, namely $x_1, x_2, \ldots, x_N$ from the information symbols $u_1, u_2, \ldots, u_N$. To this end we add a second label to each branch, which is the corresponding phasor constellation point that is transmitted when the branch is encountered.

In a trellis it is convenient to attach a time index to each column, from 0 to N, and to number the nodes in each column from 0 to $S - 1$. This allows us to introduce the concept of trellis states at time k. Specifically, during the encoding process, we say that the trellis is in state i at time k, and write $s_k = i$, if the path determined by the information sequence crosses the i-th node of the k-th column. The structure of a trellis encoder is specified by two functions. The first function is $N(j,m) \in \{0, 1, \ldots, S-1\}$, which specifies the trellis' next state, namely $s_k = N(j,m)$, when the information symbol is $u_k = m$ and the previous state is $s_{k-1} = j$ as seen in Figure 24.10. In order to specify the symbol transmitted when this branch is encountered, we use the function $L(j,m) \in X$. To summarize, there is a branch leading from state $s_{k-1} = j$ to state $s_k = N(j,m)$, which is encountered if the input symbol is $u_k = m$, and the corresponding transmitted symbol is $L(j,m)$. It is useful to consider a third function, $P(i,m) \in \{0, 1, \ldots, S-1\}$ specifying the previous state $s_{k-1} = P(i,m)$ of the trellis when the present state is $s_k = i$, and the last original information symbol is $u_k = m$ as seen in Figure 24.10. The aim of the MAP decoding algorithm is to find the path in the trellis that is associated with the most likely transmitted symbols, i.e. that of minimising

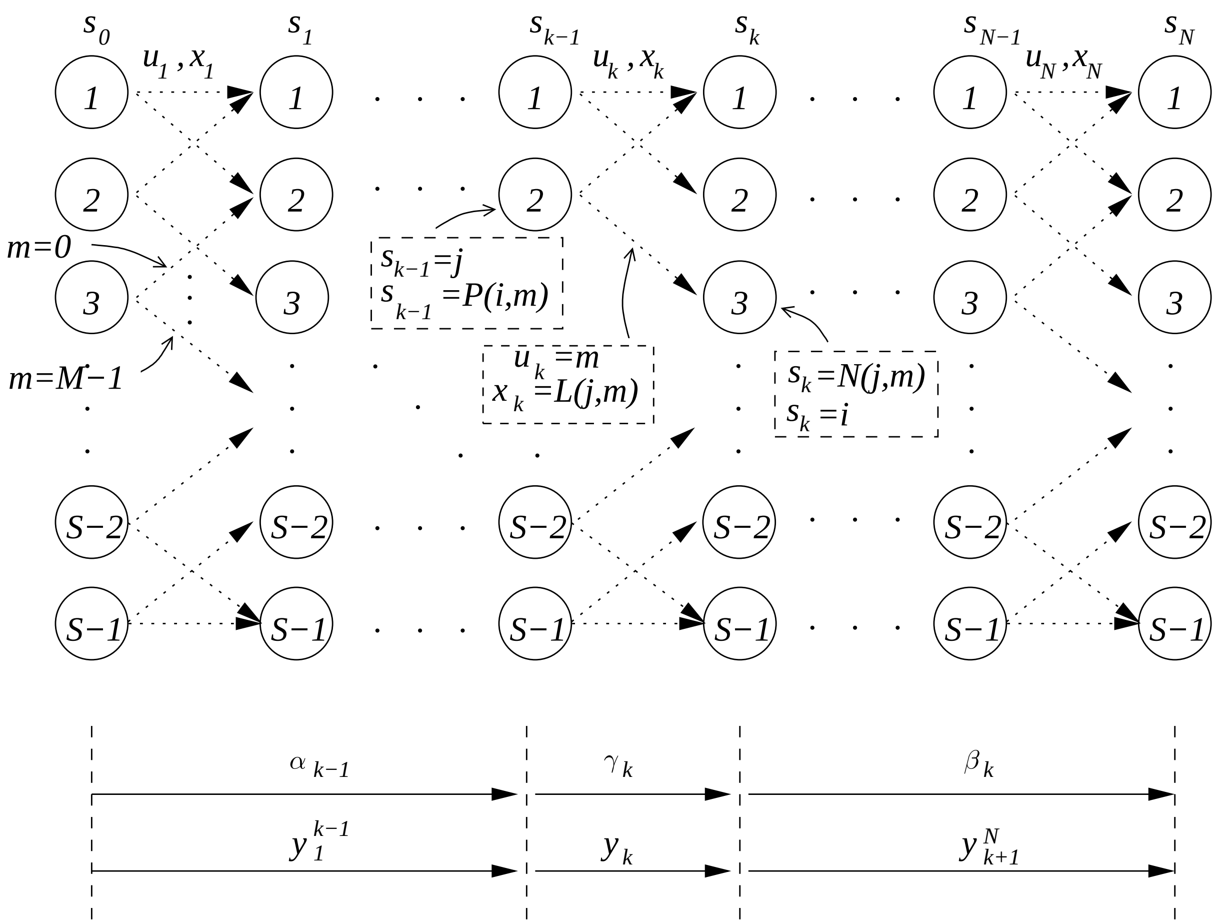

Figure 24.10: The non-binary trellis and its labelling, where there are M branches emerging from each node.

the Symbol Error Ratio (SER). By contrast, the VA-based detection of TCM signals aims for identifying the most likely transmitted symbol sequence, which does not automatically guarantee attaining the minimum SER.

24.4.2 Detailed Description of the Symbol-based MAP Algorithm

Having described the problem to be solved by the MAP decoder and the encoder structure, we now seek an algorithm capable of computing the APP, i.e. $A_{k,m} = p(u_k = m|y_1^N)$. The easiest way of computing these probabilities is by determining the sum of a different set of probabilities, namely $p(u_k = m, s_k = i, s_{k-1} = j|y_1^N)$, where again, y_1^N denotes the symbol sequence $y_1, y_2, \ldots, y_N$. This is because we can devise a recursive way of computing the second set of probabilities, as we traverse through the trellis from state to state which reduces the detection complexity. Thus we write:

$$A_{k,m} = p(u_k = m|y_1^N) = \sum_{i,j=0}^{S-1} p(u_k = m, s_k = i, s_{k-1} = j|y_1^N), \tag{24.8}$$

where the summation implies adding all probabilities associated with the nodes j and i labeled by $u_k = m$ and the problem is now that of computing $p(u_k = m, s_k = i, s_{k-1} = j|y_1^N)$. As a preliminary consideration we note that this probability is zero, if the specific branch of the trellis emerging from state j and merging into state i is not labeled with the input symbol m. Hence, we can eliminate the corresponding terms of the summation. Thus, upon denoting the specific set of pairs i, j, by I_m for which a trellis branch labeled with m exists that traverses from state j to state i, we can rewrite Equation 24.8 as:

$$A_{k,m} = \sum_{i,j \in I_m} p(u_k = m, s_k = i, s_{k-1} = j|y_1^N). \tag{24.9}$$

If $i, j \in I_m$, then we can compute the probabilities $p(u_k = m, s_k = i, s_{k-1} = j|y_1^N)$ as [583, 721]:

$$p(u_k = m, s_k = i, s_{k-1} = j|y_1^N) = \frac{1}{p(y_1^N)} \cdot \beta_k(i) \cdot \alpha_{k-1}(j) \cdot \gamma_k(j, m), \tag{24.10}$$

where

$$\begin{aligned} \beta_k(i) &= p(y_{k+1}^N|s_k = i) \\ \alpha_{k-1}(j) &= p(y_1^{k-1}, s_{k-1} = j) \\ \gamma_k(j, m) &= p(y_k, u_k = m|s_{k-1} = j). \end{aligned} \tag{24.11}$$

In order to simplify our discourse, we defer the proof of Equation 24.10 to Section 24.4.3, where we also show how the $\alpha_{k-1}(j)$ values and the $\beta_k(i)$ values can be efficiently computed using the $\gamma_k(j, m)$ values. In our forthcoming discourse we study the $\gamma_k(j, m)$ values and further simplify Equation 24.9.

The first simplification is to note that we do not necessarily need the exact $A_{k,m}$ values, but only their ratios. In fact, for a fixed k, the vector $A_{k,m}$, being a probability vector, must sum to unity. Thus, by normalising the sum in Equation 24.9 to unity, we can compute the exact value of $A_{k,m}$ from $\bar{A}_{k,m}$ with the aid of:

$$\bar{A}_{k,m} = C_k \cdot A_{k,m}. \tag{24.12}$$

For this reason we will omit the common normalisation factor of $C_k = \frac{1}{p(y_1^N)}$ in Equation 24.10. Then, upon substituting Equation 24.10 into Equation 24.9 we have:

$$\bar{A}_{k,m} = \sum_{i,j \in I_m} \beta_k(i) \cdot \alpha_{k-1}(j) \cdot \gamma_k(j, m). \tag{24.13}$$

A second simplification is to note that in Equation 24.13 the value of i is uniquely specified by the pair j and m, since $i, j \in I_m$. Specifically, since i is the state reached after emerging from state j when the input symbol is m, we have $i = N(j,m)$ where $N(j,m)$ was defined at the end of Section 24.4.1. Thus we can rewrite [1] Equation 24.13 as:

$$\bar{A}_{k,m} = \sum_{j=0}^{S-1} \beta_k(N(j,m)) \cdot \alpha_{k-1}(j) \cdot \gamma_k(j,m). \tag{24.14}$$

Before we proceed, it is worth presenting Bayes' rule, which is applied repeatedly throughout this section. This rule gives the joint probability of "a and b", $P(a,b)$, in terms of the conditional probability of "a given b", $P(a|b)$, as:

$$P(a,b) = P(a|b) \cdot P(b) = P(b|a) \cdot P(a). \tag{24.15}$$

Two useful consequences of Bayes' rule are:

$$P(a,b,c) = P(a|b,c) \cdot P(b,c) \tag{24.16}$$

and

$$\begin{aligned} P(a,b|c) &= \frac{P(a,b,c)}{P(c)} \\ &= \frac{P(a,b,c)}{P(b,c)} \cdot \frac{P(b,c)}{P(c)} \\ &= P(a|b,c).P(b|c). \end{aligned} \tag{24.17}$$

Let us now consider the term $\gamma_k(j,m) = p(y_k, u_k = m|s_{k-1} = j)$ of Equation 24.11, which can be rewritten using the relationship of Equation 24.17 as:

$$\gamma_k(j,m) = p(y_k, u_k = m|s_{k-1} = j) = p(y_k|u_k = m, s_{k-1} = j) \cdot p(u_k = m|s_{k-1} = j) \tag{24.18}$$

Let us now study the multiplicative terms at the right of Equation 24.18, where $p(y_k|u_k = m, s_{k-1} = j)$ is the probability that we receive y_k, when the branch emerging from state $s_{k-1} = j$ of Figure 24.10 labeled with the information symbol $u_k = m$ is encountered. When this branch is encountered, the symbol transmitted is $x_k = L(j,m)$, as seen in Figure 24.10. Thus, the probability of receiving the sample y_k, given that the previous state was $s_{k-1} = j$ and the transition symbol encountered was $u_k = m$ can be written as:

$$p(y_k|u_k = m, s_{k-1} = j) = p(y_k|x_k = L(j,m)) = \eta_k(j,m). \tag{24.19}$$

By remembering that $y_k = x_k + n_k$, and that n_k is the complex AWGN, we can compute $\eta_k(j,m)$ as [722]:

$$\eta_k(j,m) = e^{\frac{-|y_k - L(j,m)|^2}{2\sigma^2}}, \tag{24.20}$$

[1] Equivalently, we could note that in Equation 24.13, we have $j = P(i,m)$, since $i,j \in I_m$ and rewrite Equation 24.13 as:

$$\bar{A}_{k,m} = \sum_{i=0}^{S-1} \beta_k(i) \cdot \alpha_{k-1}(P(i,m)) \cdot \gamma_k(P(i,m),m).$$

where $\sigma^2 = N_0/2$ is the noise's variance and N_0 is the noise's Power Spectral Density (PSD). In verbal terms, Equation 24.20 indicates that the probability expressed in Equation 24.19 is a function of the distance between the received noisy sample y_k and the transmitted noiseless sample $x_k = L(j, m)$. Observe in Equation 24.20 that we dropped the multiplicative factor of $\frac{1}{2\pi\sigma^2}$, since it constitutes another scaling factor, which can be viewed as comprised in the constant C_k associated with $\bar{A}_{k,m} = C_k A_{k,m}$. As to the second multiplicative term at the righthand side of Equation 24.18, note that $p(u_k = m|s_{k-1} = j) = p(u_k = m)$, since the original information to be transmitted is independent of the previous trellis state. The probabilities:

$$\Pi_{k,m} = p(u_k = m) \tag{24.21}$$

are the $a\ priori$ probabilities of the information symbols. Typically the information symbols are independent and equiprobable, hence $\Pi_{k,m} = 1/M$. However, if we have some prior knowledge about the transmitted symbols, this can be used as their $a\ priori$ probability. As we will see, a turbo decoder will have some $a\ priori$ knowledge about the transmitted symbols after the first iteration. We now rewrite Equation 24.18 using Equation 24.19 and the $a\ priori$ probabilities as:

$$\gamma_k(j, m) = \Pi_{k,m} \cdot \eta_k(j, m). \tag{24.22}$$

Then, by substituting Equation 24.22 into Equation 24.14 and exchanging the order of summations we can portray the APPs in their final form, yielding:

$$\bar{A}_{k,m} = \Pi_{k,m} \cdot \sum_{j=0}^{S-1} \beta_k(N(j, m)) \cdot \alpha_{k-1}(j) \cdot \eta_k(j, m). \tag{24.23}$$

24.4.3 Recursive Metric Update Formulae

In this section we will deduce Equation 24.10. Figure 24.10 visualises the intervals, namely α_{k-1}, γ_k and β_k in the trellis for a given k, as well as the symbols received in these intervals, namely $\mathbf{y_1^{k-1}}, \mathbf{y_k}$ and $\mathbf{y_{k+1}^N}$, where γ is the so-called branch transition metric, α is the so-called forward recursive variable and β is the so-called backward recursive variable. As the first step of decoding, we have to compute all the values of γ_k using Equation 24.22, which depend only on the current received symbol y_k, for $k = 1, \cdots, N$. Then, we can compute α_{k-1} and β_k based on these γ_k values with the aid of Equation 24.11.

Now, we commence our discourse by considering the additive terms in Equation 24.9, which we formulated with the aids of Bayes' rule in Equations 24.15 to 24.17 as:

$$p(u_k = m, s_k = i, s_{k-1} = j|y_1^N) = \frac{1}{p(y_1^N)} \cdot p(y_1^N, u_k = m, s_k = i, s_{k-1} = j), \tag{24.24}$$

and consider the term $p(u_k = m, s_k = i, s_{k-1} = j, y_1^N)$. We can write

$$p(u_k = m, s_k = i, s_{k-1} = j, y_1^N) = p(u_k = m, s_k = i, s_{k-1} = j, y_1^k, y_{k+1}^N)$$

$$= p(y_{k+1}^N|u_k = m, s_k = i, s_{k-1} = j, y_1^k) \cdot p(u_k = m, s_k = i, s_{k-1} = j, y_1^k). \tag{24.25}$$

Let us now simplify the first multiplicative term of Equation 24.25 by noting that if the current state s_k is known, the decoded output sequence probability is not affected by either the previous state s_{k-1}, the input symbol u_k or the previous received symbol sequence y_1^k. Thus Equation 24.25 can be rewritten as

$$p(u_k = m, s_k = i, s_{k-1} = j, y_1^N) = p(y_{k+1}^N | s_k = i) \cdot p(u_k = m, s_k = i, s_{k-1} = j, y_1^k)$$

$$= p(y_{k+1}^N | s_k = i) \cdot p(y_1^{k-1} | u_k = m, s_k = i, s_{k-1} = j, y_k) \cdot p(y_k, u_k = m, s_k = i, s_{k-1} = j). \tag{24.26}$$

Again, we simplify the second multiplicative term of Equation 24.26 by noting that, if s_{k-1} is known, the received symbol sequence y_1^{k-1} is not affected by either s_k, u_k or y_k, hence we can rewrite Equation 24.26 as

$$p(u_k = m, s_k = i, s_{k-1} = j | y_1^N) = p(y_{k+1}^N | s_k = i) \cdot p(y_1^{k-1} | s_{k-1} = j) \cdot p(y_k, u_k = m, s_k = i, s_{k-1} = j). \tag{24.27}$$

By multiplying and dividing the second and the third multiplicative term, respectively, with $p(s_{k-1} = j)$, we can rearrange Equation 24.27 to

$$p(u_k = m, s_k = i, s_{k-1} = j | y_1^N) = p(y_{k+1}^N | s_k = i) \cdot p(y_1^{k-1} s_{k-1} = j) \cdot p(y_k, u_k = m, s_k = i | s_{k-1} = j). \tag{24.28}$$

Then, by introducing

$$\beta_k(i) = p(y_{k+1}^N | s_k = i) \tag{24.29}$$

and

$$\alpha_{k-1}(j) = p(y_1^{k-1}, s_{k-1} = j) \tag{24.30}$$

we have

$$p(u_k = m, s_k = i, s_{k-1} = j | y_1^N) = \beta_k(i) \cdot \alpha_{k-1}(j) \cdot p(y_k, u_k = m, s_k = i | s_{k-1} = j). \tag{24.31}$$

If $i, j \notin I_m$, the above probability is zero, since no branch exists leading from state j to state i, when the information symbol is m. Thus we assume $i, j \in I_m$. In this case we can simplify the second multiplicative term of Equation 24.31 as

$$p(y_k, u_k = m, s_k = i | s_{k-1} = j) = p(y_k, u_k = m | s_{k-1} = j). \tag{24.32}$$

Upon defining

$$\gamma_k(j, m) = p(y_k, u_k = m | s_{k-1} = j) \tag{24.33}$$

and upon substituting Equation 24.32 and Equation 24.33 in Equation 24.31 we obtain

$$p(u_k = m, s_k = i, s_{k-1} = j, y_1^N) = \beta_k(i) \cdot \alpha_{k-1}(j) \cdot \gamma_k(j, m), \tag{24.34}$$

and upon substituting Equation 24.34 in Equation 24.24 we obtain Equation 24.10, QED.

24.4.3.1 Backward Recursive Computation of $\beta_k(i)$

Let us now highlight how the values $\beta_k(i)$ can be used, in order to 'backward' recursively compute $\beta_{k-1}(P(i,m)=j)$ from $\beta_k(i)$. With the aid of the definition in Equation 24.29 we have

$$\beta_{k-1}(j) = p(y_k^N|s_{k-1}=j) = p(y_k, y_{k+1}^N|s_{k-1}=j), \tag{24.35}$$

which can be reformulated in terms of $p(y_k, y_{k+1}^N, s_k = i|s_{k-1}=j)$, by summing these probabilities for all the trellis states $i = 0\ldots(S-1)$, which are reached from $s_{k-1}=j$, yielding:

$$\beta_{k-1}(j) \;\; = \;\; \sum_{i=0}^{S-1} p(y_k, y_{k+1}^N, s_k = i|s_{k-1}=j).$$

This can be reformatted using Equations 24.15-24.17 as:

$$\beta_{k-1}(j) \;\; = \;\; \sum_{i=0}^{S-1} p(y_{k+1}^N|y_k, s_k=i, s_{k-1}=j)\cdot p(y_k, s_k=i|s_{k-1}=j). \tag{24.36}$$

With reference to the trellis diagram of Figure 24.10 we note that the received symbol sequence y_{k+1}^N is not affected by y_k and s_{k-1}, if s_k is given. Thus from Equations 24.36, 24.29 and 24.15-24.17 we obtain:

$$\beta_{k-1}(j) = \sum_{i=0}^{S-1} p(y_{k+1}^N|s_k=i)\cdot p(y_k, s_k=i|s_{k-1}=j) = \sum_{i=0}^{S-1}\beta_k(i)\cdot p(y_k, s_k=i|s_{k-1}=j). \tag{24.37}$$

Let us now consider the summation over the index range of $i = 0\ldots(S-1)$, and note that for a fixed j the probability $p(y_k, s_k=i|s_{k-1}=j)$ will be non-zero only, if a branch exists that leads from state j to state i. Thus there are only M specific values of i, which contribute to the summation, namely the values of $i = N(j,m)$ for some m. We can thus rewrite Equation 24.37 as

$$\beta_{k-1}(j) = \sum_{m=0}^{M-1}\beta_k(N(j,m))\cdot p(y_k, s_k = N(j,m)|s_{k-1}=j), \tag{24.38}$$

where for the second multiplicative term we have $p(y_k, s_k = N(j,m)|s_{k-1}=j) = p(y_k, u_k = m|s_{k-1}=j) = \gamma_k(j,m)$. Hence we can write

$$\beta_{k-1}(j) = \sum_{m=0}^{M-1}\beta_k(N(j,m))\gamma_k(j,m). \tag{24.39}$$

Equation 24.39 facilitates the 'backward' recursive calculation of the $\beta_k(N(j,m)=i)$ values, commencing from $\beta_N(N(j,m)=i)$. In order to determine this boundary value we note that by using Equation 24.39 for computing $\beta_{N-1}(j)$ we have

$$\beta_{N-1}(j) = p(y_N|s_{N-1} = j) = \sum_{m=0}^{M-1} \beta_N(N(j,m)) \cdot p(y_N, u_N = m|s_{N-1} = j) \quad (24.40)$$

and that in order to render the above expression true we have to choose

$$\beta_N(N(j,m)) = \beta_N(i) = 1. \quad (24.41)$$

24.4.3.2 Forward Recursive Computation of $\alpha_k(i)$

In this section we recursively derive the values $\alpha_k(N(j,m) = i)$ from $\alpha_{k-1}(P(i,m) = j)$. Upon exploiting Equation 24.30 we have

$$\alpha_k(i) = p(y_1^k, s_k = i) = p(y_k, y_1^{k-1}, s_k = i). \quad (24.42)$$

We can compute the right-hand side form of Equation 24.42 using the probability $p(y_k, y_1^{k-1}, s_{k-1} = j, s_k = i)$ by summing these probabilities for all the trellis states $j = 0 \ldots (S-1)$, from which the state $s_k = i$ is reached, as follows:

$$\alpha_k(i) = \sum_{j=0}^{S-1} p(y_k, y_1^{k-1}, s_{k-1} = j, s_k = i).$$

This can be reformatted using Equations 24.15-24.17 as:

$$\alpha_k(i) = \sum_{j=0}^{S-1} p(y_k, s_k = i|s_{k-1} = j, y_1^{k-1}) \cdot p(y_1^{k-1}, s_{k-1} = j). \quad (24.43)$$

With reference to the trellis diagram of Figure 24.10 we note that the received symbol sequence y_1^{k-1} has no effect on the first multiplicative term of Equation 24.43, if s_{k-1} is given. Thus from Equation 24.43 we obtain

$$\alpha_k(i) = \sum_{j=0}^{S-1} p(y_k, s_k = i|s_{k-1} = j) \cdot p(y_1^{k-1}, s_{k-1} = j)$$

and with the aid of definition in Equation 24.30 we have:

$$\alpha_k(i) = \sum_{j=0}^{S-1} p(y_k, s_k = i|s_{k-1} = j) \cdot \alpha_{k-1}(j). \quad (24.44)$$

Let us now consider the summation over the index range of $j = 0 \ldots (S-1)$ and note that for a fixed i, the probability of $p(y_k, s_k = i|s_{k-1} = j)$ will be non-zero only, if a branch exists from state j to state i. Thus there are only M non-zero values of j, which contribute to the summation in Equation 24.44, namely the values $j = P(i,m)$ for a given m. We can thus rewrite Equation 24.44 as

$$\alpha_k(i) = \sum_{m=0}^{M-1} \alpha_{k-1}(P(i,m)) \cdot p(y_k, s_k = i | s_{k-1} = P(i,m)). \tag{24.45}$$

For the second multiplicative term of Equation 24.45 we have $p(y_k, s_k = i|s_{k-1} = P(i,m)) = p(y_k, u_k = m|s_{k-1} = P(i,m)) = \gamma_k(P(i,m), m)$, hence we can write

$$\alpha_k(i) = \sum_{m=0}^{M-1} \alpha_{k-1}(P(i,m)) \cdot \gamma_k(P(i,m), m). \tag{24.46}$$

Equation 24.46 allows the recursive calculation of the $\alpha_{k-1}(P(i,m) = j)$ values, commencing from $\alpha_0(j)$. In order to determine this boundary value we note that $\alpha_0(j) = p(s_0 = j)$, i.e. $\alpha_0(j)$ is the $a\ priori$ probability of the first state j leading to state i. Conventionally, we commence the encoding from the first state, i.e. from state $j = 0$. In this case the boundary conditions are:

$$\alpha_0(j) = \begin{cases} 1 & \text{if } j = 0 \\ 0 & \text{if } j \neq 0 \end{cases} \tag{24.47}$$

Let us now consider how the above recursive computations can be carried out more efficiently in the logarithmic domain.

24.4.4 The MAP Algorithm in the Logarithmic-Domain

In this section we will describe the operation of the MAP algorithm in logarithmic domain (log-domain). In 1995, Robertson proposed the Log-Map algorithm [638], which dramatically reduces the complexity of the MAP algorithm, while attaining an identical performance to that of the MAP algorithm. The Max-Log-MAP algorithm constitutes a further substantial simplification, which performs however suboptimally compared to the Log-MAP algorithm. Specifically, in the log-domain multiplications correspond to additions, which are significantly less demanding in terms of computational complexity. A further simplification accrues by using the Jacobian logarithm [638] as follows:

$$\begin{aligned} g(\Phi_1, \Phi_2) &= ln(e^{\Phi_1} + e^{\Phi_2}) \\ &= max\{\Phi_1, \Phi_2\} + ln(1 + e^{-|\Phi_1 - \Phi_2|}) \\ &= max\{\Phi_1, \Phi_2\} + f_c(|\Phi_1 - \Phi_2|), \end{aligned} \tag{24.48}$$

where the summation of $e^{\Phi_1} + e^{\Phi_2}$ is replaced by selecting the maximum of the terms Φ_1 and Φ_2 and adding a correction term f_c that depends on the Euclidean distance of both terms. For the summation of more than two terms, i.e. for example for the summations seen in Equations 24.39 and 24.46, nesting of the $g(\Phi_1, \Phi_2)$ terms in Equation 24.48 can be carried out as follows:

$$ln(\sum_{i=1}^{I} e^{\Phi_i}) = g(\Phi_I, g(\Phi_{I-1}, \ldots g(\Phi_3, g(\Phi_2, \Phi_1)) \ldots)). \tag{24.49}$$

The correction term f_c in Equation 24.48 can be determined with the aid of three different methods:

- The Exact-Log-MAP algorithm, which is characterised by calculating the exact value of the correction term f_c as:

$$f_c = ln(1 + e^{-|\Phi_1 + \Phi_2|}). \tag{24.50}$$

  The corresponding performance is identical to that of the MAP algorithm.

- The Approx-Log-MAP algorithm invokes an approximation of the correction term f_c. Robertson [638] found that a look-up table containing eight values for f_c, ranging between 0 and 5, gives practically the same performance as the Exact-Log-MAP algorithm.

- The Max-Log-MAP algorithm, which retains only the maximum value in Equation 24.48, hence ignoring the correction term f_c. However, the Approx-Log-MAP algorithm is only marginally more complex, than the Max-Log-MAP algorithm, although it has a superior performance.

For these reasons, our simulations have been carried out by employing the Approx-Log-MAP algorithm. Explicitly, an addition operation is substituted with an addition, a subtraction, a table look-up and a maximum-search operation according to Equation 24.48, when the Approx-Log-MAP algorithm is employed.

24.4.5 Symbol-based MAP Algorithm Summary

Let us now summarize the operations of the symbol-based MAP algorithm using Figure 24.11. We assume that the $a\ priori$ probabilities $\Pi_k(i)$ in Equation 24.21 were known. These are either all equal to $1/M$ or they are constituted by additional external information. The first step is to compute the set of probabilities $\eta_k(i,m)$ from Equation 24.20 as:

$$\eta_k(j,m) = e^{\frac{-|y_k - L(j,m)|^2}{2\sigma^2}}. \tag{24.51}$$

From these and the $a\ priori$ probabilities, the $\gamma_k(i,m)$ values are computed according to Equation 24.22 as

$$\gamma_k(j,m) = \Pi_{k,m} \cdot \eta_k(j,m). \tag{24.52}$$

The above values are then used to recursively compute the values $\alpha_{k-1}(j)$ employing Equations 24.46 and 24.47 as

$$\alpha_k(i) = \sum_{m=0}^{M-1} \alpha_{k-1}(P(i,m)) \cdot \gamma_k(P(i,m),m), \tag{24.53}$$

and the values $\beta_k(i)$ using Equations 24.39 and 24.41 as

$$\beta_{k-1}(j) = \sum_{m=0}^{M-1} \beta_k(N(j,m)) \cdot \gamma_k(j,m). \tag{24.54}$$

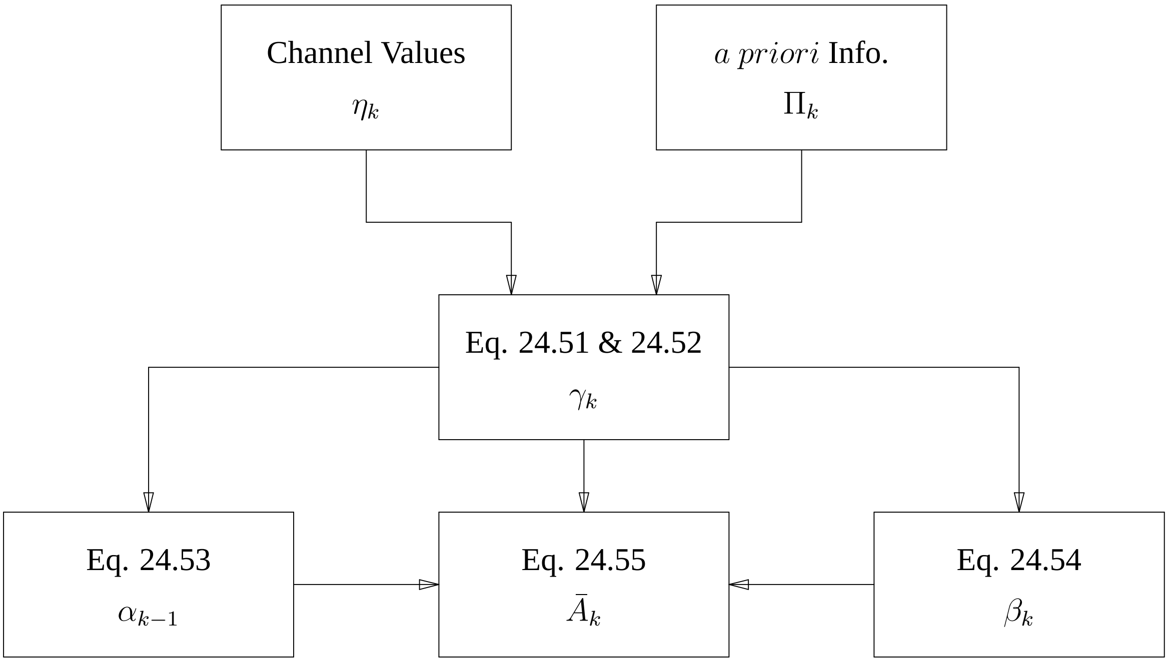

Figure 24.11: Summary of the symbol-based MAP algorithm operations.

Finally, the APP can be obtained using Equation 24.23

$$\bar{A}_{k,m} = \Pi_{k,m} \cdot \sum_{j=0}^{S-1} \beta_k(N(j,m)) \cdot \alpha_{k-1}(j) \cdot \eta_k(j,m). \tag{24.55}$$

When considering the implementation of the MAP algorithm, one can opt for computing and storing the $\eta_k(j,m)$ values, and use these values together with the $a\ priori$ probabilities for determining the values $\gamma_k(j,m)$ during decoding. In order to compute the probabilities $\eta_k(j,m)$ it is convenient to separately evaluate the exponential function of Equation 24.51 for every k and for every possible value of the transmitted symbol. As described in Section 24.4.1, a sequence of N information symbols was produced by the information source and each information symbol can assume M possible values, while the number of encoder states is S. There are $\mathsf{M} = 2 \cdot M$ possible transmitted symbols, since the size of the original signal constellation was doubled by the trellis encoder. Thus $N \cdot 2 \cdot M$ evaluations of the exponential function of Equation 24.51 are needed. Using the online computation of the $\gamma_k(j,m)$ values, two multiplications are required for computing one additive term in each of Equation 24.53 and 24.54, and there are $N \cdot S$ terms to be computed, each requiring M terms to be summed. Hence $2 \cdot N \cdot M \cdot S$ multiplications and $N \cdot M \cdot S$ additions are required for computing the forward recursion α or the backward recursion β. Approximately three multiplications are required for computing each additive term in Equation 24.55, and there are $N \cdot M$ terms to be computed, each requiring S terms to be summed. Hence, the total implementational complexity entails $7 \cdot N \cdot M \cdot S$ multiplications, $3 \cdot N \cdot M \cdot S$ summations and $N \cdot 2 \cdot M$ exponential function evaluations, which is directly proportional to the length N of the transmitted sequence, to the number of code states S and to the number of different values M assumed by the input symbols.

The computational complexity can be reduced by implementing the algorithm in the log-domain, where the evaluation of the exponential function in Equation 24.51 is avoided. The multiplications and additions in Equations 24.52 to 24.55 are replaced by additions and Jacobian comparisons, respectively. Hence the total implementational complexity imposed is $7 \cdot N \cdot M \cdot S$ additions and $3 \cdot N \cdot M \cdot S$ Jacobian comparisons.

When implementing the MAP decoder presented here it is necessary to control the dynamic range of the likelihood terms computed in Equations 24.53 to 24.55. This is because these values tend to become lower and lower due to the multiplication of small values. The dynamic range can be controlled by normalising the sum of the $\alpha_k(i)$ and the $\beta_k(i)$ values to unity at every particular k symbol. The resulting symbol values will not be affected, since the normalization only affects the scaling factors C_k in Equation 24.12. However, this problem can be avoided, when the MAP algorithm is implemented in the log-domain.

To conclude, let us note that the MAP decoder presented here is suitable for the decoding of finite-length, preferably short, sequences. When long sequences are transmitted, the employment of this decoder is impractical, since the associated memory requirements increase linearly with the sequence-length. In this case the MAP decoder has to be modified. A MAP decoder designed for long sequences was first presented in [723]. An efficient implementation, derived by adapting the algorithm of [583], was proposed by Piazzo in [724]. Having described the symbol-based MAP algorithm, let us now consider Turbo TCM (TTCM) and the way it invokes the MAP procedure.

24.5 Turbo Trellis-Coded Modulation

24.5.1 TTCM Encoder

It is worth describing the signal set dimensionality ($\bar{D}$) [725, 726] before we proceed. For a specific $2\bar{D}$ code, we have one $2\bar{D}$ symbol per codeword. For a general multidimensional code having a dimensionality of $\mathsf{D} = 2 \cdot n$ where $n > 0$ is an integer, one $\mathsf{D}\bar{D}$ codeword is comprised of n $2\bar{D}$ sub-codewords. The basic concept of the multidimensional signal mapping [725] is to assign more than one $2\bar{D}$ symbol to one codeword, in order to increase the spectral efficiency, which is defined as the number of information bits transmitted per channel symbol. For instance, a $2\bar{D}$ 8PSK TCM code seen in Table 24.2 maps $n = \frac{\mathsf{D}}{2} = 1$ three-bit $2\bar{D}$ symbol to one $2\bar{D}$ codeword, where the number of information bits per $2\bar{D}$ codeword is $\bar{\mathsf{m}} = 2$ yielding a spectral efficiency of $\bar{\mathsf{m}}/n = 2$ information bits per symbol. However, a $4\bar{D}$ 8PSK TCM code seen in Table 24.2 maps $n = \frac{\mathsf{D}}{2} = 2$ three-bit $2\bar{D}$ symbols to one six-bit $4\bar{D}$ codeword using the mapping rule of [725], where the number of information bits per $4\bar{D}$ codeword is $\bar{\mathsf{m}} = 5$, yielding a spectral efficiency of $\bar{\mathsf{m}}/n = 2.5$ information bits per symbol. However, during our further discourse we only consider $2\bar{D}$ signal sets.

Employing TTCM [709] avoids the obvious disadvantage of rate loss that one would incur when applying the principle of parallel concatenation to TCM without invoking puncturing. Specifically, this is achieved by puncturing the parity information in a particular manner, so that all information bits are sent only once, and the parity bits are provided alternatively by the two component TCM encoders. The TTCM encoder is shown in Figure 24.12, which comprises two identical TCM encoders linked by a symbol interleaver.

Let the memory of the interleaver be N symbols. The number of modulated symbols per block is $N.n$, where $n = \frac{\mathsf{D}}{2}$ is an integer and D is the number of dimensions of the signal set. The number of information bits transmitted per block is $N.\bar{\mathsf{m}}$, where $\bar{\mathsf{m}}$ is the number of information bits per symbol. The encoder is clocked at a rate of $n.T$, where T is the symbol duration of each transmitted $2^{(\bar{\mathsf{m}}+1)/n}$-ary $2\bar{D}$ symbol. At each step, $\bar{\mathsf{m}}$ information bits are input to the TTCM encoder and n symbols each constituted by $\bar{\mathsf{m}}+1$ bits are transmitted, yielding a coding rate of $\frac{\bar{\mathsf{m}}}{\bar{\mathsf{m}}+1}$.

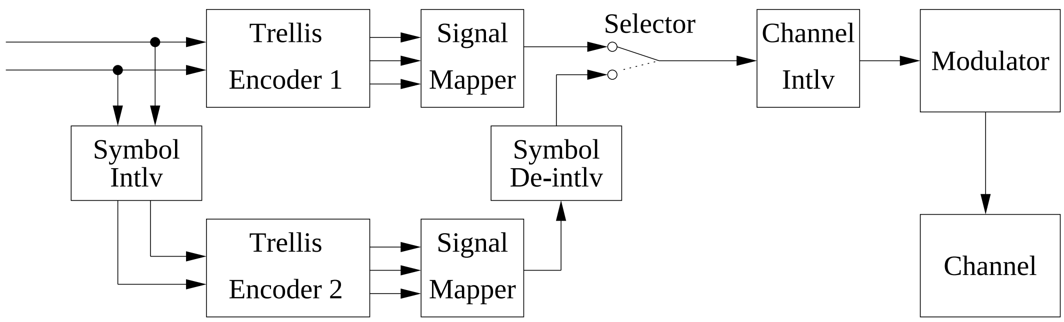

Figure 24.12: Schematic of the TTCM encoder. The selector enables the transmission of the information bits only once and selects alternative parity bits from the constituent encoders seen at the top and bottom [709] ©IEEE, 1998, Robertson and Wörz.

Each component TCM encoder consists of an Ungerböck encoder and a signal mapper. The first TCM encoder operates on the original input bit sequence, while the second TCM encoder manipulates the interleaved version of the input bit sequence. The signal mapper translates the codewords into complex symbols using the SP-based labelling method of Section 24.3.4. A complex symbol represents the amplitude and phase information passed to the modulator in the system seen in Figure 24.12. The complex output symbols of the signal mapper at the bottom of Figure 24.12 are symbol de-interleaved according to the inverse operation of the interleaver. Again, the interleaver and de-interleaver are symbol interleavers [727]. Owing to invoking the de-interleaver of Figure 24.12 at the output of the component encoder seen at the bottom, the TTCM codewords of both component encoders have identical information bits before the selector. Hence, the selector that alternatively selects the symbols of the upper and lower component encoders is effectively a puncturer that punctures the parity bits of the output symbols.

The output of the selector is then forwarded to the channel interleaver, which is, again, another symbol interleaver. The task of the channel interleaver is to effectively disperse the bursty symbol errors experienced during transmission over fading channels. This increases the diversity order of the code [708, 718]. Finally, the output symbols are modulated and transmitted through the channel.

Table 24.2 shows the generator polynomials of some component TCM codes that can be employed in the TTCM scheme. These generator polynomials were obtained by Robertson and Wörz [709] using an exhaustive computer search of all polynomials and finding the one that maximises the minimal Euclidean distance, taking also into account the alternative

Code	State, ν	$\tilde{\mathsf{m}}$	$H^0(D)$	$H^1(D)$	$H^2(D)$	$H^3(D)$	$d^2_{free}/\triangle^2_0$
$2\bar{D}$, 8PSK	4, 2	2	07	02	04	-	
$2\bar{D}$, 8PSK	8, 3	2	11	02	04	-	3
$4\bar{D}$, 8PSK	8, 3	2	11	06	04	-	3
$2\bar{D}$, 8PSK	16, 4	2	23	02	10	-	3
$4\bar{D}$, 8PSK	16, 4	2	23	14	06	-	3
$2\bar{D}$, 16QAM	8, 3	3	11	02	04	10	2
$2\bar{D}$, 16QAM	16, 4	3	21	02	04	10	3
$2\bar{D}$, 64QAM	8, 3	2	11	04	02	-	3
$2\bar{D}$, 64QAM	16, 4	2	21	04	10	-	4

Table 24.2: 'Punctured' TCM codes exhibiting the best minimum distance for 8PSK, 16QAM and 64QAM, where octal format is used for specifying the generator polynomials [709] ©IEEE, 1998, Robertson and Wörz. The notation $\bar{D}$ denotes the dimensionality of the code, ν denotes the code memory, $\triangle^2_0$ denotes the squared Euclidean distance of the signal set itself and d^2_{free} denotes the squared FED of the TCM code.

selection of parity bits for the TTCM scheme. In Table 24.2, $\tilde{\mathsf{m}}$ denotes the number of information bits to be encoded out of the total $\bar{\mathsf{m}}$ information bits in a symbol, $\triangle^2_0$ denotes the squared Euclidean distance of the signal set itself, i.e. after TCM signal expansion, and d^2_{free} denotes the squared FED of the TCM constituent codes, as defined in Section 24.3.1. Since $d^2_{free}/\triangle^2_0 > 0$, the 'punctured' TCM codes constructed in Table 24.2 exhibit a positive coding gain in comparison to the uncoded but expanded signal set, although not necessarily in comparison to the uncoded and unexpanded original signal set. Nonetheless, the design target is to provide a coding gain also in comparison to the uncoded and unexpanded original signal set at least for the targeted operational SNR range of the system.

Considering the 8PSK example of Table 24.2, where $\triangle^2_0 = d^2_{8PSK}$ applies, we have $d^2_{free}/d^2_{8PSK} = 3$. However, when we compare the 'punctured' 8PSK TCM codes to the original uncoded QPSK, signal set we have $d^2_{free}/d^2_{QPSK} = d^2_{free}/2 = 0.878$ [709], which implies attaining a negative coding gain. However, when the iterative decoding scheme of TTCM is invoked, we attain a significant positive coding gain, as we will demonstrate in the following chapters.

24.5.2 TTCM Decoder

The concept of $a\ priori$, $a\ posteriori$ and $extrinsic$ information is illustrated in Figure 24.13. The associated concept is portrayed in more detail in Figure 24.14. The TTCM decoder structure of Figure 24.14(b) is similar to that of binary turbo codes shown in Figure 24.14(a), except that there is a difference in the nature of the information passed from one decoder to the other and in the treatment of the very first decoding step. Specifically, each decoder alternately processes its corresponding encoder's channel-impaired output symbol, and then the other encoder's channel-impaired output symbol.

In a binary turbo coding scheme the component encoders' output can be split into three additive parts for each information bit u_k at step k, when operating in the logarithmic or LLR domain [638] as shown in Figure 24.14(a), which are:

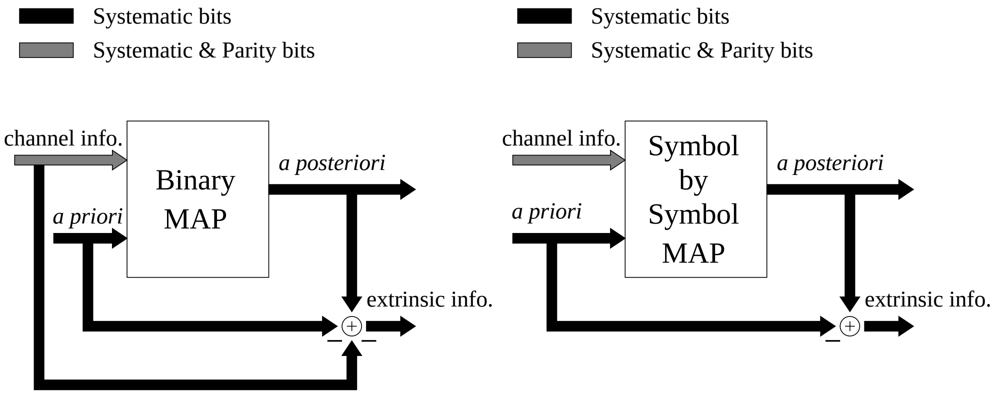

(a) A binary turbo component decoder. **(b)** A non-binary TTCM component decoder.

Figure 24.13: Schematic of the component decoders for binary turbo codes and non-binary TTCM.

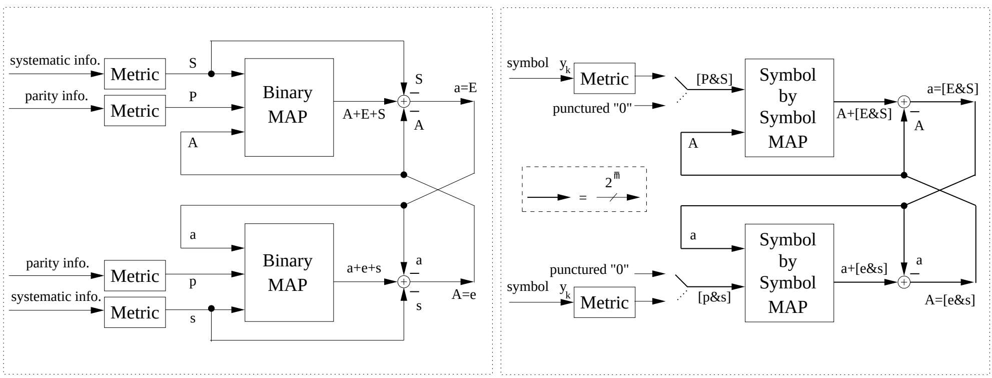

(a) Binary Turbo Decoder at step k **(b)** TTCM Decoder at step k

Figure 24.14: Schematic of the decoders for binary turbo codes and TTCM. Note that the labels and arrows apply only to one specific information bit for the binary turbo decoder, or a group of $\bar{m}$ information bits for the TTCM decoder [709] ©IEEE, 1998, Robertson and Wörz. The interleavers/de-interleavers are not shown and the notations P, S, A and E denote the parity information, systematic information, $a\ priori$ probabilities and $extrinsic$ probabilities, respectively. Upper (lower) case letters represent the probabilities of the upper (lower) component decoder.

1) the systematic component (S/s), i.e. the corresponding received systematic value for bit u_k;

2) the *a priori* or *intrinsic* component (A/a), i.e. the information provided by the other component decoder for bit u_k; and

3) the *extrinsic* information component related to bit u_k (E/e), which depends not on bit u_k itself but on the surrounding bits.

These components are impaired by independent noise and fading effects. In turbo codes, only the *extrinsic* component should be passed on to the other component decoder, so that the *intrinsic* information directly related to a bit is not reused in the other component decoder [366]. This measure is necessary in turbo codes for avoiding the prevention of achieving iterative gains, due to the dependence of the constituent decoders' information on each other.

However, in a symbol-based non-binary TTCM scheme the $\bar{\mathsf{m}}$ systematic information bits and the parity bit are transmitted together in the same non-binary symbol. Hence, the systematic component of the non-binary symbol, namely the original information bits, cannot be separated from the *extrinsic* component, since the noise and/or fading that affects the parity component also affects the systematic component. Therefore, in this scenario the symbol-based information can be split into only two components:

1) the *a priori* component of a non-binary symbol (A/a), which is provided by the other component decoder, and

2) the inseparable *extrinsic* as well as systematic component of a non-binary symbol ($[E\&S]/[e\&s]$), as can be seen from Figure 24.14(b).

Each decoder passes only the latter information to the next component decoder while the *a priori* information is removed at each component decoder's output, as seen in Figure 24.14(b), where, again, the *extrinsic* and systematic components are inseparable.

As described in Section 24.5.1, the number of modulated symbols per block is $N \cdot n$, with $n = \frac{\mathsf{D}}{2}$, where D is the number of dimensions of the signal set. Hence for a $2\bar{D}$ signal set we have $n = 1$ and the number of modulated symbols per block is N. Therefore the symbol interleaver of length N will interleave a block of N complex symbols. Let us consider $2\bar{D}$ modulation having a coding rate of $\frac{\bar{\mathsf{m}}}{\bar{\mathsf{m}}+1}$ for the following example.

The received symbols are input to the 'Metric' block of Figure 24.15, in order to generate a set of $\mathsf{M} = 2^{\bar{\mathsf{m}}+1}$ symbol probabilities for quantifying the likelihood that a certain symbol of the M-ary constellation was transmitted. The selector switches seen at the input of the 'Symbol by Symbol MAP' decoder select the current symbol's reliability metric, which is produced at the output of the 'Metric' block, if the current symbol was not punctured by the corresponding encoder. Otherwise puncturing will be applied where the probabilities of the various legitimate symbols at index k are set to 1 or to 0 in the log-domain. The upper (lower) case letters denote the set of probabilities of the upper (lower) component decoder, as shown in the figure. The 'Metric' block provides the decoder with the inseparable parity and systematic ($[P\&S]$ *or* $[p\&s]$) information, and the second input to the decoder is the *a priori* (A *or* a) information provided by the other component decoder. The MAP decoder then provides the *a posteriori* ($A + [E\&S]$ *or* $a + [e\&s]$) information at its output. Then A (*or* a) is subtracted from the *a posteriori* information, so that the same information is not used

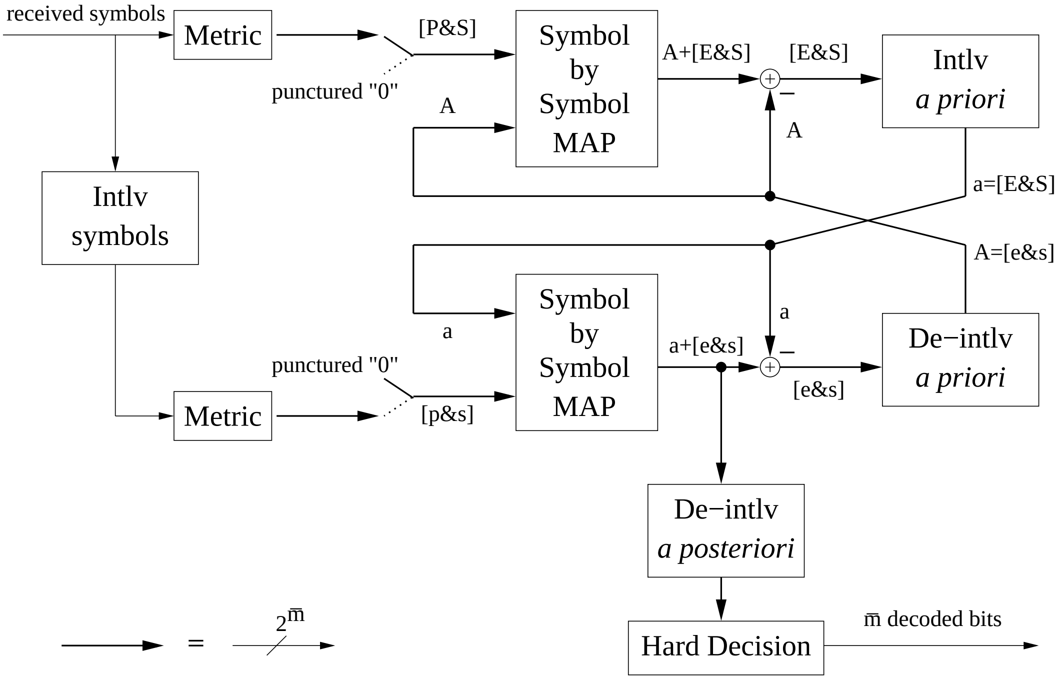

Figure 24.15: Schematic of the TTCM decoder. P, S, A and E denote the parity information, systematic information, *a priori* probabilities and *extrinsic* probabilities, respectively. Upper (lower) case letters represent the probabilities of the upper (lower) component decoder.

more than once in the other component decoder, since otherwise the component decoders' corresponding information would become dependent on each other, which would preclude the achievement of iteration gains. The resulting $[E\&S \ or \ e\&s]$ information is symbol interleaved (or de-interleaved) in order to present the $a \ (or \ A)$ input for the other component decoder in the required order. This decoding process will continue iteratively, in order to offer an improved version of the set of symbol reliabilities for the other component decoder. One iteration comprises the decoding of the received symbols by both the component decoders once. Finally, the $a \ posteriori$ information of the lower component decoder will be de-interleaved in order to extract $\bar{m}$ decoded information bits per symbol. Hard decision implies selecting the specific symbol which exhibits the maximum $a \ posteriori$ probability associated with the $\bar{m}$-bit information symbol out of the $2^{\bar{m}}$ probability values. Having described the operation of the symbol-based TTCM technique, which does not protect all transmitted bits of the symbols, let us now consider bit-interleaved coded modulation as a design alternative.

24.6 Bit-Interleaved Coded Modulation

Bit-Interleaved Coded Modulation (BICM) was proposed by [364] with the aim of increasing the diversity order of Ungerböck's TCM schemes which was quantified in Section 24.3.3.

Again, the diversity order of a code is defined as the 'length' of the shortest error event path expressed in terms of the number of trellis stages encountered, before remerging with the all-zero path [718] or, equivalently, defined as the minimum Hamming distance of the code [365] where the diversity order of TCM using a symbol-based interleaver is the minimum number of different symbols between the erroneous path and the correct path along the shortest error event path. Hence, in a TCM scenario having parallel transitions, as shown in Figure 24.5, the code's diversity order is one, since the shortest error event path consists of one branch. This implies that parallel transitions should be avoided in TCM codes if it was possible, and if there were no parallel branches, any increase in diversity would be obtained by increasing the constraint length of the code. Unfortunately no TCM codes exist where the parallel transitions associated with the unprotected bits are avoided. In order to circumvent this problem, Zehavi's idea [364] was to render the code's diversity equal to the smallest number of different bits, rather than to that of the different channel symbols, by employing bit-based interleaving, as will be highlighted below.

24.6.1 BICM Principle

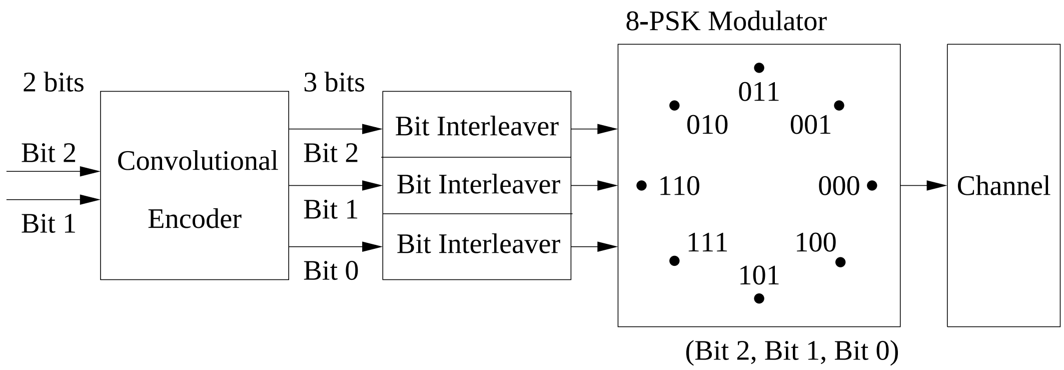

Figure 24.16: BICM encoder schematic employing independent bit interleavers and and protecting all transmitted bits. Instead of the SP-based labelling of TCM in Figure 24.2 here Gray labelling is employed [364] ©IEEE, 1992, Zehavi.

The BICM encoder is shown in Figure 24.16. In comparison to the TCM encoder of Figure 24.6, the differences are that BICM uses independent bit interleavers for all the bits of a symbol and non-systematic convolutional codes, rather than a single symbol-based interleaver and systematic RSC codes protecting some of the bits. The number of bit interleavers equals the number of bits assigned to the non-binary codeword. The purpose of bit interleaving is:

- to disperse the bursty errors induced by the correlated fading and to maximise the diversity order of the system;
- to render the bits associated with a given transmitted symbol uncorrelated or independent of each other.

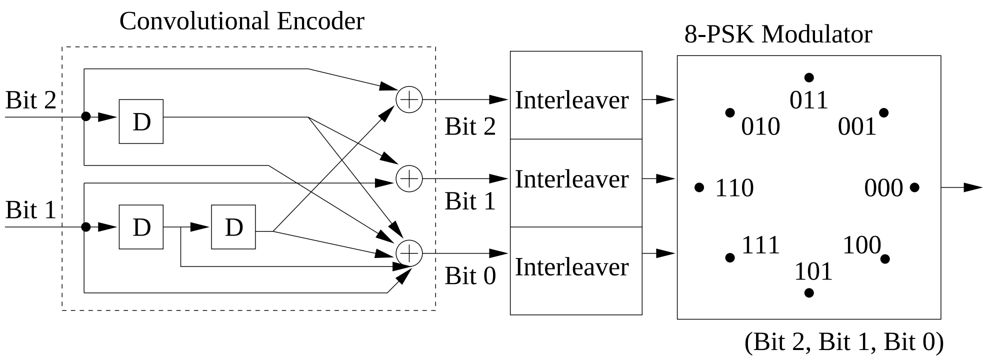

Figure 24.17: Paaske's non-systematic convolutional encoder, bit-based interleavers and modulator forming the BICM encoder [364,728], where none of the bits are unprotected and instead of the SP-based labelling as seen in Figure 24.2 here Gray labelling is employed.

The interleaved bits are then grouped into non-binary symbols, where Gray-coded labelling is used for the sake of optimising the performance of the BICM scheme. The BICM encoder uses 's non-systematic convolutional code proposed on page 331 of [728], which exhibits the highest possible free Hamming distance, hence attaining optimum performance over Rayleigh fading channels. Figure 24.17 shows Paaske's non-systematic eight-state code of rate-$2/3$, exhibiting a free bit-based Hamming distance of four. The BICM decoder im-

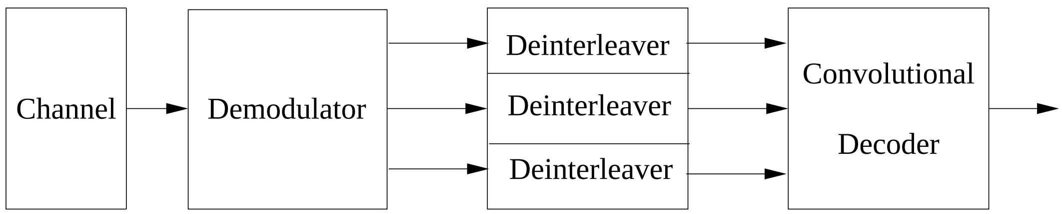

Figure 24.18: BICM decoder [364].

plements the inverse process, as shown in Figure 24.18. In the demodulator module six bit metrics associated with the three bit positions, each having binary values of 0 and 1, are generated from each channel symbol. These bit metrics are de-interleaved by three independent bit de-interleavers, in order to form the estimated codewords. Then the convolutional decoder of Figure 24.18 is invoked for decoding these codewords, generating the best possible estimate of the original information bit sequence.

From Equation 24.5 we know that the average bit error probability of a coded modulation scheme using MPSK over Rayleigh fading channels at high SNRs is inversely proportional to $(E_s/N_0)^{\mathsf{L}}$, where E_s/N_0 is the channel's symbol energy to noise spectral density ratio and L is the minimum Hamming distance or the code's diversity order. When bit-based interleavers are employed in BICM instead of the symbol-based interleaver employed in TCM, the minimum Hamming distance of BICM is quantified in terms of the number of different bits between the erroneous path in the shortest error event and the correct path. Since in BICM the bit-based minimum Hamming distance is maximised, BICM will give a lower bit error probability in Rayleigh fading channels than that of TCM that maximises the FED. Again, the design of BICM is aimed at providing maximum minimum Hamming distance, rather than providing maximum FED, as in TCM schemes. Moreover, we note that attaining a maximum FED is desired for transmission over Gaussian channels, as shown in Section 24.3.1. Hence, the performance of BICM is not as good as that of TCM in AWGN channels. The reduced FED of BICM is due to the 'random' modulation imposed by the 'random' bit interleavers [364], where the m-bit BICM symbol is randomised by the m number of bit interleavers. Again, $\bar{\mathsf{m}}$ denotes the number of information bits, while m denotes the total number of bits in a 2^{m}-ary modulated symbol.

Rate	State, ν	$g^{(1)}$	$g^{(2)}$	$g^{(3)}$	$g^{(4)}$	d_{free}
1/2 (4QAM)	8, 3	15	17	-	-	5
	16, 4	23	35	-	-	7
	64, 6	133	171	-	-	10
2/3 (8PSK)	8, 3	4	2	6	-	4
		1	4	7	-	
	16, 4	7	1	4	-	5
		2	5	7	-	
	64, 6	64	30	64	-	7
		30	64	74	-	
3/4 (16QAM)	8, 3	4	4	4	4	4
		0	6	2	4	
		0	2	5	5	
	32, 5	6	2	2	6	5
		1	6	0	7	
		0	2	5	5	
	64, 6	6	1	0	7	6
		3	4	1	6	
		2	3	7	4	

Table 24.3: Paaske's non-systematic convolutional codes, page 331 of [728], where ν denotes the code memory and d_{free} denotes the free Hamming distance. Octal format is used for representing the generator polynomial coefficients.

Rate	State, ν	$g^{(1)}$	$g^{(2)}$	puncturing matrix	d_{free}
5/6 (64QAM)	8, 3	15	17	1 0 0 1 0 0 1 1 1 1	3
	64, 6	133	171	1 1 1 1 1 1 0 0 0 0	3

Table 24.4: Rate-Compatible Punctured Convolutional (RCPC) codes [729, 730], where ν denotes the code memory and d_{free} denotes the free Hamming distance. Octal format is used for representing the generator polynomial coefficients.

Table 24.3 summarises the parameters of a range of Paaske's non-systematic codes utilised in BICM. For a rate-k/n code there are k generator polynomials, each having n

coefficients. For example, $\mathbf{g_i} = (g^0,\ g^1,\ \ldots,\ g^n),\ i \le k$, is the generator polynomial associated with the ith information bit. The generator matrix of the encoder seen in Figure 24.17 is:

$$\mathbf{G}(\mathbf{D}) = \begin{bmatrix} 1 & D & 1+D \\ D^2 & 1 & 1+D+D^2 \end{bmatrix}, \tag{24.56}$$

while the equivalent polynomial expressed in octal form is given by:

$$\mathbf{g_1} = \begin{bmatrix} 4 & 2 & 6 \end{bmatrix} \ \mathbf{g_2} = \begin{bmatrix} 1 & 4 & 7 \end{bmatrix}. \tag{24.57}$$

Observe in Table 24.3 that Paaske generated codes of rate-$1/2$, $2/3$ and $3/4$, but not $5/6$. In order to study rate-$5/6$ BICM/64QAM, we created the required punctured code from the rate-$1/2$ code of Table 24.3. Table 24.4 summarises the parameters of the Rate-Compatible Punctured Convolutional (RCPC) codes that can be used in rate=$5/6$ BICM/64QAM schemes. Specifically, rate-$1/2$ codes were punctured according to the puncturing matrix of Table 24.4 in order to obtain the rate-$5/6$ codes, following the approach of [729, 730]. Let us now consider the operation of BICM with the aid of an example.

24.6.2 BICM Coding Example

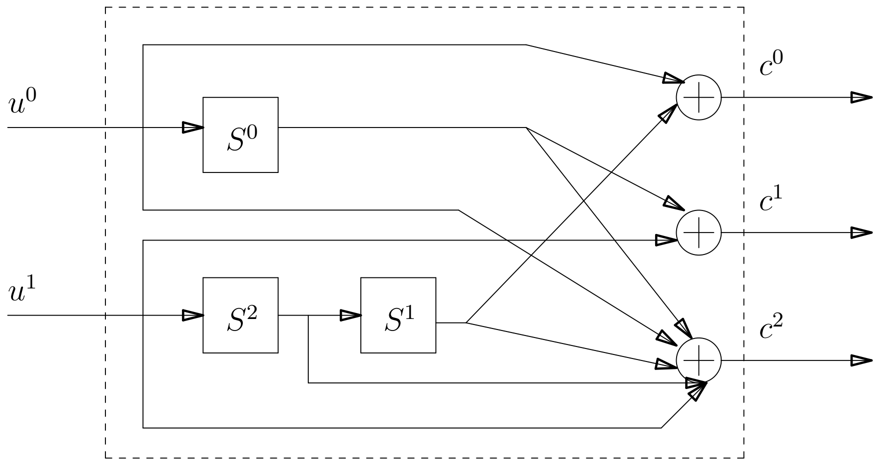

Figure 24.19: Paaske's non-systematic convolutional encoder [728].

Considering Paaske's eight-state convolutional code [728] in Figure 24.19 as an example, the BICM encoding process is illustrated here. The corresponding generator polynomial is shown in Equation 24.57. A two-bit information word, namely $u = (u^1,\ u^0)$, is encoded in each cycle in order to form a three-bit codeword, $c = (c^2,\ c^1,\ c^0)$. The encoder has three shift registers, namely S^0, S^1 and S^2, as shown in the figure. The three-bit binary contents of these registers represent eight states, as follows:

$$S = (S^2,\ S^1,\ S^0) \in \{000,\ 001,\ \ldots,\ 111\} = \{0,\ 1,\ \ldots,\ 7\}. \tag{24.58}$$

The input sequence, u, generates a new state S and a new codeword c at each encoding

State	Information Word $u = (u^1,\ u^0)$			
$S = (S^2, S^1, S^0)$	$00 = 0$	$01 = 1$	$10 = 2$	$11 = 3$
$000 = 0$	$000 = 0$	$101 = 5$	$110 = 6$	$011 = 3$
$001 = 1$	$110 = 6$	$011 = 3$	$000 = 0$	$101 = 5$
$010 = 2$	$101 = 5$	$000 = 0$	$011 = 3$	$110 = 6$
$011 = 3$	$011 = 3$	$110 = 6$	$101 = 5$	$000 = 0$
$100 = 4$	$100 = 4$	$001 = 1$	$010 = 2$	$111 = 7$
$101 = 5$	$010 = 2$	$111 = 7$	$100 = 4$	$001 = 1$
$110 = 6$	$001 = 1$	$100 = 4$	$111 = 7$	$010 = 2$
$111 = 7$	$111 = 7$	$010 = 2$	$001 = 1$	$100 = 4$
Codeword $c = (c^2,\ c^1, c^0)$				
$000 = 0$	$000 = 0$	$001 = 1$	$100 = 4$	$101 = 5$
$001 = 1$	$000 = 0$	$001 = 1$	$100 = 4$	$101 = 5$
$010 = 2$	$000 = 0$	$001 = 1$	$100 = 4$	$101 = 5$
$011 = 3$	$000 = 0$	$001 = 1$	$100 = 4$	$101 = 5$
$100 = 4$	$010 = 2$	$011 = 3$	$110 = 6$	$111 = 7$
$101 = 5$	$010 = 2$	$011 = 3$	$110 = 6$	$111 = 7$
$110 = 6$	$010 = 2$	$011 = 3$	$110 = 6$	$111 = 7$
$111 = 7$	$010 = 2$	$011 = 3$	$110 = 6$	$111 = 7$
Next State $S = (S^2,\ S^1,\ S^0)$				

Table 24.5: The codeword generation and state transition table of the non-systematic convolutional encoder of Figure 24.19. The state transition diagram is seen in Figure 24.20.

cycle. Table 24.5 illustrates the codewords generated and the associated state transitions. The encoding process can also be represented with the aid of the trellis diagram of Figure 24.20. Specifically, the top part of Table 24.20 contains the codewords $c = (c^2,\ c^1, c^0)$ as a function of the encoder state $S = (S^2, S^1, S^0)$ as well as that of the information word $u = (u^1,\ u^0)$, while the bottom section contains the next states, again as a function of S and u. For example, if the input is $u = (u^1,\ u^0) = (1, 1) = 3$ when the shift register is in state $S = (S^2, S^1, S^0) = (1, 1, 0) = 6$, the shift register will change its state to state $S = (S^2, S^1, S^0) = (1, 1, 1) = 7$ and $c = (c^2,\ c^1, c^0) = (0, 1, 0) = 2$ will be the generated codeword. Hence, if the input binary sequence is $\{01\ 10\ 01\ 00\ 10\ 10 \rightarrow\}$ with the rightmost being the first input bit, the corresponding information words are $\{1\ 2\ 1\ 0\ 2\ 2 \rightarrow\}$. Before any decoding takes place, the shift register is initialised to zero. Therefore, as seen at the right of Figure 24.20, when the first information word of $u_1 = 2$ arrives, the state changes from $S^{-1} = 0$ to $S = 4$, generating the first codeword $c_1 = 6$ as seen in the bottom and top sections of Table 24.5, respectively. Then the second information word of $u_2 = 2$ changes the state from $S^{-1} = 4$ to $S = 6$, generating the second codeword of $c_2 = 2$. The process continues in a similiar manner according to the transition table, namely Table 24.5. The codewords generated as seen at the right of Figure 24.20 are $\{4\ 0\ 0\ 1\ 2\ 6 \rightarrow\}$, and the state transitions are $\{2 \leftarrow 4 \leftarrow 1 \leftarrow 2 \leftarrow 6 \leftarrow 4 \leftarrow 0\}$. Then the bits constituting the codeword sequence are interleaved by the three bit interleavers of Figure 24.17, before they are assigned to the corresponding 8PSK constellation points.

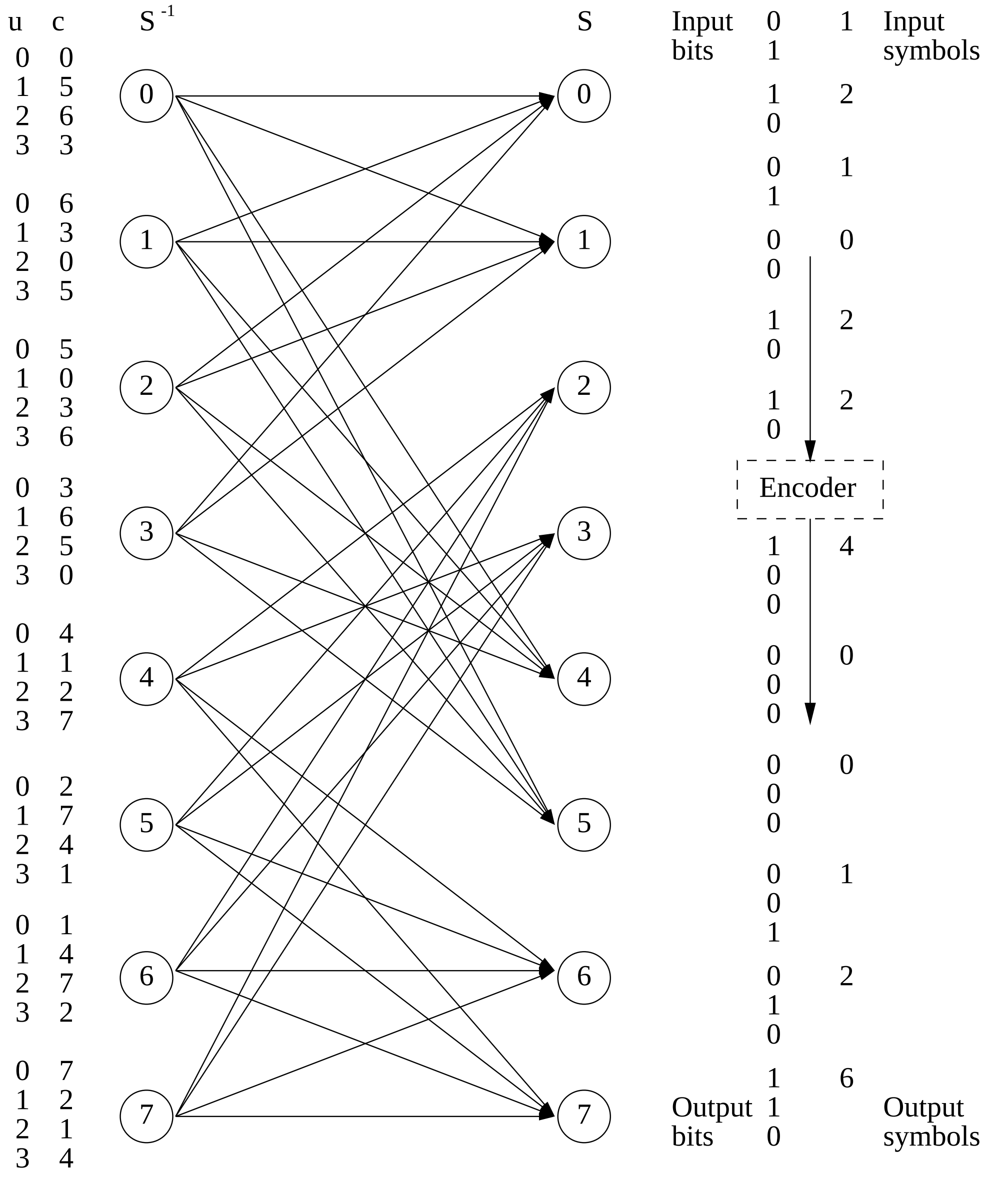

Figure 24.20: Trellis diagram for Paaske's eight-state convolutional code, where u indicates the information word, c indicates the codeword, S^{-1} indicates the previous state and S indicates the current state. As an example, the encoding of the input bit sequence of $\{011001001010 \rightarrow\}$ is shown at the right. The encoder schematic is portrayed in Figure 24.19, while the state transitions are summarised in Table 24.5.

24.7 Bit-Interleaved Coded Modulation with Iterative Decoding

BICM using Iterative Decoding (BICM-ID) was proposed by [373, 710] for further improving the FED of Zehavi's BICM scheme, although BICM already improved the diversity order of Ungerböck's TCM scheme. This FED improvement can be achieved with the aid of combining SP-based constellation labelling, as in TCM, and by invoking soft-decision feedback from the decoder's output to the demodulator's input, in order to exchange soft-decision-based information between them. As we will see below, this is advantageous, since upon each iteration the channel decoder improves the reliability of the soft information passed to the demodulator.

24.7.1 Labelling Method

Let us now consider the mapping of the interleaved bits to the phasor constellation in this section. Figure 24.21 shows the process of subset partitioning for each of the three bit positions for both Gray labelling and in the context of SP labelling. The shaded regions shown inside the circle correspond to the subset $\chi(i,1)$ defined in Equation 24.64, and the unshaded regions to $\chi(i,0)$, $i = 0,1,2$, where i indicates the bit position in the three-bit BICM/8PSK symbol. These are also the decision regions for each bit, if hard-decision-based BICM demodulation is used for detecting each bit individually. The two labelling methods seen in Figure 24.21 have the same intersubset distances, although a different number of nearest neighbours. For example, $\chi(0,1)$, which denotes the region where bit 0 equals to 1, is divided into two regions in the context of Gray labelling, as can be seen in Figure 24.21(a). By contrast, in the context of SP labelling seen in Figure 24.21(b), $\chi(0,1)$ is divided into four regions. Clearly, Gray labelling has a lower number of nearest neighbours compared to SP-based labelling. The higher the number of nearest neighbours, the higher the chances for a bit to be decoded into the wrong region. Hence, Gray labelling is a more appropriate mapping during the first decoding iteration, and hence it was adopted by the non-iterative BICM scheme of Figure 24.18.

During the second decoding iteration in BICM-ID, given the feedback information representing Bit 1 and Bit 2 of the coded symbol, the constellation associated with Bit 0 is confined to a pair of constellation points, as shown at the right of Figure 24.22. Therefore, as far as Bit 0 is concerned, the 8PSK phasor constellation is translated into four binary constellations, where one of the four possible specific BPSK constellations is selected by the feedback Bit 1 and Bit 2. The same is true for the constellations associated with both Bit 1 and Bit 2, given the feedback information of the corresponding other two bits.

In order to optimise the second-pass decoding performance of BICM-ID, one must maximise the minimum Euclidean distance between any two points of all the $2^{\mathsf{m}-1} = 4$ possible phasor pairs at the left (Bit 2), centre (Bit 1) and the right (Bit 0) of Figure 24.22. Clearly, SP-based labelling serves this aim better, when compared to Gray labelling, since the corresponding minimum Euclidean distance of SP-based labelling is higher than that of Gray labelling for both Bit 1 and Bit 2, as illustrated at the left and the centre of Figure 24.22. Although the first-pass performance is important, in order to prevent error precipitation due to erroneous feedback bits, the error propagation is effectively controlled by the soft feedback of the decoder. Therefore, BICM-ID assisted by soft decision feedback uses SP labelling.

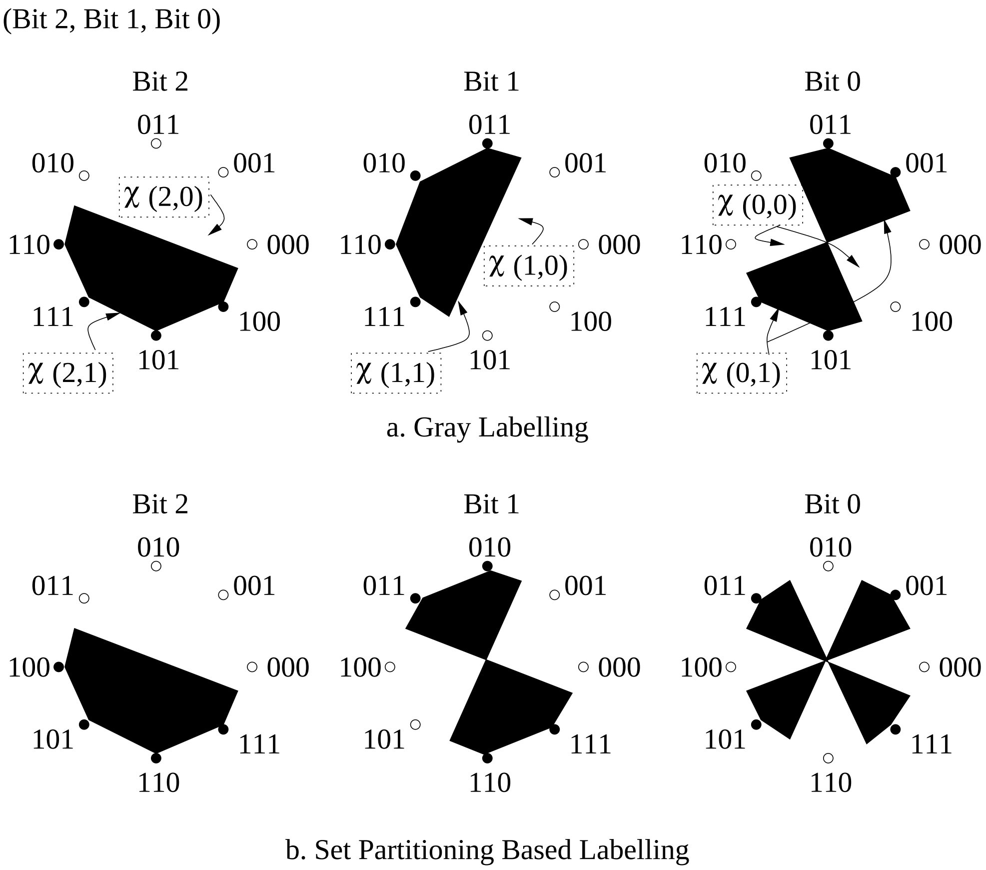

Figure 24.21: SP and Gray labelling methods for 8PSK and the corresponding subset partitioning for each bit, where $\chi(i, b)$ defined in Equation 24.64 refers to the subset of the modulation constellation for Bit i where Bit $i = b \in \{0, 1\}$ [373] ©IEEE, 1999, Li and Ritcey.

Specifically, the desired high Euclidean distance for Bit 2 in Figure 24.22(b) is only attainable when Bit 1 and Bit 0 are correctly decoded and fed back to the SP-based demodulator. If the values to be fed back are not correctly decoded, the desired high Euclidean distance will not be achieved and error propagation will occur. On the other hand, an optimum convolutional code having a high binary Hamming distance is capable of providing a high reliability for the decoded bits. Therefore, an optimum convolutional code using appropriate signal labelling is capable of 'indirectly' translating the high binary Hamming distance between coded bits into a high Euclidean distance between the phasor pairs portrayed in Figure 24.22. In short, BICM-ID converts a 2^{m}-ary signalling scheme to m independent parallel binary schemes by the employment of m number of independent bit interleavers and involves an iterative decoding method. This simultaneously facilitates attaining a high diversity order with the advent of the bit interleavers, as well as achieving a high FED with the aid of the iterative decoding and SP-based labelling. Hence, BICM-ID effectively combines powerful binary codes with bandwidth-efficient modulation.

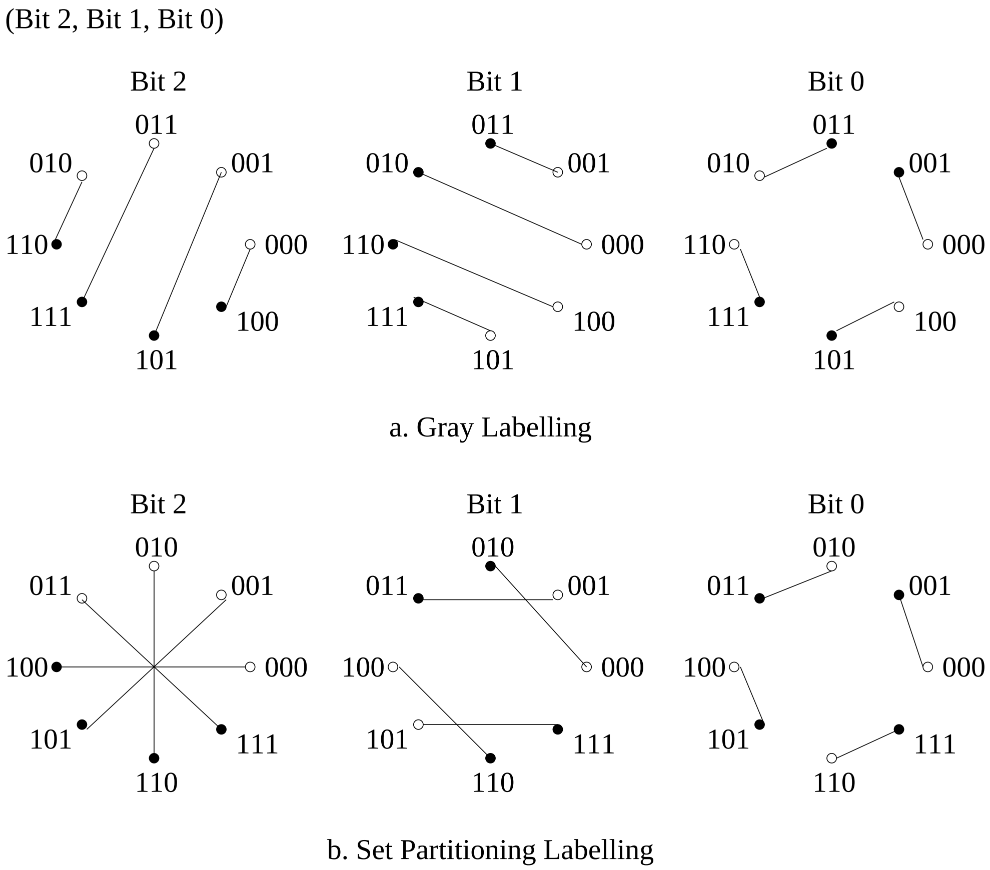

Figure 24.22: Iterative decoding translates the 8PSK scheme into three parallel binary sub-channels, each associated with a BPSK constellation selected from the four possible signal sets [373] ©IEEE, 1999, Li and Ritcey.

24.7.2 Interleaver Design

The interleaver design is important as regards the performance of BICM-ID. In [711], Li introduced certain constraints on the design of the interleaver, in order to maximise the minimum Euclidean distance between the two points in the 2^{m-1} possible specific BPSK constellations. However, we advocate a more simple approach, where the m number of interleavers used for the 2^m-ary modulation scheme are generated randomly and separately, without any interactions between them. The resultant minimum Euclidean distance is less than that of the scheme proposed in [711], but the error bursts inflicted by correlated fading are expected to be randomised effectively by the independent bit interleavers. This was expected to give a better performance over fading channels at the cost of a slight performance degradation over AWGN channels, when compared to Li's scheme [711]. However, as we will demonstrate in the context of our simulation results in Section 25.2.2, our independent random interleaver design and Li's design perform similarly.

Having described the labelling method and the interleaver design in the context of BICM-ID, let us now consider the operation of BICM-ID with the aid of an example.

24.7.3 BICM-ID Coding Example

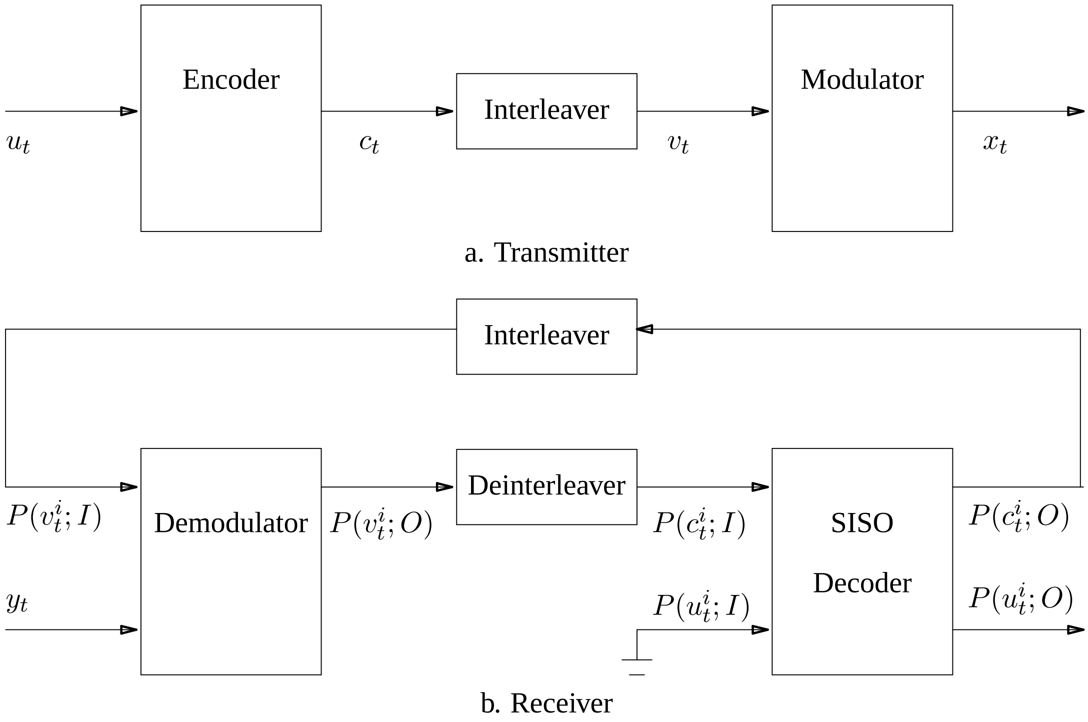

Figure 24.23: The transmitter and receiver modules of the BICM-ID scheme using soft-decision feedback [710] ©IEEE, 1998, Li.

The BICM-ID scheme using soft-decision feedback is shown in Figure 24.23. The interleavers used are all bit-based, as in the BICM scheme of Figure 24.17, although for the sake of simplicity here only one interleaver is shown. A Soft-Input Soft-Output (SISO) [731] decoder is used in the receiver module and the decoder's output is fed back to the input of the demodulator. The SISO decoder of the BICM-ID scheme is actually a MAP decoder that computes the $a\ posteriori$ probabilities for the non-systematically channel-coded bits and the original information bits.

For an $(n,\ k)$ binary convolutional code the encoder's input symbol at time t is denoted by $u_t = [u_t^0,\ u_t^1,\ \ldots,\ u_t^{k-1}]$ and the coded output symbol by $c_t = [c_t^0,\ c_t^1,\ \ldots,\ c_t^{n-1}]$, where u_t^i or c_t^i is the ith bit in a symbol as defined in the context of Table 24.5 and Figure 24.20. The coded bits are interleaved by m independent bit interleavers, then m interleaved bits are grouped together in order to form a channel symbol $v_t = [v_t^0,\ v_t^1,\ \ldots,\ v^{\mathsf{m}-1}]$ as seen in Figure 24.23(a), for transmission using 2^{m}-ary modulation. Let us consider 8PSK modulation, i.e. $\mathsf{m} = 3$ as an example.

A signal labelling method μ maps the symbol v_t to a complex phasor according to $x_t = \mu(v_t)$, $x_t \in \chi$, where the 8PSK signal set is defined as $\chi = \{\sqrt{E_s}\, e^{j2n\pi/8},\ n = 0, \ldots, 7\}$ and E_s is the energy per transmitted symbol. In conjunction with a rate-$2/3$ code, the energy per information bit is $E_b = E_s/2$. For transmission over Rayleigh fading channels using coherent detection, the received discrete time signal is:

$$y_t = \rho_t x_t + n_t, \tag{24.59}$$

where ρ_t is the Rayleigh-distributed fading amplitude [370] having an expectation value of $\mathrm{E}[\rho_t^2] = 1$, while n_t is the complex AWGN exhibiting a variance of $\sigma^2 = N_0/2$ where N_0 is the noise's PSD. For AWGN channels we have $\rho_t = 1$ and the Probability Density Function (PDF) of the non-faded but noise-contaminated received signal is expressed as [722]:

$$P(y_t|x_t, \rho_t) = \frac{1}{2\pi\sigma^2}\, e^{-\frac{1}{2}\left(\frac{n_t}{\sigma}\right)^2}, \tag{24.60}$$

where $\sigma^2 = N_0/2$ and the constant multiplicative factor of $\frac{1}{2\pi\sigma^2}$ does not influence the shape of the distribution and hence can be ignored when calculating the branch transition metric η, as described in Section 24.4.5. For AWGN channels, the conditional PDF of the received signal can be written as:

$$P(y_t|x_t) = e^{-\frac{|y_t\ -\ x_t|^2}{2\sigma^2}}. \tag{24.61}$$

Considering AWGN channels, the demodulator of Figure 24.23(b) takes y_t as its input for computing the confidence metrics of the bits using the maximum APP criterion [374]:

$$P(v_t^i = b|y_t) \quad = \sum_{x_t \in \chi(i,b)} P(x_t|y_t), \tag{24.62}$$

where $i \in \{0, 1, 2\}$, $b \in \{0, 1\}$ and $x_t = \mu(v_t)$. Furthermore, the signal after the demodulator of Figure 24.23 is described by the demapping of the bits $[\nabla^0(x_t), \nabla^1(x_t), \nabla^2(x_t)]$ where $\nabla^i(x_t) \in \{0, 1\}$ is the value of the ith bit of the three-bit label assigned to x_t. With the aid of Bayes' rule in Equations 24.15 to 24.17 we obtain:

$$P(v_t^i = b|y_t) \quad = \sum_{x_t \in \chi(i,b)} P(y_t|x_t)P(x_t), \tag{24.63}$$

where the subset $\chi(i, b)$ is described as:

$$\chi(i, b) = \{\mu([\nabla^0(x_t), \nabla^1(x_t), \nabla^2(x_t)])\ \mid\ \nabla^j(x_t) \in \{0, 1\}, j \neq i\}, \tag{24.64}$$

which contains all the phasors for which $\nabla^i(x_t) = b$ holds. For 8PSK, where $\mathsf{m} = 3$, the size of each such subset is $2^{\mathsf{m}-1} = 4$ as portrayed in Figure 24.21. This implies that only the $a\ priori$ probabilities of $\mathsf{m} - 1 = 2$ bits out of the total of $\mathsf{m} = 3$ bits per channel symbol have to be considered, in order to compute the bit metric of a particular bit.

Now using the notation of *et al.* [731], the $a\ priori$ probabilities of an original uncoded information bit at time index t and bit index i, namely u_t^i being 0 and 1, are denoted by $P(u_t^i = 0; I)$ and $P(u_t^i = 1; I)$ respectively, while I refers to the $a\ prIori$ probabilities of the bit. This notation is simplified to $P(u_t^i; I)$, when no confusion arises, as shown in Figure 24.23. Similarly, $P(c_t^i; I)$ denotes the $a\ priori$ probabilities of a legitimate coded bit at time index t and position index i. Finally, $P(u_t^i; O)$ and $P(c_t^i; O)$ denote the $extrinsic$ $a\ pOsteriori$ information of the original information bits and coded bits, respectively.

The $a\ priori$ probability $P(x_t)$ in Equation 24.63 is unavailable during the first-pass decoding, hence an equal likelihood is assumed for all the 2^{m} legitimate symbols. This renders the $extrinsic\ a\ posteriori$ bit probabilities, $P(v_t^i = b; O)$, equal to $P(v_t^i = b|y_t)$, when ignoring the common constant factors. Then, the SISO decoder of Figure 24.23(b) is used for generating the $extrinsic\ a\ posteriori$ bit probabilities $P(u_t^i; O)$ of the information bits, as well as the $extrinsic\ a\ posteriori$ bit probabilities $P(c_t^i; O)$ of the coded bits, from the de-interleaved probabilities $P(v_t^i = b; O)$, as seen in Figure 24.23(b). Since $P(u_t^i; I)$ is unavailable, it is not used in the entire decoding process.

During the second iteration $P(c_t^i; O)$ is interleaved and fed back to the input of the demodulator in the correct order in the form of $P(v_t^i; I)$, as seen in Figure 24.23(b). Assuming that the probabilities $P(v_t^0; I)$, $P(v_t^1; I)$ and $P(v_t^2; I)$ are independent by the employment of three independent bit interleavers, we have for each $x_t \in \chi$:

$$\begin{aligned} P(x_t) &= P(\mu([\nabla^0(x_t), \nabla^1(x_t), \nabla^2(x_t)])) \\ &= \prod_{j=0}^{2} P(v_t^j = \nabla^j(x_t); I), \end{aligned} \tag{24.65}$$

where $\nabla^j(x_t) \in \{0, 1\}$ is the value of the jth bit of the three-bit label for x_t. Now that we have the $a\ priori$ probability $P(x_t)$ of the transmitted symbol x_t, the $extrinsic\ a\ posteriori$ bit probabilities for the second decoding iteration can be computed using Equations 24.63 and 24.65, yielding:

$$\begin{aligned} P(v_t^i = b; O) &= \frac{P(v_t^i = b|y_t)}{P(v_t^i = b; I)} \\ &= \sum_{x_t \in \chi(i,b)} \left(P(y_t|x_t) \prod_{j \neq i} P(v_t^j = \nabla^j(x_t); I) \right) \\ & \quad i \in \{0, 1, 2\}, \quad b \in \{0, 1\}. \end{aligned} \tag{24.66}$$

As seen from Equation 24.66, in order to recalculate the metric for a bit we only need the $a\ priori$ probabilities of the other two bits in the same channel symbol. After interleaving in the feedback loop of Figure 24.23, the regenerated bit metrics are tentatively soft demodulated again and the process of passing information between the demodulator and decoder is continued. The final decoded output is the hard-decision-based $extrinsic$ bit probability $P(u_t^i; O)$.

24.8 Summary

In this chapter we have studied the conceptual differences between four coded modulation schemes in terms of coding structure, signal labelling philosophy, interleaver type and decoding philosophy. The symbol-based non-binary MAP algorithm was also highlighted, when operating in the log-domain.

In the next chapter, we will proceed to study the performance of TCM, BICM, TTCM and BICM-ID over non-dispersive propagation environments.

Glossary

16QAM	16-level Quadrature Amplitude Modulation
3G	Third generation
4PSK	4-level Phase Shift Keying
4QAM	4-level Quadrature Amplitude Modulation
64QAM	64-level Quadrature Amplitude Modulation
8-DPSK	8-Phase Differential Phase Shift Keying
8PSK	8-level Phase Shift Keying
ACF	autocorrelation function
ADC	Analog–to–Digital Converter
ADM	adaptive delta modulation
ADPCM	Adaptive Differential Pulse Coded Modulation.
AGC	Automatic Gain Control
AM-PM	amplitude modulation and phase modulation
AOFDM	Adaptive Orthogonal Frequency Division Multiplexing
APP	A Posteriori Probability
ARQ	Automatic Repeat Request, Automatic request for retransmission of corrupted data
ATM	Asynchronous Transfer Mode
AWGN	Additive White Gaussian Noise

BbB	Burst-by-Burst
BCH	Bose-Chaudhuri-Hocquenghem, A class of forward error correcting codes (FEC)
BCM	block code modulation
BER	Bit error rate, the fraction of the bits received incorrectly
BICM	Bit Interleaved Coded Modulation
BICM-ID	Bit-Interleaved Coded Modulation with Iterative decoding
BPF	Bandpass Filter
BPS	Bits Per Symbol
BPSK	Binary Phase Shift Keying
BS	A common abbreviation for Base Station
CCI	Co-Channel Interference
CCITT	Now ITU, standardisation group
CD	Code Division, a multiplexing technique where signals are coded and then combined, in such a way that they can be separated using the assigned user signature codes at a later stage.
CDMA	Code Division Multiple Access
CIR	Carrier to Interference Ratio, same as SIR.
CISI	controlled inter-symbol interference
CM	Coded Modulation
CM-GA-MUD	Coded Modulation assisted Genetic Algorithm based Multiuser Detection
CM-JD-CDMA	Coded Modulation-assisted Joint Detection-based CDMA
CRC	Cyclic Redundancy Checksum
CT-TEQ	Conventional Trellis-based Turbo Equalisation
D/A	Digital to Analogue
DAB	Digital Audio Broadcasting

DC	Direct Current, normally used in electronic circuits to describe a power source that has a constant voltage, as opposed to AC power in which the voltage is a sine-wave. It is also used to describe things which are constant, and hence have no frequency component.
DECT	A Pan-European digital cordless telephone standard.
DFE	Decision Feedback Equalizer
DFT	Discrete Fourier Transform
DoS-RR	Double-Spreading aided Rake Receiver
DS	Direct Sequence
DTTB	Digital Terrestrial Television Broadcast
DTX	discontinuous transmission
DVB	Digital Video Broadcasting
ECL	The Effective Code Length or the "length" of the shortest error event path.
EFF	Error Free Feedback
EQ	Equaliser
E_b/N_0	Ratio of bit energy to noise power spectral density.
FD	Frequency Division, a multiplexing technique, where different frequencies are used for each communications link.
FDM	Frequency Division Multiplexing
FEC	Forward Error Correction
FED	Free Euclidean distance
FER	Frame error rate
FFT	Fast Fourier Transform
FSK	Frequency Shift Keying
G	Coding Gain
GA	Genetic Algorithm
GF	Galois field

GMSK	Gaussian Mean Shift Keying, a modulation scheme used by the Pan-European GSM standard by virtue of its spectral compactness.
GSM	A Pan-European digital mobile radio standard, operating at 900MHz.
HT	Hilly Terrain, channel impulse response of a hilly terrain environment.
I	The In-phase component of a complex quantity.
I/Q-TEQ	In-phase/Quadrature-phase Turbo Equalisation
IC	Interference Cancellation
ICI	Inter–Channel Interference
IF	Intermediate Frequency
IFFT	Inverse Fast Fourier Transform
IL	interleaver block length
IMD	Intermodulation Distortion
IQ-CM	IQ-interleaved Coded Modulation
ISI	Inter Symbol Interference, Inter Subcarrier Interference
JD	Joint Detection
JD-MMSE-DFE	Joint Detection scheme employing MMSE-DFE
LAR	Logarithmic area ratio
LMS	Least Mean Square, a stochastic gradient algorithm used in adapting the equalizer's coefficients in a non-stationary environment
log-domain	logarithmic-domain
LOS	Line–Of–Sight
LP	Logarithmic-domain Probability
LPF	low pass filter
LS	Least Square, a category of adaptive algorithms which uses recursive least squres methods in adapting the equalizer or channel estimators in a non-stationary environment
LSB	least significant bit

LSF	Least Squares Fitting
LTP	long term predictor
MAI	Multiple Access Interference
MAP	Maximum–A–Posteriori
MC-CDMA	Multi-Carrier Code Division Multiple Access
MDI	multi-dimensional interference
MIMO	Multi-Input Multi-Output
ML	Maximum Likelihood
MMSE	Minimum Mean Square Error
MMSE-BLE	Minimum Mean Square Error based Block Linear Equaliser
MMSE-DFE	Minimum Mean Square Error based Decision Feedback Equaliser
MPSK	M-ary Phase Shift Keying
MRC	Mixed Radix Conversion
MS	A common abbreviation for Mobile Station
MSE	Mean Square Error, a criterion used to optimised the coefficients of the equalizer such that the ISI and the noise contained in the received signal is jointly minimised.
MUD	Multi-User Detection
NLA	non-linear amplification
NLF	non-linear filtering
OFDM	Orthogonal Frequency Division Multiplexing
OMPX	Orthogonal Multiplexing
OOB	out of band
OQAM	offset quadrature amplitude modulation
OQPSK	offset quadrature phase shift keying
OSWE	one-symbol window equaliser
PAM	pulse amplitude modulation
PCM	pulse code modulation

PCN	Personal Communications Network
PD	phase detector
PDF	Probability Density Function
PLL	phase locked loop
PLMR	Public Land Mobile Radio
PN	Pseudo-Noise
PR	PseudoRandom
PSAM	Pilot symbol assisted modulation, a technique where known symbols (pilots) are transmitted regularly. The effect of channel fading on all symbols can then be estimated by interpolating between the pilots
PSD	Power Spectral Density
PSK	Phase Shift Keying
PSTN	Public switched telephone network
Q	The Quadrature-phase component of a complex quantity.
QAM	Quadrature Amplitude Modulation
QMF	Quadrature Mirror Filtering
QOS	Quality of Service
QPSK	Quaternary Phase Shift Keying
RBF	Radial Basis Function
RBF-DFE	RBF assisted Decision Feedback Equaliser
RBF-TEQ	Radial Basis Function based Turbo Equalisation
RCPC	Rate-Compatible Puncture Convolutional
RF	radio frequency
RLS	Recursive Least Squares, an adaptive filtering technique where a recursive method is used to adapt the filter tap weights such that the square of the error between the filter output and the desired response is minimized
RPE	regular pulse excited

RPE-LTP Regular pulse excited codec with long term predictor

RRNS Redundant Residual Number System

RS Reed Solomon Codes

RSC Recursive Systematic Convolutional

RSSI Received Signal Strength Indicator, commonly used as an indicator of channel quality in a mobile radio network.

SbS Symbol-by-Symbol

SER Symbol Error Ratio

SINR Signal to Interference plus Noise ratio, same as signal to noise ratio (SNR), when there is no interference.

SIR Signal to Interference ratio

SISO Soft-Input-Soft-Output

SNR Signal to Noise Ratio, noise energy compared to the signal energy

SOVA Soft-Output Viterbi Algorithm

SP Set Partitioning

STB Space-Time Block

STBC Space-Time Block Coding

STBC-DoS-RR Space-Time Block Coding-assisted Double-Spread Rake Receiver

STBC-IQ Space-Time Block Coding based IQ-interleaved

STC Space-Time Coding

STP Short term predictor

STS Space-Time Spreading

STT Space-Time Trellis

STTC Space-Time Trellis Coding

TC Trellis Coded

TCM trellis code modulation

TDD	Time-Division Duplex, a technique where the forward and reverse links are multiplexed in time.
TDMA	Time Division Multiple Access
TEQ	Turbo Equalisation
TTCM	Turbo Trellis Coded Modulation
TTIB	transparent tone in band
TU	Typical Urban, channel impulse response of an urban environment.
TuCM	Turbo Coded Modulation
TWT	travelling wave tube
UHF	ultra high frequency
UMTS	Universal Mobile Telecommunications System, a future Pan-European third generation mobile radio standard.
UTRA	UMTS Terrestrial Radio Access
VA	Viterbi Algorithm
VCO	voltage controlled oscillator
VE	Viterbi equalizer
WATM	Wireless Asynchronous Transfer Mode (ATM)
WMF	Whitening Matched Filter
WN	white noise
ZF	Zero Forcing, a criterion used to optimised the coefficients of the equalizer such that the ISI contained in the received signal is totally eliminated.
ZFE	Zero Forcing Equalizer.

Bibliography

[1] C. Cahn, "Performance of digital phase modulation communication systems," *IRE Transactions on Communications*, vol. CS-7, pp. 3–6, May 1959.

[2] C. Cahn, "Combined digital phase and amplitude modulation communication system," *IRE Transactions on Communications*, vol. CS-8, pp. 150–155, September 1960.

[3] J. Hancock and R. Lucky, "Performance of combined amplitude and phase modulated communications system," *IRE Transactions on Communicationss*, vol. CS-8, pp. 232–237, December 1960.

[4] C. Campopiano and B. Glazer, "A coherent digital amplitude and phase modulation scheme," *IRE Transactions on Communications Systems*, vol. CS-10, pp. 90–95, 1962.

[5] R. Lucky and J. Hancock, "On the optimum performance of m-ary systems having two degrees of freedom," *IRE Transactions on Communications*, vol. CS-10, pp. 185–192, June 1962.

[6] R. Lucky, J. Salz, and E. Weldon, *Principles of Data Communication*. New York, USA: McGraw-Hill, 1968.

[7] J. Salz, J. Sheenhan, and D. Paris, "Data transmission by combined AM and PM," *Bell Systems Technical Journal*, vol. 50, pp. 2399–2419, September 1971.

[8] E. Ho and Y. Yeh, "Error probability of a multilevel digital system with intersymbol interference and gaussian noise," *Bell Systems Technical Journal*, vol. 50, pp. 1017–1023, March 1971.

[9] G. Foschini, R. Gitlin, and S. Weinstein, "Optimization of two-dimensional signal constellations in the presence of gaussian noise," *IEEE Transactions on Communications*, vol. COM-22, pp. 28–38, January 1974.

[10] C. Thomas, M. Weidner, and S. Durrani, "Digital amplitude-phase keying with m-ary alphabets," *IEEE Transactions on Communications*, vol. COM-22, pp. 168–180, February 1974.

[11] M. Simon and J. Smith, "Carrier synchronization and detection of QASK signal sets," *IEEE Transactions on Communications*, vol. COM-22, pp. 98–106, February 1974.

[12] M. Simon and J. Smith, "Offset quadrature communications with decision feedback carrier synchronization," *IEEE Transactions on Communications*, vol. COM-22, pp. 1576–1584, October 1974.

[13] J. Smith, "Odd-bit quadrature amplitude-shift keying," *IEEE Transactions on Communications*, vol. COM-23, pp. 385–389, March 1975.

[14] K. Miyauchi, S. Seki, and H. Ishio, "New techniques for generating and detecting multilevel signal formats," *IEEE Transactions on Communications*, vol. COM-24, pp. 263–267, February 1976.

[15] W. Weber, "Differential encoding for multiple amplitude and phase shift keying systems," *IEEE Transactions on Communications*, vol. COM-26, pp. 385–391, March 1978.

[16] P. Dupuis, M. Joindot, A. Leclert, and D. Soufflet, "16 QAM modulation for high capacity digital radio system," *IEEE Transactions on Communications*, vol. COM-27, pp. 1771–1781, December 1979.

[17] I. Horikawa, T. Murase, and Y. Saito, "Design and performance of a 200mbit/s 16 QAM digital radio system," *IEEE Transactions on Communications*, vol. COM-27, pp. 1953–1958, December 1979.

[18] V. Prabhu, “The detection efficiency of 16-ary QAM,” *Bell Systems Technical Journal*, vol. 59, pp. 639–656, April 1980.

[19] D. Morais and K. Feher, “NLA-QAM: A method for generating high power QAM signals through non-linear amplification,” *IEEE Transactions on Communications*, vol. COM-30, pp. 517–522, March 1982.

[20] T. Hill and K. Feher, “A performance study of NLA 64-state QAM,” *IEEE Transactions on Communications*, vol. COM-31, pp. 821–826, June 1983.

[21] D. Tufts, “Nyquist’s problem - the joint optimisation of the transmitter and receiver in pulse amplitude modulation,” *Proceedings of the IEEE*, vol. 53, pp. 248–260, March 1965.

[22] J. Smith, “The joint optimization of transmitted signal and receiving filter for data transmission filters,” *Bell Systems Technical Journal*, vol. 44, pp. 2363–2392, December 1965.

[23] E. Hänsler, “Some properties of transmission systems with minimum mean square error,” *IEEE Transactions on Communications Technology (Corresp)*, vol. COM-19, pp. 576–579, August 1971.

[24] T. Ericson, “Structure of optimum receiving filters in data transmission systems,” *IEEE Transactions on Information Theory (Corresp)*, vol. IT-17, pp. 352–353, May 1971.

[25] G. Forney Jr, “Maximum likelihood sequence estimation of digital sequences in the presence of intersymbol interference,” *IEEE Transactions on Information Theory*, vol. IT-18, pp. 363–378, May 1972.

[26] M. Austin, “Decision feedback equalization for fading dispersive channels,” Tech. Rep. 461, M.I.T Research Lab. Electron, August 1971.

[27] P. Monsen, “Feedback equalization for fading dispersive channels,” *IEEE Transactions on Information Theory*, vol. IT-17, pp. 1144–1153, January 1971.

[28] J. Salz, “Optimum mean square decision feedback equalization,” *Bell Systems Techncial Journal*, vol. 52, pp. 1341–1373, October 1973.

[29] D. Falconer and G. Foschini, “Theory of mmse qam system employing decision feedback equalization,” *Bell Systems Technical Journal*, vol. 52, pp. 1821–1849, November 1973.

[30] R. Price, “Non-linearly feedback equalized pam versus capacity for noisy filter channels,” in *Rec. Int. Conf. Communication*, pp. 12–17, 1972.

[31] R. Lucky, “A survey of the communication theory literature : 1968–1973,” *IEEE Transactions on Information Theory*, vol. IT-19, pp. 725–739, July 1973.

[32] C. Belfiore and J. Park Jr, “Decision feedback equalization,” *Proceedings of the IEEE*, vol. 67, pp. 1143–1156, August 1979.

[33] S. Qureshi, “Adaptive equalization,” in *Advanced Digital Communications Systems and Signal Processing Techniques* (K.Feher, ed.), pp. 640–713, Englewood Cliffs NJ, USA: Prentice-Hall, 1987.

[34] J.C. Cheung, *Adaptive Equalisers for Wideband TDMA Mobile Radio*. PhD thesis, Department of Electronics and Computer Science, University of Southampton, UK, 1991.

[35] J. Cheung and R. Steele, “Soft-decision feedback equalizer for continuous-phase modulated signals in wide-band mobile radio channels,” *IEEE Transactions on Communications*, vol. 42, pp. 1628–1638, February/March/April 1994.

[36] J. Wu, A. Aghvami, and J. Pearson, “A reduced state soft decision feedback viterbi equaliser for mobile radio communications,” in *Proceedings of IEEE International Symposium on Personal, Indoor and Mobile Radio Communications*, (Stockholm, Sweden), pp. 234–242, June 1994.

[37] J. Wu and A. Aghvami, “A new adaptive equalizer with channel estimator for mobile radio communications,” *IEEE Transactions on Vehicular Technology*, vol. 45, pp. 467–474, August 1996.

[38] Y. Gu and T. Le-Ngoc, “Adaptive combined DFE/MLSE techniques for ISI channels,” *IEEE Transactions on Communications*, vol. 44, pp. 847–857, July 1996.

[39] D. Duttweiler, J. Mazo, and D. Messerschmitt, “An upper bound on the error probability on decision feedback equalization,” *IEEE Transactions on Information Theory*, vol. IT-20, pp. 490–497, July 1974.

[40] J. Smee and N. Beaulieu, “Error-rate evaluating of linear equalization and decision feedback equalization with error rate performance,” *IEEE Transactions On Communications*, vol. 46, pp. 656–665, May 1998.

[41] S. Altekar and N. Beaulieu, "Upper bounds to the error probability of decision feedback equalization," *IEEE Transactions on Communications*, vol. 39, pp. 145–157, January 1993.

[42] M. Tomlinson, "New automatic equalizer employing modulo arithmetic," *IEE Electronics Letters*, vol. 7, pp. 138–139, March 1971.

[43] H. Harashima and H. Miyakawa, "Matched transmission technique for channels with intersymbol interference," *IEEE Transactions on Communications*, vol. COM-20, pp. 774–780, August 1972.

[44] M. Russell and J. Bergmans, "A technique to reduce error propagation in M-ary decision feedback equalization," *IEEE Transactions on Communications*, vol. 43, pp. 2878–2881, December 1995.

[45] M. Chiani, "Introducing erasures in decision feedback equalization to reduce error propagation," *IEEE Transactions on Communications*, vol. 45, pp. 757–760, July 1997.

[46] Y. Sato, "A method of self–recovering equalization for multilevel amplitude–modulation systems," *IEEE Transactions on Communications*, vol. COM–23, pp. 679–682, June 1975.

[47] A. Benveniste, M. Goursat, and G. Ruget, "Robust identification of a nonminimum phase system: Blind adjustment of a linear equalizer in data communications," *IEEE Transactions on Automatic Control*, vol. 25, pp. 385–399,, June 1980.

[48] M. Goursat and A. Benveniste, "Blind equalizers," *IEEE Transactions on Communications*, vol. COM–28, pp. 871–883, August 1984.

[49] D. Godard, "Self–recovering equalization and carrier tracking in two–dimensional data communication systems," *IEEE Transactions on Communications*, vol. COM–28, pp. 1867–1875, November 1980.

[50] G. Foschini, "Equalizing without altering or deleting data," *AT&T Technical Journal*, vol. 64, pp. 1885–1911, October 1985.

[51] Z. Ding, R. Kennedy, B. Anderson, and R. Johnson, "Ill-convergence of Godard blind equalizers in data communications systems," *IEEE Transactions on Communications*, vol. COM-39, pp. 1313–1327, September 1991.

[52] S. Bellini, "Bussgang techniques for blind equalisation," in *Proceedings of the IEEE Global Telecommunications Conference*, (Houston, TX, USA), pp. 1634–1640, December 1986.

[53] J. Bussgang, "Cross–correlation functions of amplitude-distorted Gaussian signals," *MIT Research Laboratory Technical Report*, no. 216, 1952.

[54] G. Picchi and G. Prati, "Blind equalization and carrier recovery using a "stop–and–go" decision–directed algorithm," *IEEE Transactions on Communications*, vol. COM–35, pp. 877–887, September 1987.

[55] S. Haykin, *Adaptive Filter Theory*. Englewood Cliffs, NJ, USA: Prentice-Hall, 1996.

[56] N. Seshadri, "Joint data and channel estimation using blind Trellis search techniques," *IEEE Transactions on Communications*, vol. 42, pp. 1000–1011, February–April 1994.

[57] D. Forney, "Maximum-likelihood sequence estimation of digital sequences in the presence of intersymbol interference," *IEEE Transactions on Information Theory*, vol. 18, pp. 363–378, May 1972.

[58] A. Polydoros, R. Raheli, and C. Tzou, "Per–survivor processing: a general approach to MLSE in uncertain environments," *IEEE Transactions on Communications*, vol. COM–43, pp. 354–364, February–April 1995.

[59] A. Polydoros and K. Chugg, "MLSE for an unknown channel - Part I: Optimality considerations," *IEEE Transactions on Communications*, vol. 44, pp. 836–846, July 1996.

[60] K. Chugg and A. Polydoros, "MLSE for an unknown channel - Part II: Tracking performance," *IEEE Transactions on Communications*, vol. 44, pp. 949–958, August 1996.

[61] C. Antón-Haro, J. Fonolossa, and J. Fonolossa, "Blind channel estimation and data detection using hidden Markov models," *IEEE Transactions on Signal Processing*, vol. 45, pp. 241–247, January 1997.

[62] H. Cirpan and M. Tsatsanis, "Blind receivers for nonlinearly modulated signals in multipath," *IEEE Transactions on Signal Processing*, vol. 47, pp. 583–586, February 1999.

[63] L. Favalli, A. Mecocci, and P. Savazzi, "Blind MLSE equalizer with fuzzy metric calculation for mobile radio environments," *Electronics Letters*, vol. 33, pp. 1841–1842, October 1997.

[64] K. Chugg, "Acquisition performance of blind sequence detectors using per-survivor processing," in *Proceedings of the 1997 47th IEEE Vehicular Technology Conference*, (Phoenix, USA), pp. 539–543, May 1997.

[65] K. Chugg, “Blind acquisition characteristics of PSP-based sequence detectors,” *International Journal on Selected Areas in Communications*, vol. 16, pp. 1518–1529, October 1998.

[66] E. Baccarelli and R. Cusani, “Combined channel estimation and data detection using soft statistics for frequency selective fast-fading digital links,” *IEEE Transactions on Communications*, vol. 46, pp. 424–427, April 1998.

[67] S. Chen and Y. Wu, “Maximum likelihood joint channel and data estimation using genetic algorithms,” *IEEE Transactions on Signal Processing*, vol. 46, pp. 1469–1473, May 1998.

[68] L. Tong, G. Xu, and T. Kailath, “A new approach to blind identification and equalization of multipath channels,” in *Proceedings of the 25th Asilomar Conference*, (Pacific Grive, Canada), pp. 856–860, 4–6 November 1991.

[69] E. Mulines, J. Cardoso, and S. Mayrargue, “Subspace methods for the blind identification of multichannel fir filters,” *IEEE Transactions on Signal Processing*, vol. 43, pp. 516–525, February 1995.

[70] M. Tsatsanis and G. Giannakis, “Transmitter induced cyclostationarity for blind channel equalization,” *IEEE Transactions on Signal Processing*, vol. 45, pp. 1785–1794, July 1997.

[71] A. Chevreuil, F. Desbouvries, A. Gorokhov, P. Loubaton, and C. Vignat, “Blind equalization in the presence of jammers and unknown noise: Solutions based on second-order cyclostationary statistics,” *IEEE Transactions on Signal Processing*, vol. 46, pp. 259–263, January 1998.

[72] A. Chevreuil and P. Loubaton, “Blind second–order identification of FIR channels: Forced cyclostationarity and structured subspace method,” *IEEE Signal Processing Letters*, vol. 4, pp. 204–206, July 1997.

[73] M. Tsatsanis and G. Giannakis, “Subspace methods for blind estimation of time-varying FIR channels,” *IEEE Transactions on Signal Processing*, vol. 45, pp. 3084–3093, December 1997.

[74] Z. Ding, “Matrix outer-product decomposition method for blind multiple channel identification,” *IEEE Transactions on Signal Processing*, vol. 45, pp. 3053–3061, December 1997.

[75] G. Giannakis and E. Serpedin, “Blind identification of ARMA channels with periodically modulated inputs,” *IEEE Transactions on Signal Processing*, vol. 46, pp. 3099–3104, November 1998.

[76] G. Giannakis, “Filterbanks for blind channel identification and equalization,” *IEEE Signal Processing Letters*, vol. 4, pp. 184–187, June 1997.

[77] R. Heath Jr. and G. Giannakis, “Exploiting input cyclostationarity for blind channel identification in OFDM systems,” *IEEE Transactions on Signal Processing*, vol. 47, pp. 848–856, March 1999.

[78] H. Wong and J. Chambers, “Two-stage interference immune blind equaliser which exploits cyclostationary statistics,” *Electronics Letters*, vol. 32, pp. 1763–1764, September 1996.

[79] H. Liu, G. Xu, L. Tong, and T. Kailath, “Recent developments in blind channel equalization: From cyclostationarity to subspace,” *Signal Processing*, vol. 50, pp. 83–99, April 1996.

[80] Y. Hua, H. Yang, and W. Qiu, “Source correlation compensation for blind channel identification based on second order statistics,” *IEEE Signal Processing Letters*, vol. 1, pp. 119–120, August 1994.

[81] Z. Ding, “Characteristics of band-limited channels unidentifiable from second-order cyclostationary statistics,” *IEEE Signal Processing Letters*, vol. 3, pp. 150–152, May 1996.

[82] J. Xavier, V. Barroso, and J. Moura, “Closed-form blind channel identification and sourse separation in SDMA systems through correlative coding,” *International Journal on Selected Areas in Communications*, vol. 16, pp. 1506–1517, October 1998.

[83] X. Wang and H. Poor, “Blind equalization and multiuser detection in dispersive CDMA channels,” *IEEE Transactions on Communications*, vol. 46, pp. 91–103, January 1998.

[84] X. Wang and H. Poor, “Blind joint equalization and multiuser detection for DS-CDMA in uknowon correlated noise,” *IEEE Transactions on Circuits and Systems II: Analog and Digital Signal Processing*, vol. 46, pp. 886–895, July 1999.

[85] J. Zhu, Z. Ding, and X.-R. Cao, “Column–anchored zeroforcing blind equalization for multiuser wireless FIR channels,” *International Journal on Selected Areas in Communications*, vol. 17, pp. 411–423, March 1999.

[86] H. Zeng and L. Tong, “Blind channel–estimation using the second–order statistics algorithms,” *IEEE Transactions on Signal Processing*, vol. 45, pp. 1919–1930, August 1997.

[87] D. Hatzinakos and C. Nikias, "Blind equalization using a tricepstrum based algorithm," *IEEE Transactions on Communications*, vol. 39, pp. 669–682, May 1991.

[88] D. Boss, K. Kammeyer, and T. Petermann, "Is blind channel estimation feasible in mobile communication systems ?; a study based on GSM," *International Journal on Selected Areas in Communications*, vol. 16, pp. 1479–1492, October 1998.

[89] T. Endres, S. Halford, C. Johnson, and G. Giannakis, "Blind adaptive channel equalization using fractionally-spaced receivers: A comparison study," in *Proceedings of the Conference on Information Sciences and Systems*, (Princeton, USA), 20–22 March 1996.

[90] C. Johnson Jr. and B. Anderson, "Godard blind equalizer error surface characteristics: White, zero–mean binary source case," *International Journal of Adaptive Control and Signal Processing*, vol. 9, pp. 301–324, July–August 1995.

[91] L. Tong and S. Perreau, "Analysis of a nonparametric blind equalizer for discrete-valued signals," *Proceedings of the IEEE*, vol. 86, pp. 1951–1968, March 1996.

[92] J. Proakis, *Digital Communications*. New York, USA: McGraw-Hill, 3rd ed., 1995.

[93] A. Nandi, *Blind Estimation using Higher-Order Statistics*. Dordrecht: Kluwer Academic Publishers, 1999.

[94] C. Becchetti, A. Cocco, and G. Jacovitti, "Performance comparison of second order based blind equalizers in data communication channels," in *Proceedings of the 1997 13th International Conference on Digital Signal Processing, DSP. Part 1 (of 2)*, vol. 1, (Santorini, Greece), pp. 147–150, 2–4 July 1997.

[95] M. Kristensson and B. Ottersten, "Asymptotic comparison of two blind channel identification algorithms," in *Proceedings of the 1997 1st IEEE Signal Processing Workshop on Signal Processing Advances in Wireless Communications, SPAWC'97*, pp. 361–364, 16–18 April 1997.

[96] J. Altuna and B. Mulgrew, "Comparison of cyclostationary blind equalization algorithms in the mobile radio environment," *International Journal of Adaptive Control and Signal Processing*, vol. 12, pp. 267–282, May 1998.

[97] K. Skowratananont and J. Chambers, "Comparison of blind channel estimation and equalisation techniques for a fading environment," in *Proceedings of the 1998 6th IEE Conference on Telecommunications*, no. 451, (Edinburgh, UK), pp. 27–31, 21 March – 2 April 1998.

[98] J. Shynk, P. Gooch, G. Krishnamurthy, and C. Chan, "Comparative performance study of several blind equalization algorithms," in *Proceedings of SPIE — The International Society for Optical Engineering*, vol. 1565, (San Diego, CA, USA), pp. 102–117, 22–24 July 1991.

[99] T. Schirtzinger, X. Li, and W. Jenkins, "Comparison of three algorithms for blind equalization based on the constant modulus error criterion," in *Proceedings of the 1995 International Conference on Acoustics, Speech, and Signal Processing*, vol. Part 2 (of 5), (Detroit, USA), pp. 1049–1052, 9–12 May 1995.

[100] T. Endres, S. Halford, C. Johnson Jr., and G. Giannakis, "Simulated comparisons of blind equalization algorithms for cold start-up applications," *International Journal of Adaptive Control and Signal Processing*, vol. 12, pp. 283–301, May 1998.

[101] K. Feher, ed., *Digital Communications—Satellite/Earth Station Engineering*. Englewood Cliffs, NJ, USA: Prentice-Hall, 1983.

[102] K.-T. Wu and K. Feher, "256-QAM modem performance in distorted channels," *IEEE Transactions on Communications*, vol. COM-33, pp. 487–491, May 1985.

[103] P. Mathiopoulos and K. Feher, "Performance evaluation of a 512-QAM system in distorted channels," *Proceedings Pt F*, vol. 133, pp. 199–204, April 1986.

[104] M. Borgne, "Comparison of high level modulation schemes for high capacity digital radio systems," *IEEE Transactions on Communications*, vol. COM-33, pp. 442–449, May 1985.

[105] M. Shafi and D. Moore, "Further results on adaptive equalizer improvements for 16 QAM and 64 QAM digital radio," *IEEE Transactions on Communications*, vol. COM-34, pp. pp59–66, January 1986.

[106] Y. Saito and Y. Nakamura, "256 QAM modem for high capacity digital radio system," *IEEE Transactions on Communications*, vol. COM-34, pp. 799–805, August 1986.

[107] A. Rustako, L. Greenstein, R. Roman, and A. Saleh, "Using times four carrier recovery in M-QAM digital radio receivers," *IEEE Journal on Selected Areas of Communications*, pp. 524–533, April 1987.

[108] C.-E. Sundberg, W. Wong, and R. Steele, “Logarithmic PCM weighted QAM transmission over gaussian and rayleigh fading channels,” *IEE Proceedings Pt. F*, vol. 134, pp. 557–570, October 1987.

[109] R. Steele, C.-E. Sundberg, and W. Wong, “Transmission of log-PCM via QAM over Gaussian and Rayleigh fading channels,” *IEE Proceedings*, vol. 134, Pt. F, pp. 539–556, October 1987.

[110] L. Hanzo, R. Steele, and P. Fortune, “A subband coding, BCH coding and 16-QAM system for mobile radio speech communication,” *IEEE Transactions on Vehicular Technology*, vol. 39, pp. 327–340, November 1990.

[111] H. Sari and S. Moridi, “New phase and frequency detectors for carrier recovery in PSK and QAM systems,” *IEEE Transactions on Communications*, vol. COM-36, pp. 1035–1043, September 1988.

[112] J.-I. Chuang, “The effects of time-delay spread on QAM with non-linearly switched filters in a portable radio communications channel,” *IEEE Transactions on Communications*, vol. 38, pp. 9–13, February 1989.

[113] J. McGeehan and A. Bateman, “Phase-locked transparent tone in band (TTIB): A new spectrum configuration particularly suited to the transmission of data over SSB mobile radio networks,” *IEEE Transactions on Communications*, vol. COM-32, no. 1, pp. 81–87, 1984.

[114] J. Matthews, “Cochannel performance of 16-level QAM with phase locked TTIB/FFSR processing,” *IEE colloquium on multi-level modulation*, March 1990.

[115] P. Huish and G. Richman, “Increasing the capacity and quality of digital microwave radio,” *IEE colloquium on multi-level modulation*, March 1990.

[116] W. Webb and R. Steele, “16-level circular QAM transmissions over a rayleigh fading channel,” *IEE colloquium on multi-level modulation*, March 1990.

[117] E. Issman and W. Webb, “Carrier recovery for 16-level QAM in mobile radio,” *IEE colloquium on multi-level modulation*, March 1990.

[118] W. Peterson and E. Weldon Jr., *Error Correcting Codes*. Cambridge, MA, USA: MIT. Press, 2nd ed., August 1972. ISBN: 0262160390.

[119] W. Webb and R. Steele, “Equaliser techniques for QAM transmissions over dispersive mobile radio channels,” *IEE Proceedings, Pt. I*, vol. 138, pp. 566–576, December 1991.

[120] W. Webb, “QAM, the modulation scheme for future mobile radio communications?,” *IEE Electronics & Communications Journal*, vol. 4, pp. 1167–176, August 1992.

[121] W. Webb, “Modulation methods for PCNs,” *IEEE Communications magazine*, vol. 30, pp. 90–95, December 1992.

[122] R. Steele and W. Webb, “Variable rate QAM for data transmission over Rayleigh fading channels,” in *Proceeedings of Wireless ’91*, (Calgary, Alberta), pp. 1–14, IEEE, 1991.

[123] K. Feher, “Modems for emerging digital cellular mobile systems,” *IEEE Transactions on Vehicular Technology*, vol. 40, pp. 355–365, May 1991.

[124] M. Iida and K. Sakniwa, “Frequency selective compensation technology of digital 16-QAM for microcellular mobile radio communication systems,” in *Proceedings of IEEE VTC ’92*, (Denver, CO, USA), pp. 662–665, IEEE, 10–13 May 1992.

[125] R. Castle and J. McGeehan, “A multilevel differential modem for narrowband fading channels,” in *Proceedings of IEEE VTC ’92*, (Denver, CO, USA), pp. 104–109, IEEE, 10–13 May 1992.

[126] D. Purle, A. Nix, M. Beach, and J. McGeehan, “A preliminary performance evaluation of a linear frequency hopped modem,” in *Proceedings of IEEE VTC ’92*, (Denver, CO, USA), pp. 120–124, IEEE, 10–13 May 1992.

[127] Y. Kamio and S. Sampei, “Performance of reduced complexity DFE using bidirectional equalizing in land mobile communications,” in *Proceedings of IEEE VTC ’92*, (Denver, CO, USA), pp. 372–376, IEEE, 10–13 May 1992.

[128] S. S. T. Nagayasu and Y. Kamio, “Performance of 16-QAM with decision feedback equalizer using interpolation for land mobile communications,” in *Proceedings of IEEE VTC ’92*, (Denver, CO, USA), pp. 384–387, IEEE, 10–13 May 1992.

[129] E. Malkamaki, “Binary and multilevel offset QAM, spectrum efficient modulation schemes for personal communications,” in *Proceedings of IEEE VTC ’92*, (Denver, CO, USA), pp. 325–328, IEEE, 10–13 May 1992.

[130] Z. Wan and K. Feher, “Improved efficiency CDMA by constant envelope SQAM,” in *Proceedings of IEEE VTC ’92*, (Denver, CO, USA), pp. 51–55, IEEE, 10–13 May 1992.

[131] H. Sasaoka, “Block coded 16-QAM/TDMA cellular radio system using cyclical slow frequency hopping,” in *Proceedings of IEEE VTC ’92*, (Denver, CO, USA), pp. 405–408, IEEE, 10–13 May 1992.

[132] P. Kenington, R. Wilkinson, and J. Marvill, “Broadband linear amplifier design for a PCN base-station,” in *Proceedings of IEEE Vehicular Technology Conference (VTC’91)*, (St. Louis, MO, USA), pp. 155–160, IEEE, 19–22 May 1991.

[133] R. Wilkinson et al., “Linear transmitter design for MSAT terminals,” in *Proceedings of 2nd International Mobile Satellite Conference*, June 1990.

[134] S. Stapleton and F. Costescu, “An adaptive predistorter for a power amplifier based on adjacent channel emissions,” *IEEE Transactions on Vehicular Technology*, vol. 41, pp. 49–57, February 1992.

[135] S. Stapleton, G. Kandola, and J. Cavers, “Simulation and analysis of an adaptive predistorter utilizing a complex spectral convolution,” *IEEE Transactions on Vehicular Technology*, vol. 41, pp. 387–394, November 1992.

[136] A. Wright and W. Durtler, “Experimental performance of an adaptive digital linearized power amplifier,” *IEEE Transactions on Vehicular Technology*, vol. 41, pp. 395–400, November 1992.

[137] M. Faulkner and T. Mattson, “Spectral sensitivity of power amplifiers to quadrature modulator misalignment,” *IEEE Transactions on Vehicular Technology*, vol. 41, pp. 516–525, November 1992.

[138] J. Cavers, “An analysis of pilot symbol assisted modulation for rayleigh fading channels,” *IEEE Transactions on Vehicular Technology*, vol. 40, pp. 686–693, November 1991.

[139] S. Sampei and T. Sunaga, “Rayleigh fading compensation for QAM in land mobile radio communications,” *IEEE Transactions on Vehicular Technology*, vol. 42, pp. 137–147, May 1993.

[140] T. Sunaga and S. Sampei, “Performance of multi-level QAM with post-detection maximal ratio combining space diversity for digital land-mobile radio communications,” *IEEE Transactions on Vehicular Technology*, vol. 42, pp. 294–301, August 1993.

[141] F. Adachi and M. Sawahashi, “Performance analysis of various 16 level modulation schemes under Rrayleigh fading,” *Electronics Letters*, vol. 28, pp. 1579–1581, November 1992.

[142] R. W. Chang, “Synthesis of Band-Limited Orthogonal Signals for Multichannel Data Transmission,” *Bell Systems Technical Journal*, vol. 46, pp. 1775–1796, December 1966.

[143] M.S. Zimmermann and A.L. Kirsch, “The AN/GSC-10/KATHRYN/Variable Rate Data Modem for HF Radio,” *IEEE Transactions on Communication Technology*, vol. CCM–15, pp. 197–205, April 1967.

[144] S. B. Weinstein and P. M. Ebert, “Data transmission by frequency division multiplexing using the discrete fourier transform,” *IEEE Transactions on Communication Technology*, vol. COM–19, pp. 628–634, October 1971.

[145] L.J. Cimini, “Analysis and Simulation of a Digital Mobile Channel Using Orthogonal Frequency Division Multiplexing,” *IEEE Transactions on Communications*, vol. 33, pp. 665–675, July 1985.

[146] M. Alard and R. Lassalle, “Principles of modulation and channel coding for digital broadcasting for mobile receivers,” *EBU Review, Technical No. 224*, pp. 47–69, August 1987.

[147] *Proceedings of 1st International Symposium,DAB*, (Montreux, Switzerland), June 1992.

[148] A. Peled and A. Ruiz, “Frequency domain data transmission using reduced computational complexity algorithms,” in *Proceedings of International Conference on Acoustics, Speech, and Signal Processing, ICASSP’80*, vol. 3, (Denver, CO, USA), pp. 964–967, IEEE, 9–11 April 1980.

[149] B. Hirosaki, “An orthogonally multiplexed QAM system using the discrete fourier transform,” *IEEE Transactions on Communications*, vol. COM-29, pp. 983–989, July 1981.

[150] H. Kolb, “Untersuchungen über ein digitales mehrfrequenzverfahren zur datenübertragung,” in *Ausgewählte Arbeiten über Nachrichtensysteme*, no. 50, Universität Erlangen-Nürnberg, 1982.

[151] H. Schüssler, “Ein digitales Mehrfrequenzverfahren zur Datenübertragung,” in *Professoren-Konferenz, Stand und Entwicklungsaussichten der Daten und Telekommunikation*, (Darmstadt, Germany), pp. 179–196, 1983.

[152] K. Preuss, “Ein Parallelverfahren zur schnellen Datenübertragung Im Ortsnetz,” in *Ausgewählte Arbeiten über Nachrichtensysteme*, no. 56, Universität Erlangen-Nürnberg, 1984.

[153] R. Rückriem, "Realisierung und messtechnische Untersuchung an einem digitalen Parallelverfahren zur Datenübertragung im Fernsprechkanal," in *Ausgewählte Arbeiten über Nachrichtensysteme*, no. 59, Universität Erlangen-Nürnberg, 1985.

[154] I. Kalet, "The multitone channel," *IEEE Transactions on Communications*, vol. 37, pp. 119–124, February 1989.

[155] B. Hirosaki, "An analysis of automatic equalizers for orthogonally multiplexed QAM systems," *IEEE Transactions on Communications*, vol. COM-28, pp. 73–83, January 1980.

[156] L. Hanzo, R. Salami, R. Steele, and P. Fortune, "Transmission of digitally encoded speech at 1.2 Kbaud for PCN," *IEE Proceedings, Part I*, vol. 139, pp. 437–447, August 1992.

[157] P. Fortune, L. Hanzo, and R. Steele, "On the computation of 16-QAM and 64-QAM performance in rayleigh-fading channels," *IEICE Transactions on Communications*, vol. E75-B, pp. 466–475, June 1992.

[158] R. Stedman, H. Gharavi, L. Hanzo, and R. Steele, "Transmission of subband-coded images via mobile channels," *IEEE Transactions on Circuits and Systems for Video Technology*, vol. 3, pp. 15–27, February 1993.

[159] X. Lin, L. Hanzo, R. Steele, and W. Webb, "A subband-multipulse digital audio broadcasting scheme for mobile receivers," *IEEE Transactions on Broadcasting*, vol. 39, pp. 373–382, December 1993.

[160] W. Webb, R. Steele, J. Cheung, and L. Hanzo, "A packet reservation multiple access assisted cordless telecommunications scheme," *IEEE Transactions on Vehicular Technology*, vol. 43, pp. 234–245, May 1994.

[161] L. Hanzo, W. Webb, R. Salami, and R. Steele, "On QAM speech transmission schemes for microcellular mobile PCNs," *European Transactions on Communications*, pp. 495–510, September/October 1993.

[162] L. Hanzo, J. Streit, R. Salami, and W. Webb, "A low-rate multi-level voice/video transceiver for personal communications," *Wireless Personal Communications, Kluwer Academic Publishers*, vol. 2, no. 3, pp. 217–234, 1995.

[163] L. Hanzo, R. Stedman, R. Steele, and J. Cheung, "A mobile speech/video/data transceiver scheme," in *Proceedings of IEEE VTC '94*, (Stockholm, Sweden), pp. 452–456, IEEE, 8–10 June 1994.

[164] L. Hanzo, X. Lin, R. Steele, and W. Webb, "A mobile hi-fi digital audio broadcasting scheme," in *Proceedings of IEEE VTC '94*, (Stockholm, Sweden), pp. 1035–1039, IEEE, 8–10 June 1994.

[165] J. Woodard and L. Hanzo, "A dual-rate algebraic CELP-based speech transceiver," in *Proceedings of IEEE VTC '94*, vol. 3, (Stockholm, Sweden), pp. 1690–1694, IEEE, 8–10 June 1994.

[166] J. Streit and L. Hanzo, "A fractal video communicator," in *Proceedings of IEEE VTC '94*, (Stockholm, Sweden), pp. 1030–1034, IEEE, 8–10 June 1994.

[167] L. Hanzo and P. Cherriman and J. Streit, "Wireless Video Communications: From Second to Third Generation Systems, WLANs and Beyond." IEEE Press, 2001. (For detailed contents please refer to http://www-mobile.ecs.soton.ac.uk.).

[168] L. Hanzo, F. Somerville, and J. Woodard, "Voice compression and communications: Principles and applications for fixed and wireless channels." 2001 (For detailed contents, please refer to http://www-mobile.ecs.soton.ac.uk.).

[169] L. Hanzo, C. Wong, and M. Yee, *Adaptive Wireless Transceivers*. John Wiley, IEEE Press, 2002. (For detailed contents, please refer to http://www-mobile.ecs.soton.ac.uk.).

[170] L. Hanzo, T. Liew, and B. Yeap, *Turbo Coding, Turbo Equalisation and Space-Time Coding*. John Wiley, IEEE Press, 2002. (For detailed contents, please refer to http://www-mobile.ecs.soton.ac.uk.).

[171] L. Hanzo, L. L. Yang, E. L. Kuan, and K. Yen, *Single- and Multi-Carrier CDMA*. John Wiley and IEEE press, 2003.

[172] L. Hanzo and M. Münster and B-J. Choi and T. Keller, *OFDM versus MC-CDMA for broadband multi-user communications, WLANs and broadcasting*. John Wiley and IEEE press, 2003.

[173] J. F. Hayes, "Adaptive feedback communications," *IEEE Transactions on Communication Technology*, vol. 16, no. 1, pp. 29–34, 1968.

[174] A. Duel-Hallen and S. Hu and H. Hallen, "Long Range Prediction of Fading Signals," *IEEE Signal Processing Magazine*, vol. 17, pp. 62–75, May 2000.

[175] J. K. Cavers, "Variable rate transmission for rayleigh fading channels," *IEEE Transactions on Communications Technology*, vol. COM-20, pp. 15–22, February 1972.

[176] W. T. Webb and R. Steele, “Variable rate QAM for mobile radio,” *IEEE Transactions on Communications*, vol. 43, no. 7, pp. 2223–2230, 1995.

[177] M. Moher and J. Lodge, “TCMP—a modulation and coding strategy for rician fading channels,” *IEEE Journal on Selected Areas in Communications*, vol. 7, pp. 1347–1355, December 1989.

[178] S. Otsuki, S. Sampei, and N. Morinaga, “Square QAM adaptive modulation/TDMA/TDD systems using modulation level estimation with Walsh function,” *Electronics Letters*, vol. 31, pp. 169–171, February 1995.

[179] L. Hanzo, W. Webb, and T. Keller, *Single- and Multi-carrier Quadrature Amplitude Modulation*. New York, USA: IEEE Press-John Wiley, April 2000.

[180] W. Lee, “Estimate of channel capacity in Rayleigh fading environment,” *IEEE Transactions on Vehicular Technology*, vol. 39, pp. 187–189, August 1990.

[181] A. Goldsmith and P. Varaiya, “Capacity of fading channels with channel side information,” *IEEE Transactions on Information Theory*, vol. 43, pp. 1986–1992, November 1997.

[182] M. S. Alouini and A. J. Goldsmith, “Capacity of Rayleigh fading channels under different adaptive transmission and diversity-combining technique,” *IEEE Transactions on Vehicular Technology*, vol. 48, pp. 1165–1181, July 1999.

[183] A. Goldsmith and S. Chua, “Variable rate variable power MQAM for fading channels,” *IEEE Transactions on Communications*, vol. 45, pp. 1218–1230, October 1997.

[184] J. Torrance and L. Hanzo, “Optimisation of switching levels for adaptive modulation in a slow Rayleigh fading channel,” *Electronics Letters*, vol. 32, pp. 1167–1169, 20 June 1996.

[185] B. J. Choi and L. Hanzo, “Optimum mode-switching levels for adaptive modulation systems,” in *Submitted to IEEE GLOBECOM 2001*, 2001.

[186] B. J. Choi, M. Münster, L. L. Yang, and L. Hanzo, “Performance of Rake receiver assisted adaptive-modulation based CDMA over frequency selective slow Rayleigh fading channel,” *Electronics Letters*, vol. 37, pp. 247–249, February 2001.

[187] W. H. Press, S. A. Teukolsky, W. T. Vetterling, and B. P. Flannery, *Numerical Recipies in C*. Cambridge University Press, 1992.

[188] C. Tang, “An Intelligent Learning Scheme for Adaptive Modulation,” *In Proceedings of the IEEE Vehicular Technology Conference*, pp. 718–719, Oct 2001.

[189] J. Torrance and L. Hanzo, “Upper bound performance of adaptive modulation in a slow Rayleigh fading channel,” *Electronics Letters*, vol. 32, pp. 718–719, 11 April 1996.

[190] C. Wong and L. Hanzo, “Upper-bound of a wideband burst-by-burst adaptive modem,” in *Proceeding of VTC’99 (Spring)*, (Houston, TX, USA), pp. 1851–1855, IEEE, 16–20 May 1999.

[191] C. Wong and L. Hanzo, “Upper-bound performance of a wideband burst-by-burst adaptive modem,” *IEEE Transactions on Communications*, vol. 48, pp. 367–369, March 2000.

[192] H. Matsuoka and S. Sampei and N. Morinaga and Y. Kamio, “Adaptive Modulation System with Variable Coding Rate Concatenated Code for High Quality Multi-Media Communications Systems,” in *Proceedings of IEEE VTC’96*, vol. 1, (Atlanta, GA, USA), pp. 487–491, IEEE, 28 April–1 May 1996.

[193] A. J. Goldsmith and S. G. Chua, “Adaptive coded modulation for fading channels,” in *Proceedings of IEEE International Conference on Communications*, vol. 3, (Montreal, Canada), pp. 1488–1492, 8–12 June 1997.

[194] A.J. Goldsmith and S. Chua, “Variable-rate variable-power MQAM for fading channels,” *IEEE Transactions on Communications*, vol. 45, pp. 1218–1230, October 1997.

[195] J. Torrance and L. Hanzo, “Demodulation level selection in adaptive modulation,” *Electronics Letters*, vol. 32, pp. 1751–1752, 12 September 1996.

[196] V. Lau and S. Maric, “Variable rate adaptive modulation for DS-CDMA,” *IEEE Transactions on Communications*, vol. 47, pp. 577–589, April 1999.

[197] S. Sampei, N. Morinaga, and Y. Kamio, “Adaptive modulation/TDMA with a BDDFE for 2 mbit/s multi-media wireless communication systems,” in *Proceedings of IEEE Vehicular Technology Conference (VTC’95)*, vol. 1, (Chicago, USA), pp. 311–315, IEEE, 15–28 July 1995.

[198] J. Torrance and L. Hanzo, “Latency considerations for adaptive modulation in a slow Rayleigh fading channel,” in *Proceedings of IEEE VTC’97*, vol. 2, (Phoenix, AZ, USA), pp. 1204–1209, IEEE, 4–7 May 1997.

[199] J. Torrance and L. Hanzo, "Statistical multiplexing for mitigating latency in adaptive modems," in *Proceedings of IEEE International Symposium on Personal, Indoor and Mobile Radio Communications, PIMRC'97*, (Marina Congress Centre, Helsinki, Finland), pp. 938–942, IEEE, 1–4 September 1997.

[200] T. Ue, S. Sampei, and N. Morinaga, "Symbol rate controlled adaptive modulation/TDMA/TDD for wireless personal communication systems," *IEICE Transactions on Communications*, vol. E78-B, pp. 1117–1124, August 1995.

[201] M. Yee and L. Hanzo, "Radial Basis Function decision feedback equaliser assisted burst-by-burst adaptive modulation," in *Proceedings of IEEE Global Telecommunications Conference (GLOBECOM)*, (Rio de Janeiro, Brazil), 5–9 December 1999.

[202] M. Yee, T. Liew, and L. Hanzo, "Radial basis function decision feedback equalisation assisted block turbo burst-by-burst adaptive modems," in *Proceedings of VTC '99 Fall*, (Amsterdam, Holland), pp. 1600–1604, 19-22 September 1999.

[203] M. S. Yee, B. L. Yeap, and L. Hanzo, "Radial basis function assisted turbo equalisation," in *Proceedings of IEEE Vehicular Technology Conference*, (Japan, Tokyo), pp. 640–644, IEEE, 15-18 May 2000.

[204] M. S. Yee and T. H. Liew and L. Hanzo, "Burst-by-burst adaptive turbo-coded radial basis function-assisted decision feedback equalization," *IEEE Transactions on Communications*, pp. 1935–1945, Nov. 2001.

[205] M. S. Yee and B. L. Yeap and L. Hanzo, "RBF-based decision feedback aided turbo equalisation of convolutional and space-time trellis coded systems," *IEE Electronics Letters*, pp. 1298–1299, October 2001.

[206] M. S. Yee, B. L. Yeap, and L. Hanzo, "Turbo equalisation of convolutional coded and concatenated space time trellis coded systems using radial basis function aided equalizers," in *Proceedings of Vehicular Technology Conference*, (Atlantic City, USA), pp. 882–886, Oct 7-11 2001.

[207] D. Goeckel, "Adaptive Coding for Fading Channels using Outdated Fading Estimates," *IEEE Transactions on Communications*, vol. 47, pp. 844–855, June 1999.

[208] K. J. Hole, H. Holm, and G. E. Oien, "Adaptive multidimensional coded modulation over flat fading channels," *IEEE Journal on Selected Areas in Communications*, vol. 18, pp. 1153–1158, July 2000.

[209] D. Pearce, A. Burr, and T. Tozer, "Comparison of counter-measures against slow Rayleigh fading for TDMA systems," in *IEE Colloquium on Advanced TDMA Techniques and Applications*, (London, UK), pp. 9/1–9/6, IEE, 28 October 1996. digest 1996/234.

[210] V.K.N. Lau and M.D. Macleod, "Variable rate adaptive trellis coded QAM for high bandwidth efficiency applications in rayleigh fading channels," in *Proceedings of IEEE Vehicular Technology Conference (VTC'98)*, (Ottawa, Canada), pp. 348–352, IEEE, 18–21 May 1998.

[211] S. X. Ng, C. H. Wong and L. Hanzo, "Burst-by-Burst Adaptive Decision Feedback Equalized TCM, TTCM, BICM and BICM-ID," in *International Conference on Communications (ICC)*, (Helsinki, Finland), pp. 3031–3035, June 2001.

[212] T. Suzuki, S. Sampei, and N. Morinaga, "Space and path diversity combining technique for 10 Mbits/s adaptive modulation/TDMA in wireless communications systems," in *Proceedings of IEEE VTC'96*, (Atlanta, GA, USA), pp. 1003–1007, IEEE, 28 April–1 May 1996.

[213] K. Arimochi, S. Sampei, and N. Morinaga, "Adaptive modulation system with discrete power control and predistortion-type non-linear compensation for high spectral efficient and high power efficient wireless communication systems," in *Proceedings of the IEEE International Symposium on Personal, Indoor and Mobile Radio Communications (PIMRC)*, (Helsinki, Finland), pp. 472–477, 1–4 September 1997.

[214] T. Ikeda, S. Sampei, and N. Morinaga, "TDMA-based adaptive modulation with dynamic channel assignment (AMDCA) for high capacity multi-media microcellular systems," in *Proceedings of IEEE Vehicular Technology Conference*, (Phoenix, USA), pp. 1479–1483, May 1997.

[215] T. Ue, S. Sampei, and N. Morinaga, "Adaptive modulation packet radio communication system using NP-CSMA/TDD scheme," in *Proceedings of IEEE VTC'96*, (Atlanta, GA, USA), pp. 416–421, IEEE, 28 April–1 May 1996.

[216] M. Naijoh, S. Sampei, N. Morinaga, and Y. Kamio, "ARQ schemes with adaptive modulation/TDMA/TDD systems for wireless multimedia communication systems," in *Proceedings of the IEEE International Symposium on Personal, Indoor and Mobile Radio Communications (PIMRC)*, (Helsinki, Finland), pp. 709–713, 1–4 September 1997.

[217] S. Sampei, T. Ue, N. Morinaga, and K. Hamguchi, "Laboratory experimental results of an adaptive modulation TDMA/TDD for wireless multimedia communication systems," in *Proceedings of IEEE International Symposium on Personal, Indoor and Mobile Radio Communications, PIMRC'97*, (Marina Congress Centre, Helsinki, Finland), pp. 467–471, IEEE, 1–4 September 1997.

[218] J.M. Torrance and L. Hanzo, "Latency and Networking Aspects of Adaptive Modems over Slow Indoors Rayleigh Fading Channels," *IEEE Transactions on Vehicular Technology*, vol. 48, no. 4, pp. 1237–1251, 1998.

[219] J. Torrance, L. Hanzo, and T. Keller, "Interference aspects of adaptive modems over slow Rayleigh fading channels," *IEEE Transactions on Vehicular Technology*, vol. 48, pp. 1527–1545, September 1999.

[220] A. Czylwik, "Adaptive OFDM for wideband radio channels," in *Proceeding of IEEE Global Telecommunications Conference, Globecom 96*, (London, UK), pp. 713–718, IEEE, 18–22 November 1996.

[221] P. Chow, J. Cioffi, and J. Bingham, "A practical discrete multitone transceiver loading algorithm for data transmission over spectrally shaped channels," *IEEE Transactions on Communications*, vol. 48, pp. 772–775, 1995.

[222] P. Bello, "Selective fading limitations of the KATHRYN modem and some system design considerations," *IEEE Trabsactions on Communications Technology*, vol. COM–13, pp. 320–333, September 1965.

[223] E. Powers and M. Zimmermann, "A digital implementation of a multichannel data modem," in *Proceedings of the IEEE International Conference on Communications*, (Philadelphia, USA), 1968.

[224] R. Chang and R. Gibby, "A theoretical study of performance of an orthogonal multiplexing data transmission scheme," *IEEE Transactions on Communication Technology*, vol. COM–16, pp. 529–540, August 1968.

[225] B. R. Saltzberg, "Performance of an efficient parallel data transmission system," *IEEE Transactions on Communication Technology*, pp. 805–813, December 1967.

[226] K. Fazel and G. Fettweis, eds., *Multi-Carrier Spread-Spectrum*. Dordrecht: Kluwer, 1997. ISBN 0-7923-9973-0.

[227] F. Classen and H. Meyr, "Synchronisation algorithms for an OFDM system for mobile communications," in *Codierung für Quelle, Kanal und Übertragung*, no. 130 in ITG Fachbericht, (Berlin), pp. 105–113, VDE–Verlag, 1994.

[228] F. Classen and H. Meyr, "Frequency synchronisation algorithms for OFDM systems suitable for communication over frequency selective fading channels," in *Proceedings of IEEE VTC '94*, (Stockholm, Sweden), pp. 1655–1659, IEEE, 8–10 June 1994.

[229] S. Shepherd, P. van Eetvelt, C. Wyatt-Millington, and S. Barton, "Simple coding scheme to reduce peak factor in QPSK multicarrier modulation," *Electronics Letters*, vol. 31, pp. 1131–1132, July 1995.

[230] A. E. Jones, T. A. Wilkinson, and S. K. Barton, "Block coding scheme for reduction of peak to mean envelope power ratio of multicarrier transmission schemes," *Electronics Letters*, vol. 30, pp. 2098–2099, December 1994.

[231] D. Wulich, "Reduction of peak to mean ratio of multicarrier modulation by cyclic coding," *Electronics Letters*, vol. 32, pp. 432–433, 1996.

[232] S. Müller and J. Huber, "Vergleich von OFDM–Verfahren mit reduzierter Spitzenleistung," in *2. OFDM–Fachgespräch in Braunschweig*, 1997.

[233] M. Pauli and H.-P. Kuchenbecker, "Neue Aspekte zur Reduzierung der durch Nichtlinearitäten hervorgerufenen Außerbandstrahlung eines OFDM–Signals," in *2. OFDM–Fachgespräch in Braunschweig*, 1997.

[234] T. May and H. Rohling, "Reduktion von Nachbarkanalstörungen in OFDM–Funkübertragungssystemen," in *2. OFDM–Fachgespräch in Braunschweig*, 1997.

[235] D. Wulich, "Peak factor in orthogonal multicarrier modulation with variable levels," *Electronics Letters*, vol. 32, no. 20, pp. 1859–1861, 1996.

[236] H. Schmidt and K. Kammeyer, "Adaptive Subträgerselektion zur Reduktion des Crest faktors bei OFDM," in *3. OFDM Fachgespräch in Braunschweig*, 1998.

[237] R. Dinis and A. Gusmao, "Performance evaluation of OFDM transmission with conventional and 2-branch combining power amplification schemes," in *Proceeding of IEEE Global Telecommunications Conference, Globecom 96*, (London, UK), pp. 734–739, IEEE, 18–22 November 1996.

[238] R. Dinis, P. Montezuma, and A. Gusmao, “Performance trade-offs with quasi-linearly amplified OFDM through a 2-branch combining technique,” in *Proceedings of IEEE VTC’96*, (Atlanta, GA, USA), pp. 899–903, IEEE, 28 April–1 May 1996.

[239] R. Dinis, A. Gusmao, and J. Fernandes, “Adaptive transmission techniques for the mobile broadband system,” in *Proceeding of ACTS Mobile Communication Summit ’97*, (Aalborg, Denmark), pp. 757–762, ACTS, 7–10 October 1997.

[240] B. Daneshrad, L. Cimini Jr., and M. Carloni, “Clustered-OFDM transmitter implementation,” in *Proceedings of IEEE International Symposium on Personal, Indoor, and Mobile Radio Communications (PIMRC’96)*, (Taipei, Taiwan), pp. 1064–1068, IEEE, 15–18 October 1996.

[241] M. Okada, H. Nishijima, and S. Komaki, “A maximum likelihood decision based nonlinear distortion compensator for multi-carrier modulated signals,” *IEICE Transactions on Communications*, vol. E81B, no. 4, pp. 737–744, 1998.

[242] R. Dinis and A. Gusmao, “Performance evaluation of a multicarrier modulation technique allowing strongly nonlinear amplification,” in *Proceedings of ICC 1998*, pp. 791–796, IEEE, 1998.

[243] T. Pollet, M. van Bladel, and M. Moeneclaey, “BER sensitivity of OFDM systems to carrier frequency offset and wiener phase noise,” *IEEE Transactions on Communications*, vol. 43, pp. 191–193, February/March/April 1995.

[244] H. Nikookar and R. Prasad, “On the sensitivity of multicarrier transmission over multipath channels to phase noise and frequency offset,” in *Proceedings of IEEE International Symposium on Personal, Indoor, and Mobile Radio Communications (PIMRC’96)*, (Taipei, Taiwan), pp. 68–72, IEEE, 15–18 October 1996.

[245] W. Warner and C. Leung, “OFDM/FM frame synchronization for mobile radio data communication,” *IEEE Transactions on Vehicular Technology*, vol. 42, pp. 302–313, August 1993.

[246] H. Sari, G. Karam, and I. Jeanclaude, “Transmission techniques for digital terrestrial TV broadcasting,” *IEEE Communications Magazine*, pp. 100–109, February 1995.

[247] P. Moose, “A technique for orthogonal frequency division multiplexing frequency offset correction,” *IEEE Transactions on Communications*, vol. 42, pp. 2908–2914, October 1994.

[248] K. Brüninghaus and H. Rohling, “Verfahren zur Rahmensynchronisation in einem OFDM-System,” in *3. OFDM Fachgespräch in Braunschweig*, 1998.

[249] F. Daffara and O. Adami, “A new frequency detector for orthogonal multicarrier transmission techniques,” in *Proceedings of IEEE Vehicular Technology Conference (VTC’95)*, (Chicago, USA), pp. 804–809, IEEE, 15–28 July 1995.

[250] M. Sandell, J.-J. van de Beek, and P. Börjesson, “Timing and frequency synchronisation in OFDM systems using the cyclic prefix,” in *Proceedings of International Symposium on Synchronisation*, (Essen, Germany), pp. 16–19, 14–15 December 1995.

[251] N. Yee, J.-P. Linnartz, and G. Fettweis, “Multicarrier CDMA in indoor wireless radio networks,” in *PIMRC’93*, pp. 109–113, 1993.

[252] A. Chouly, A. Brajal, and S. Jourdan, “Orthogonal multicarrier techniques applied to direct sequence spread spectrum CDMA systems,” in *Proceedings of the IEEE Global Telecommunications Conference 1993*, (Houston, TX, USA), pp. 1723–1728, 29 November – 2 December 1993.

[253] G. Fettweis, A. Bahai, and K. Anvari, “On multi-carrier code division multiple access (MC-CDMA) modem design,” in *Proceedings of IEEE VTC ’94*, (Stockholm, Sweden), pp. 1670–1674, IEEE, 8–10 June 1994.

[254] K. Fazel and L. Papke, “On the performance of convolutionally-coded CDMA/OFDM for mobile communication system,” in *PIMRC’93*, pp. 468–472, 1993.

[255] R. Prasad and S. Hara, “Overview of multicarrier CDMA,” *IEEE Communications Magazine*, pp. 126–133, December 1997.

[256] B.-J. Choi, E.-L. Kuan, and L. Hanzo, “Crest–factor study of MC-CDMA and OFDM,” in *Proceeding of VTC’99 (Fall)*, vol. 1, (Amsterdam, Netherlands), pp. 233–237, IEEE, 19–22 September 1999.

[257] Y. Li and N. Sollenberger, “Interference suppression in OFDM systems using adaptive antenna arrays,” in *Proceedings of Globecom’98*, (Sydney, Australia), pp. 213–218, IEEE, 8–12 November 1998.

[258] Y. Li and N. Sollenberger, “Adaptive antenna arrays for OFDM systems with cochannel interference,” *IEEE Transactions on Communications*, vol. 47, pp. 217–229, February 1999.

[259] Y. Li, L. Cimini, and N. Sollenberger, "Robust channel estimation for OFDM systems with rapid dispersive fading channels," *IEEE Transactions on Communications*, vol. 46, pp. 902–915, April 1998.

[260] C. Kim, S. Choi, and Y. Cho, "Adaptive beamforming for an OFDM sytem," in *Proceeding of VTC'99 (Spring)*, (Houston, TX, USA), IEEE, 16–20 May 1999.

[261] L. Lin, L. Cimini Jr., and J.-I. Chuang, "Turbo codes for OFDM with antenna diversity," in *Proceeding of VTC'99 (Spring)*, (Houston, TX, USA), IEEE, 16–20 May 1999.

[262] M. Münster, T. Keller, and L. Hanzo, "Co–channel interference suppression assisted adaptive OFDM in interference limited environments," in *Proceeding of VTC'99 (Fall)*, vol. 1, (Amsterdam, Netherlands), pp. 284–288, IEEE, 19–22 September 1999.

[263] J. Blogh and L. Hanzo, *3G Systems and Intelligent Networking*. John Wiley and IEEE Press, 2002. (For detailed contents, please refer to http://www-mobile.ecs.soton.ac.uk.).

[264] P. Höher, "TCM on frequency-selective land-mobile fading channels," in *International Workshop on Digital Communications*, (Tirrenia, Italy), pp. 317–328, September 1991.

[265] J. Chow, J. Cioffi, and J. Bingham, "Equalizer training algorithms for multicarrier modulation systems.," in *International Conference on Communications*, (Geneva, Switzerland), pp. 761–765, IEEE, May 1993.

[266] S. Wilson, R. E. Khayata, and J. Cioffi, "16QAM Modulation with Orthogonal Frequency Division Multiplexing in a Rayleigh-Fading Environment," in *Vehicular Technology Conference*, vol. 3, (Stockholm, Sweden), pp. 1660–1664, IEEE, June 1994.

[267] J.-J. van de Beek, O. Edfors, M. Sandell, S. Wilson, and P. Börjesson, "On channel estimation in OFDM systems," in *Proceedings of Vehicular Technology Conference*, vol. 2, (Chicago, IL USA), pp. 815–819, IEEE, July 1995.

[268] O. Edfors, M. Sandell, J. van den Beek, S. K. Wilson, and P. Börjesson, "OFDM Channel Estimation by Singular Value Decomposition," in *Proceedings of Vehicular Technology Conference*, vol. 2, (Atlanta, GA USA), pp. 923–927, IEEE, April 28 - May 1 1996.

[269] P. Frenger and A. Svensson, "A Decision Directed Coherent Detector for OFDM," in *Proceedings of Vehicular Technology Conference*, vol. 3, (Atlanta, GA USA), pp. 1584–1588, IEEE, Apr 28 - May 1 1996.

[270] V. Mignone and A. Morello, "CD3-OFDM: A Novel Demodulation Scheme for Fixed and Mobile Receivers," *IEEE Transactions on Communications*, vol. 44, pp. 1144–1151, September 1996.

[271] F. Tufvesson and T. Maseng, "Pilot Assisted Channel Estimation for OFDM in Mobile Cellular Systems," in *Proceedings of Vehicular Technology Conference*, vol. 3, (Phoenix, Arizona), pp. 1639–1643, IEEE, May 4-7 1997.

[272] P. Höher, S. Kaiser, and P. Robertson, "Two-dimensional pilot-symbol-aided channel estimation by Wiener filtering," in *International Conference on Acoustics, Speech and Signal Processing*, (Munich, Germany), pp. 1845–1848, IEEE, April 1997.

[273] P. Höher, S. Kaiser, and P. Robertson, "Pilot–symbol–aided channel estimation in time and frequency," in *Proceedings of Global Telecommunications Conference: The Mini–Conf.*, (Phoenix, AZ), pp. 90–96, IEEE, November 1997.

[274] Y. Li, L. Cimini, and N. Sollenberger, "Robust Channel Estimation for OFDM Systems with Rapid Dispersive Fading Channels," *IEEE Transactions on Communications*, vol. 46, pp. 902–915, April 1998.

[275] O. Edfors, M. Sandell, J.-J. van den Beek, S. Wilson, and P. Börjesson, "OFDM Channel Estimation by Singular Value Decomposition," *IEEE Transactions on Communications*, vol. 46, pp. 931–939, April 1998.

[276] F. Tufvesson, M. Faulkner, and T. Maseng, "Pre-Compensation for Rayleigh Fading Channels in Time Division Duplex OFDM Systems," in *Proceedings of 6th International Workshop on Intelligent Signal Processing and Communications Systems*, (Melbourne, Australia), pp. 57–33, IEEE, November 5-6 1998.

[277] M. Itami, M. Kuwabara, M. Yamashita, H. Ohta, and K. Itoh, "Equalization of Orthogonal Frequency Division Multiplexed Signal by Pilot Symbol Assisted Multipath Estimation," in *Proceedings of Global Telecommunications Conference*, vol. 1, (Sydney, Australia), pp. 225–230, IEEE, November 8-12 1998.

[278] E. Al-Susa and R. Ormondroyd, "A Predictor-Based Decision Feedback Channel Estimation Method for COFDM with High Resilience to Rapid Time-Variations," in *Proceedings of Vehicular Technology Conference*, vol. 1, (Amsterdam, Netherlands), pp. 273–278, IEEE, September 19-22 1999.

[279] B. Yang, K. Letaief, R. Cheng, and Z. Cao, "Robust and Improved Channel Estimation for OFDM Systems in Frequency Selective Fading Channels," in *Proceedings of Global Telecommunications Conference*, vol. 5, (Rio de Janeiro, Brazil), pp. 2499–2503, IEEE, December 5-9 1999.

[280] Y. Li, "Pilot-Symbol-Aided Channel Estimation for OFDM in Wireless Systems," *IEEE Transactions on Vehicular Technology*, vol. 49, pp. 1207–1215, July 2000.

[281] B. Yang, K. Letaief, R. Cheng, and Z. Cao, "Channel Estimation for OFDM Transmission in Multipath Fading Channels Based on Parametric Channel Modeling," *IEEE Transactions on Communications*, vol. 49, pp. 467–479, March 2001.

[282] S. Zhou and G. Giannakis, "Finite-Alphabet Based Channel Estimation for OFDM and Related Multicarrier Systems," *IEEE Transactions on Communications*, vol. 49, pp. 1402–1414, August 2001.

[283] X. Wang and K. Liu, "OFDM Channel Estimation Based on Time-Frequency Polynomial Model of Fading Multipath Channel," in *Proceedings of Vehicular Technology Conference*, vol. 1, (Atlantic City, NJ USA), pp. 460–464, IEEE, October 7-11 2001.

[284] B. Yang, Z. Cao, and K. Letaief, "Analysis of Low-Complexity Windowed DFT-Based MMSE Channel Estimator for OFDM Systems," *IEEE Transactions on Communications*, vol. 49, pp. 1977–1987, November 2001.

[285] B. Lu and X. Wang, "Bayesian Blind Turbo Receiver for Coded OFDM Systems with Frequency Offset and Frequency-Selective Fading," *IEEE Journal on Selected Areas in Communications*, vol. 19, pp. 2516–2527, December 2001.

[286] Y. Li and N. Sollenberger, "Clustered OFDM with Channel Estimation for High Rate Wireless Data," *IEEE Transactions on Communications*, vol. 49, pp. 2071–2076, December 2001.

[287] M. Morelli and U. Mengali, "A Comparison of Pilot-Aided Channel Estimation Methods for OFDM Systems," *IEEE Transactions on Signal Processing*, vol. 49, pp. 3065–3073, December 2001.

[288] M.-X. Chang and Y. Su, "Model-Based Channel Estimation for OFDM Signals in Rayleigh Fading," *IEEE Transactions on Communications*, vol. 50, pp. 540–544, April 2002.

[289] M. Necker and G. Stüber, "Totally Blind Channel Estimation for OFDM over Fast Varying Mobile Channels," in *Proceedings of International Conference on Communications*, (New York, NY USA), IEEE, April 28 - May 2 2002.

[290] B. Yang, Z. Cao, and K. Letaief, "Low Complexity Channel Estimator Based on Windowed DFT and Scalar Wiener Filter for OFDM Systems," in *Proceedings of International Conference on Communications*, vol. 6, (Helsinki, Finnland), pp. 1643–1647, IEEE, June 11-14 2001.

[291] J. Deller, J. Proakis, and J. Hansen, *Discrete-Time Processing of Speech Signals*. Macmillan Publishing Company, 1993.

[292] A. Duel-Hallen, S. Hu, and H. Hallen, "Long Range Prediction of Fading Signals," *IEEE Signal Processing Magazine*, vol. 17, pp. 62–75, May 2000.

[293] F. Tufvesson, *Design of Wireless Communication Systems - Issues on Synchronization, Channel Estimation and Multi-Carrier Systems*. Department of Applied Electronics, Lund University, Sweden, 2000.

[294] W.H. Press and S.A. Teukolsky and W.T. Vetterling and B.P. Flannery, *Numerical Recipes in C*. Cambridge: Cambridge University Press, 1992.

[295] T. Moon and W. Stirling, *Mathematical Methods and Algorithms for Signal Processing*. Prentice Hall, 2000.

[296] Y. Li, N. Seshadri, and S. Ariyavisitakul, "Channel Estimation for OFDM Systems with Transmitter Diversity in Mobile Wireless Channels," *IEEE Journal on Selected Areas in Communications*, vol. 17, pp. 461–471, March 1999.

[297] W. Jeon, K. Paik, and Y. Cho, "An Efficient Channel Estimation Technique for OFDM Systems with Transmitter Diversity," in *Proceedings of International Symposium on Personal, Indoor and Mobile Radio Communications*, vol. 2, (Hilton London Metropole Hotel, London, UK), pp. 1246–1250, IEEE, September 18-21 2000.

[298] Y. Li, "Optimum Training Sequences for OFDM Systems with Multiple Transmit Antennas," in *Proc. of Global Telecommunications Conference*, vol. 3, (San Francisco, United States), pp. 1478–1482, IEEE, November 27 - December 1 2000.

[299] A. Mody and G. Stüber, "Parameter Estimation for OFDM with Transmit Receive Diversity," in *Proceedings of Vehicular Technology Conference*, vol. 2, (Rhodes, Greece), pp. 820–824, IEEE, May 6-9 2001.

[300] Y. Gong and K. Letaief, "Low Rank Channel Estimation for Space-Time Coded Wideband OFDM Systems," in *Proceedings of Vehicular Technology Conference*, vol. 2, (Atlantic City Convention Center, Atlantic City, NJ USA), pp. 772–776, IEEE, October 7-11 2001.

[301] W. Jeon, K. Paik, and Y. Cho, "Two-Dimensional MMSE Channel Estimation for OFDM Systems with Transmitter Diversity," in *Proceedings of Vehicular Technology Conference*, vol. 3, (Atlantic City Convention Center, Atlantic City, NJ USA), pp. 1682–1685, IEEE, October 7-11 2001.

[302] F. Vook and T. Thomas, "MMSE Multi-User Channel Estimation for Broadband Wireless Communications," in *Proceedings of Global Telecommunications Conference*, vol. 1, (San Antonio, Texas, USA), pp. 470–474, IEEE, November 25-29 2001.

[303] Y. Xie and C. Georghiades, "An EM-based Channel Estimation Algorithm for OFDM with Transmitter Diversity," in *Proceedings of Global Telecommunications Conference*, vol. 2, (San Antonio, Texas, USA), pp. 871–875, IEEE, November 25-29 2001.

[304] Y. Li, "Simplified Channel Estimation for OFDM Systems with Multiple Transmit Antennas," *IEEE Transactions on Wireless Communications*, vol. 1, pp. 67–75, January 2002.

[305] H. Bölcskei, R. Heath, and A. Paulraj, "Blind Channel Identification and Equalization in OFDM-Based Multi-Antenna Systems," *IEEE Transactions on Signal Processing*, vol. 50, pp. 96–109, January 2002.

[306] H. Minn, D. Kim, and V. Bhargava, "A Reduced Complexity Channel Estimation for OFDM Systems with Transmit Diversity in Mobile Wireless Channels," *IEEE Transactions on Wireless Communications*, vol. 50, pp. 799–807, May 2002.

[307] S. Slimane, "Channel Estimation for HIPERLAN/2 with Transmitter Diversity," in *International Conference on Communications*, (New York, NY USA), IEEE, April 28 - May 2 2002.

[308] C. Komninakis, C. Fragouli, A. Sayed, and R. Wesel, "Multi-Input Multi-Output Fading Channel Tracking and Equalization Using Kalman Estimation," *IEEE Transactions on Signal Processing*, vol. 50, pp. 1065–1076, May 2002.

[309] G. Foschini, "Layered Space-Time Architecture for Wireless Communication in a Fading Environment when using Multi-Element Antennas"," *Bell Labs Technical Journal*, vol. Autumn, pp. 41–59, 1996.

[310] F. Vook and K. Baum, "Adaptive antennas for OFDM," in *Proceedings of IEEE Vehicular Technology Conference (VTC'98)*, vol. 2, (Ottawa, Canada), pp. 608–610, IEEE, 18–21 May 1998.

[311] X. Wang and H. Poor, "Robust Adaptive Array for Wireless Communications," *IEEE Transactions on Communications*, vol. 16, pp. 1352–1366, October 1998.

[312] K.-K. Wong, R.-K. Cheng, K. Letaief, and R. Murch, "Adaptive Antennas at the Mobile and Base Station in an OFDM/TDMA System," in *Proceedings of Global Telecommunications Conference*, vol. 1, (Sydney, Australia), pp. 183–190, IEEE, November 8-12 1998.

[313] Y. Li and N. Sollenberger, "Interference Suppression in OFDM Systems using Adaptive Antenna Arrays," in *Proceedings of Global Telecommunications Conference*, vol. 1, (Sydney, Australia), pp. 213–218, IEEE, November 8-12 1998.

[314] G. Golden, G. Foschini, R. Valenzuela, and P. Wolniansky, "Detection Algorithms and Initial Laboratory Results using V-BLAST Space-Time Communication Architecture," *IEE Electronics Letters*, vol. 35, pp. 14–16, January 1999.

[315] Y. Li and N. Sollenberger, "Adaptive Antenna Arrays for OFDM Systems with Cochannel Interference," *IEEE Transactions on Communications*, vol. 47, pp. 217–229, February 1999.

[316] P. Vandenameele, L. Van der Perre, M. Engels, and H. Man, "A novel class of uplink OFDM/SDMA algorithms for WLAN," in *Proceedings of Global Telecommunications Conference — Globecom'99*, vol. 1, (Rio de Janeiro, Brazil), pp. 6–10, IEEE, 5–9 December 1999.

[317] M. Speth, A. Senst, and H. Meyr, "Low complexity space-frequency MLSE for multi-user COFDM," in *Proceedings of Global Telecommunications Conference — Globecom'99*, vol. 1, (Rio de Janeiro, Brazil), pp. 2395–2399, IEEE, 5–9 December 1999.

[318] C. H. Sweatman, J. Thompson, B. Mulgrew, and P. Grant, "A Comparison of Detection Algorithms including BLAST for Wireless Communication using Multiple Antennas," in *Proceedings of International Symposium on Personal, Indoor and Mobile Radio Communications*, vol. 1, (Hilton London Metropole Hotel, London, UK), pp. 698–703, IEEE, September 18-21 2000.

[319] R. van Nee, A. van Zelst, and G. Awater, "Maximum Likelihood Decoding in a Space-Division Multiplexing System," in *Proceedings of Vehicular Technology Conference*, vol. 1, (Tokyo, Japan), pp. 6–10, IEEE, May 15-18 2000.

[320] G. Awater, A. van Zelst, and R. van Nee, "Reduced Complexity Space Division Multiplexing Receivers," in *Proceedings of Vehicular Technology Conference*, vol. 1, (Tokyo, Japan), pp. 11–15, IEEE, May 15-18 2000.

[321] A. van Zelst, R. van Nee, and G. Awater, "Space Division Multiplexing (SDM) for OFDM systems," in *Proceedings of Vehicular Technology Conference*, vol. 2, (Tokyo, Japan), pp. 1070–1074, IEEE, May 15-18 2000.

[322] P. Vandenameele, L. V. D. Perre, M. Engels, B. Gyselinckx, and H. D. Man, "A Combined OFDM/SDMA Approach," *IEEE Journal on Selected Areas in Communications*, vol. 18, pp. 2312–2321, November 2000.

[323] X. Li, H. Huang, A. Lozano, and G. Foschini, "Reduced-Complexity Detection Algorithms for Systems Using Multi-Element Arrays," in *Proc. of Global Telecommunications Conference*, vol. 2, (San Francisco, United States), pp. 1072–1076, IEEE, November 27 - December 1 2000.

[324] C. Degen, C. Walke, A. Lecomte, and B. Rembold, "Adaptive MIMO Techniques for the UTRA-TDD Mode," in *Proceedings of Vehicular Technology Conference*, vol. 1, (Rhodes, Greece), pp. 108–112, IEEE, May 6-9 2001.

[325] X. Zhu and R. Murch, "Multi-Input Multi-Output Maximum Likelihood Detection for a Wireless System," in *Proceedings of Vehicular Technology Conference*, vol. 1, (Rhodes, Greece), pp. 137–141, IEEE, May 6-9 2001.

[326] J. Li, K. Letaief, R. Cheng, and Z. Cao, "Joint Adaptive Power Control and Detection in OFDM/SDMA Wireless LANs," in *Proceedings of Vehicular Technology Conference*, vol. 1, (Rhodes, Greece), pp. 746–750, IEEE, May 6-9 2001.

[327] F. Rashid-Farrokhi, K. Liu, and L. Tassiulas, "Transmit Beamforming and Power Control for Cellular Wireless Systems," *IEEE Journal on Selected Areas in Communications*, vol. 16, pp. 1437–1450, October 1998.

[328] A. van Zelst, R. van Nee, and G. Awater, "Turbo-BLAST and its Performance," in *Proceedings of Vehicular Technology Conference*, vol. 2, (Rhodes, Greece), pp. 1282–1286, IEEE, May 6-9 2001.

[329] A. Benjebbour, H. Murata, and S. Yoshida, "Performance of Iterative Successive Detection Algorithm with Space-Time Transmission," in *Proceedings of Vehicular Technology Conference*, vol. 2, (Rhodes, Greece), pp. 1287–1291, IEEE, May 6-9 2001.

[330] M. Sellathurai and S. Haykin, "A Simplified Diagonal BLAST Architecture with Iterative Parallel-Interference Cancellation Receivers," in *Proceedings of International Conference on Communications*, vol. 10, (Helsinki, Finnland), pp. 3067–3071, IEEE, June 11-14 2001.

[331] A. Bhargave, R. Figueiredo, and T. Eltoft, "A Detection Algorithm for the V-BLAST System," in *Proceedings of Global Telecommunications Conference*, vol. 1, (San Antonio, Texas, USA), pp. 494–498, IEEE, November 25-29 2001.

[332] S. Thoen, L. Deneire, L. V. D. Perre, and M. Engels, "Constrained Least Squares Detector for OFDM/SDMA-based Wireless Networks," in *Proceedings of Global Telecommunications Conference*, vol. 2, (San Antonio, Texas, USA), pp. 866–870, IEEE, November 25-29 2001.

[333] Y. Li and Z.-Q. Luo, "Parallel Detection for V-BLAST System," in *Proceedings of International Conference on Communications*, (New York, NY USA), IEEE, April 28 - May 2 2002.

[334] S. Verdú, *Multiuser Detection*. Cambridge, UK: Cambridge University Press, 1998.

[335] J. Litva and T.-Y. Lo, *Digital Beamforming in Wireless Communications*. London: Artech House Publishers, 1996.

[336] P. Vandenameele, L. Van der Perre, M. Engels, B. Gyselinckx, and H. Man, "A novel class of uplink OFDM/SDMA algorithms: A statistical performance analysis," in *Proceedings of Vehicular Technology Conference*, vol. 1, (Amsterdam, Netherlands), pp. 324–328, IEEE, 19–22 September 1999.

[337] F. Mueller-Roemer, “Directions in audio broadcasting,” *Journal Audio Engineering Society*, vol. 41, pp. 158–173, March 1993.

[338] G. Plenge, “DAB — a new radio broadcasting system — state of development and ways for its introduction,” *Rundfunktech. Mitt.*, vol. 35, no. 2, 1991.

[339] ETSI, *Digital Audio Broadcasting (DAB)*, 2nd ed., May 1997. ETS 300 401.

[340] ETSI, *Digital Video Broadcasting (DVB); Framing structure, channel coding and modulation for digital terrestrial television*, August 1997. EN 300 744 V1.1.2.

[341] P. Chow, J. Tu, and J. Cioffi, “A discrete multitone transceiver system for HDSL applications,” *IEEE journal on selected areas in communications*, vol. 9, pp. 895–908, August 1991.

[342] P. Chow, J. Tu, and J. Cioffi, “Performance evaluation of a multichannel transceiver system for ADSL and VHDSL services,” *IEEE journal on selected areas in communications*, vol. 9, pp. 909–919, August 1991.

[343] K. Sistanizadeh, P. Chow, and J. Cioffi, “Multi-tone transmission for asymmetric digital subscriber lines (ADSL),” in *Proceedings of ICC’93*, pp. 756–760, IEEE, 1993.

[344] ANSI, *ANSI/T1E1.4/94-007, Asymmetric Digital Subscriber Line (ADSL) Metallic Interface.*, August 1997.

[345] A. Burr and P. Brown, “Application of OFDM to powerline telecommunications,” in *3rd International Symposium On Power-Line Communications*, (Lancaster, UK), 30 March – 1 April 1999.

[346] M. Deinzer and M. Stoger, “Integrated PLC-modem based on OFDM,” in *3rd International Symposium On Power-Line Communications*, (Lancaster, UK), 30 March – 1 April 1999.

[347] R. Prasad and H. Harada, “A novel OFDM based wireless ATM system for future broadband multimedia communications,” in *Proceeding of ACTS Mobile Communication Summit ’97*, (Aalborg, Denmark), pp. 757–762, ACTS, 7–10 October 1997.

[348] C. Ciotti and J. Borowski, “The AC006 MEDIAN project — overview and state–of–the–art,” in *Proc. ACTS Summit ’96*, (Granada, Spain), pp. 362–367, 27–29 November 1996.

[349] J. Borowski, S. Zeisberg, J. Hübner, K. Koora, E. Bogenfeld, and B. Kull, “Performance of OFDM and comparable single carrier system in MEDIAN demonstrator 60GHz channel,” in *Proceeding of ACTS Mobile Communication Summit ’97*, (Aalborg, Denmark), pp. 653–658, ACTS, 7–10 October 1997.

[350] M. D. Benedetto, P. Mandarini, and L. Piazzo, “Effects of a mismatch in the in–phase and in–quadrature paths, and of phase noise, in QDCPSK-OFDM modems,” in *Proceeding of ACTS Mobile Communication Summit ’97*, (Aalborg, Denmark), pp. 769–774, ACTS, 7–10 October 1997.

[351] T. Rautio, M. Pietikainen, J. Niemi, J. Rautio, K. Rautiola, and A. Mammela, “Architecture and implementation of the 150 Mbit/s OFDM modem (invited paper),” in *IEEE Benelux Joint Chapter on Communications and Vehicular Technology, 6th Symposium on Vehicular Technology and Communications*, (Helsinki, Finland), p. 11, 12–13 October 1998.

[352] J. Ala-Laurila and G. Awater, “The magic WAND — wireless ATM network demondtrator system,” in *Proceeding of ACTS Mobile Communication Summit ’97*, (Aalborg, Denmark), pp. 356–362, ACTS, 7–10 October 1997.

[353] J. Aldis, E. Busking, T. Kleijne, R. Kopmeiners, R. van Nee, R. Mann-Pelz, and T. Mark, “Magic into reality, building the WAND modem,” in *Proceeding of ACTS Mobile Communication Summit ’97*, (Aalborg, Denmark), pp. 775–780, ACTS, 7–10 October 1997.

[354] E. Hallmann and H. Rohling, “OFDM-Vorschläge für UMTS,” in *3. OFDM Fachgespräch in Braunschweig*, 1998.

[355] “Universal mobile telecommunications system (UMTS); UMTS terrestrial radio access (UTRA); concept evaluation,” tech. rep., ETSI, 1997. TR 101 146.

[356] C. E. Shannon, “A mathematical theory of communication,” *Bell System Technical Journal*, pp. 379–427, 1948.

[357] R. Hamming, “Error detecting and error correcting codes,” *Bell System Technical Journal*, vol. 29, pp. 147–160, 1950.

[358] M. Golay, “Notes on digital coding,” *Proceedings of the IEEE*, vol. 37, p. 657, 1949.

[359] P. Elias, “Coding for noisy channels,” *IRE Conv. Rec. pt.4*, pp. 37–47, 1955.

[360] A. Viterbi, "Error bounds for convolutional codes and an asymphotically optimum decoding algorithm," *IEEE Transactions on Information Theory*, vol. IT-13, pp. 260–269, April 1967.

[361] G. Ungerböck, "Trellis-coded modulation with redundant signal sets. Part 1 and 2," *IEEE Communications Magazine*, vol. 25, pp. 5–21, February 1987.

[362] D. Divsalar and M. K. Simon, "The design of trellis coded MPSK for fading channel: Set partitioning for optimum code design," *IEEE Transactions on Communications*, vol. 36, pp. 1013–1021, September 1988.

[363] C. Schlegel, *Trellis Coding*. The Institute of Electrical and Electronics Engineers, Inc., New York: IEEE Press, 1997.

[364] E. Zehavi, "8-PSK trellis codes for a Rayleigh fading channel," *IEEE Transactions on Communications*, vol. 40, pp. 873–883, May 1992.

[365] G. Caire and G. Taricco and E. Biglieri, "Bit-Interleaved Coded Modulation," *IEEE Transactions on Information Theory*, vol. 44, pp. 927–946, May 1998.

[366] C. Berrou and A. Glavieux and P. Thitimajshima, "Near Shannon Limit Error-Correcting Coding and Decoding: Turbo Codes," in *Proceedings of the International Conference on Communications*, (Geneva, Switzerland), pp. 1064–1070, May 1993.

[367] *Proceedings of the International Symposium on Turbo Codes & Related Topics*, (Brest, France), 3–5 September 1997.

[368] D. J. Costello, A. Banerjee, T. E. Fuja and P. C. Massey, "Some Reflections on the Design of Bandwidth Efficient Turbo Codes," in *Proceedings of 4th ITG Conference on Source and Channel Coding*, no. 170 in ITG Fachbericht, (Berlin), pp. 357–363, VDE–Verlag, 28–30 January 2002.

[369] L. Hanzo, T.H. Liew and B.L. Yeap, *Turbo Coding, Turbo Equalisation and Space Time Coding for Transmission over Wireless channels*. New York, USA: John Willy IEEE Press, 2002.

[370] R. Steele and L. Hanzo, eds., *Mobile Radio Communications: Second and Third Generation Cellular and WATM Systems*. New York, USA: IEEE Press - John Wiley & Sons, 2nd ed., 1999.

[371] S. L. Goff, A. Glavieux, and C. Berrou, "Turbo-codes and high spectral efficiency modulation," in *Proceedings of IEEE International Conference on Communications*, pp. 645–649, 1994.

[372] P. Robertson and T. Worz, "Bandwidth-Efficient Turbo Trellis-Coded Modulation Using Punctured Component Codes," *IEEE Journal on Selected Areas in Communications*, vol. 16, pp. 206–218, Feb 1998.

[373] X. Li and J.A. Ritcey, "Trellis-Coded Modulation with Bit Interleaving and Iterative Decoding," *IEEE Journal on Selected Areas in Communications*, vol. 17, April 1999.

[374] X. Li and J.A. Ritcey, "Bit-interleaved coded modulation with iterative decoding using soft feedback," *IEE Electronics Letters*, vol. 34, pp. 942–943, May 1998.

[375] J. Winters, "Smart antennas for wireless systems," *IEEE Personal Communications*, vol. 5, pp. 23–27, February 1998.

[376] R. Derryberry, S. Gray, D. Ionescu, G. Mandyam, and B. Raghothaman, "Transmit diversity in 3g cdma systems," *IEEE Communications Magazine*, vol. 40, pp. 68–75, April 2002.

[377] A. Molisch, M. Win, and J. Winters, "Space-time-frequency (stf) coding for mimo-ofdm systems," *IEEE Communications Letters*, vol. 6, pp. 370–372, September 2002.

[378] A. Molisch, M. Steinbauer, M. Toeltsch, E. Bonek, and R. Thoma, "Capacity of mimo systems based on measured wireless channels," *IEEE Journal on Selected Areas in Communications*, vol. 20, pp. 561–569, April 2002.

[379] D. Gesbert, M. Shafi, D.-S. Shiu, P. Smith, and A. Naguib, "From theory to practice: an overview of mimo space-time coded wireless systems," *IEEE Journal on Selected Areas in Communications*, vol. 21, pp. 281–302, April 2003.

[380] M. Shafi, D. Gesbert, D.-S. Shiu, P. Smith, and W. Tranter, "Guest editorial: Mimo systems and applications," *IEEE Journal on Selected Areas in Communications*, vol. 21, pp. 277–280, April 2003.

[381] W. Jakes Jr., ed., *Microwave Mobile Communications*. New York, USA: John Wiley & Sons, 1974.

[382] W. Lee, *Mobile Cellular Communications*. New York, USA: McGraw-Hill, 1989.

[383] R. Steele and L. Hanzo, eds., *Mobile Radio Communications*. Piscataway, NJ, USA: IEEE Press, 1999.

[384] D. Parsons, *The Mobile Radio Propagation Channel*. London: Pentech Press, 1992.

[385] D. Greenwood and L. Hanzo, "Characterisation of mobile radio channels," in Steele and Hanzo [383], ch. 2, pp. 92–185.

[386] R. Steele and V. Prabhu, "Mobile radio cellular structures for high user density and large data rates," *Proceedings of the IEE*, pp. 396–404, August 1985. Pt F.

[387] R. Steele, "The cellular environment of lightweight hand-held portables," *IEEE Communications Magazine*, pp. 20–29, July 1989.

[388] J. G. Proakis, *Digital Communications*. Mc-Graw Hill International Editions, 3rd ed., 1995.

[389] K. Bullington, "Radio propagation at frequencies above 30 Mc/s," *Proceedings IRE 35*, pp. 1122–1136, 1947.

[390] R. Edwards and J. Durkin, "Computer prediction of service area for VHF mobile radio networks," *Proc of IRE*, vol. 116, no. 9, pp. 1493–1500, 1969.

[391] W. Webb, "Sizing up the microcell for mobile radio communications," *IEE Electronics and communications Journal*, vol. 5, pp. 133–140, June 1993.

[392] M. Hata, "Empirical formula for propagation loss in land mobile radio," *IEEE Transactions on Vehicular Technology*, vol. 29, pp. 317–325, August 1980.

[393] Y. Okumura, E. Ohmori, T. Kawano, and K. Fukuda, "Field strength and its variability in VHF and UHF land mobile service," *Review of the Electrical Communication Laboratory*, vol. 16, pp. 825–873, September–October 1968.

[394] E. Green, "Radio link design for microcellular systems," *British Telecom Technology Journal*, vol. 8, pp. 85–96, January 1990.

[395] G. O. A. Rustako, N. Amitay and R. Roman, "Propagation measurements at microwave frequencies for microcellular mobile and personal communications," *Proceedings of 39th IEEE VTC*, pp. 316–320, 1989.

[396] J. Kiebler, "The design and planning of feeder links to broadcasting satellites," *IEEE Journal on Selected Areas of Communications*, vol. SAC-3, pp. 181–185, January 1985.

[397] C. Loo, "A statistical model for a land mobile radio satellite link," *IEEE Transactions on Vehicular Technology*, vol. VT-34, pp. 122–127, August 1985.

[398] C. Loo, "Digital transmission through a land mobile satellite channel," *IEEE Transactions on Communications*, vol. 38, pp. 693–697, May 1990.

[399] E. Lutz, D. Cygan, M. Dippold, F. Dolainsky, and W. Papke, "The land mobile satellite communications channel - recording, statistics and channel model," *IEEE Transactions on Vehicular Technology*, vol. 40, pp. 375–386, May 1991.

[400] J. Hagenauer, F. Dolainsky, E. Lutz, W. Papke, and R. Schweikert, "The maritime satellite communication channel – channel model, performance of modulation and coding," *IEEE Journal on Selected Areas in Communications*, vol. 5, pp. 701–713, May 1987.

[401] C. Loo, "Measurements and models of a land mobile satellite channel and their application to MSK signals," *IEEE Transactions on Vehicular Technology*, vol. VT-35, pp. 114–121, August 1987.

[402] H. Nyquist, "Certain factors affecting telegraph speed," *Bell System Technical Journal*, p. 617, April 1928.

[403] H. Raemer, *Statistical Communication Theory and Applications*. Englewood Cliffs, NJ, USA: Prentice-Hall, 1969.

[404] Y. Chow, A. Nix, and J. McGeehan, "Analysis of 16-APSK modulation in AWGN and rayleigh fading channel," *Electronics Letters*, vol. 28, pp. 1608–1610, November 1992.

[405] N. Kingsbury, "Transmit and receive filters for QPSK signals to optimise the performance on linear and hard limited channels," *IEE Proceedings*, vol. 133, pp. 345–355, July 1986. Pt.F.

[406] B. Sklar, *Digital Communications—Fundamentals and Applications*. Englewood Cliffs, NJ, USA: Prentice-Hall, 1988.

[407] M. Schwartz, *Information Transmission, Modulation and Noise*. New York, USA: McGraw-Hill, 1990.

[408] K. Feher, ed., *Advanced Digital Communications: Systems and Signal Processing*. Englewood Cliffs, NJ, USA: Prentice-Hall, 1987.

[409] A. Saleh and D. Cox, "Improving the power-added efficiency of FET amplifiers operating with varying envelope signals," *IEEE Transactions on Microwave Theory Technology*, vol. MTT-31, pp. 51–56, January 1983.

[410] D. Green, "Characterisation and compensation of nonlinearities in microwave transmitters," *IEEE Transactions on Microwave Theory Technology.*, vol. MTT-30, pp. 213–217, 1982.

[411] F. Casadevall, "The LINC transmitter," *RF Design*, pp. 41–48, February 1990.

[412] Y. Akaiwa and Y. Nagata, "Highly efficient digital mobile communications with a linear modulation method," *IEEE Journal on Selected Areas in Communications*, vol. SAC-5, pp. 890–895, June 1987.

[413] D. H. A. Bateman and R. Wilkinson, "Linear transceiver architectures," in *Proceedings of IEEE Vehicular Technology Conference*, pp. 478–484, 1988.

[414] A. Wright and W. Duntler, "Experimental performance of an adaptive digital linearised power amplifier," *IEEE Transactions on Vehicular Technology*, vol. 41, pp. 395–400, November 1992.

[415] S. Stapleton and L. Quach, "Reduction of adjacent channel interference using postdistortion," in *Proceedings of IEEE VTC '92*, (Denver, CO, USA), pp. 915–918, IEEE, 10–13 May 1992.

[416] J. Namiki, "An automatically controlled predistorter for multilevel quadrature amplitude modulation," *IEEE Transactions on Communications*, vol. COM-31, pp. 707–712, May 1983.

[417] T. Nojima and T. Konno, "Cuber predistortion linearizer for relay equipment in the 800 MHz band land mobile telephone system," *IEEE Transactions on Vehicular Technology*, vol. VT-34, pp. 169–177, November 1985.

[418] P. M. M. Nannicini and F. Oggioni, "Temperature controlled predistortion circuits for 64 QAM microwave power amplifiers," *IEEE Microwave Theory Tech. Dig.*, pp. 99–102, 1985.

[419] Y. Nagata, "Linear amplification technique for digital mobile communications," in *Proceedings of IEEE Vehicular Technology Conference (VTC'89)*, (San Francisco, CA, USA), pp. 159–164, IEEE, 1–3 May 1989.

[420] A. Saleh and J. Salz, "Adaptive linearization of power amplifiers in digital radio systems," *Bell Systems Technical Journal*, vol. 62, pp. 1019–1033, April 1983.

[421] B. Bunday, *Basic Optimisation Methods*. London: Edward Arnold, 1984.

[422] S. Stapleton and F. Costesu, "An adaptive pre-distortion system," in *Proceedings of IEEE VTC '92*, (Denver, CO, USA), pp. 690–693, IEEE, 10–13 May 1992.

[423] S. S. L.D. Quach, "A post-distortion receiver for mobile communications," *IEEE Transactions on Vehicular Technology*, vol. 42, pp. 604–616, November 1993.

[424] M. K. Simon, S. M. Hinedi, and W. C. Lindsey, *Communication Techniques - Signal Design and Detection*. Prentice Hall, 1995.

[425] L. Franks, "Carrier and bit synchronization — a tutorial review," *IEEE Transactions on Communications*, vol. COM-28, pp. 1107–1121, August 1980.

[426] R. Ziemer and R. Peterson, *Digital Communications and Spread Spectrum System*. New York, USA: Macmillan Publishing Company, 1985.

[427] L. Franks, "Synchronisation subsystems: Analysis and design," in Feher [101], ch. 7.

[428] A. Carlson, *Communication Systems*. New York, USA: McGraw-Hill, 1975.

[429] I. Wassell, *Digital mobile radio communication*. PhD thesis, University of Southampton, UK, 1991.

[430] R. Cupo. and R. Gitlin, "Adaptive carrier recovery systems for digital data communications receivers," *IEEE Journal on Selected Areas of Communications*, vol. 7, pp. 1328–1339, December 1989.

[431] W. Lindsey and M. Simon, "Carrier synchronisation and detection of polyphase signals," *IEEE Transactions on Communications*, pp. 441–454, June 1972.

[432] J. Smith, *Modern communications circuits*. New York, USA: McGraw Hill, 1986.

[433] M. Woodbury, "Inverting modified matrices," tech. rep., Statistical Research Group, Princeton University, Princeton, NJ, USA. Mem.Rep. 42.

[434] B. Picinbono, "Adaptive signal processing for detection and communication," in *Communication Systems and Random Process Theory* (J. Skwirzinsky, ed.), Alphen aan den Rijn, The Netherlands: Sijthof and Noordhoff, 1978.

[435] K. Murota and K. Hirade, "GMSK modulation for digital mobile radio telephony," *IEEE Transactions on Communications*, vol. 29, pp. 1044–1050, July 1981.

[436] L. Lopes, "GSM radio link simulation," tech. rep., University research in Mobile Radio, 1990. IEE Colloquium.

[437] J. Anderson, T. Aulin, and C. Sundberg, *Digital phase modulation*. Plenum Press, 1986.

[438] ETSI, *Digital Video Broadcasting (DVB); Framing structure, channel coding and modulation for 11/12 GHz Satellite Services*, August 1997. ETS 300 421.

[439] ETSI, *Digital Video Broadcasting (DVB); Framing structure, channel coding and modulation for digital terrestrial television*, August 1997. ETS 300 744.

[440] ETSI, *Digital Video Broadcasting (DVB); Framing structure, channel coding and modulation for cable systems*, December 1997. ETS 300 429.

[441] L. Hanzo, W. Webb, and T. Keller, *Single- and Multi-carrier Quadrature Amplitude Modulation*. New York: John Wiley-IEEE Press, April 2000.

[442] L. Hanzo and W. Webb, *Modern Quadrature Amplitude Modulation — Principles and Applications for Fixed and Wireless Channels*. New York, USA: IEEE Press – John Wiley,, 1994.

[443] S. Haykin, *Blind Deconvolution*. Prentice-Hall, 1st ed., 1994.

[444] D. Lainiotis, S. Katsikas, and S. Likothanassis, "Optimal seismic deconvolution," *Signal Processing*, vol. 15, pp. 375–404, December 1988.

[445] D. Huang and F. Gustafsson, "Sufficient output conditions for identifiability in blind equalization," *IEEE Transactions on Communications*, vol. 47, pp. 191–194, February 1999.

[446] L. Tong, G. Xu, and T. Kailath, "Blind identification and equalization based on second-order statistics: a time domain approach," *IEEE Transactions on Information Theory*, vol. 40, pp. 380–389, December 1994.

[447] S.-C. Pei and M.-F. Shih, "Fractionally spaced blind equalization using polyperiodic linear filtering," *IEEE Transactions on Communications*, vol. 46, pp. 16–19, January 1998.

[448] K. Dogancay and R. Kennedy, "Least squares approach to blind channel equalization," *Signal Processing*, vol. 58, pp. 63–78, April 1997.

[449] T. Endres, C. Johnson, and M. Green, "Robustness to fractionally-spaced equalizer length using the constant modulus criterion," *IEEE Transactions on Signal Processing*, vol. 47, pp. 544–548, February 1999.

[450] J. LeBlanc, I. Fijalkow, and C. Johnson Jr., "CMA fractionally spaced equalizers: Stationary points and stability under iid and temporally correlated sources," *International Journal of Adaptive Control and Signal Processing*, vol. 12, pp. 135–155, March 1998.

[451] M. Magarini, A. Spalvieri, and G. Tartara, "Asymptotic analysis of stabilisation technique for the blind fractionally spaced equaliser," *Electronics Letters*, vol. 32, pp. 1947–1948, October 1996.

[452] C. Papadias and D. Slock, "Fractionally spaced equalization of linear polyphase channels and related blind techniques based on multichannel linear prediction," *IEEE Transactions on Signal Processing*, vol. 47, pp. 641–654, March 1999.

[453] V. Yang and D. Jones, "A vector constant modulus algorithm for shaped constellation equalization," *IEEE Signal Processing Letters*, vol. 5, pp. 89–91, April 1998.

[454] O. Shalvi and E. Weinstein, "New criteria for blind deconvolution of nonminimum phase systems (channels)," *IEEE Transactions on Information Theory*, vol. 36, pp. 312–321, March 1990.

[455] O. Shalvi and E. Weinstein, "Super-exponential methods for blind deconvolution," *IEEE Transactions on Information Theory*, vol. 39, pp. 504–519, March 1993.

[456] H. Chiang and C. Nikias, "Adaptive deconvolution and identification of nonminimum phase FIR systems based on cumulants," *IEEE Transactions on Automatic Control*, vol. 35, pp. 36–47, January 1990.

[457] D. Boss and K.-D. Kammeyer, "Blind GSM channel estimation," in *Proceedings of the 1997 47th IEEE Vehicular Technology Conference*, (Phoenix, USA), pp. 1044–1048, 4–7 May 1997.

[458] K. Wesolowsky, "Analysis and properties of the modified constant modulus algorithm for blind equalization," *European Transactions on Telecommunication*, vol. 3, pp. 225–230, May–June 1992.

[459] J. Choi, I. Song, and R. Park, "Some convergence properties of Godard's quartic algorithm," *Signal Processing*, vol. 56, pp. 313–320, February 1997.

[460] Z. Ding, R. Johnson, and R. Kennedy, "On the (non)existence of undesirable equilibria of Godard blind equalizers," *IEEE Transactions on Signal Processing*, vol. 40, pp. 2425–2432, October 1992.

[461] Y. Li, K. Liu, and Z. Ding, "Length -and cost- dependent local minima of unconstrained blind channel equalizers," *IEEE Transactions on Signal Processing*, vol. 44, pp. 2726–2735, November 1996.

[462] Z. Ding, R. Kennedy, B. Anderson, and R. Johnson Jr., "Local convergence of the Sato blind equalizer and generalizations under practical constraints," *IEEE Transactions on Information Theory*, vol. 39, pp. 129–144, January 1993.

[463] Z. Ding and R. Kennedy, "On the whereabouts of local minima for blind adaptive equalizers," *IEEE Transactions on Circuits and Systems II: Analog and Digital Signal Processing*, vol. 39, pp. 119–123, February 1992.

[464] Z. Ding and R. Johnson Jr., "On the nonvanishing stability of undesirable equilibria for FTR Godard blind equalizers," *IEEE Transactions on Signal Processing*, vol. 41, pp. 1940–1944, May 1993.

[465] Y. Li and Z. Ding, "Convergence analysis of finite length blind adaptive equalizers," *IEEE Transactions on Signal Processing*, vol. 43, pp. 2120–2129, September 1995.

[466] H. Zeng, L. Tong, and C. Johnson, "Relationships between the constant modulus and Wiener receivers," *IEEE Transactions on Information Theory*, vol. 44, pp. 1523–1539, July 1998.

[467] P. Regalia and M. Mboup, "Undermodeled equalization: A characterization of stationary points for a family of blind criteria," *IEEE Transactions on Signal Processing*, vol. 47, pp. 760–770, March 1999.

[468] M. Gu and L. Tong, "Geometrical characterizations of constant modulus receivers," *IEEE Transactions on Signal Processing*, vol. 47, pp. 2745–2756, October 1999.

[469] Y. Li and K. Liu, "Static and dynamic convergence behaviour of adaptive blind equalizers," *IEEE Transactions on Signal Processing*, vol. 44, pp. 2736–2745, November 1996.

[470] V. Weerackody, S. Kassam, and K. Laker, "Convergence analysis of an algorithm for blind equalization," *IEEE Transactions on Communications*, vol. 39, pp. 856–865, June 1991.

[471] W. Lee and K. Cheun, "Convergence analysis of the stop-and-go blind equalization algorithm," *IEEE Transactions on Communications*, vol. 47, pp. 177–180, February 1999.

[472] Y. Li and Z. Ding, "Global convergence of fractionally spaced Godard (CMA) adaptive equalizers," *IEEE Transactions on Signal Processing*, vol. 44, pp. 818–826, April 1996.

[473] Z. Ding, "On convergence analysis of fractionally spaced adaptive blind equalizers," *IEEE Transactions on Signal Processing*, vol. 45, pp. 650–657, March 1997.

[474] J. J. Shynk and C. K. Chan, "Performance surfaces of the constant modulus algorithm based on a conditional gaussian model," *IEEE Transactions on Signal Processing*, vol. 41, pp. 1965–1969, May 1993.

[475] S. Douglas, A. Cichocki, and S. Amari, "Fast-convergence filtered regressor algorithms for blind equalisation," *Electronics Letters*, vol. 32, pp. 2114–2115, November 1996.

[476] C. Papadias and D. Slock, "Normalized sliding window constant modulus (CM) and decision-directed algorithms: a link between blind equalization and classical adaptive filtering," *IEEE Transactions on Signal Processing*, vol. 45, pp. 231–235, January 1997.

[477] J. Anderson and S. Mohan, "Sequential coding algorithms: A survey and cost analysis," *IEEE Transactions on Communications*, vol. 32, pp. 1689–1696, February 1984.

[478] Z. Xie, C. Rushforth, R. Short, and T. Moon, "Joint signal detection and parameter estimation in multiuser communications," *IEEE Transactions on Communications*, vol. 41, pp. 1208–1216, August 1993.

[479] A. Papoulis, *Probability, Random Variables, and Stochastic Processes*. New York, USA: McGraw-Hill, 2nd ed., 1984.

[480] S. Haykin, *Communications Systems*. New York, USA: John Willey and Sons, 2nd ed., 1994.

[481] B. Noble and J. Daniel, *Applied Linear Algebra*. Englewood Cliffs, NJ, USA: Prentice-Hall, 3rd ed., 1986.

[482] D. Hatzinakos, "Blind equalization based on prediction and polycepstra principles," *IEEE Transactions on Communications*, vol. 43, pp. 178–181, February–April 1995.

[483] D. Hatzinakos, “Blind equalization using decision feedback prediction and tricepstrum principles,” *Signal Processing*, vol. 36, pp. 261–276, April 1994.

[484] A. Bessios and C. Nikias, “POTEA: the power cepstrum and tricoherence equalization algorithm,” *IEEE Transactions on Communications*, vol. 43, pp. 2667–2671, November 1995.

[485] A. Petropulu and C. Nikias, “Blind deconvolution of coloured signals based on higher–order cepstra and data fusion,” *IEE Proceedings, Part F: Radar and Signal Processing*, vol. 140, pp. 356–361, December 1993.

[486] G. Kechriotis, E. Zervas, and E. Manolakos, “Using recurrent neural networks for adaptive communication channel equalization,” *IEEE Transactions on Neural Networks*, vol. 5, pp. 267–278, March 1994.

[487] S. Amari and A. Cichocki, “Adaptive blind signal processing - neural network approaches,” *Proceedings of the IEEE*, vol. 86, pp. 2026–2048, October 1998.

[488] C. You and D. Hong, “Nonlinear blind equalization scheme using complex-valued multilayer feedforward neural networks,” *IEEE Transactions on Neural Networks*, vol. 9, pp. 1442–1455, November 1998.

[489] Y. Fang and T. Chow, “Blind equalization of a noisy channel by linear neural network,” *IEEE Transactions on Neural Networks*, vol. 10, no. 4, pp. 918–924, 1999.

[490] S. Choi. and A. Cichocki, “Cascade neural networks for multichannel blind deconvolution,” *Electronics Letters*, vol. 34, pp. 1186–1187, June 1998.

[491] S. Mo and B. Shafai, “Blind equalization using higher order cumulants and neural network,” *IEEE Transactions on Signal Processing*, vol. 42, pp. 3209–3217, November 1994.

[492] L. H. C.S. Lee, S. Vlahoyiannatos, “Satellite based turbo-coded, blind-equalised 4-QAM and 16-QAM digital video broadcasting,” *IEEE Transactions on Broadcasting*, vol. 46, pp. 23–34, March 2000.

[493] G. Forney Jr, R. Gallager, G. Lang, F. Longstaff, and S. Qureshi, “Efficient modulation for band-limited channels,” *IEEE Journal on Selected Areas in Communications*, vol. 2, pp. 632–647, September 1984.

[494] J. Massey, “Coding and modulation in digital communications,” in *Proceedings of International Zurich Seminar on Digital Communications 1994*, (Zurich, Switzerland), March 1974.

[495] H. Imai and S. Hirakawa, “A new multi-level coding method using error correcting codes,” *IEEE Transactions on Information Theory*, vol. 23, pp. 371–377, May 1977.

[496] G. Ungerböck, “Channel Coding with Multilevel/Phase Signals,” *IEEE Transactions on Information Theory*, vol. IT-28, pp. 55–67, January 1982.

[497] G. Ungerboeck, “Treliis-coded modulation with redundant signal sets part 1: Introduction,” *IEEE Communications Magazine*, vol. 25, pp. 5–11, February 1987.

[498] E. Biglieri and M. Luise, “Coded modulation and bandwidth-efficient transmission,” in *Proceedings of the Fifth Tirrenia Internatioanal Workshop*, (Netherlands), 8–12 September 1991.

[499] “Special issue on coded modulation,” *IEEE Communications Magazine*, vol. 29, December 1991.

[500] E. Biglieri, D. Divsalar, P. McLane, and M. Simon, *Introduction to trellis coded modulation with applications*. New York, USA: MacMillan Publishing Co., 1991.

[501] C. E. Shannon, *Mathematical Theory of Communication*. University of Illinois Press, 1963.

[502] J. Wozencraft and R. Kennedy, “Modulation and demodulation for probabilistic coding,” *IEEE Transactions on Information Theory*, vol. IT-12, pp. 291–297, 1966.

[503] J. Wozencraft and I. Jacobs, *Principles of communications engineering*. New York, USA: John Wiley, 1965.

[504] R. Blahut, *Theory and Practice of Error Control Codes*. Reading, MA, USA: Addison-Wesley, 1983. ISBN 0-201-10102-5.

[505] E. Berlekamp, *Algebraic Coding Theory*. New York, USA: McGraw-Hill, 1968.

[506] W. Peterson, *Error Correcting Codes*. Cambridge, MA, USA: MIT Press, 1st ed., 1961.

[507] A. Michelson and A. Levesque, *Error Control Techniques for Digital Communication*. New York, USA: John Wiley and Sons, 1985.

[508] K. Wong and L. Hanzo, “Channel coding,” in Steele and Hanzo [383], ch. 4, pp. 347–488.

[509] *International Consultative Committee for Telephone and Telegraph Recommendations*. Geneva. V.29 - V.33.

[510] L. Wei, "Rotationally-invariant convolutional channel coding with expanded signal space, part I and II," *IEEE Transactions on Selected Areas in Comms*, vol. SAC-2, pp. 659–686, September 1984.

[511] K. Shanmugam, *Digital and Analog Communications Systems*. New York, USA: John Wiley and Sons, 1979.

[512] W. Lee, *Mobile communications engineering*. New York, USA: McGraw-Hill, 1982.

[513] I. Gradshteyn and I. Ryzhik, *Table of integrals, series and products*. New York, USA: Academic Press, 1980.

[514] D. Yoon, D. Chang, N. Kim, and H. Woo, "Linear diversity analysis for M-ary square quadrature amplitude modulation over Nakagami fading channels," *ETRI Journal*, vol. 25, pp. 231–237, August 2003.

[515] P. Vitthaladevuni and M. Alouini, "A recursive algorithm for the exact BER computation of generalized hierarchical QAM constellations," *IEEE Transactions on Information Theroy*, vol. 49, pp. 297–307, January 2003.

[516] D. Y. K.K. Cho, "On the general BER expression of one- and two-dimensional amplitude modulations," *IEEE Transactions on Communications*, vol. 50, pp. 1074–1080, July 2002.

[517] P. Vitthaladevuni and M. Alouini, "BER computation of 4/M-QAM hierarchical constellations," *IEEE Transactions on Broadcasting*, vol. 47, pp. 228–239, September 2001.

[518] G. Saulnier and W. Raffety, "Pilot-aided modulation for narrowband satellite communications," in *Procedings of Mobile Satellite Conference*, pp. 329–336, 1988.

[519] A. Bateman and J. McGeehan, "Feedforward transparent tone in band for rapid fading protection in multipath fading," in *IEE International Conference on Communications*, vol. 68, pp. 9–13, 1986.

[520] A. Bateman and J. McGeehan, "The use of transparent tone in band for coherent data schemes," in *IEEE International Conference on Communications*, (Boston, MA, USA), 1983.

[521] A. Bateman, G. Lightfoot, A. Lymer, and J. McGeehan, "Speech and data transmissions over a 942MHz TAB and TTIB single sideband mobile radio system," *IEEE Transactions on Vehicular Technology*, vol. VT-34, pp. 13–21, February 1985.

[522] A. Bateman and J. McGeehan, "Data transmissions over UHF fading mobile radio channels," *Proceedings of IEE*, vol. 131, no. Pt.F, pp. 364–374, 1984.

[523] J. McGeehan and A. Bateman, "A simple simultaneous carrier and bit synchronisation system for narrowband data transmissions," *Proceedings of IEE*, vol. 132, no. Pt.F, pp. 69–72, 1985.

[524] J. McGeehan and A. Bateman, "Theoretical and experimental investigation of feedforward signal regeneration," *IEEE Transactions on Vehicular Technology*, vol. VT-32, pp. 106–120, 1983.

[525] A. Bateman, "Feedforward transparent tone in band: Its implementation and applications," *IEEE Transactions on Vehicular Technology*, vol. 39, pp. 235–243, August 1990.

[526] M. Simon, "Dual pilot tone calibration technique," *IEEE Transactions on Vehicular Technology*, vol. VT-35, pp. 63–70, May 1986.

[527] M. Fitz, "A dual-tone reference digital demodulator for mobile communications," *IEEE Transactions on Vehicular Technology*, vol. VT-42, pp. 156–166, May 1993.

[528] S. Gamnathan and K. Feher, "Pilot tone aided QPRS systems for digital audio broadcasting," *IEEE Transactions on Broadcasting*, vol. 38, pp. 1–6, March 1992.

[529] F. Davarrin, "Mobile digital communications via tone calibration," *IEEE Transactions on Vehicular Technology*, vol. VT-36, pp. 55–62, May 1987.

[530] J. Cavers, "The performance of phase locked transparent tone in band with symmetric phase detection," *IEEE Transactions on Communications*, vol. 39, pp. 1389–1399, September 1991.

[531] J. Cavers, "Performance of tone calibration with frequency offset and imperfect pilot filter," *IEEE Transactions on Vehicular Technology*, vol. 40, pp. 426–434, May 1991.

[532] P. Martin and A. Bateman, "Practical results for a modem using linear mobile radio channels," in *Proceedings of IEEE Vehicular Technology Conference (VTC'91)*, (St. Louis, MO, USA), pp. 386–392, IEEE, 19–22 May 1991.

[533] D. Esteban and C. Galand, "Application of quadrature mirror filters to split band voice coding scheme," in *Proceedings of International Conference on Acoustics, Speech, and Signal Processing, ICASSP'77*, (Hartford, CT, USA), pp. 191–195, IEEE, 9–11 May 1977.

[534] J. Johnston, “A filter family designed for use in quadrature mirror filter banks,” in *Proceedings of International Conference on Acoustics, Speech, and Signal Processing, ICASSP’80*, (Denver, CO, USA), pp. 291–294, IEEE, 9–11 April 1980.

[535] J. Lodge and M. Moher, “Time diversity for mobile satellite channels using trellis coded modulations,” in *IEEE Global Telecommunications Conference*, (Tokyo, Japan), 1987.

[536] S. Sampei and T. Sunaga, “Rayleigh fading compensation method for 16-QAM in digital land mobile radio channels,” in *Proceedings of IEEE Vehicular Technology Conference (VTC’89)*, (San Francisco, CA, USA), pp. 640–646, IEEE, 1–3 May 1989.

[537] J. Cavers, “Pilot symbol assisted modulation in fading and delay spread,” in *Proceedings of IEEE VTC ’93*, (Secaucus, NJ, USA), pp. 13–16, IEEE, 18–20 May 1993.

[538] M. F. J.P. Seymour, “Improved carrier synchronisation techniques for mobile communications,” in *Proceedings of IEEE VTC ’93*, (Secaucus, NJ, USA), pp. 901–904, IEEE, 18–20 May 1993.

[539] AT&T Information Services, *A trellis coded modulation scheme that includes differential encoding for 9600 bit/sec full-duplex,two-wire modems*, August 1983. CCITT SG XVII.

[540] R. Salami, L. Hanzo, R. Steele, K. Wong, and I. Wassell, “Speech coding,” in Steele and Hanzo [383], ch. 3, pp. 186–346.

[541] K. Larsen, “Short convolutional codes with maximal free distance for rate 1/2, 1/3 and 1/4,” *IEEE Transactions on Information Theory*, vol. IT-19, pp. 371–372, May 1973.

[542] K. Wong, L. Hanzo, and R. Steele, “Channel coding for satellite mobile channels,” *International Journal on Satellite Communications*, vol. 7, pp. 143–163, July–September 1989.

[543] P. Ho, J. Cavers, and J. Varaldi, “The effect of constellation density on trellis coded modulation in fading channels,” in *Proceedings of IEEE VTC ’92*, (Denver, CO, USA), pp. 463–467, IEEE, 10–13 May 1992.

[544] S. Fechtel and H. Meyr, “Combined equalisation, decoding and antenna diversity combining for mobile personal digital radiotransmission using feedforward synchronisation,” in *Proceedings of IEEE VTC ’93*, (Secaucus, NJ, USA), IEEE, 18–20 May 1993.

[545] R. Bultitude and G. Bedal, “Propagation characteristics on microcellular urban mobile radio channels at 910MHz,” *IEEE Journal on Selected Areas in Communications*, vol. 7, pp. 31–39, January 1989.

[546] R. Bultitude, S. Mahmoud, and W. Sullivan, “A comparison of indoor radio propagation characteristics at 910MHz and 1.75GHz,” *IEEE Journal on Selected Areas in communications*, vol. 7, pp. 20–30, January 1989.

[547] H. Harmuth, *Transmission of Information by Orthogonal Time Functions*. Berlin: Springer Verlag, 1969.

[548] H. Harmuth, “On the transmission of information by orthogonal time functions,” *AIEE*, July 1960.

[549] H. Harmuth, “Die orthogonalteilung als verallgemeinerung der zeit- und frequenzteilung,” *AEÜ*, vol. 18, pp. 43–50, 1964.

[550] D. Saha and T. Birdsall, “Quadrature-quadrature phase shift keying,” *IEEE Transactions on Communications*, vol. 37, pp. 437–448, May 1989.

[551] C. E. Shannon, “A mathematical theory of communication,” *Bell System Technical Journal*, vol. 27, pp. 379–423 and 623–656, June and October 1948.

[552] H. Landau and H. Pollak, “Prolate spheroidal wave functions...,” *Bell Systems Technical Journal*, vol. 41, pp. 1295–1336, July 1962.

[553] W. Lee, “Spectrum efficiency in cellular,” *IEEE Transactions on Vehicular Technology*, vol. 38, pp. 69–75, May 1989.

[554] H. Kolb Private Communications.

[555] J. Lindner Private Communications.

[556] D. Schnidman, “A generalized nyquist criterion and an optimum linear receiver for a pulse modulation system,” *Bell Systems Technical Journal*, pp. 2163–2177, November 1967.

[557] W. V. Etten, “An optimum linear receiver for multiple channel digital transmission systems,” *IEEE Transactions on Communications*, vol. COM-23, pp. 828–834, August 1975.

[558] A. Kaye and D. George, "Transmission of multiplexed PAM signals over multiple channel and diversity systems," *IEEE Tranactions on Communications Technology*, vol. COM-18, pp. 520–525, October 1970.

[559] M. Aaron and D. Tufts, "Intersymbol interference and error probability," *IEEE Transactions on Information Theory*, vol. IT-12, pp. 26–34, January 1966.

[560] D. Tufts, "Nyquist's problem: The joint optimization of transmitter and receiver in pulse amplitude modulation," *Proceedings of IEEE*, vol. 53, pp. 248–259, March 1965.

[561] H. Schüssler, *Digitale Systeme zur Signalverarbeitung*. Berlin, Heidelberg, and New York: Springer Verlag, 1974.

[562] R. O'Neill and L. Lopes, "Performance of amplitude limited multitone signals," in *Proceedings of IEEE VTC '94*, (Stockholm, Sweden), IEEE, 8–10 June 1994.

[563] X. Li and L. Cimini, "Effects of clipping and filtering on the performance of OFDM," in *Proceedings of IEEE VTC'97*, (Phoenix, AZ, USA), pp. 1634–1638, IEEE, 4–7 May 1997.

[564] A. Garcia and M. Calvo, "Phase noise and sub–carrier spacing effects on the performance of an OFDM communications system," *IEEE Communications Letters*, vol. 2, pp. 11–13, January 1998.

[565] W. Robins, *Phase Noise in signal sources*, vol. 9 of *IEE Telecommunication series*. Peter Peregrinus Ltd., 1982.

[566] C. Tellambura, Y. Guo, and S. Barton, "Equaliser performance for HIPERLAN in indoor channels," *Wireless Personal Communications*, vol. 3, no. 4, pp. 397–410, 1996.

[567] T. Ojanperä, M. Gudmundson, P. Jung, J. Sköld, R. Pirhonen, G. Kramer, and A. Toskala, "FRAMES: - hybrid multiple access technology," in *Proceedings of IEEE ISSSTA'96*, (Mainz, Germany), pp. 334–338, IEEE, September 1996.

[568] M. Failli, "Digital land mobile radio communications COST 207," tech. rep., European Commission, 1989.

[569] J. Torrance and L. Hanzo, "Comparative study of pilot symbol assisted modem schemes," in *Proceedings of IEE Conference on Radio Receivers and Associated Systems (RRAS'95)*, pp. 36–41, September 1995.

[570] K. Fazel, S. Kaiser, P. Robertson, and M. Ruf, "A concept of digital terrestrial television broadcasting," *Wireless Personal Communications*, vol. 2, pp. 9–27, 1995.

[571] J. Kuronen, V.-P. Kaasila, and A. Mammela, "An all-digital symbol tracking algorithm in an OFDM system by using the cyclic prefix," in *Proc. ACTS Summit '96*, (Granada, Spain), pp. 340–345, 27–29 November 1996.

[572] M. Kiviranta and A. Mammela, "Coarse frame synchronization structures in OFDM," in *Proc. ACTS Summit '96*, (Granada, Spain), pp. 464–470, 27–29 November 1996.

[573] Z. Li and A. Mammela, "An all digital frequency synchronization scheme for OFDM systems," in *Proceedings of the IEEE International Symposium on Personal, Indoor and Mobile Radio Communications (PIMRC)*, (Helsinki, Finland), pp. 327–331, 1–4 September 1997.

[574] J. Bingham, "Method and apparatus for correcting for clock and carrier frequency offset, and phase jitter in multicarrier modems." U.S. Patent No. 5206886, 27 April 1993.

[575] T. de Couasnon, R. Monnier, and J. Rault, "OFDM for digital TV broadcasting," *Signal Processing*, vol. 39, pp. 1–32, 1994.

[576] P. Mandarini and A. Falaschi, "SYNC proposals." MEDIAN Design Note, January 1996.

[577] T. Keller and L. Hanzo, "Orthogonal frequency division multiplex synchronisation techniques for wireless local area networks," in *Proceedings of IEEE International Symposium on Personal, Indoor, and Mobile Radio Communications (PIMRC'96)*, vol. 3, (Taipei, Taiwan), pp. 963–967, IEEE, 15–18 October 1996.

[578] S.-G. Chua and A. Goldsmith, "Variable-rate variable-power mQAM for fading channels," in *Proceedings of IEEE VTC'96*, (Atlanta, GA, USA), pp. 815–819, IEEE, 28 April–1 May 1996.

[579] J. Torrance, *Adaptive Full Response Digital Modulation for Wireless Communications Systems*. PhD thesis, Department of Electronics and Computer Science, University of Southampton, UK, 1997.

[580] K. Miya, O. Kato, K. Homma, T. Kitade, M. Hayashi, and T. Ue, "Wideband CDMA systems in TDD-mode operation for IMT-2000," *IEICE Transactions on Communications*, vol. E81-B, pp. 1317–1326, July 1998.

[581] O. Kato, K. Miya, K. Homma, T. Kitade, M. Hayashi, and M. Watanabe, "Experimental performance results of coherent wideband DS-CDMA with TDD scheme," *IEICE Transactions on Communications.*, vol. E81-B, pp. 1337–1344, July 1998.

[582] T. Keller and L. Hanzo, "Blind-detection assisted sub-band adaptive turbo-coded OFDM schemes," in *Proceeding of VTC'99 (Spring)*, (Houston, TX, USA), pp. 489–493, IEEE, 16–20 May 1999.

[583] L.R. Bahl and J. Cocke and F. Jelinek and J. Raviv, "Optimal Decoding of Linear Codes for Minimising Symbol Error Rate," *IEEE Transactions on Information Theory*, vol. 20, pp. 284–287, March 1974.

[584] T. Keller, M. Muenster, and L. Hanzo, "A burst–by–burst adaptive OFDM wideband speech transceiver." submitted to IEEE JSAC, 1999.

[585] T. Keller, J. Woodard, and L. Hanzo, "Turbo-coded parallel modem techniques for personal communications," in *Proceedings of IEEE VTC'97*, (Phoenix, AZ, USA), pp. 2158–2162, IEEE, 4–7 May 1997.

[586] T. Keller and L. Hanzo, "Adaptive orthogonal frequency division multiplexing schemes," in *Proceeding of ACTS Mobile Communication Summit '98*, (Rhodes, Greece), pp. 794–799, ACTS, 8–11 June 1998.

[587] C. E. Shannon, "Communication in the presence of noise," *Proceedings of the I.R.E.*, vol. 37, pp. 10–22, January 1949.

[588] L. Piazzo, "A fast algorithm for near-optimum power and bit allocation in OFDM systems." to appear in Electronics Letters, December 1999.

[589] T. Willink and P. Wittke, "Optimization and performance evaluation of multicarrier transmission," *IEEE Transactions on Information Theory*, vol. 43, pp. 426–440, March 1997.

[590] R. Fischer and J. Huber, "A new loading algorithm for discrete multitone transmission," in *Proceeding of IEEE Global Telecommunications Conference, Globecom 96*, (London, UK), pp. 713–718, IEEE, 18–22 November 1996.

[591] S. Lai, R. Cheng, K. Letaief, and R. Murch, "Adaptive trellis coded mqam and power optimization for ofdm transmission," in *Proceeding of VTC'99 (Spring)*, (Houston, TX, USA), IEEE, 16–20 May 1999.

[592] D. Hughes-Hartogs, "Ensemble modem structure for imperfect transmission media." U.S Patents Nos. 4,679,227 (July 1988) 4,731,816 (March 1988) and 4,833,796 (May 1989).

[593] J. Bingham, "Multicarrier modulation for data transmission: an idea whose time has come," *IEEE Communications Magazine*, pp. 5–14, May 1990.

[594] L. Godara, "Applications of antenna arrays to mobile communications, part II: Beam-forming and direction-of-arrival considerations," *Proceedings of the IEEE*, vol. 85, pp. 1193–1245, August 1997.

[595] Y. Li, "Pilot-symbol-aided channel estimation for OFDM in wireless systems," in *Proceeding of VTC'99 (Spring)*, (Houston, TX, USA), IEEE, 16–20 May 1999.

[596] N. Szabo and R. Tanaka, *Residue Arithmetic and Its Applications to Computer Technology*. New York, USA: McGraw-Hill, 1967.

[597] R. Watson and C. Hastings, "Self-checked computation using residue arithmetic," *Proceedings of the IEEE*, vol. 54, pp. 1920–1931, December 1966.

[598] R. Pyndiah, "Iterative decoding of product codes: Block turbo codes," in ISTC'97 [367], pp. 71–79.

[599] P. Adde, R. Pyndiah, O. Raoul, and J.-R. Inisan, "Block turbo decoder design," in Copied [367], pp. 166–169.

[600] W. Jenkins and B. Leon, "The use of residue number system in the design of finite impulse response filters," *IEEE Transactions on Circuits Systems*, vol. CAS-24, pp. 191–201, April 1977.

[601] M. Soderstrand, "A high-speed, low-cost, recursive digital filter using residue number arithmetic," *Proceedings of IEEE*, vol. 65, pp. 1065–1067, July 1977.

[602] M. Soderstrand and E. Fields, "Multipliers for residue number arithmetic digital filters," *Electronics Letters*, vol. 13, pp. 164–166, March 1977.

[603] M. Soderstrand, W. Jenkins, and G. Jullien, *Residue Number System Arithmetic: Modern Applications in Digital Signal Processing*. New York, USA: IEEE Press, 1986.

[604] E. Claudio, G. Orlandi, and F. Piazza, "A Systolic Redundant Residue Arithmetic Error Correction Circuit," *IEEE Transactions on Computers*, vol. 42, pp. 427–432, April 1993.

[605] H. Krishna, K.-Y. Lin, and J.-D. Sun, “A coding theory approach to error control in redundant residue number systems - part I: theory and single error correction,” *IEEE Transactions on Circuits Systems*, vol. 39, pp. 8–17, January 1992.

[606] J.-D. Sun and H. Krishna, “A coding theory approach to error control in redundant residue number systems — part II: multiple error detection and correction,” *IEEE Transactions on Circuits Systems*, vol. 39, pp. 18–34, January 1992.

[607] T. Liew, L.-L. Yang, and L. Hanzo, “Soft-decision redundant residue number system based error correction coding,” in *Proceeding of VTC'99 (Fall)*, (Amsterdam, Netherlands), pp. 2974–2978, IEEE, 19–22 September 1999.

[608] L.-L. Yang and L. Hanzo, “Residue number system arithmetic assisted m-ary modulation,” *IEEE Communications Letters*, vol. 3, pp. 28–30, February 1999.

[609] L.-L. Yang and L. Hanzo, “Performance of residue number system based DS-CDMA over multipath fading channels using orthogonal sequences,” *ETT*, vol. 9, pp. 525–536, November–December 1998.

[610] H. Krishna and J.-D. Sun, “On theory and fast algorithms for error correction in residue number system product codes,” *IEEE Transactions on Comput.*, vol. 42, pp. 840–852, July 1993.

[611] D. Chase, “A class of algorithms for decoding block codes with channel measurement information,” *IEEE Transactions on Information Theory*, vol. IT-18, pp. 170–182, January 1972.

[612] J. Hagenauer, E. Offer, and L. Papke, “Iterative decoding of binary block and convolutional codes,” *IEEE Transactions on Information Theory*, vol. 42, pp. 429–445, March 1996.

[613] H. Nickl, J. Hagenauer, and F. Burkett, “Approaching shannon's capacity limit by 0.27 dB using simple hamming codes,” *IEEE Communications Letters*, vol. 1, pp. 130–132, September 1997.

[614] T. Liew, C. Wong, and L. Hanzo, “Block turbo coded burst-by-burst adaptive modems,” in *Proceedings of Microcoll'99, Budapest, Hungary*, pp. 59–62, 21–24 March 1999.

[615] B. Yeap, T. Liew, J. Hamorsky, and L. Hanzo, “Comparative study of turbo equalisers using convolutional codes and block-based turbo-codes for GMSK modulation,” in *Proceedings of VTC 1999 Fall*, (Amsterdam, Holland), pp. 2974–2978, 19-22 September 1999.

[616] C.H. Wong, T. H. Liew and L. Hanzo, “Burst-by-Burst Turbo Coded Wideband Adaptive Modulation with Blind Modem Mode Detection,” *Proceedings of 4th ACTS Mobile Communications Summit 1999, Sorrento, Italy*, pp. 303–308, 8–11 June 1999.

[617] S. M. Alamouti, “A Simple Transmit Diversity Technique for Wireless Communications,” *IEEE Journal on Selected Areas in Communications*, vol. 16, pp. 1451–1458, October 1998.

[618] H. J. V. Tarokh and A. Calderbank, “Space-time block codes from orthogonal designs,” *IEEE Transactions on Information Theory*, vol. 45, pp. 1456–1467, May 1999.

[619] V. Tarokh, H. Jafarkhani, and A. R. Calderbank, “Space-time block coding for wireless communications: Performance results,” *IEEE Journal on Selected Areas in Communications*, vol. 17, pp. 451–460, March 1999.

[620] V. Tarokh, N. Seshadri, and A. R. Calderbank, “Space-Time Codes for High Data Rate Wireless Communication: Performance Criterion and Code Construction,” *IEEE Transactions on Information Theory*, vol. 44, pp. 744–765, March 1998.

[621] N. Seshadri, V. Tarokh, and A. Calderbank, “Space-Time Codes for High Data Rate Wireless Communications: Code Construction,” in *Proceedings of IEEE Vehicular Technology Conference '97*, (Phoenix, Arizona), pp. 637–641, 1997.

[622] V. Tarokh and N. Seshadri and A. Calderbank, “Space-time codes for high data rate wireless communications: Performance criterion and code construction,” in *Proc IEEE International Conference on Communications '97*, (Montreal, Canada), pp. 299–303, 1997.

[623] N. S. V. Tarokh, A. Naguib and A. Calderbank, “Space-time codes for high data rate wireless communications: Mismatch analysis,” in *Proc IEEE International Conference on Communications '97*, (Montreal, Canada), pp. 309–313, 1997.

[624] A. F. Naguib, V. Tarokh, N. Seshadri, and A. R. Calderbank, “A Space-Time Coding Modem for High-Data-Rate Wireless Communications,” *IEEE Journal on Selected Areas in Communications*, vol. 16, pp. 1459–1478, October 1998.

[625] V. Tarokh, A. Naguib, N. Seshadri, and A. R. Calderbank, "Space-time codes for high data rate wireless communication: Performance criteria in the presence of channel estimation errors, mobility, and multile paths," *IEEE Transactions on Communications*, vol. 47, pp. 199–207, February 1999.

[626] R. Horn and C. Johnson, *Matrix Analysis*. New York: Cambridge University Press, 1988.

[627] A. Naguib and N. Seshdri and A. Calderbank, "Increasing Data Rate Over Wireless Channels: Space-Time Coding for High Data Rate Wireless Communications," *IEEE Signal Processing Magazine*, vol. 17, pp. 76–92, May 2000.

[628] G. Bauch, A. Naguib, and N. Seshadri, "MAP Equalization of Space-Time Coded Signals over Frequency Selective Channels," in *Proceedings of Wireless Communications and Networking Conference*, (New Orleans, USA), September 1999.

[629] G. Bauch and N. Al-Dhahir, "Reduced-complexity turbo equalization with multiple transmit and receive antennas over multipath fading channels," in *Proceedings of Information Sciences and Systems*, (Princeton, USA), pp. WP3 13–18, March 2000.

[630] D. Agrawal, V. Tarokh, A. Naguib, and N. Seshadri, "Space-time coded OFDM for high data-rate wireless communication over wideband channels," in *Proceedings of IEEE Vehicular Technology Conference*, (Ottawa, Canada), pp. 2232–2236, May 1998.

[631] Y. Li, N. Seshadri, and S. Ariyavisitakul, "Channel estimation for OFDM systems with transmitter diversity in mobile wireless channels," *IEEE Journal on Selected Areas in Communications*, vol. 17, pp. 461–471, March 1999.

[632] Y. Li, J. Chuang, and N. Sollenberger, "Transmitter diversity for OFDM systems and its impact on high-rate data wireless networks," *IEEE Journal on Selected Areas in Communications*, vol. 17, pp. 1233–1243, July 1999.

[633] W. Choi and J. Cioffi, "Space-Time Block Codes over Frequency Selective Fading Channels," in *Proceedings of VTC 1999 Fall*, (Amsterdam, Holland), pp. 2541–2545, 19-22 September 1999.

[634] Z. Liu, G. Giannakis, A. Scaglione, and S. Barbarossa, "Block precoding and transmit-antenna diversity for decoding and equalization of unknown multipath channels," in *Proc 33rd Asilomar Conference Signals, Systems and Computers*, (Pacific Grove, Canada), pp. 1557–1561, 1-4 November 1999.

[635] Z. Liu and G. Giannakis, "Space-time coding with transmit antennas for multiple access regardless of frequency-selective multipath," in *Proc 1st Sensor Array and Multichannel SP Workshop*, (Boston, USA), 15-17 March 2000.

[636] T. Liew, J. Pliquett, B. Yeap, L.-L. Yang, and L. Hanzo, "Comparative study of space time block codes and various concatenated turbo coding schemes," in *PIMRC 2000*, (London, UK), pp. 741–745, 18-21 September 2000.

[637] T. Liew, J. Pliquett, B. Yeap, L.-L. Yang, and L. Hanzo, "Concatenated space time block codes and TCM, turbo TCM, convolutional as well as turbo codes," in *GLOBECOM 2000*, (San Francisco, USA), 27 Nov -1 Dec 2000.

[638] P. Robertson and E. Villebrun and P. Höher, "A Comparison of Optimal and Sub-Optimal MAP Decoding Algorithms Operating in the Log Domain," in *Proceedings of the International Conference on Communications*, (Seattle, United States), pp. 1009–1013, June 1995.

[639] G. Bauch, "Concatenation of space-time block codes and Turbo-TCM," in *Proceedings of IEEE International Conference on Communications*, (Vancouver, Canada), pp. 1202–1206, June 1999.

[640] G. Forney, "The Viterbi algorithm," *Proceedings of the IEEE*, vol. 61, pp. 268–278, March 1973.

[641] W. Webb and R. Steele, "Variable rate QAM for mobile radio," *IEEE Transactions on Communications*, vol. 43, pp. 2223–2230, July 1995.

[642] J. Torrance and L. Hanzo, "Performance upper bound of adaptive QAM in slow Rayleigh-fading environments," in *Proceedings of IEEE ICCS'96/ISPACS'96*, (Singapore), pp. 1653–1657, IEEE, 25–29 November 1996.

[643] H. Matsuako, S. Sampei, N. Morinaga, and Y. Kamio, "Adaptive modulation systems with variable coding rate concatenated code for high quality multi-media communication systems," in *Proceedings of IEEE Vehicular Technology Conference*, (Atlanta, USA), pp. 487–491, April 1996.

[644] T. Keller and L. Hanzo, "Adaptive multicarrier modulation: A convenient framework for time-frequency processing in wireless communications," *Proceedings of the IEEE*, vol. 88, pp. 611–642, May 2000.

[645] J. Torrance and L. Hanzo, "On the upper bound performance of adaptive QAM in a slow Rayleigh fading," *IEE Electronics Letters*, pp. 169–171, April 1996.

[646] Ömer. F. Açikel and W. E. Ryan, "Punctured turbo-codes for BPSK/QPSK channels," *IEEE Transactions on Communications*, vol. 47, pp. 1315–1323, September 1999.

[647] L. Hanzo, "Bandwidth-efficient wireless multimedia communications," *Proceedings of the IEEE*, vol. 86, pp. 1342–1382, July 1998.

[648] S. Nanda, K. Balachandran, and S. Kumar, "Adaptation techniques in wireless packet data services," *IEEE Communications Magazine*, vol. 38, pp. 54–64, January 2000.

[649] T. Liew and L. Hanzo, "Space-time block coded adaptive modulation aided ofdm," in *Proceedings of GLOBE-COM'2001*, (San Antonio, USA), pp. 136–140, IEEE, 26-29 November 2001.

[650] T. Ottosson and A. Svensson, "On schemes for multirate support in DS-CDMA systems," *Wireless Personal Communications (Kluwer)*, vol. 6, pp. 265–287, March 1998.

[651] S. Spangenberg, D. Cruickshank, S. McLaughlin, G. Povey, and P. Grant, "Advanced multiuser detection techniques for downlink CDMA, version 2.0," tech. rep., Virtual Centre of Excellence in Mobile and Personal Communications Ltd (Mobile VCE), July 1999.

[652] S. Ramakrishna and J. Holtzman, "A comparison between single code and multiple code transmission schemes in a CDMA system," in *Proceedings of IEEE Vehicular Technology Conference (VTC'98)*, (Ottawa, Canada), pp. 791–795, IEEE, 18–21 May 1998.

[653] F. Adachi, K. Ohno, A. Higashi, T. Dohi, and Y. Okumura, "Coherent multicode DS-CDMA mobile Radio Access," *IEICE Transactions on Communications*, vol. E79-B, pp. 1316–1324, September 1996.

[654] T. Dohi, Y. Okumura, A. Higashi, K. Ohno, and F. Adachi, "Experiments on coherent multicode DS-CDMA," *IEICE Transactions on Communications*, vol. E79-B, pp. 1326–1332, September 1996.

[655] H. Schotten, H. Elders-Boll, and A. Busboom, "Adaptive multi-rate multi-code CDMA systems," in *Proceedings of the IEEE Vehicular Technology Conference (VTC)*, (Ottawa, Canada), pp. 782–785, 18–21 May 1998.

[656] M. Saquib and R. Yates, "Decorrelating detectors for a dual rate synchronous DS/CDMAchannel," *Wireless Personal Communications (Kluwer)*, vol. 9, pp. 197–216, May 1999.

[657] A.-L. Johansson and A. Svensson, "Successive interference cancellation schemes in multi-rateDS/CDMA systems," in *Wireless Information Networks (Baltzer)*, pp. 265–279, 1996.

[658] A. Johansson and A. Svensson, "Multistage interference cancellation in multirate DS/CDMA on a mobile radio channel," in *Proceedings of the IEEE Vehicular Technology Conference (VTC)*, (Atlanta, GA, USA), pp. 666–670, 28 April–1 May 1996.

[659] M. Juntti, "Multiuser detector performance comparisons inmultirate CDMA systems," in *Proceedings of the IEEE Vehicular Technology Conference (VTC)*, (Ottawa, Canada), pp. 36–40, 18–21 May 1998.

[660] S. Kim, "Adaptive rate and power DS/CDMA communications in fading channels," *IEEE Communications Letters*, vol. 3, pp. 85–87, April 1999.

[661] S. Abeta, S. Sampei, and N. Morinaga, "Channel activation with adaptive coding rate and processing gain control for cellular DS/CDMA systems," in *Proceedings of IEEE VTC'96*, (Atlanta, GA, USA), pp. 1115–1119, IEEE, 28 April–1 May 1996.

[662] M. Hashimoto, S. Sampei, and N. Morinaga, "Forward and reverse link capacity enhancement of DS/CDMA cellular system using channel activation and soft power control techniques," in *Proceedings of the IEEE International Symposium on Personal, Indoor and Mobile Radio Communications (PIMRC)*, (Helsinki, Finland), pp. 246–250, 1–4 September 1997.

[663] S. Tateesh, S. Atungsiri, and A. Kondoz, "Link adaptive multi-rate coding verification system for CDMA mobile communications," in *Proceedings of the IEEE Global Telecommunications Conference (GLOBECOM)*, (London, UK), pp. 1969–1973, 18–22 November 1996.

[664] Y. Okumura and F. Adachi, "Variable-rate data transmission with blind rate detection for coherent DS-CDMA mobile radio," *IEICE Transactions on Communications*, vol. E81B, pp. 1365–1373, July 1998.

[665] J. Blogh, P. Cherriman, and L. Hanzo, "Adaptive beamforming assisted dynamic channel allocation," in *Proceeding of VTC'99 (Spring)*, (Houston, TX, USA), pp. 199–203, IEEE, 16–20 May 1999.

[666] I. Jeong and M. Nakagawa, "A novel transmission diversity system in TDD-CDMA," *IEICE Transactions on Communications*, vol. E81-B, pp. 1409–1416, July 1998.

[667] M. S. Alouini, X. Tand, and A. J. Goldsmith, "An adaptive modulation scheme for simultaneous voice and data transmission over fading channels," *IEEE Journal on Selected Areas in Communications*, vol. 17, pp. 837–850, May 1999.

[668] D. Yoon, K. Cho, and J. Lee, "Bit error probability of M-ary Quadrature Amplitude Modulation," in *Proc. IEEE VTC 2000-Fall*, vol. 5, pp. 2422–2427, IEEE, September 2000.

[669] E. L. Kuan, C. H. Wong, and L. Hanzo, "Burst-by-burst adaptive joint-detection CDMA," in *Proc. of IEEE VTC'99 Fall*, vol. 2, (Amsterdam, Netherland), pp. 1628–1632, September 1999.

[670] M. Nakagami, "The m-distribution - A general formula of intensity distribution of rapid fading," in *Statistical Methods in Radio Wave Propagation* (W. C. Hoffman, ed.), pp. 3–36, Pergamon Press, 1960.

[671] I. S. Gradshteyn and I. M. Ryzhik, *Table of Integrals, Series and Products*. New York, USA: Academic Press, 1980.

[672] E. Kreyszig, *Advanced engineering mathematics*. John Wiley & Sons, Inc., 7th ed., 1993.

[673] J. Lu, K. B. Letaief, C. I. J. Chuang, and M. L. Lio, "M-PSK and M-QAM BER computation using signal-space concepts," *IEEE Transactions on Communications*, vol. 47, no. 2, pp. 181–184, 1999.

[674] T. Keller and L. Hanzo, "Adaptive modulation technique for duplex OFDM transmission," *IEEE Transactions on Vehicular Technology*, vol. 49, pp. 1893–1906, September 2000.

[675] G. S. G. Beveridge and R. S. Schechter, *Optimization: Theory and Practice*. McGraw-Hill, 1970.

[676] "COST 207 : Digital land mobile radio communications, final report," tech. rep., Luxembourg, 1989.

[677] R. Price and E. Green Jr., "A communication technique for multipath channels," *Proceedings of the IRE*, vol. 46, pp. 555–570, March 1958.

[678] M. K. Simon and M. S. Alouini, *Digital Communication over Fading Channels: A Unified Approach to Performance Analysis*. John Wiley & Sons, Inc., 2000. ISBN 0471317799.

[679] C. Y. Wong, R. S. Cheng, K. B. Letaief, and R. D. Murch, "Multiuser OFDM with adaptive subcarrier, bit, and power allocation," *IEEE Journal on Selected Areas in Communications*, vol. 17, pp. 1747–1758, October 1999.

[680] A. Klein, G. Kaleh, and P. Baier, "Zero forcing and minimum mean square error equalization for multiuser detection in code division multiple access channels," *IEEE Transactions on Vehicular Technology*, vol. 45, pp. 276–287, May 1996.

[681] B. J. Choi, T. H. Liew, and L. Hanzo, "Concatenated space-time block coded and turbo coded symbol-by-symbol adaptive OFDM and multi-carrier CDMA systems," in *Proceedings of IEEE VTC 2001-Spring*, p. P.528, IEEE, May 2001.

[682] B. Vucetic, "An adaptive coding scheme for time-varying channels," *IEEE Transactions on Communications*, vol. 39, no. 5, pp. 653–663, 1991.

[683] S. M. Alamouti and S. Kallel, "Adaptive Trellis-Coded Multiple-Phased-Shift Keying Rayleigh fading channels," *IEEE Transactions on Communications*, vol. 42, pp. 2305–2341, June 1994.

[684] S. Chua and A. Goldsmith, "Adaptive coded modulation for fading channels," *IEEE Transactions on Communications*, vol. 46, pp. 595–602, May 1998.

[685] T. Keller, T. Liew, and L. Hanzo, "Adaptive rate RRNS coded OFDM transmission for mobile communication channels," in *Proceedings of VTC 2000 Spring*, (Tokyo, Japan), pp. 230–234, 15-18 May 2000.

[686] T. Keller, T. H. Liew, and L. Hanzo, "Adaptive redundant residue number system coded multicarrier modulation," *IEEE Journal on Selected Areas in Communications*, vol. 18, pp. 1292–2301, November 2000.

[687] T. Liew, C. Wong, and L. Hanzo, "Block turbo coded burst-by-burst adaptive modems," in *Proceedings of Microcoll'99*, (Budapest, Hungary), pp. 59–62, 21-24 March 1999.

[688] C. Wong, T. Liew, and L. Hanzo, "Turbo coded burst by burst adaptive wideband modulation with blind modem mode detection," in *ACTS Mobile Communications Summit*, (Sorrento, Italy), pp. 303–308, 8-11 June 1999.

[689] C. Berrou and A. Glavieux, "Near optimum error correcting coding and decoding: Turbo codes," *IEEE Transactions on Communications*, vol. 44, pp. 1261–1271, October 1996.

[690] P. Jung and J. Blanz, "Joint detection with coherent receiver antenna diversity in CDMA mobile radio systems," *IEEE Transactions on Vehicular Technology*, vol. 44, pp. 76–88, February 1995.

[691] J. Wozencraft and B. Reiffen, *Sequential Decoding*. Cambridge, MA, USA: MIT Press, 1961.

[692] R. Gallager, *Information Theory and Reliable Communication*. John Wiley and Sons, 1968.

[693] S. G. Wilson, *Digital Modulation and Coding*. Englewood Cliffs, NJ, USA: Prentice-Hall International Editions, 1996.

[694] M. Campanella and G. Mamola, "On the channel capacity for constant envelope signals with effective bandwidth constraint," *IEEE Transactions on Communications*, vol. 38, pp. 1164–1172, August 1990.

[695] P. E. McIllree, "Channel capacity calculations for m-ary n-dimensional signal sets," M.Eng thesis, The University of South Australia, 1995.

[696] P. E. McIllree, "Calculation of channel capacity for m-ary digital modulation signal sets," in *IEEE Singapore International Conference on Information Engineering*, (Singapore), pp. 639–643, September 1993.

[697] G. J. Foschini and M. J. Gans, "On limits of wireless communications in a fading environment when using multiple antennas," *Wireless Personal Communications*, vol. 6, pp. 311–335, March 1998.

[698] I. S. Reed and R. A. Scholtz, "N-orthogonal phase modulated codes," *IEEE Transactions on Information Theory*, vol. 12, pp. 388–395, July 1966.

[699] W. C. Lindsey, M. K. Simon, "L-orthogonal signal transmission and detection," *IEEE Transactions on Communications*, vol. COM-20, pp. 953–960, October 1972.

[700] A. Viterbi and J. Omura, *Principles of Digital Communication and Coding*. New York, USA: McGraw-Hill, 1979.

[701] C. Schlegel and D. J. Costello, "Bandwidth Efficient Coding for Fading Channels: Code Construction and Performance Analysis," *IEEE Journal on Selected Areas in Communications*, vol. 7, pp. 1356–1368, December 1989.

[702] S. Al-Semari and T. Fuja, "Performance analysis of coherent tcm systems with diversity reception in slow rayleigh fading," *IEEE Transactions on Vehicular Technology*, vol. 48, pp. 198–212, January 1999.

[703] J. Ventura-Traveset, G. Caire, E. Biglieri and G. Taricco, "Impact of diversity reception on fading channels with coded modulation–part i: Coherent detection," *IEEE Transactions on Communications*, vol. 45, pp. 563–572, May 1997.

[704] D. Divsalar and M.K. Simon, "Trellis Coded Modulation for 4800-9600 bits/s Transmission over a Fading Mobile Satellite Channel," *IEEE Journal on Selected Areas in Communications*, vol. 5, pp. 162–175, February 1987.

[705] R. E. Blahut, *Principles and Practice of Information Theory*. Reading, MA, USA: Addison-Wesley, 1987.

[706] L. Hanzo and L-L. Yang, E. L. Kuan and K. Yen, *Single- and Multi-Carrier CDMA*. New York, USA: John Wiley, IEEE Press, 2003.

[707] M. Kanefsky, *Communication Techniques for Digital and Analog Signals*. New York, USA: John Wiley, 1987.

[708] D. Divsalar and M. K. Simon, "The design of trellis coded MPSK for fading channel: Performance criteria," *IEEE Transactions on Communications*, vol. 36, pp. 1004–1012, September 1988.

[709] P. Robertson, T. Wörz, "Bandwidth-Efficient Turbo Trellis-Coded Modulation Using Punctured Component Codes," *IEEE Journal on Selected Areas in Communications*, vol. 16, pp. 206–218, February 1998.

[710] X. Li and J.A. Ritcey, "Bit-interleaved coded modulation with iterative decoding," *IEEE Communications Letters*, vol. 1, November 1997.

[711] X. Li and J.A. Ritcey, "Bit-interleaved coded modulation with iterative decoding — Approaching turbo-TCM performance without code concatenation," in *Proceedings of CISS 1998*, (Princeton University, USA), March 1998.

[712] S. X. Ng, T. H. Liew, L-L. Yang and L. Hanzo, "Comparative Study of TCM, TTCM, BICM and BICM-ID schemes," in *IEEE Vehicular Technology Conference*, (Rhodes, Greece), pp. 2450–2454, May 2001.

[713] C. S. Lee, S. X. Ng, L. Piazzo and L. Hanzo, "TCM, TTCM, BICM and Iterative BICM Assisted OFDM-Based Digital Video Broadcasting to Mobile Receivers," in *IEEE Vehicular Technology Conference*, (Rhodes, Greece), pp. 732–736, May 2001.

[714] J.-H. Chen and A. Gersho, "Gain-adaptive vector quantization with application to speech coding," *IEEE Transactions on Communications*, vol. 35, pp. 918–930, September 1987.

[715] R. Blahut, *Theory and Practice of Error Control Codes*, ch. 6, pp. 130–160. IBM Corporation, Owego, NY 13827, USA: Addison-Wesley Publishing Company, 1983.

[716] S. S. Pietrobon, G. Ungerböck, L. C. Perez and D. J. Costello, "Rotationally invariant nonlinear trellis codes for two-dimensional modulation," *IEEE Transactions on Information Theory*, vol. IT-40, pp. 1773–1791, November 1994.

[717] C. Schlegel, "Chapter 3: Trellis Coded Modulation," in *Trellis Coding*, (New York), pp. 43–89, IEEE Press, September 1997.

[718] J. K. Cavers and P. Ho, "Analysis of the Error Performance of Trellis-Coded Modulations in Rayleigh-Fading Channels," *IEEE Transactions on Communications*, vol. 40, pp. 74–83, January 1992.

[719] J. Du, B. Vucetic and L. Zhang, "Construction of New MPSK Trellis Codes for Fading Channels," *IEEE Transactions on Communications*, vol. 43, pp. 776–784, February/March/April 1995.

[720] G. D. Forney, "The Viterbi ALgorithm," in *Proceedings of the IEEE*, vol. 61, pp. 268–277, March 1973.

[721] L. Piazzo, "TTCM-OFDM over Wideband Fading Channels," tech. rep., University of Southampton, December 1999.

[722] J. G. Proakis, "Optimum Receivers for the Additive White Gaussian Noise Channel," in *Digital Communication*, (New York), pp. 260–274, September 1995.

[723] K. Abend and B. D. Fritchman, "Statistical detection for communication channels with intersymbol interference," *Proceedings of the IEEE*, vol. 58, pp. 779–785, May 1970.

[724] L. Piazzo, "An algorithm for SBS Receivers/Decoders," *IEE Electronics Letters*, vol. 32, pp. 1058–1060, Jun 1996.

[725] S.S. Pietrobon, R.H. Deng, A. Lafanechére, G. Ungerböck and D.J. Costello, "Trellis-Coded Multidimensional Phase Modulation," *IEEE Transactions on Information Theory*, vol. 36, pp. 63–89, January 1990.

[726] L.-F. Wei, "Trellis-coded modulation with multidimensional constellations," *IEEE Transactions on Information Theory*, vol. IT-33, pp. 483–501, July 1987.

[727] P. Robertson, "An Overview of Bandwidth Efficient Turbo Coding Schemes," in ISTC'97 [367], pp. 103–110.

[728] S. Lin and D. Constello Jr., *Error Control Coding: Fundamentals and Applications*. Englewood Cliffs, NJ, USA: Prentice-Hall, October 1982. ISBN: 013283796X.

[729] J. Hagenauer, "Rate-compatible puncture convolutional codes (RCPC) and their application," *IEEE Transactions on Communications*, vol. 36, pp. 389–400, April 1988.

[730] L. Lee, "New rate-compatible puncture convolutional codes for viterbi decoding," *IEEE Transactions on Communications*, vol. 42, pp. 3073–3079, December 1994.

[731] S. Benedetto, D. Divsalar, G. Montorsi and F. Pollara, "A Soft-Input Soft-Output APP Module for Iterative Decoding of concatenated codes," *IEEE Communications Letter*, vol. 1, pp. 22–24, January 1997.

[732] L. Piazzo and L. Hanzo, "TTCM-OFDM over Dispersive Fading Channels," *IEEE Vehicular Technology Conference*, vol. 1, pp. 66–70, May 2000.

[733] R.F.H. Fischer, L.H.-J. Lampe and S.H. Muller-Weinfurtner, "Coded modulation for noncoherent reception with application to OFDM," *IEEE Transactions on Vehicular Technology*, vol. 50, pp. 74–88, January 2001.

[734] C. Douillard, A. Picart, M. Jézéquel, P. Didier, C. Berrou, and A. Glavieux, "Iterative correction of intersymbol interference: Turbo-equalization," *European Transactions on Communications*, vol. 6, pp. 507–511, 1995.

[735] B. L. Yeap, T. H. Liew and L. Hanzo, "Turbo Equalization of Serially Concatenated Systematic Convolutional Codes and Systematic Space Time Trellis Codes," *IEEE Vehicular Technology Conference*, p. 119 (CDROM), May 2001.

[736] L. Hanzo and C. H. Wong and M. S. Yee, *Adaptive Wireless Transceivers: Turbo-Coded, Turbo-Equalized and Space-Time Coded TDMA, CDMA and OFDM Systems.* New York, USA: John Wiley, IEEE Press, 2002.

[737] S. Chen, S. McLaughlin, and B. Mulgrew, "Complex-valued radial basis function network, Part II: Application to digital communications channel equalisation," *EURASIP Signal Processing*, vol. 36, pp. 175–188, March 1994.

[738] J. G. Proakis, "Chapter 10: Communication Through Band-Limited Channels," in *Digital Communications*, (New York), pp. 583–635, McGraw-Hill International Editions, 3rd Edition, September 1995.

[739] C. H. Wong, *Wideband Adaptive Full Response Multilevel Transceivers and Equalizers*. PhD thesis, University of Southampton, United Kingdom, November 1999.

[740] D.F. Mix, *Random Signal Processing*. Englewood Cliffs NJ, USA: Prentice-Hall, 1995.

[741] S. Sampei and S. Komaki and N. Morinaga, "Adaptive Modulation/TDMA Scheme for large capacity personal Multi-Media Communication Systems," *IEICE Transactions on Communications (Japan)*, vol. E77-B, pp. 1096–1103, September 1994.

[742] J.M. Torrance and L. Hanzo, "Interference Aspects of adaptive modems over slow Rayleigh fading channels," *IEEE Vehicular Technology Conference*, vol. 48, pp. 1527–1545, September 1999.

[743] V.K.N. Lau and M.D. Macleod, "Variable rate adaptive trellis coded QAM for flat-fading channels," *IEEE Transactions on Communications*, vol. 49, pp. 1550–1560, September 2001.

[744] A.J. Goldsmith and S. Chua, "Adaptive Coded Modulation for fading channels," *IEEE Transactions on Communications*, vol. 46, pp. 595–602, May 1998.

[745] P. Ormeci, X. Liu, D. Goeckel and R. Wesel, "Adaptive bit-interleaved coded modulation," *IEEE Transactions on Communications*, vol. 49, pp. 1572–1581, September 2001.

[746] V.K.N. Lau, "Performance analysis of variable rate: symbol-by-symbol adaptive bit interleaved coded modulation for Rayleigh fading channels," *IEEE Transactions on Vehicular Technology*, vol. 51, pp. 537–550, May 2002.

[747] S. Falahati, *Adaptive Modulation and Coding in Wireless Communications with Feedback.* PhD thesis, Communication Systems Group, Department of Signals and Systems, School of Electrical and Computer Engineering, Chalmers University of Technology, Sweden, 2002.

[748] "COST 207: Digital land mobile radio communications, final report." Office for Official Publications of the European Communities, 1989. Luxembourg.

[749] A. Klein and R. Pirhonen and J. Skoeld and R. Suoranta, "FRAMES Multiple Access MODE 1 — Wideband TDMA with and without Spreading," in *Proceedings of the IEEE International Symposium on Personal, Indoor and Mobile Radio Communications (PIMRC)*, vol. 1, (Helsinki, Finland), pp. 37–41, 1–4 September 1997.

[750] G. Bauch, H. Khorram, and J. Hagenauer, "Iterative equalization and decoding in mobile communications systems," in *European Personal Mobile Communications Conference*, (Bonn, Germany), pp. 301–312, 30 September - 2 October 1997.

[751] G. J. Gibson, S. Siu, and C. F. N. Cowan, "The application of nonlinear structures to the reconstruction of binary signals," *IEEE Transactions on Signal Processing*, vol. 39, pp. 1877–1884, August 1991.

[752] S. Chen, G. J. Gibson, and C. F. N. Cowan, "Adaptive channel equalisation using a polynomial-perceptron structure," *IEE Proceedings*, vol. 137, pp. 257–264, October 1990.

[753] H. L. V. Trees, *Detection, Estimation and Modulation Theory, Part 1.* New York: John Wiley and Sons, 1968.

[754] S. Chen, B. Mulgrew, and P. M. Grant, "A clustering technique for digital communications channel equalization using radial basis function networks," *IEEE Transactions on Neural Networks*, vol. 4, pp. 570–579, July 1993.

[755] S. Haykin, *Neural Networks: A Comprehensive Foundation*. Macmillan Publishing Company, 1994.

[756] S. K. Patra and B. Mulgrew, "Computational aspects of adaptive radial basis function equalizer design," in *IEEE International Symposium on Circuits and Systems, ISCAS'97*, vol. 1, pp. 521–524, IEEE, Piscataway, NJ, USA, June 1997.

[757] M. Gertsman and J. Lodge, "Symbol-by-symbol MAP demodulation of CPM and PSK signals on Rayleigh flat-fading channels," *IEEE Transactions on Communications*, vol. 45, pp. 788–799, July 1997.

[758] D. Raphaeli and Y. Zarai, "Combined turbo equalization and turbo decoding," *IEEE Communications Letters*, vol. 2, pp. 107–109, April 1998.

[759] A. Knickenberg, B. L. Yeap, J. Hamorsky, M. Breiling, and L. Hanzo, "Non-iterative joint channel equalisation and channel decoding," in *Proceedings of Globecom'99*, (Rio de Janeiro, Brazil), pp. 442–446, 5-9 December 1999.

[760] A. Glavieux, C. Laot, and J. Labat, "Turbo equalization over a frequency selective channel," in *Proceedings of the International Symposium on Turbo Codes*, (Brest, France), pp. 96–102, 3-5 September 1997.

[761] M. Yee and L. Hanzo, "Multi-level Radial Basis Function network based equalisers for Rayleigh channel," in *Proceeding of VTC'99 (Spring)*, (Houston, TX, USA), pp. 707–711, IEEE, 16–20 May 1999.

[762] S. Chen, B. Mulgrew, and S. McLaughlin, "Adaptive Bayesian equalizer with decision feedback," *IEEE Transactions on Signal Processing*, vol. 41, pp. 2918–2927, September 1993.

[763] E.-S. Chng, H. Yang, and W. Skarbek, "Reduced complexity implementation of Bayesian equaliser using local RBF network for channel equalisation problem," *Electronics Letters*, vol. 32, pp. 17–19, January 1996.

[764] M. S. Yee, T. H. Liew and L. Hanzo, "Burst-by-Burst Adaptive Turbo-Coded Radial Basis Function-Assisted Decision Feedback Equalization," *IEEE Transactions on Communications*, vol. 49, pp. 1935–1945, November 2001.

[765] B. L. Yeap, C. H. Wong, and L. Hanzo, "Reduced complexity in-phase/quadrature-phase turbo equalisation with iterative channel estimation," in *IEEE International Communications Conference 2001*, (Helsinki, Finland), pp. 1395–1399, 11-15 June 2001. Accepted for publication.

[766] E.L. Kuan and C.H. Wong and L. Hanzo, "Comparative study of joint-detection and interference cancellation based burst-by-burst adaptive CDMA schemes," in *Proceedings of the IEEE Vehicular Technology Conference (VTC Fall)*, (Amsterdam, The Netherlands), pp. 653–657, 19–22 September 1999.

[767] J. R. Foerster and L. B. Milstein, "Coded Modulation for a Coherent DS-CDMA System Employing an MMSE Receiver in a Fading Channel," *IEEE Transactions on Communications*, vol. 48, pp. 1909–1918, November 2000.

[768] D. E. Goldberg, *Genetic Algorithms in Search, Optimization, and Machine Learning*. Reading, Massachusetts: Addison-Wesley, 1989.

[769] K. Yen and L. Hanzo, "Hybrid genetic algorithm based multi-user detection schemes for synchronous CDMA systems," in *submitted to the IEEE Vehicular Technology Conference (VTC)*, (Tokyo, Japan), 2000.

[770] K. Yen and L. Hanzo, "Genetic Algorithm Assisted Joint Multiuser Symbol Detection and Fading Channel Estimation for Synchrono us CDMA Systems," *IEEE Journal on Selected Areas in Communications*, vol. 19, pp. 985–998, June 2001.

[771] S. Abedi and R. Tafazolli, "Genetically Modified Multiuser Detection for Code Division Multiple Access Systems," *IEEE Journal on Selected Areas in Communications*, vol. 20, pp. 463–473, February 2002.

[772] A. Whalen, *Detection of signals in noise*. New York, USA: Academic Press, 1971.

[773] E.A. Lee and D.G. Messerschmitt, *Digital Communication*. Dordrecht: Kluwer Academic Publishers, 1988.

[774] G. Golub and C. van Loan, *Matrix Computations*. North Oxford Academic, 1983.

[775] T. Ojanperä, A. Klein, and P.-O. Anderson, "FRAMES multiple access for UMTS," *IEE Colloquium (Digest)*, pp. 7/1–7/8, May 1997.

[776] V.K.N. Lau and M.D. Macleod, "Variable-Rate Adaptive Trellis Coded QAM for Flat-Fading Channels," *IEEE Transactions on Communications*, vol. 49, pp. 1550–1560, September 2001.

[777] T.S. Lee and T.C. Tsai, "A partially adaptive CDMA interference canceller for multipath channels," *IEEE Vehicular Technology Conference*, vol. 2, pp. 917–921, May 2000.

[778] S. Kazi and L. Lucke, "A convolutionally-coded adaptive CDMA receiver architecture," *Signals, Systems and Computers. Thirty-Second Asilomar Conference*, vol. 2, pp. 1199–1203, 1998.

[779] S.W. Lei and V.K.N. Lau, "Adaptive interleaving for OFDM in TDD system," *IEE Proceedings on Communications*, vol. 148, no. 2, pp. 77–80, 2001.

[780] Special Mobile Group of ETSI, "UMTS: Selection procedures for the choice of radio transmission technologies of the UMTS," tech. rep., European Telecommunications Standard Institute (ETSI), France, 1998.

[781] S. Verdú, “Minimum probability of error for asynchronous Gaussian multiple-access channel,” *IEEE Transactions on Communications*, vol. 32, pp. 85–96, January 1986.

[782] S. Moshavi, “Multi-user detection for DS-CDMA communications,” *IEEE Communications Magazine*, vol. 34, pp. 124–136, October 1996.

[783] M. Mitchell, *An Introduction to Genetic Algorithms*. Cambridge, Massachusetts: MIT Press, 1996.

[784] L. J. Eshelman and J. D. Schaffer, “Preventing premature convergence in genetic algorithms by preventing incest,” in *Proceedings of the Fourth International Conference on Genetic Algorithms* (R. K. Belew and L. B. Booker, eds.), (California, USA), pp. 115–122, Morgan Kaufmann, 1991.

[785] M. J. Juntti, T. Schlösser, and J. O. Lilleberg, “Genetic algorithms for multiuser detection in synchronous CDMA,” in *IEEE International Symposium on Information Theory – ISIT’97*, (Ulm, Germany), p. 492, 1997.

[786] G. Syswerda, “Uniform crossover in genetic algorithms,” in *Proceedings of the Third International Conference on Genetic Algorithms* (J. D. Schaffer, ed.), (California, USA), pp. 2–9, Morgan Kaufmann, 1989.

[787] W. Spears and K. De Jong, *Foundations of Genetic Algorithms*, ch. An Analysis of Multi-Point Crossover, pp. 301–315. California, USA: G. Rawlins, ed., Morgan Kaufmann, 1991.

[788] J. Anderson and S. Mohan, “Sequential coding algorithms: a survey and cost analysis,” *IEEE Transactions on Communications*, vol. 32, pp. 169–176, February 1984.

[789] T. Hashimoto, “A list-type reduced-constraint generalization of the viterbi algorithm,” *IEEE Transactions on Information Theory*, vol. 33, pp. 866–876, November 1987.

[790] S. J. Simmons, “Breadth-first trellis decoding with adaptive effort,” *IEEE Transactions on Communications*, vol. 38, pp. 3–12, January 1990.

[791] L. Rasmussen, T. Lim, and T. Aulin, “Breadth-first maximum likelihood detection in multiuser CDMA,” *IEEE Transactions on Communications*, vol. 45, pp. 1176–1178, October 1997.

[792] P. Balaban, J. Salz, “Optimum diversity combining and equalization in digital data transmission with application to cellular mobile radio – Part I: Theoretical considerations,” *IEEE Transactions on Communications*, vol. 40(5), pp. 885–894, 1992.

[793] A. Wittneben, “Base station modulation diversity for digital SIMULCAST,” in *Proceedings of IEEE Vehicular Technology Conference*, pp. 505–511, May 1993.

[794] S. Al-Semari and T. Fuja, “I-Q TCM: Reliable communication over the rayleigh fading channel close to the cuttoff rate,” *IEEE Transactions on Information Theory*, vol. 43, pp. 250–262, January 1997.

[795] B. D. Jelicic and S. Roy, “Design of trellis coded QAM for flat fading and AWGN channels,” *IEEE Transactions on Vehicular Technology*, vol. 44, pp. 192–201, February 1994.

[796] G. Klang, A. F. Naguib, “Transmit Diversity Based On Space-Time Block Codes In Frequency Selective Rayleigh Fading DS-CDMA Systems,” *IEEE Vehicular Technology Conference*, pp. 264–268, Spring 2000.

[797] L.-L. Yang and L. Hanzo, “Performance of wideband CDMA using adaptive space-time spreading over multipath nakagami fading channels,” *IEEE Vehicular Technology Conference*, pp. 615–619, May 2002.

[798] L. Miller and J. Lee, *CDMA Systems Engineering Handbook*. London, UK: Artech House, 1998.

[799] J. Mar and H. Chen, “Performance Analysis of Cellular CDMA Networks over Frequency-Selective Fading Channel,” *IEEE Transactions on Vehicular Technology*, vol. 47, pp. 1234–1244, November 1998.

[800] M. C. Reed, C. B. Schlegel, P. D. Alexander, and J. A. Asenstorfer, “Iterative Multiuser Detection for CDMA with FEC: Near single user performance,” *IEEE Transactions on Communication*, pp. 1693–1699, December 1998.

[801] R. Prasad and S. Hara, “Overview of multi-carrier CDMA,” in *Proceedings of the IEEE International Symposium on Spread Spectrum Techniques and Applications (ISSSTA)*, (Mainz, Germany), pp. 107–114, 22–25 September 1996.

[802] C. Tidestav, A. Ahl$\acute{e}$n and M. Sternad, “Realiazable MIMO Decision Feedback Equalizer: Structure and Design,” *IEEE Transactions on Signal Processing*, vol. 49, pp. 121–133, January 2001.

[803] R. Gallager, “Low-density parity-check codes,” *IEEE Transactions on Information Theory*, pp. 21–28, 1962.

[804] ETSI, *Digital Video Broadcasting (DVB); Framing structure, channel coding and modulation for cable systems*, December 1997. EN 300 429 V1.2.1.

[805] ETSI, *Digital Video Broadcasting (DVB); Framing structure, channel coding and modulation for 11/12 GHz Satellite Services*, August 1997. EN 300 421 V1.1.2.

[806] A. Michelson and A. Levesque, *Error Control Techniques for Digital Communication*. New York, USA: Wiley-Interscience, 1985.

[807] S. O'Leary and D. Priestly, "Mobile broadcasting of DVB-T signals," *IEEE Transactions on Broadcasting*, vol. 44, pp. 346–352, September 1998.

[808] W.-C. Lee, H.-M. Park, K.-J. Kang, and K.-B. Kim, "Performance analysis of viterbi decoder using channel state information in COFDM system," *IEEE Transactions on Broadcasting*, vol. 44, pp. 488–496, December 1998.

[809] S. O'Leary, "Hierarchical transmission and COFDM systems," *IEEE Transactions on Broadcasting*, vol. 43, pp. 166–174, June 1997.

[810] L. Thibault and M. Le, "Performance evaluation of COFDM for digital audoo broadcasting Part I: parametric study," *IEEE Transactions on Broadcasting*, vol. 43, pp. 64–75, March 1997.

[811] P. Shelswell, "The COFDM modulation system: the heart of digital audio broadcasting," *Electronics & Communication Engineering Journal*, vol. 7, pp. 127–136, June 1995.

[812] S. Wicker, *Error Control Systems for Digital Communication and Storage*. Englewood Cliffs, NJ, USA: Prentice-Hall, 1994.

[813] A. Barbulescu and S. Pietrobon, "Interleaver design for turbo codes," *IEE Electronics Letters*, pp. 2107–2108, December 1994.

[814] C. Lee, T. Keller, and L. Hanzo, "Turbo-coded hierarchical and non-hierarchical mobile digital video broadcasting," *IEEE Transaction on Broadcasting*, March 2000.

[815] B. Haskell, A. Puri, and A. Netravali, *Digital Video: An Introduction To MPEG-2*. Digital Multimedia Standards Series, London, UK: Chapman and Hall, 1997.

[816] G. Reali, G. Baruffa, S. Cacopardi, and F. Frescura, "Enhancing satellite broadcasting services using multiresolution modulations," *IEEE Transactions on Broadcasting*, vol. 44, pp. 497–506, December 1998.

[817] Y. Hsu, Y. Chen, C. Huang, and M. Sun, "MPEG-2 spatial scalable coding and transport stream error concealment for satellite TV broadcasting using Ka-band," *IEEE Transactions on Broadcasting*, vol. 44, pp. 77–86, March 1998.

[818] L. Atzori, F. D. Natale, M. D. Gregario, and D. Giusto, "Multimedia information broadcasting using digital TV channels," *IEEE Transactions on Broadcasting*, vol. 43, pp. 383–392, December 1997.

[819] W. Sohn, O. Kwon, and J. Chae, "Digital DBS system design and implementation for TV and data broadcasting using Koreasat," *IEEE Transactions on Broadcasting*, vol. 44, pp. 316–323, September 1998.

[820] J. Griffiths, *Radio Wave Propagation and Antennas — An Introduction*. Englewood Cliffs, NJ, USA: Prentice-Hall, 1987.

[821] M. Karaliopoulos and F.-N. Pavlidou, "Modelling the land mobile satellite channel: a review," *Electronics and Communication Engineering Journal*, vol. 11, pp. 235–248, October 1999.

[822] J. Goldhirsh and W. Vogel, "Mobile satellite system fade statistics for shadowing and multipath from roadside trees at UHF and L-band," *IEEE Transactions on Antennas and Propagation*, vol. 37, pp. 489–498, April 1989.

[823] W. Vogel and J. Goldhirsh, "Multipath fading at L band for low elevation angle, land mobile satellite scenarios," *IEEE Journal on Selected Areas in Communications*, vol. 13, pp. 197–204, February 1995.

[824] W. Vogel and G. Torrence, "Propagation measurements for satellite radio reception inside buildings," *IEEE Transactions on Antennas and Propagation*, vol. 41, pp. 954–961, July 1993.

[825] W. Vogel and U. Hong, "Measurement and modelling of land mobile satellite propagation at UHF and L-band," *IEEE Transactions on Antennas and Propagation*, vol. 36, pp. 707–719, May 1988.

[826] S. Saunders, C. Tzaras, and B. Evans, "Physical statistical propagation model for mobile satellite channel," tech. rep., European Commission, 1998.

[827] S. Saunders, *Antennas and Propagation for Wireless Communication Systems Concept and Design*. New York, USA: John Wiley and Sons, 1999.

[828] H. Gharavi and L. Hanzo, eds., *Proceedings of the IEEE*, vol. 87, October 1999.

[829] F. Adachi, "Error rate analysis of differentially encoded and detected 16APSK under rician fading," *IEEE Transactions on Vehicular Technology*, vol. 45, pp. 1–12, February 1996.

[830] Y. C. Chow, A. R. Nix, and J. P. McGeehan, "Diversity improvement for 16-DAPSK in Rayleigh fading channel," *Electronics Letters*, vol. 29, pp. 387–389, February 1993.

[831] Y. C. Chow, A. R. Nix, and J. P. McGeehan, "Error analysis for circular 16-DAPSK in frquency-selective Rayleigh fading channels with diversity reception," *Electronics Letters*, vol. 30, pp. 2006–2007, November 1994.

[832] C. M. Lo and W. H. Lam, "Performance analysis of bandwidth efficient coherent modulation schems with L-fold MRC and SC in Nakagami-m fading channels," in *Proceedings of IEEE PIMRC 2000*, vol. 1, pp. 572–576, September 2000.

[833] S. Benedetto, E. Biglierri, and V. Castellani, *Digital Transmission Theory*. Prentice-Hall, 1987.